CHARACTERISTICS OF CAVITIES DURING START TRANSIENT AND ESTABLISHED FLOW CONDITIONS AT SUPERSONIC MACH NUMBER

A thesis

Submitted in Partial Fulfilment of the Requirement for

The Award of the Degree of

DOCTOR OF PHILOSOPHY

By

S. Pandian

DEPARTMENT OF MECHANICAL ENGINEERING

INDIAN INSTITUTE OF TECHNOLOGY GUWAHATI

February 2020

DECLARATION

I hereby certify that the work compiled in this dissertation is the outcome of the research work, performed by myself, under the guidance of Dr. Desikan SLN, Scientist, Vikram Sarabhai Space Centre and Prof. Niranjan Sahoo, Department of Mechanical Engineering, Indian Institute of Technology Guwahati.

Any part of this work has not been submitted for the award of any degree or diploma, associate fellowship or its equivalent to any university or institution.

S. Pandian

Registration No. : 156103021

Department of Mechanical Engineering

Indian Institute of Technology Guwahati

THESIS CERTIFICATE

This is to certify that the thesis entitled “Characteristics of cavities during start transient and established flow conditions at supersonic Mach number” submitted by Shri. S. Pandian to the Indian Institute of Technology Guwahati, for the award of the degree of Doctor of Philosophy is a bonafide record of research work carried out by him under our supervision. The contents of this thesis, in full or parts have not been submitted to any other Institute or University for the award of any degree or diploma.

Dr. Desikan. SLN

Scientist and Research Supervisor
Wind Tunnel Data Division
Aeronautics Entity
Vikram Sarabhai Space Centre
Thiruvananthapuram – 695022
Kerala, India

Prof. Niranjan Sahoo

Professor and Research Supervisor
Department of Mechanical Engineering
Indian Institute of Technology Guwahati
Guwahati – 781039, Assam, India

Date: February 28, 2020

CONTENTS

LIST OF FIGURES

LIST OF TABLES

ACKNOWLEDGEMENTS

Successful completion of my doctoral thesis was possible with the encouragement and help of many persons. I would like to place on record and express my sincere gratitude to all of them.

First and foremost, I am extremely grateful to my organizational guide (internal guide) Dr SLN Desikan, Senior Scientist, Aeronautics Entity, Vikram Sarabhai Space Centre, ISRO for his valuable contributions in terms of scholarly inputs, planning, conceiving, execution and encouragements I received throughout the research work. This feat was possible only because of unconditional support provided by Dr Desikan. He is a person with lot of energy, amicable and positive disposition. He made available himself for each step of this thesis work for the last four years. I am very fortunate to have him as my internal guide. I don't have words to express my heartiest appreciation and thanks to him.

I express my sincere and deepest gratitude to my guide Prof. Niranjan Saboo, Mechanical Engineering department, Indian Institute of Technology, Guwahati who has guided me throughout this thesis work, made critical suggestions and gave valuable inputs. To complete this thesis Dr Desikan's expertise, understanding and positive criticism added value. Without his continuous inspiration, it would not have been possible to complete the thesis timely.

I am immensely indebted to lab mates Mr. K. Suresh for the realization of various models and I gratefully acknowledge Mrs.Sajitha, Mr.Binu, Mr. Chandrasekar, Mr. Shyju and Mr. Salam for providing all supports in terms of providing high pressure air,

instrumenting the model, integrating it, carrying out hundreds of blow downs, data acquisition, processing the data, etc.

I acknowledge the Doctoral committee Chairman and members of IITG for their support at various phases of this thesis work.

I am grateful to my wife Mrs Hemavathy, siblings, my mother and family members who have provided me moral and emotional support in my life.

ABSTRACT

Experiments are carried out to study the cavity flow physics for a range of Length/Depth ratios (L/D ratios 1, 2, 3, 4, 5, 6, 7.5 and 10) at supersonic condition in a confined duct. These cavities are categorized into (a) transition from deep to shallow open cavities ($1 \leq L/D \leq 3$), (b) shallow open cavities (L/D = 4 and 5) and (c) transition from shallow open to shallow closed cavities ($6 \leq L/D \leq 10$). The studies consist of (i) transient starting process in which the stagnation pressures varied from $P_{01}/P_0 = 0.41$ to 0.63 to comprehend the transient shocks interaction with cavity shear layer and, (ii) fully established supersonic conditions (M = 1.8) at $P_{01}/P_0 = 1$.The cavity flow physics is brought out by analyzing the unsteady pressure data and time resolved optical images (both shadowgraph and schlieren). Further, from unsteady pressure signals, FFT, cross correlation, coherence coefficients, spectrogram and wavelet transform are derived to bring out the flow physics.

The transient starting characteristics obtained from shadowgraph images show the existence of bifurcated shock system and associated shock train phenomena. This shock train interacts with cavity shear layer, which produces number of small amplitude modes/tones inside the cavity. During start transient process, a mode switching phenomena is observed. The overall sound pressure level (OASPL) measured is181 dB and hence, the airframe structure and electronics packages have to be designed to take care of this effect.

Experiments are carried out on L/D = 1, 2 and 3 cavities at Mach number 1.8 to comprehend cavity oscillation from transverse to longitudinal mode. The mode transition is studied through unsteady pressure measurements and time resolved schlieren images. It is noticed that the mode transition depends on cavity L/D ratio and shear layer. Results reveal that the transverse oscillation is characterized by a single vortex while transition and longitudinal oscillation is dictated by two vortices. The mode transition takes place between L/D = 2 and 3, where the cavity shear layer is thicker (with respect L/D =1) and the vortex convection velocity is not constant along the shear layer. Time dependent data are compared with the modified Rossiter relation that necessitates in development of a suitable model for transitional cavities. In-depth analyses in terms of cross correlation as well as wavelet transform divulge the source of cavity modes/tones and mode switching phenomena.

For L/D = 4 and 5, number of modes/tones is increased. In these cases, the vortex convection velocity inside the cavity shear layer is not constant and the vortex velocity varies from 230 to 305 m/s. The cross correlation analyses reveal that the 1st mode/tone is due to wave propagation inside the cavity, 2nd mode/tone is due to vortex shedding and one time period indicates the maximum mode/tone. In both the cavities, wavelet analysis shows no mode switching phenomena.

Time resolved schlieren images for L/D = 6, 7.5 and 10 show the cavity shear layer impinges on cavity floor and hence, modes/tones of the cavity are affected. As the cavity L/D increases, shear layer impingement on cavity floor moves upstream with

respect to the trailing edge, and the cavity floor experiences more attached flow region. The velocity of the vortex convection varies from 256 to 344 m/s, for L/D = 6 and 7.5, indicate the non-linear behavior of the cavity flow physics. Coherence coefficients show a poor value, which indicates a non-existence of a feedback mechanism. The absence of feedback mechanism is also confirmed through cross correlation.

NOMENCLATURE

C_{xy}	Coherence between two signals *x* and *y* in frequency domain
D(H)	Depth(height) of cavity (mm)
G_{xy}	Cross spectral density between two signals *x* and *y* in time domain
L	Length of cavity (mm)
M	Mach number
M_C	Convective Mach number
P_{ref}	Reference pressure (= 20 μPa)
P_0	Tunnel stagnation pressure (bar)
P_{01}	Settling Chamber pressure (bar)
P_{02}	Stagnation pressure behind normal shock (bar)
P'	Fluctuating pressure (bar)
P	Freestream pressure (bar)
Re	Reynolds number
rms	Root Mean Square value
x, y	Cartesian coordinates
δ	Boundary layer thickness (mm)
V_C	Convective velocity (m/s)
V_∞	Freestream velocity (m/s)
Υ	Specific heat ratio
m	Mode number
ρ	Density (kg/m^3)

ABBREVIATION

ADC	Analog-to-Digital Converter
CIAM	Central Institute Of Aviation Motors
FFT	Fast Fourier Transformation
LPSC	Liquid Propulsion System Centre
NASA	National Aeronautics and Space Administration
OASPL	Overall Sound Pressure Level (dB)
PMMA	Poly-Methyl-Meth Acrylate
PSD	Power Spectral Density
SERN	Single Expansion Ramp Nozzle
SPL	Sound Pressure Level
TSTO	Two Stage To Orbit

LIST OF PUBLICATIONS

1. S. Pandian, S. L. N. Desikan and Sahoo Niranjan, Experimental investigation of starting characteristics and wave propagation from a shallow open cavity and its acoustic emission at supersonic speed, AIP Publication, Physics of Fluids, 30, 016104 (2018)

2. S. Pandian, S. L. N. Desikan and Sahoo Niranjan, Onset of transient shock interaction with cavity shear layer". AIAA Journal, Vol. 57, No. 9, pp. 3773-3778 (2019)

3. S. Pandian, S. L. N. Desikan and Sahoo Niranjan, Non-linear characteristics of a rectangular cavity in supersonic flow, AIAA Journal, Article in Advance (2020) https://doi.org/10.2514/1.J058709

4. S. Pandian, S. L. N. Desikan and Sahoo Niranjan, Onset of cavity oscillation from transverse to longitudinal mode in a supersonic flow, ASME Journal of Fluids Engineering, Article in Press (2020) doi:10.1115/1.4046369

CHAPTER 1

INTRODUCTION

1.1. Introduction

Supersonic combustion ramjet engine (scramjet) is being considered as a feasible propulsion system for hypersonic cruise missiles, passenger transport vehicles for long-range operation, faster inter-continental travel and for low cost access to space. Some of the programs to demonstrate scramjet technology include Dual Mode Ramjet Jet (DMRJ) of India, Kholod of Russia, SCRAM, X43, X51 of USA, Hyshot and Scram Space Experiments by Australia.

Fig 1.1 shows the overall performance range of various propulsion systems in terms of their operating Mach number range and specific impulse. Ramjet engines may be used for flight Mach numbers of 3-6. It may be seen that the Mach number higher than 6-7, the only available propulsion systems are scramjets and rockets. Compared to rocket, scramjet specific impulse is high because it need not carry oxidizer, as the air breathing engine collect oxygen from the atmosphere. Apart from the above, there are other reasons that highlight the advantage of scramjet. Air breathing engines produce higher efficiency, have longer powered range, the thrust modulations ensure efficient operation, higher versatility and are reusable.

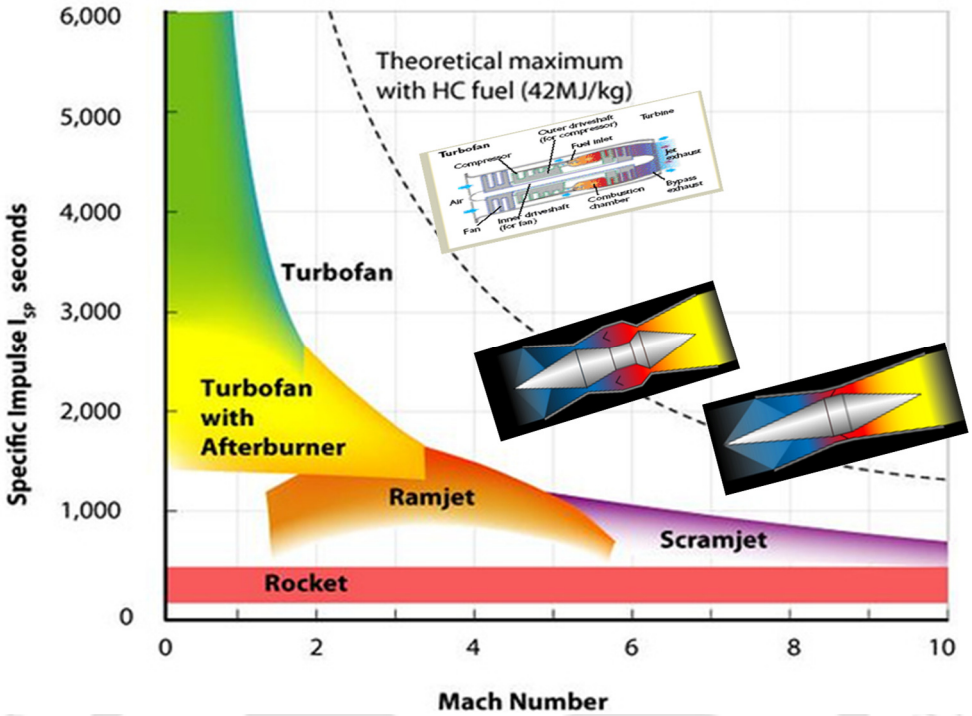

Fig.1.1: Performance of various propulsions [1]

At higher Mach numbers, many of the problems precipitating the transition from ramjets to scramjets and vice versa as major issues, thus limiting “scramjet” practically. The increased flow path velocity associated with increased free stream Mach number result in significantly increased heat transfer levels. Consequently, fuel cooling Equivalence Ratio (ER) can be considerably higher than required for stoichiometric combustion, resulting in reduction in Specific Impulse and increasing fuel volume requirements. Severe thermal environment demands higher mass thermal protection systems, which lead to mass and cost increase, which becomes limiting factors.

The scramjet engine conceptually is an extension of the ramjet engine where in the flow through the engine is fully supersonic, whereas, in a ramjet engine the flow is decelerated to subsonic speeds at combustor entry. The scramjet is so designed that

the flow Mach number at entry to the combustor is supersonic and it is usually around 2 - 2.5. The scramjet engine is fundamentally simple in concept but is not so easy to operationalize. Figure 1.2 shows a typical scramjet engine consists of four main parts namely the inlet, isolator, combustor and exhaust nozzle. The fuel is injected into the main supersonic flow in the combustor where the air is at high temperature and pressure for the fuel to combust and resulting mixture is expelled from engine at high pressure through a divergent nozzle (which is typically a Single Expansion Ramp Nozzle- SERN) to produce large thrust. To facilitate heat addition at such high speeds, the combustion occurs at supersonic Mach numbers, which enable the vehicle to reach up to hypersonic Mach numbers as high as 15.

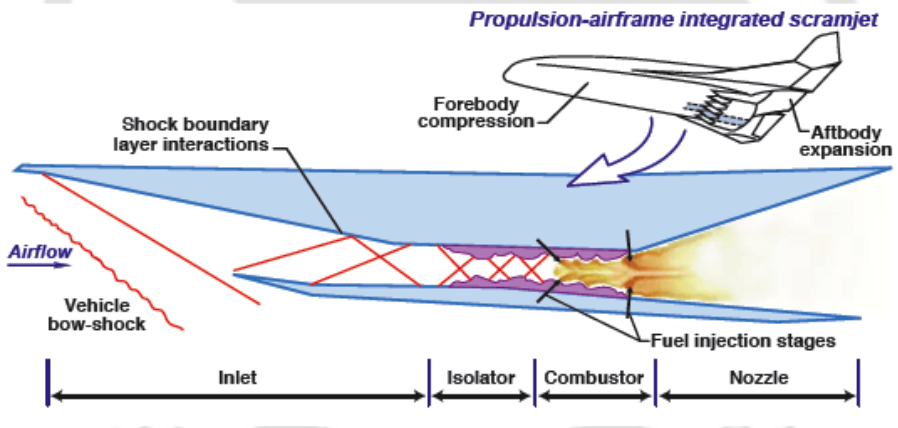

Fig. 1.2: Schematic illustration of a scramjet engine
(www. nasa.gov/centers/dryden/news/factsheets/FS.040-DFRC.html)

The major challenges involved in the development of scramjet engine are; accomplishing stable, efficient mixing and combustion in a supersonic flow and to handle severe aero-thermal environments of the engine system. Although the concept of scramjet engine appeared to be simple, supersonic combustion remains a formidable

task due to the association of chemical kinetics, temperature, pressure, equivalence ratio, mixing rate, etc. Perhaps mixing in the high speed flows is a key problem associated with the combustion due to very small residential time. Many mixing /flame holding devices are being attempted both in ground testing and in flight. Fundamentally, the fluid mechanics of mixing needs to be understood so that it may be used gainfully. In scramjet engine, the incoming boundary layer is compressible. When a mixing layer is formed between two supersonic streams, the compressibility causes less growth rate of mixing layer/ less spreading rate of the layer and hence the mixing extent is less compared to incompressible flows. Thus, the injection of fuel in the above scenario leads to inefficient mixing. In addition to the problem of mixing, ignition and flame holding at these high velocities are extremely difficult. To overcome these challenges, several solutions have been proposed by many researchers viz., strut mounted injection, wall mounted injection system, cavity mounted, etc. One of the viable solutions is the cavity assisted supersonic combustion.

In recent times, focus is made to implement wall-mounted cavities to augment mixing and flame stabilization with less total pressure losses at higher thrust, as compared to other active and passive devices. Since the acoustic feedback mechanism associated with the cavities can influence the compressible shear layer at high speed to oscillate, this effect can be utilized for mixing augmentation. The cavities that are acoustically stable with large recirculation zone are used for flame holding purpose. Though cavities are noticed to be suitable candidate for supersonic mixing and flame holding capability, still its flow physics is not completely understood. This includes the

characteristics of the shear layer over the cavity and its interaction with the start transient shock train, its behavior, vortex convection, waves both inside and outside the cavity, origin of the modes/tones, etc.

In Dual Mode ramjet-scramjet combustion engine (combined propulsion system), mode transition takes place. When the engine undergoes transition from Ramjet to Scram jet or vice versa, the inflow variation has a great impact on the ramjet-scramjet mode transition and it makes a great difference to the variation of the Equivalence Ratio. Hence, this information needs further investigation. In transient starting/stopping, there exists shock train, which interacts with the cavity shear layer. This may alter the shear layer characteristics and the impinging pattern at cavity aft wall. Though this kind of phenomena prevails for short duration, its effect has to be quantified in the design phase. For example, in the present studies, these effects produce mode switching phenomena which may have impact on mixing, flame holding and on structure. Hence, it is essential to study them in detail and account the same in the design suitably.

The cavities, which are acoustically stable with large recirculation zone, are used for flame holding purpose. These are termed as “stable cavities” where the flow resident time inside the cavity is relatively large. In contrary, for certain cavities, the flow reattaches at the cavity trailing edge. As a result, the flow unsteadiness inside the cavity is more that aid mixing of fuel and air. This type of cavity is called “unstable cavity”.

The present experimental work, mainly intended to bring out the influence/interaction of starting transient shocks with cavity shear layer and its effect on cavity acoustic field. The stable/unstable behavior of the cavity flow physics for different cavity L/D ratios are brought out.

1.2. Delineation of the Thesis

In Chapter II, a detailed review of the literature pertaining high speed mixing layer flows, cavity flow physics and transition from ramjet to scramjet are presented.

Details of the models configuration, experimental facility, test set-up, measurement techniques, data reduction schemes and flow field visualization studies are presented in Chapter III. The interaction between transient starting shock systems with shear layer of different cavities are studied through unsteady pressure measurements and high-speed shadowgraph images which are presented in Chapter IV. This study finds importance in the transition from Ramjet to Scramjet mode and Scramjet to Ramjet mode in a combined propulsion system. Chapter V deals with the onset of cavity oscillation from transverse to longitudinal mode and their characteristics for L/D = 1 to 3 cavities (transition to open cavity) for fully established flow condition. These results are obtained through unsteady pressure measurements and time resolved schlieren images.

Detailed results on shallow open cavities (L/D = 4 and 5) obtained from unsteady pressure measurements and time resolved schlieren images are presented in Chapter VI. These include non-linear behavior of the cavities flow physics and wave structures both inside and outside the cavity. In Chapter VII, the transitional behavior of the open and close cavity (L/D = 6, 7.5 and 10) are discussed. The cavities oscillatory modes and drag aspects are discussed in Chapter VIII. The conclusions are presented in Chapter IX.

CHAPTER 2

LITERATURE REVIEW AND SCOPE OF THE WORK

The objective of present work is to study the flow physics of wall-mounted cavities in a confined supersonic flow to understand their behavior at different L/D ratios. In this chapter, the relevant literatures pertaining to cavity flow, start transient studies, shear layer / mixing characteristics are presented. Subsequently, motivation and objectives of the present studies are outlined.

2.1. Cavity flow

The cavity flow consists of three main regimes namely flow inside the cavity, flow outside the cavity and cavity shear layer. Irrespective of the nature of approaching flow (laminar or turbulent) to the cavity, the flow separation occurs at the leading edge of the cavity and shear layer is formed. This shear layer reattaches either at cavity aft wall or at cavity floor depending upon the cavity L/D ratio. In general, two fundamental types of cavity exist based on length-to depth ratio (L/D). The first type is known as open cavity (L/D < 10) and the second one is closed cavity (L/D > 10). In the former, the shear layer reattaches at the cavity aft wall whereas, in the latter, the shear layer reattaches at the cavity floor. The open cavity is further classified into deep cavity (when L/D < 1) and shallow cavity (L/D > 1). The basic difference between these two is the way in which the oscillation takes place. In the case of deep cavity, the oscillation is predominantly in transverse mode whereas; in shallow cavity the oscillation occurs in longitudinal mode. The (L/D) of the cavity is the primary factor for the self-sustained oscillation which is very strong and coherent up to certain L/D values. Beyond certain L/D value, oscillations are

reduced and their frequencies are broadband in nature. The changes occur in the flow up to L/D = 5 beyond which, there is no appreciable change in the dominant frequencies [2].

Cavities are used in many practical applications, among them scramjet engine is one where they play pivotal role in terms of efficient mixing, flame holding and sustained combustion. Depending upon the application, the cavity configuration is chosen. The stable cavity is the one used for the flame holding, where the cavity oscillations are controlled using several active and passive control methods. The unstable cavities are used for mixing and its enhancement. In unstable cavities, the acoustic waves emitted from cavity are impinging on the mixing layer.

Investigation on cavity was carried out way back in 1950s where the acoustic emission and the flame holding concepts were established [3-4]. The acoustic emission from cavity and its dependence on cavity parameters (length, depth and width) shows self-sustained oscillation which produces fluctuation in pressure, velocity and density leading to increase in drag [3,5]. Many researchers [6-14] studied the complex flow features of the cavity, its oscillation and the control mechanisms. It is understood that the cavity flow oscillation occurs at certain dominant frequencies and the feedback mechanism, which produces the self-sustained oscillation mainly, depends on shear layer fluctuation and the wave propagation inside the cavity. Hence, to control and suppress the cavity instability, relation between wave propagation and shear layer oscillation has to be well understood.

Earlier investigations suggested that the cavity oscillations were due to linear response caused by unsteadiness inside the turbulent boundary layer [15]. However, it

was demonstrated that the pressure fluctuations induced by the laminar boundary layer [3] is found to be more intensive than the turbulent boundary layer. Hence, the empirical relation [8] is modified by accounting laminar to turbulent transition and turbulent boundary layer [17] to explain cavity induced oscillations at discrete frequencies.

Krishnamurty [3] investigated the acoustic radiation from two-dimensional rectangular cut-outs in aerodynamic surfaces. The acoustic radiation is found to be very intense and the frequency measured in the gap is inversely proportional to gap breadth in both laminar and turbulent flow. His studies showed that there is an interaction of the oscillatory shear layer with the cavity trailing edge.

The definition of open or closed cavity was introduced by Charawat et al. [17] on their investigations in subsonic and supersonic cavities flows. Also, their studies revealed that the flow entrainment takes place from free stream to cavity and vice versa due to unstable behavior of the cavity flow. Probably, the first published investigation of cavity flame-holder is by Huellmantel et al [4], who studied various cavity shapes for sustained combustion in low speeds.

Rossiter [8] observed the phenomenon of flow induced noise radiations and acoustic oscillations in a rectangular cavity at subsonic and transonic flows. The results indicated that small-scale vortices are formed at the leading edge of the cavity and grow in size as they move downstream. When they impinge on the trailing edge of the cavity, a feedback mechanism is set within the cavity. As a result, pressure pulses are generated

inside the cavity, which propagates upstream with local speed. When the pressure pulse reaches the leading edge, new vortices are shed and thus complete one feedback cycle. These studies assumed that the vortex convection speed is linear with respect to cavity length. Based on these observations, an empirical formula for tone frequencies in the form of Strouhal number (Stn) is derived which is limited to subsonic and transonic flows as given below.

$$Stn = \frac{fL}{V_\infty} = \frac{(m - \alpha)}{(\frac{1}{K} + M)} \quad (2.1)$$

Where, f is the mode/tone frequency, L is the length of the cavity, V_∞ is the free stream velocity, m is an integer (1, 2, 3), M is the Mach number, K is the ratio of convective velocity of vortices to the free stream velocity, α is the factor to account for the time lag between the passage of a vortex and emission of acoustic pulses at downstream corner of the cavity. The values of the empirical constants are evaluated through the best fit of measured data as α = 0.25 and 1/k = 1.75.

Plentovich et al. [13] carried out experimental investigation of cavity flow at subsonic and transonic speeds (M = 0.2 - 0.99). It is found that for a given L/D ratio, when the cavity volume is increased the pressure coefficient values considerably change, especially in the open cavity flow regime.

Chung [18] carried out experimental study on the characteristics of compressible rectangular cavity flows by varying cavity geometry and flow Mach number. The study

indicated that the ratio of depth to incoming boundary layer thickness has significant impact on the pressure coefficient distribution.

The experiments performed by Tracy et al. [19] in transonic and subsonic flows showed that the mode amplitude depends on Mach number. It was also shown that the deeper cavity experiences higher acoustic pressure. A similar study conducted by Tracy et al. [20] to characterize L/D variation by keeping constant cavity length for range of Mach numbers from 0.2 to 0.9 indicated that the Sound Pressure Level (SPL) on the floor showed sufficient increase in its magnitude with increase in cavity depth. An experimental study [21] of the flow over an open shallow cavity at free stream Mach numbers 0.3, 0.5, and 0.6 showed that the high intensity fluctuations occurs even if the resonance criteria $\delta/L < 0.066$ is not met. It showed that the above criterion needs refinement. Using wavelet transform, it was found that the high intensity fluctuations at Rossiter frequencies are usually generated in the flow.

The generation of tones in an axisymmetric cavity [22] for turbulent flow with acoustic wavelength much longer than the cavity length was studied. For a sufficiently long cavity, the fully evolved axisymmetric instability yields a large-scale mode. When the cavity length is decreased to progressively smaller values, the mode of oscillation transforms from high amplitude to low amplitude mode. Below certain cavity length, distinct oscillations do not occur. The existence of pronounced oscillations, i.e., flow tones, is also related to the cavity dimensions. Oscillations are suppressed when the cavity depth is sufficiently small relative to the on-coming boundary layer momentum thickness.

Numerical studies [23] to investigate the resonant instabilities in two dimensional flows past an open cavity were carried out. For low Mach numbers, shorter cavities exhibit shear layer mode whereas at higher Mach number, longer cavities exhibit wake mode. The shear-layer mode is well characterized by the acoustic feedback process and disturbances in the shear layer compare well with predictions based on linear stability analysis of the Kelvin-Helmholtz mode. The wake mode is characterized by a large-scale vortex shedding and it is independent of Mach number. Transition to wake mode occurs as the cavity L/D becomes large compared to the upstream boundary-layer thickness, or as the Mach and/or Reynolds numbers are increased. Under these conditions, it is shown that the Kelvin Helmholtz instability grows to sufficient strength which leads to a strong recirculating flow in the cavity.

An experimental investigation [24] of flow over an axisymmetric cavity shows self-sustained oscillations with low cavity drag. In this low-drag mode, the flow gets adjusted such a way that the mean shear layer stagnation point gets fixed at the downstream corner. Above a critical value of the cavity width-to-depth ratio, there is an abrupt and large increase of drag due to the onset of the wake mode of instability. Wall pressure fluctuation due to turbulent boundary layers over a shallow cavity [25] is similar to flow around a backward facing step.

The flow over a non-resonating shallow cavity at low Mach numbers [26] shows a strong vortex inside the cavity aft wall region in laminar case as compared to turbulent

case. The laminar upstream conditions lead to a vortex, which remains more localized towards trailing edge. In addition, laminar upstream conditions produce a weak counter-rotating vortex near the upstream corner that is not seen for the turbulent upstream condition case. Incompressible flow computations [27] on L/D = 2 cavity shows three regimes depending upon the Reynolds number. In the first regime, a second Rossiter mode dominates, in the second (transitional) regime two incommensurable frequencies compete with each other via mode switching, and finally, in the third (suppressed) regime a lower frequency dominates.

The fluid-acoustic interactions in a turbulent flow over a two-dimensional rectangular cavity [28] of L/D = 0.5 reveal the mechanism for the acoustic radiation. Large-scale vortices form in the shear layer that separates from the upstream edge of the cavity. When a large-scale vortex impinges on the downstream wall, low-pressure fluid in the vortex spreads along the downstream wall. As a result, local downward velocity is induced by the local pressure gradient, causing the upstream fluid to expand. Finally, an expansion wave propagates outside of the cavity. The large-scale vortices grow due to Kelvin–Helmholtz instability, similar to the growth of those in a laminar cavity flow.

2.2. Supersonic cavity and start transient studies

Considering the buffeting of bomb bays and cockpits, early investigations of cavities focused mainly on subsonic and transonic flows. In 1993, cavity flame-holders

designed by CIAM (Central Institute of Aviation Motors), were used for the first time in a joint Russian/French dual-mode scramjet flight test. Further experiments showed that the use of a cavity after the ramp injector significantly improved the hydrocarbon combustion efficiency in a supersonic flow. Similar flame stabilization zones, investigated by Ben-Yakar et al [29], have been employed within a solid-fuel supersonic combustor, demonstrating self-ignition and sustained combustion of PMMA under supersonic flow conditions. In 1994, under a contract from NASA, CIAM extended the scramjet operating envelope from dual-mode operation to full supersonic combustion mode at Mach 6.5. Owing to the results obtained in flight tests and feasibility demonstrations in laboratory scale, cavities have gained attention towards effective injection, mixing, auto-ignition and flame-holding devices in supersonic combustors.

Bilanin and Covert [30] improved the Rossiter feedback model by relating the driving mechanism of cavity oscillation to the instabilities of the free shear layer. They assumed that the shear layer being agitated periodically at the upstream lip of the cavity, which excites the flow instability as, they propagate downstream. The fluctuating motion of the shear layer at the downstream wall of the cavity induces a periodic inflow of fluid in to the cavity and a half period later, it gets discharge from the cavity in to the external flow. This action of mass inflow and outflow acts as the source of acoustic radiation. Further, the model is modified based on the assumption that equal fluid temperature inside and outside the cavity, separated by the shear layer. The temperature difference is taken in to account by Heller and Bliss [31] to modify the relation as:

$$Stn = \frac{m - \alpha}{\left\{ \frac{M}{[1 + (\gamma - 1)M^2 / 2]^{1/2}} + \frac{1}{K} \right\}} \tag{2.2}$$

It was also found that the transition from laminar to turbulent boundary layer can severely affect the cavity-induced oscillations. The pressure oscillation in the cavity is insensitive to Reynolds number once the upstream boundary layer is turbulent.

Water table experiments [32] on deep cavity explained that the wave propagation around the cavity was due to shear layer impingement at cavity aft wall. As a consequence of shear layer impingement, a compression wave was generated which was responsible for the flow oscillation. This compression wave was found to move upstream inside the cavity with reflection from the cavity front wall after incident. This reflected wave was observed to be in phase with the shear layer vortex in the course of its downstream movement. On the other hand, outside the cavity, a compression/ expansion wave appeared periodically at the cavity leading edge depending upon the nature of shear layer deflection (flapping up or down). Also, generation and downstream propagation of a shock wave owing to vortex convection in the shear layer was seen. At the cavity aft wall, a quasi-steady bow shock and formation of a compression wave were observed. In order to confirm the water table studies, wind tunnel experiments were carried out [32] at high Mach number that revealed most of the flow features.

Further, studies on cavity explored three types of shear layer impingement mechanism [33]. In the first type, a full clipping was seen where the shear layer was

found to impinge directly on the cavity aft wall and hence, full entrainment into the cavity is observed. In the second type, a partial clipping was noticed where a portion of the shear layer was found to impinge on the cavity trailing edge and hence, the entrainment is limited. The third type was no clipping where the shear layer was observed to be fully escaped from the cavity aft wall. The flow development inside and outside the cavity at supersonic Mach numbers is given in reference [32]. Whenever the shear layer deflects upward a quasi-steady compression shock is generated at the front wall. Subsequently, the expansion wave is generated one-half cycle later due to shear layer oscillation. Hence the shock and expansion waves appear and disappear periodically. The upstream travelling wave front inside the cavity trails with an external wave front, which detaches from the internal stem of the front and swims off into the external medium, on reaching the front wall. Hence, in the course of repeated oscillation cycles one would expect a periodic pattern of such wave fronts propagating outward into the free medium, while at the same time they are convected with the free flow in a downstream direction. The internal wave front being reflected off the trailing edge, now moves upstream, again approximately with the speed of sound. For every cycle the shear layer dives down into the cavity at the trailing edge thus exposing the trailing edge to free stream (supersonic).This causes outward/inward mass transfer.

Tam [34] indicated that the flow induced cavity oscillations are affected not only by Mach number but also by cavity L/D. The empirically determined constants in Rossiter formula for excitation frequencies are computed and it appears that instability of the shear layer as well as interaction between the shear layer and the cavity trailing edge are required to sustain discrete-frequency oscillation. It is suggested that the simultaneous

excitation of two or more discrete frequencies are observed, correspond to the simultaneous participation of two or more vortices.

Tam and Block [35] observed that upward deflection of the shear layer shield the cavity from external flow and hence, the free stream moves above the cavity trailing edge. When the shear layer deflects downwards, free stream entrains into the cavity produce a high-pressure region (stagnation point) near the trailing edge of the cavity. The transient nature of flow causes emission of compression waves and these waves propagate in all directions away from the trailing edge of the cavity.

Consistent with the above findings it is understood that the self-sustained oscillations are strongly influenced by shear layer instability acting in conjunction with disturbance feedback and resonant wave condition or a complex combination of these effects. Rockwell and Naudascher [36] analyzed these effects separately in their general classification of self-sustained oscillation of cavities: (i) fluid dynamic, where the oscillations are due to amplification of unstable disturbance in the shear layer and are enhanced through the feedback mechanism or (ii) fluid resonant in which cavity oscillations are strongly coupled with the resonant wave effect within the cavity.

Hankey and Shang [37] obtained complete viscous solutions of pressure oscillations for supersonic flow over an open cavity, which fairly matches with experimental data. A similar solution for the unsteady flow over a three dimensional cavity at M=1.5 was presented by Rizetta [38]. Zhang and Edwards [39] simulated cavity flow

driven by thick shear layer at Mach numbers 1.5 and 2.5 and concluded that dominant oscillation resulted in shallow cavity is longitudinal and it is a purely fluid dynamic mechanism rather than a purely acoustic one. Baysal and Stallings [40] extended their work for the numerical prediction of flow features over open, transitional and closed cavities also.

Stallings and Wilcox [41] experimentally studied the pressure distribution inside rectangular cavities over a range of free steam Mach numbers from 1.5 to 2.86 with different cavity dimensions. The critical value of L/D ratio that separates open cavity from closed one are studied through pressure distribution along with schlieren images and a marked differences of pressure coefficient is observed depending on cavity volume.

Zhang and Edwards [42], visualized flow features such as the trailing edge vortex, large density gradient at the trailing edge of a fluid dynamic cavity and single large vortex in the case of a short cavity. The study also found that the convective speed of the vertical structure in the shear layer is not constant, but depends on Mach number.

A computational analysis is performed for L/D = 3 cavity at M = 1.5 and 2.5 by Zhang [43] where a self-sustained flow oscillatory state is achieved. The shock and expansion wave patterns above the cavity are simulated which resemble the experimentally observed images. The wave emission is caused by the shear layer deflection, which in turn associated with the vortex production and convection in the

cavity. It is observed that the form drag coefficient varies with the shear layer impingement and mass ejection near the cavity tailing edge.

Tam et al [44] carried out the unsteady numerical simulation, which reveals a new oscillation cycle and several noteworthy wave signatures inside the cavity that are entirely different from Heller and Bliss [10]. In this cycle, it is argued that unlike Heller and Bliss [10], the vortex impingement at the lip of the trailing edge does not form an upstream traveling wave. It is mentioned that the vortex, when impinges on the cavity aft wall lip, produces a pressure pulse. This forces an upstream moving wave, which is reflected from the cavity aft wall lower corner at the vortex shedding frequency. This wave after reflecting from the cavity front wall moves downstream and disappear due to dissipation before reaching the cavity aft wall. During the process of impingement on the front wall, this wave forces a shedding of a new vortex. Hence, a new wave is generated behind the shed vortex and reflects from the cavity aft corner at shedding frequency.

Experiments [45] on cavity with L/D =3 at M=1.5 show that the flow consists of five types of wave pattern such as leading edge shock-expansion, acoustic wave inside the cavity, shock wave due to roll-up of vortices, shock due to periodic interaction of shear layer with the trailing edge and quasi-stationary waves downstream of the trailing edge.

For unconfined separated flows and cavity flows [46] at relatively high convective Mach number, the primary mechanism for unsteadiness near reattachment is due to

perturbation by organized structures in the shear layer. The spectrum of the wall pressure fluctuations near reattachment was found to scale on the characteristic length and convection velocity of the organized structures in the incoming free shear layer. There is a strong link between large-scale structures and unsteadiness at reattachment, hence accurate characterization of the mixing layer turbulence is important. The driving mechanism for the cavity flow unsteadiness is related to the broadband turbulent fluctuations rather than discrete acoustic resonances.

The shear layer-acoustic coupling was shown [47] for open cavity, high Mach number and turbulent flow conditions. In these studies, cavities with and without cover plate (80 % of the length was covered with plate) were studied through experiments. The uncovered-cavity resonance frequencies at M = 2 agree well with those predicted by Rossiter's model. On the other hand, the resonance frequencies measured in the covered cavity do not agree with Rossiter's model but instead are consistent with a model that is based on closed-box acoustics. At Mach 5, both the uncovered and covered cavities have resonance frequencies, which are agreeing well with both Rossiter's model and closed-box acoustics. The results suggest that the coupling between the shear-layer dynamics and the cavity acoustics is greatly reduced at high Mach numbers. Based on a consideration of the physical mechanisms implicit in Rossiter's model, it is argued that its successful prediction of the resonance frequencies in high-Mach-number cavity flows is largely coincidental and likely does not reflect the correct modeling of the flow physics.

The frequency jump observed in an oscillating supersonic flow over a rectangular cavity [48] is studied analytically by incorporating the phase delay in Rossiter's formula. The phase delay is caused by the acoustic field inside the cavity and is estimated by positioning a monopole source and its image sources at the trailing edge of the cavity. The results agree reasonably with experimental results with respect to both frequency jump and variation in frequency with the length-to-depth ratio. Further, to understand the frequency jump occurrence, a simple model is developed. In this model, two one-dimensional planar waves are considered: "Wave I" generated at the trailing edge, and "Wave II" generated by the reflection of "Wave I" at the bottom wall. These two waves are superposed at the leading edge of the cavity, and frequency of the superposed wave is calculated by changing the cavity depth. The results showed that the frequency jumps when the phase of the superposed wave abruptly changed. The simple model is found to explain the frequency jumps observed in experiments when the length to-depth ratio of the cavity is changed.

The feedback mechanism and effects of upstream boundary layer in supersonic cavity flows was investigated by implicit large-eddy simulations [49]. It was shown that the feedback mechanism is the cause for driving the self-sustained oscillations and does not alter regardless of the upstream turbulent state and boundary-layer thickness. It was demonstrated that the generation of discrete large-scale vortices in the cavity shear layer is highly related to acoustic excitations at the cavity leading edge rather than natural instabilities. Successive passage of large-scale vortices over the cavity trailing edge plays important role in the generation of acoustic disturbances near the cavity

trailing edge. Based on the shear-layer growth rate, three different regions were identified in the supersonic turbulent cavity flows. In the laminar cavity flow, the identification was different since a transition procedure from laminar inflow to turbulence appears near the leading edge. More severe shear-layer motions were found in the laminar cavity flow.

Higher-order spectral technique [50] is implemented to ascertain the multiple tones in the cavity which are due to nonlinear interactions between the primary cavity modes (Rossiter modes). The spectra of the cavity with L/D ratio 2 show distinct peaks due to nonlinear interactions while cavity with L/D ratio 3 does not exhibit observable peaks. The spectra of both the cavities show presence of low-frequency peaks of significant amplitudes.

A mixed shear layer/wake mode in supersonic cavity flow was numerically captured [51]; it shows that the shear layer mode is driven by the vortex convection – acoustic feedback mechanism while the wake mode is probably induced by absolute instability. In particular, the results indicate that the feedback-acoustic-wave in the shear-layer mode is probably generated (from the aft wall) by the reflection of the downstream traveling pressure wave associated with the shed vortex in the shear layer

Schmit et al [52] show that from the shear-layer vortices, the flow physics inside the cavity is non-linear. It is explained that the formation of large-scale vortices in the shear layer is non-periodic in nature and the shear-layer convection velocity is determined to be $0.9U_\infty$ which is significantly higher than Rossiter's equation value. The

low frequency pumping action inside the cavity controls the broadband pressure on the aft wall by controlling the vertical motion of the vortices as they traverse downstream. This pumping action may be exploited to develop a new control method and force the developing vortices to be lifted above the cavity possibly reducing the broadband noise and (even possibly) the acoustic tones. The numerous acoustic waves inside the cavity at any given time, especially when the cavity has multiple cavity tones, are created from the free stream fluid entrained between the vortices in the shear layer. Because numerous acoustic waves are traversing back and forth inside the cavity, a significantly higher number of cavity tones are observed in the frequency spectrum, indicating that a non-linear acoustic model is needed.

Nair et al [53] numerically simulated subsonic as well as supersonic flow past cavity using LES. The results indicate the aerodynamic instability leading to rollup of shear layer and vortex impingement, giving rise to changes in velocity and pressure field, is the cause of self-sustained oscillation for subsonic cavity flow where the validity of acoustic waves is questionable. However, supersonic flow over the cavity shows very complex features with appearance of traveling lambda-shock and compression waves, which interact with the shear layer forming large-scale eddies which in turn generate Mach waves. This elucidates that the reflection of the Mach wave from the bottom corner of the aft wall creates the feedback acoustic wave within the cavity. Hence, the mutual interactions of this feedback acoustic wave with shear layer and the compression wave result in its flapping and self-sustained oscillation. Further, the acoustic wave's feedback is related to reflection of the Mach waves, rather than by

vortex impingement on the aft wall for the supersonic flow. Vortex dynamics illustrates that the amplitude of pressure oscillation becomes maximum as the large-scale vortex interacts with the aft wall, and there is no time lag between generation of pressure waves and vortex impingement for the subsonic flow. Thus, the vortex impingement at the aft wall is the cause of pressure waves, resulting in a convection current that in turn excites the shear layer attributing to self-sustained oscillation. But there exists a considerable time lag between pressure amplification and vortex impingement, illustrating that vortex impingement is not the primary cause of self-sustained oscillation for the supersonic flow.

A digital streak schlieren technique [54] is used to investigate cavity flow characteristics from unprocessed visualization records. Although the application of this method makes it possible to capture most of the modes and to quantify the associated flow phenomena, one cannot quantify the amplitude of pressure fluctuations or detect features that do not generate a large-enough signal on the original visualization records. The propagation of waves inside the cavity leads to flow oscillation at certain frequencies which were obtained through the high speed schlieren video. The results from these measurements showed excellent agreement with independently conducted pressure measurements, simulations and analytical predictions. The technique also provides a measurement of the convective flow velocity within the cavity.

Experiments on a shallow open cavity at Mach 2 showed that the basic flow features are consistent with moderately shallow cavity experiments [55]. The

experiments reveled good correlation of tonal frequencies with those calculated from the well-known Rossiter formula. A new relation valid for shallow cavity flow at supersonic Mach numbers has been suggested based on the low speed relation. Its comparison with the experimental data and the Rossiter relation is found to be reasonable especially for higher mode frequencies.

Settles, et al [56] carried out experimental studies at Mach 2.92, in which a two dimensional turbulent shear layer reattachment takes place on a cavity trailing edge, which is inclined. Measured turbulent fluctuation levels reach a maximum of 40-50 % in the compression region near flow reattachment, then fall off rapidly in the redeveloping boundary layer downstream. The delayed detached eddy simulation was carried out by Timothy, et al [57] for two dimensional cavity with inclined trailing edge at Mach 2.9. It was found that the fluctuation magnitude differ by a factor of two with respect to experimental data and the pressure fluctuation spectral shape is captured well.

Wei Huang, et al [58] has made excellent survey on mode transition in combined cycle propulsion system. The ramjet to scramjet transition occurs during ascent phase of a hypersonic vehicle. In the ram mode, a normal shock wave train is generated due to the thermally chocked downstream boundary condition. Ramjet to scramjet mode transition can be obtained by varying the fuel Equivalence Ratio (ER),the wall heating temperature and the combustor configuration, namely the operational and structural parameters. The inflow variation has a great impact on the ramjet-scramjet mode

transition and it makes a great difference to the variation of ER. This area may be further explored.

Mode transition process in a typical strut based scramjet combustor based on a parametric study has been brought out [59]. The cavity adapted in this study would prevent the pre-combustion shock waves from pushing out of the isolator and help to stabilize the flow field. In this study, the cavity has been shown to reduce the transition time from scram mode to the ram mode. Wei Huang, et al [60] brought out the operational conditions and the geometric parameters effect on flame propagation and stabilization in a dual mode scramjet combustor. The mode transition process is very crucial for the design of the Dual Mode Scramjet combustor and it should be taken in to consideration seriously for the design of hypersonic plane.

Xi-Peng Li, et al [61] mentioned that the boundary layer separation and upstream movement of the pre-combustion shock train is responsible for the contra-flow flame propagation process. Also unstable boundary layer cavity stabilized combustion was found during the flame transition process. This phenomenon results from the interaction between the cavity recirculation zones and the separation zone immediately upstream of the cavity, which was caused by the strong shock wave -boundary layer interaction, as the shock train is pushed upstream. Chenlin Zhang, et al [62] studied the effect of continuous Mach number variation of incoming flow on ram-scram transition in a Dual Mode combustor. Heiser and Pratt (Ref 63) brought out an analytical method for scramjet to ramjet transition process in which they considered a variable area scramjet.

Using the above analytical tool, they analysed the scramjet without shock, with oblique shock train and normal shock train.

2.3. Shear/mixing layer characteristics

In a typical cavity flow, shear layer is formed at its leading edge irrespective of free stream Mach number. The cavity flow physics is stable or unstable depending upon the shear layer fluctuation, reattachment location, etc. Generally, the cavity with unstable flow physics is used for mixing process whereas; a cavity with stable flow physics is best suited for flame holding concepts. In this regards, the free shear layer characteristics are summarized for high-speed flows.

Brown and Roshko [64] reported that the mixing is greatly affected by the density ratio. Their studies revealed that the effect is small in the case of incompressible shear layer as compared to supersonic shear layer. When a shear layer is formed between two supersonic streams, the compressibility causes less growth rate of shear layer/less spreading rate of the layer compared to incompressible flows. Hence, injection of fuel in the above scenario leads to less efficient mixing. This is because disturbances cannot propagate upstream in supersonic flow but are restricted to a narrow region downstream, and hence the growth rate is very slow.

Chinzei et al. [65] investigated the effect of free-stream Mach numbers on velocity ratio and the spreading rate of two-stream mixing layers. A large-scale vortical structure was believed to dominate the development of supersonic mixing layer, just as

in the case of the incompressible mixing layer. The spreading rate was correlated with velocity ratio of the free stream and Mach number based on the velocity difference across the streams (convective Mach number). They concluded that the compressibility effect for single stream mixing layers becomes significant for Mach number (M) above unity. For two stream layers, on the other hand, the compressibility effect cannot be represented by M alone but also by the velocity ratio.

An experimental study of reattaching compressible turbulent, free shear layer was conducted by Elliot and Saimmy [66]. Local similarity of the mean flow was observed through the shear layer, the reattachment, and the initial part of the redeveloping boundary layer. The mean flow and the turbulence field above the sonic line correlated with the local shear or the local boundary layer thickness. They found that the growth rate of the shear layer was 1.74 times lesser than that of incompressible shear layer. The turbulence intensities, shear stress, and turbulent triple product were significantly increased through reattachment as compared to the incompressible reattaching shear layers.

Papamoschou and Roshko [67] conducted experiments on mixing layers at different supersonic Mach numbers with different fluids and derived a correlation between incompressible and compressible mixing layers. This is given by

$$\frac{\delta}{\delta_0} = \left[0.8e^{-3M^2_c} + 0.2\right] \qquad (2.3)$$

Where, δ and δ_0 are the compressible and incompressible mixing layer thickness and M_c is the convective Mach number. It is given as

$$M_C = \frac{\sqrt{\rho_1}M_2 - \sqrt{\rho_2}M_1}{\sqrt{\rho_2} + \sqrt{\rho_1}} \qquad (2.4)$$

When M_c is above 1 (supersonic), the resulting growth rate of compressible mixing layer thickness is reduced by a factor of 4 to 5 as compared to the incompressible mixing layer.

Dimotakis [68] experimentally and analytically investigated mixing layers in incompressible flows and proposed a relation for the growth of mixing layer as,

$$\frac{\delta_0}{x} = \delta_0' = C_\delta \frac{(1-r)(1+\sqrt{S})}{1+r\sqrt{S}} \qquad (2.5)$$

Where C_δ is a constant and r is the velocity ratio and S is the density ratio. Based on the cumulative experimental evidence, it has been concluded that C_δ varies from 0.025 to 0.45. The wide range in the constant is related to the sensitivity of the turbulent mixing layer to initial profile and the nature of disturbance. Heat release due to combustion reduces the growth rate by about 15%. This is primarily due to the lowering of the density in the mixing zone, as a result of which the amount of fluid entrained in the mixing layer goes down by as much as 40%.

The computational work of Sekar and Mukunda [69] showed that at the temperatures prevailing in the combustors, the heat release did not affect the growth of the mixing layer. They pointed out that changes in enthalpy due to gas dynamics is more significant compared to that by chemical heat release and hence the mixing layer was not sensitive to the heat release.

An experimental study by Clemens and Mungal [70] on supersonic mixing layers showed that the structure of the supersonic mixing layer depends on the convective Mach number. In this study, the effect of convective Mach number on mixing layers was investigated and it was found that 3-D effects were significant for M_c = 0.79, whereas, at M_c = 0.28, the flow was essentially two dimensional.

Papamoschou [71] measured the speed of observable turbulent structures movement at high convective Mach numbers. It showed different convective Mach numbers for the two streams rather than a single value normally ascribed to the layer in the early studies. This has been attributed to the presence of shock waves in the shear layer. This was investigated further by Erdos et al. [72] in connection with their experimental studies of reacting mixing layers. The time variation of pressure node along the mean mixing layer was used to assess the speed of the structures. This calculation showed that at M_c~ 0.38, the speed was constant along the layer for its entire length. However, it varied by 30% between structures for high M_c case. In addition, the structure of the pressure variation was highly skewed. It is clear from these

studies that the notion of a unique convective speed is inconsistent with the physics of the flow.

The slow growth rate of the mixing layer in the case of compressible flows has led to considerable work on enhanced mixing schemes. Marble et al. [73] showed experimentally and computationally that a jet of low density in a stream of higher density gas flow can be mixed faster by impinging it with a weak shock. It was argued that by arranging the density and pressure gradients non-aligned to each other, streamwise vorticity can be generated which in turn cause the development of additional structures. Drummond et al. [74] has found that the process of break up initiated thus has been shown to be adequate to cause intense mixing and hasten the completion of the combustion process.

These fundamental studies on shear layers have brought out a very important fact that, when compared to the incompressible mixing layer the compressible shear layer spreads much more slowly. As mentioned earlier, a supersonic combustor demands a rapid mixing of the fuel and air owing to constraints on the combustor length. Hence it is essential to understand the mechanism of mixing under start transient conditions and under fully established conditions for various cavities.

2.4. Motivation and scope of the present study

The foregoing literature review shows that the fluid dynamic oscillations in the cavity are produced due to shear layer impingement at the cavity aft wall. The cavity

oscillations are produced due to the amplification of the vorticity fluctuations inside the shear layer, which is enhanced by the downstream edge of the cavity. The cavity oscillations are produced when the self-sustained oscillations inside the cavity are coupled to the resonant wave effects. These oscillations are produced when the ratio of characteristic length (length L or depth D of the cavity) to the acoustic wavelength (λa) is greater than unity. Depending on the cavity dimensions, the acoustic oscillations inside the cavity could be longitudinal or transverse. If L/D ratio is greater than unity, the oscillations are longitudinal and the cavity is termed as a shallow cavity and for L/D ratio less than unity, the oscillations are transverse in direction and such cavities are termed as deep cavities.

Owing to the increasing demand of space transportation, either low cost access to the space or passenger vehicles for long-range operation or faster inter-continental travel, supersonic combustion ramjet engine (scramjet) is a viable option. However, design of a scramjet engine for long duration operation is a highly challenging task due to the complex flow physics involving shock waves-boundary layer interaction, poor mixing characteristics of high speed flows with fuel, flame holding, combustion instability, etc. Hence, the flow physics of such propulsion system need to be understood. Cavities have been proposed as one of the candidates for mixing enhancement and flame holding in scramjet engines. They are preferred over other options such as ramps, struts, pylons because of the inherent advantage of lower drag. Though lot of studies (both experimental and numerical) has been reported in literature on the cavity flows, still the complete flow physics of cavities has not been fully

understood especially the unsteady flow oscillations and their effects on mixing phenomenon, flame holding, etc. In this context, the flow feature of the combustion chamber with a rectangular cavity is a good option. Since, the use of cavity as a mixing and flame holding device can certainly reduce the drag and in turn help in producing positive thrust as compared to other devices such as strut, pylon, ramps etc.

In Dual Mode ramjet scramjet combustion engine (combined propulsion system), mode transition takes place. When the engine undergoes transition from Ramjet to Scram jet or vice versa, the inflow variation has a great impact on the ramjet scramjet mode transition and it makes a great difference to the variation of the Equivalence Ratio. Hence this information has to be explored further. In transient starting/stopping, there exists shock train, which interacts with the cavity shear layer. This may alter the shear layer characteristics and the impinging pattern at cavity aft wall. Though this kind of phenomena prevails for short duration, its effect has to be quantified in the design phase. Internationally to cover wide range of Mach number, the ramjet and scramjet combination is being pursued as a viable propulsion option. The ramjet and scramjet are independently studied. While in combination, it has to undergo transition from ramjet to scramjet or scramjet to ramjet at different phases of the mission.

Investigations under fully established flow condition are carried out to find answer for the following: whether the shear layer vortex dynamics linearity assumption valid for entire range of cavities, whether the modified Rossiter relation valid for the transitional cavities .In order to have continuity in thrust and positive acceleration, the transition has a vital role to play. This transition characteristic has not been explored enough. Hence,

it is essential to analyze and understands the start transients' characteristics and the established flow characteristics for the same configuration under same flow conditions. Hence an attempt is made to study the flow field for various types of cavities. In this attempt more of unsteady characteristics are focused which is important from the mixing point of view.

With these broad aims the specific objective of the present work are listed below: Fundamental studies of shallow rectangular cavities of various dimensions (L/D) for its ability to adopt in a scramjet combustor by

- Its starting transient characteristics
  - Flow features through high speed shadowgraph images
  - Unsteady pressure measurements
- Its fully established condition
  - Flow features inside and outside the cavity through time resolved schlieren images
  - Shear layer dynamics through time resolved schlieren images
  - Unsteady pressure measurements

The complete flow physics is obtained through various data processing techniques:

- Fast Fourier Transform
- Optical technique
- Cross correlation
- Coherence
- Spectrogram
- Wavelet transform

CHAPTER 3

FACILITY AND EXPERIMENTAL DETAILS

The start transient characteristics are in the cavity flows need extensive investigation. Hence, this study is carried out for Deep cavity, Shallow open cavities, Closed cavities and their transition cavity ranges. For various cavities, the unsteady pressures on different faces of the cavities are measured and the overall flow field is obtained from shadow graph and high speed schlieren videos.

3.1. Cavity model details

The schematic of a typical cavity is shown in Fig. 3.1 and various cavities dimensions are given in Table 3.1. The test section is provided with a cavity block (Fig.3.2) to accommodate various cavity geometries both length (L) and depth (D) using suitable inserts. Experiments are carried out for different cavity configurations which are categorized into three types namely;

(a) Transitional cavities L/D = 1, 2 and 3

(b) Shallow open cavities L/D = 4 and 5

(c) Transitional cavities from open to closed L/D = 6, 7.5 and 10.

Table 3. 1 Cavity details

Sl. No.	L(mm)	D(mm)	L/D
Transitional cavity from deep to shallow			
1	6	6	1
2	12	6	2
3	18	6	3
Rectangular shallow open cavity			
4	24	6	4
5	30	6	5
Transition from shallow open to closed cavity			
6	30	5	6
7	30	4	7.5
8	30	3	10

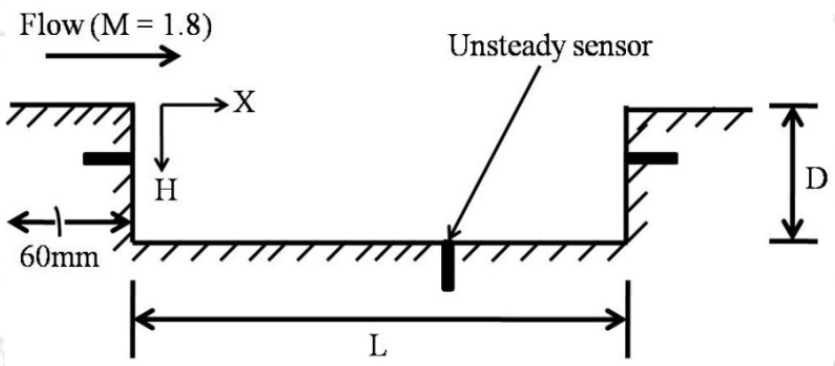

Fig. 3.1: Typical cavity details (dimensions in mm)

In all cases, three unsteady pressure ports are provided along the center line of the cavity. These unsteady pressure ports are located at a distance 2mm below the leading edge and trailing edge while, the third port is located on cavity floor (bottom wall) at L/X = 1.5 where X is the starting point of cavity leading edge. In all the cases, the cavity is located at a distance 60 mm from the test section inlet (shown in Fig 3.1).

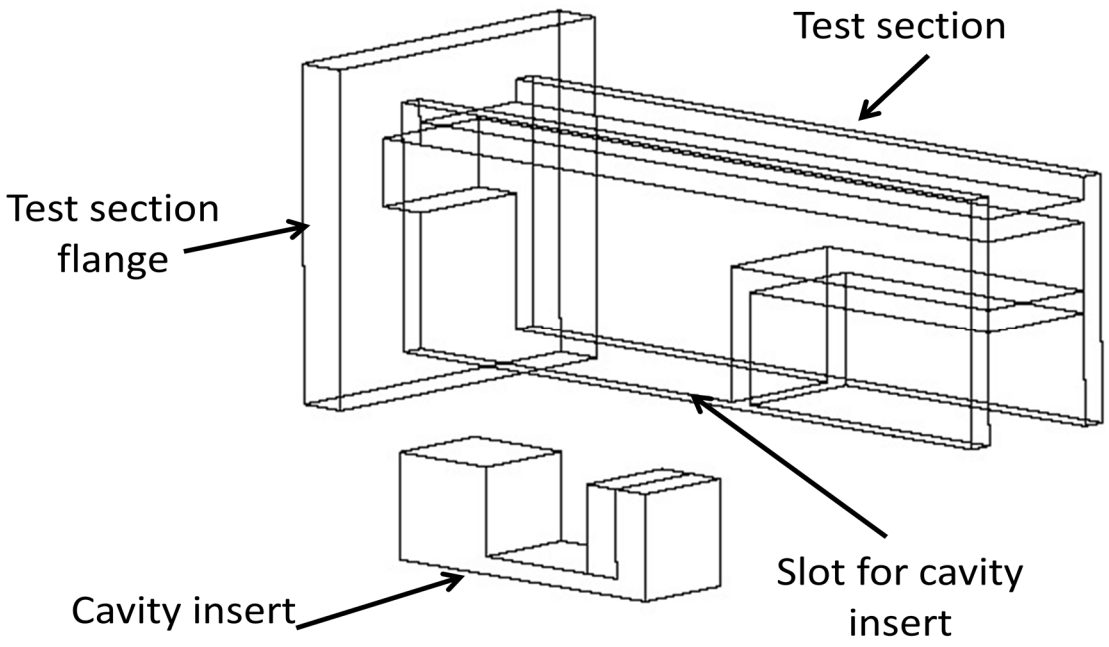

Fig. 3.2: Test section with cavity block and inserts

3.2. Experimental Facility

The experiments are carried out at Open Jet Facility (OJF), Vikram Sarabhai Space Centre, Thiruvananthapuram. The OJF (Fig. 3.3) consists of air supply system, pressure regulating system, settling chamber, CD nozzle, model, instrumentation system and optical system. A two stage, two cylinder double acting compressor is used to charge the reservoirs (2 nos) of 27cubic meter capacity. The compressed air is passed through (before the reservoirs) a desiccant based drier unit, desiccant unit, air filters and charcoal filters in order to remove the moisture, oil content and carbon content. The reservoir maximum storage pressure is 40 bar. From the reservoir, the moisture free air is supplied through 200 mm diameter pipeline to the Open Jet Facility.

The pressure is regulated through a pressure regulation system .Pressure monitoring gauges are mounted in the facility.

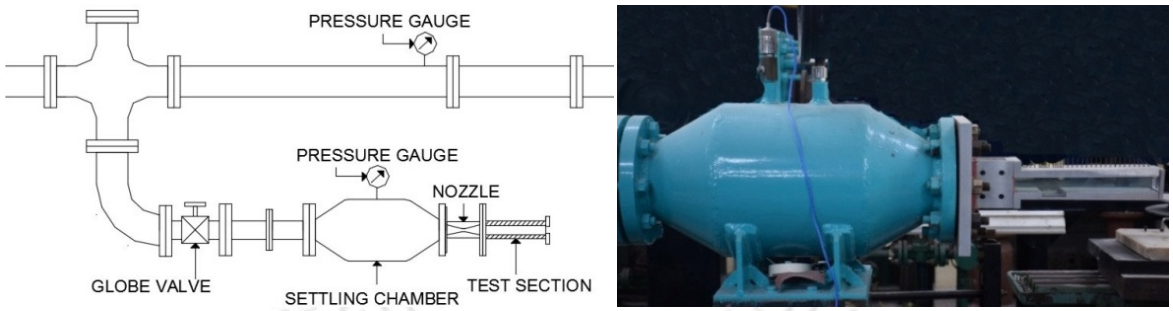

Fig. 3. 3 Experimental facility

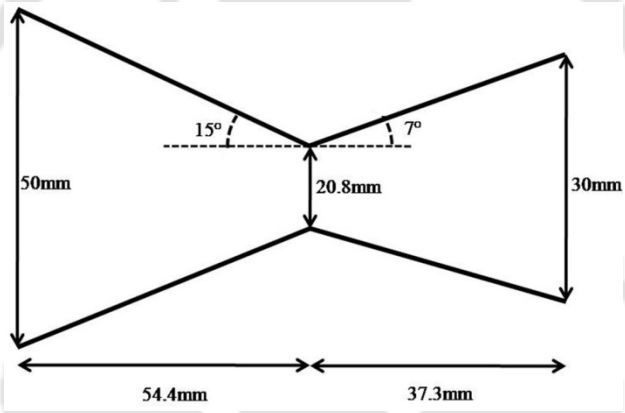

Fig. 3. 4: Convergent-Divergent nozzle details

A convergent-divergent (C-D) nozzle is connected to the settling chamber through a suitable flange. The C-D nozzle as shown in Fig. 3.4 is of rectangular cross section made of Aluminum on top and bottom sides of convergent and divergent parts with sidewalls being parallel. The convergent and divergent lengths of the nozzle are 54.4 mm and 37.3 mm, respectively, the convergent and the divergent angles of the nozzle are 15° and 7° respectively. Throat and exit height of the nozzle are 20.8 mm and 30 mm, respectively. The nozzle exits into a rectangular (30 mm height and 60 mm width)300 mm long test section made of Aluminum alloy (AA7075). The nozzle exit

Mach number is 1.8 and mass flow rate is 1.46 kg/s. An absolute pressure transducer (20 bar) is used to measure the settling chamber pressure and a Bourdon dial gauge is used to monitor the settling chamber pressure. For calibrating the nozzle exit flow, total pressure (P_{02}) is measured across the exit of the nozzle using 1bar differential pressure transducer. The operating pressure (P_{01}) is maintained at 5 bar absolute.

Where,

P_{02} – pitot pressure

P_{01} – Settling chamber pressure

Mach number is calculated using P_{02} and P_{01} relationship (3.1). It is observed that the distribution is fairly uniform. Average Mach number is 1.8 with ±0.03 variations.

$$\frac{P_{02}}{P_{01}} = \left[1 + \frac{2\gamma}{\gamma+1}\left(M^2 - 1\right)\right]^{-1/(\gamma-1)} \left[\frac{(\gamma+1)M^2}{(\gamma-1)M^2 + 2}\right]^{\gamma/(\gamma-1)} \tag{3.1}$$

Measurement error in Mach number is obtained by using method of propagation of error [75] given by the following relation

$$\frac{dM}{M} = \frac{-(\gamma-1)\left[M^2 + 2/(\gamma-1)\right]\left[2\gamma M^2 - (\gamma-1)\right]}{4\gamma(M^2-1)^2}\left(\frac{dP_{01}}{P_{01}} - \frac{dP_{02}}{P_{02}}\right) \tag{3.2}$$

Using chain calibration, uncertainty of P_{01} and P_{02} sensors are found to be 0.5% and 0.1% of full scale respectively. Substituting these in equation, the measurement uncertainty in Mach number estimated is± 0.015.

3.3. Test conditions

The test conditions are presented in Table 3.2. The approaching free stream conditions of the cavity are calculated based on isentropic relation and boundary layer thickness (δ) is estimated from Crocco relation [76] as given by.

$$\frac{\delta}{L} = \frac{0.037}{(R_e)^{1/5}} \frac{C_{fm}}{C_{fi}} \frac{1}{(\delta^{**}/\delta)} \tag{3.3}$$

Where δ^{**}/δ = 0.801 is based on 1/7th power velocity distributed and the compressibility correction ($\frac{C_{fm}}{C_{fi}}$) = 0.84.

Table3.2: Experimental test conditions & their uncertainties

Parameter	Value
Stagnation pressure, P_0 (bar)	5.4 ±0.2
Stagnation temperature, T_0 (K)	300 ± 3
Freestream/ambient pressure, P_∞ (bar)	0.94±0.08
Free stream/ambient temperature, T_∞ (K)	182±2
Freestream velocity, V_∞ (m/s)	487±9
Mach number, M	1.8 ± 0.035
Reynolds number, R_e /m	(7.38±0.07)x10^7
Boundary layer thickness, δ (mm)	1.04±0.01

3.4. Flow visualization techniques used

(a) Schlieren technique

Conventional Z-type schlieren flow visualization technique is used to capture the starting characteristics and flow features around the cavity. The schlieren system consists of a 250 Watts light source (Halogen lamp) and two 150mm paraboloidal mirror with a focal length of 1.5 m. In order to fold the beams, two flat fold mirrors of 100 mm diameter is used. A vertical knife-edge cutting is done to capture the shock structure in the flow field. The schlieren set-up is shown in Fig.3.5. The light from the source is focused on a slit using a condenser lens to generate a point source. This slit is placed at the focus of the paraboloidal mirror on one side of the test section. Once the light rays fall on the paraboloidal mirror, a collimated beam is generated which passes through the test section. The collimated beam after passing through the test section is captured by the second spherical mirror on the other side of the test section. A knife-edge placed at the focus of the second parabiloidal mirror blocks 30% of the image and the shadow

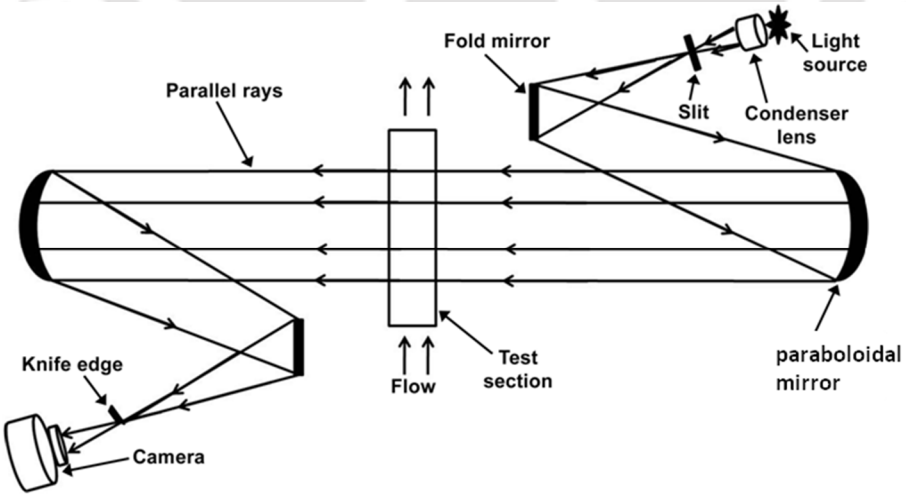

Fig. 3. 5: Schematic of schlieren set-up

images is viewed on a camera (Photron Fastcam SA 1.1, frame rate of 125000 fps) placed outside the focus. The density variations associated with the flow lead to change in the refractive index of the medium. Thus, the collimated beam passing through the test section experiences different refractive indices at different regions and refracted in different directions. Some of the deviated beam blocked by the knife-edge produces dark regions in the image and other portions of the beam deviated away from the knife-edge produces bright portions in the image. Depending on the vertical knife-edge cutting (right or left), the shock waves or the expansion fans appear to be dark or white.

(b) Shadowgraph Technique

Shadowgraph optical system is similar to schlieren optical system. In place of knife edge in the schlieren system, the image is directly focused and captured through camera (in shadowgraph technique). Shadowgraph is sensitive to the changes of the density second derivative (whereas schlieren gives the changes of density first derivative). In this study, shadowgraph technique is used to capture the shear layer during start transient process.

3.5. Instrumentation and Data Acquisition

An absolute pressure sensor (20 bar) with a sampling rate 1 kHz measures stagnation pressure (P_0) in the settling chamber. The cavity is instrumented with three unsteady pressure sensors of Kulite make (model XCS-062-15D) of 1.6mm diameter and pressure range of 15 psid located along the center line of the cavity (Fig. 3.1). The natural frequency of the sensors is 200 kHz with an input impedance of 1KΩ. The hysteresis and the non-linearity of the sensors is ± 0.5%. For high-speed cavity flows,

measurement of unsteady pressures using such sensors is well-established [76-78]. These transducers are flush-mounted with wall. The transducers are connected to a power supply unit through coaxial cable and are interfaced with computer through an Analog to Digital (A/D) converter card of 12 bit resolution. The schematic diagram of unsteady pressure measurement unit connected to a data acquisition system (Preston Make) is shown in Fig. 3.6.

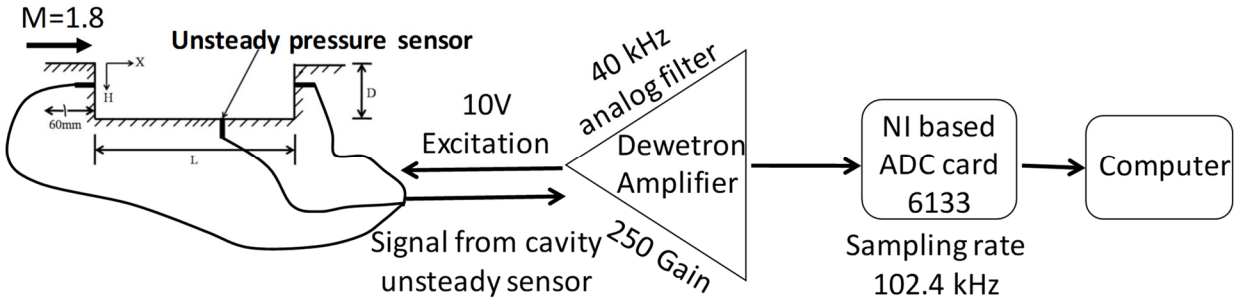

Fig. 3.6: Schematic of unsteady pressure measurements

Simultaneous sampling (102.4 kHz) of the signals from all the sensors are done for 4s (409600 samples). The unsteady pressure signals are divided into 200 segments (2048 points/segment) to obtain pressure spectra. In order to get a reliable value of the pressure spectra, averaging is done using hamming window (50% overlapping). A cut-off frequency of 40 kHz is used to avoid aliasing effect. A 50Hz resolution in the frequency on each segment is obtained after performing Fast Fourier Transformation (FFT). Continuous wavelet transform is performed to analyze the non-stationery, non-linear and intermittent signal. The non-stationary data statistics are time variant that can be further categorized depending upon the specific type of non-stationary properties viz. intermittent, non-linear, etc. When the non-stationary data is processed using wavelet, it

is found that the signal is intermittent, because the frequency at which certain event occurs is not repeating with respect to time. Because the signal is non-stationary and intermittent, the energy with respect to time is non-linear. Based on five repeat tests under identical test conditions, uncertainty in the dominant frequencies are derived as, ± 130 Hz.

3.6. Data reduction

Fast Fourier Transformation is used to derive spectrogram and Power Spectral Density (PSD) from unsteady pressure signals. Spectrogram gives the dominant frequency components, their powers and mode switching with respect to time [77, 80-81]. In addition to the above, the total acoustic energy levels produced by the cavity are studied through Overall Sound Pressure Level (OASPL) and its relation is given below.

$$OASPL = 20log_{10}\frac{P'_{rms}}{P_{ref}} \quad (3.4)$$

Where, P'_{rms} is the root mean square of the pressure fluctuation and P_{ref} of 20μPais used (which is the minimum audible sound pressure level).

In order to establish a similarity between two signals (x, y) in frequency domain, coherence coefficient (C_{xy}) is derived from following relation [82-83].

$$C_{xy} = \frac{|G_{xy}|^2}{G_{xx}G_{yy}} \quad (3.5)$$

An optimum linear least square function is used to estimate the coherence that gives the extent to which output y(t) is predicted from input x(t). The coherence

coefficient is one for an ideal system where single input x (t) and single output y (t) is sufficient to define the dynamics of the system. Thus, Cauchy–Schwarz inequality is used which gives a value of C_{xy}≤ 1 and satisfy 0 ≤C_{xy}≤ 1.The coherence coefficient C_{xy} close to 1 implies that the common source is responsible for both the signals. In case if the coherence coefficient C_{xy} is close to zero, it implies that the signals x (t) and y (t) are not related.

From the unsteady pressure measurements, wavelet transformation is also carried out to bring out the localized fluctuations of power within the specified time. Wavelet analysis is a comprehensive method to understand localized fluctuations of power within a time series that lies in a convolution operation between the signal and a wavelet function. By decomposing a time-series into time-frequency space, both the dominant mode of a given signal and its time variance can be determined. Unlike the conventional Fourier transformation (inability to extricate the temporal features of the signals) and modified Short-time Fourier transform (fixed time and frequency resolution), continuous wavelet transform analyzes the non-stationery, non-linear and intermittent signal with temporal-spectral information and multi-resolution concept. Multi resolution is particularly useful while analyzing signals, which contain frequencies of interest ranging from very low to high. The wavelet transform uses the basic wavelet functions, known as mother wavelets, that can dilate/compress and translate based on two parameters namely frequency and time shift, to apply short windows at high frequency and long windows at low frequency. Wavelet transform is classified as continuous wavelets transform or discrete wavelets transform depending on the way it is

discretized. Continuous wavelet transform is being used in high-speed turbulent flows [84-85] to understand the temporal-spectral information of unsteady pressure inside the cavity. In the present study, a continuous wavelet transform is used which is defined as,

$$W(\tau, a) = \int_{-\infty}^{+\infty} x(t)\varphi_{a,\tau}^{*}(t)dt \tag{3.6}$$

The mother wavelet is defined as,

$$\varphi(t) = \exp\left(i\omega_{\psi}t\right)\exp(-|t|^2/2) \tag{3.7}$$

In the present study, Morlet wavelet is used as the wavelet function. The translated and scaled version of mother wavelet is defined as,

$$\varphi_{a,\tau}^{*} = a^{-1/2}\varphi\left(\frac{t-\tau}{a}\right) \tag{3.8}$$

The factor $a^{-1/2}$assures the same energy in all the scaled versions of the mother wavelet. In a frequency domain, the wavelet transform at a specific scale acts as a band-pass filter. In the present study, continuous wavelet transform from the digitized time series data [86] is obtained to understand whether the spectral details are importunate during entire time or show any variations.

CHAPTER 4

RESULTS AND DISCUSSIONS

ONSET OF TRANSIENT SHOCK INTERACTION WITH CAVITY SHEAR LAYER AND THEIR CHARACTERISTICS

4.1 Introduction

In numerous practical applications whether internal or external flows, shock waves (normal/oblique) appear in the flow field. When these waves interact with the shear/boundary layer, they produce complex flow structures that significantly affect the entire flow field particularly very strong interaction leads to flow separation. This interaction frequently occurs in various fluid dynamic problems such as flow over the aerofoil, supersonic wind tunnel test section as well as diffuser, pipe flow, duct flow, air intake, isolator, combustion chamber etc. The factors that mainly affect the interaction are the boundary layer (laminar/turbulent), Mach number (M), passage geometry and pressure conditions.

The pioneering experiments [87-88] in a constant area duct show that an ideal normal shock in the absence of a boundary layer is never achieved. Shock compression [89] in a duct shows curved/oblique shock that generates a regular or Mach reflections due to boundary layer interaction. Also, in a constant area duct, series of bifurcated shock system [87, 90] is observed due to shock wave boundary layer interaction. As reported in literature [90-94], the interaction between normal shock and turbulent boundary layer in a constant area duct produces flow structure [95] of different

categories depending upon Mach number. When the Mach number upstream of the normal shock is $1 \leq M \leq 1.2$, a weak interaction occurs where the normal shock is appeared to be upright and may be considered as an inviscid normal shock. If $1.2 \leq M \leq 1.3$, the normal shock continuously changes its shape and become concave due to fair interaction with boundary layer where the boundary layer separation may or may not happen. Further increase in the Mach number ($1.3 \leq M \leq 1.5$), a bifurcated shock system is formed due to large boundary layer separation. For $M > 1.5$, number of shocks (shock train) appears downstream of the bifurcated shock system.

In a typical Scramjet engine, a constant/divergent duct is used as a combustion chamber where fuel-air mixing, flame holding and sustained combustion occurs. Since the resident time of the flow in the duct is very small owing to supersonic nature of the flow, effective devices are required to achieve rapid fuel-air mixing, efficient flame holding capability and sustained combustion. These devices are either active (struts, pylon, etc.) or passive (cavity) and alter the shape of the combustor as compared to a simple duct. These devices generate shock/expansion waves and interact with the boundary layer to produce complex flow features. Among these devices, cavity is a potential candidate due to reduced drag (positive thrust) and excellent flame holding capability.

Generally, the cavity flow is unsteady due to shear layer that produces modes/tones at some dominant frequencies upon impinging at cavity aft wall. Also, a mode/tone switching phenomena is observed in some cavities at certain conditions.

Hence, the structure experiences vibration that has to be accounted properly in the design phase. In addition to the above phenomenon, during starting of the engine, depending on the pressure differences and passage shape, there exists a flow that contains propagation of the transient shock. This transient shock after interacting with the cavity shear layer can alter the size and growth of the shear layer. The transition from scramjet to ramjet or vice versa in dual mode combustion encounters the starting transient, which in turn changes the incoming flow to the combustion chamber. During this kind of transition, the cavity plays crucial role in the performance of the engine. In fact the cavity reduces the transition time from one mode to another mode of combustion. This particular area is not explored extensively.

Some of the flow phenomena during the starting process that are not fully understood are; (a) how is the transient shock system during starting process ? (b) How does the transient shock affect the cavity shear layer? (c) Once the cavity shear layer impinges at aft wall, is there any modes/tones experienced by the cavity during transient process? (d) Are these modes/tones can happen at the same frequencies (global instability) irrespective of different pressures during starting process at different locations inside the cavity? (e) Are there any mode/tone switching phenomena at different pressures during starting process? (e) How significant the OASPL inside the cavity during transient process? The present investigation is aimed to address the above questions, which are not reported in the literature. The interaction of transient shock system with cavity shear layer is captured through high-speed shadowgraph images while the cavity response is measured by unsteady pressure sensors.

4.2 Results and discussions

The present studies focused on to bring out the flow features during transient starting process of the cavity flow through time resolved shadowgraph images. A series of tests are carried out on cavity configurations to bring out the transient starting process. Transient starting characteristics of the flow with cavity are presented in this section where the flow is from left to right. Time resolved shadowgraph images with an exposure time of 10 μs are obtained using a high speed camera (Photron Fastcam SA 1.1) at a frame rate of 250 fps with a resolution of 250×580 pixels. A 250W Tungsten-Halogen lamp is used as light source for obtaining shadowgraph pictures. The stagnation pressure (P_0) in the settling chamber is measured by a 5bar (Gauge - GP50 make) and a 20 bar (Absolute - LPSC make) pressure sensors with a sampling rate of 1 kHz. The 5 bar sensor is synchronized with the camera and an external trigger was given to obtain pressure-time stamping data for transient starting characteristics.

4.2.1. Transient starting shocks associated flow features and unsteadiness

4.2.1.1. *Case-I Flow features of transitional cavities (1 ≤ L/D ≤ 3)*

4.2.1.1a *L/D = 1*

Figure 4.1 shows the flow features of the L/D = 1 cavity. The flow features are quite similar to that of without cavity case. The main flow features are bifurcated shock system consisting of normal shock (point 1), leading shock (point 2), trailing shock (point 3), boundary layer separation (point 4) and the normal shock train behind the bifurcated shock system. As the pressure is increased further, the boundary layer gets separated.

The boundary layer separation is symmetry both at top as well as the bottom wall up to P_{01}/P_0 = 0.41 and 0.46 (Figs. 4.1a and 4.1b).

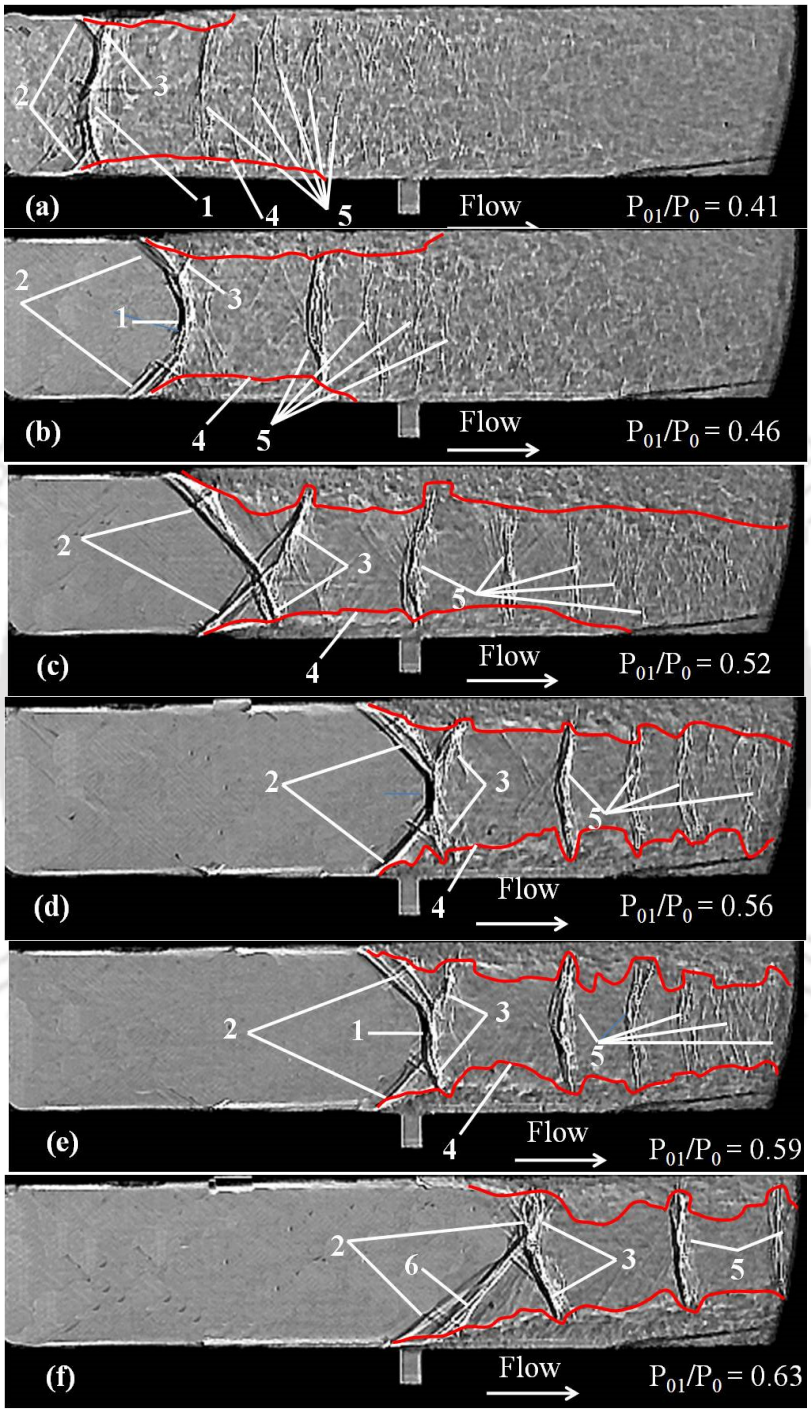

Fig. 4.1: Sequential images of transient starting shocks in a confined duct (L/D = 1)

The boundary layer separation becomes asymmetric for P_{01}/P_0 greater than 0.52 (Fig.4.1c to 4.1f). At P_{01}/P_0 = 0.52 (Fig.4.1c), the flow experiences the presence of the cavity. As the flow passes over the cavity, there exists a favorable pressure gradient due to area increase, and hence the flow accelerates. Though the separation/leading shock (point 2) of the bifurcated shock system produces adverse pressure gradient, its effect is reduced due to cavity. Since the cavity is much downstream of the bifurcated shock system, sufficient distance is available to accelerate the boundary layer flow. Thus to make the pressure to equalize with the ambient, the bifurcated shock system becomes asymmetry. In this case, the bifurcation is large on top wall as compared to bottom wall. It activates early boundary layer separation on top wall against the bottom wall. This trend is seen up to P_{01}/P_0 = 0.59 (Fig.4.1d and 4.1e). However, the difference in boundary layer separation for both top and bottom wall decreases from P_{01}/P_0 = 0.52 to 0.59. This is due to the fact that the expansion produced by the cavity is suppressed by the separation shock (point 2) standing just upstream of the cavity. At P_{01}/P_0 = 0.63 (Fig.4.1f), the cavity trailing edge shock (point 6) is formed and is merged with the leading shock (point 2) of the bifurcated shock system. It may be noticed that the presence of the cavity is felt on the boundary layer at P_{01}/P_0 = 0.63 where the boundary layer separation is seen right at the leading edge of the cavity whereas, on the top wall, the separation is delayed. The fact is that the flow over the cavity produces expansion due to sudden area change and generates shear layer.

4.2.1.1b **L/D = 2**

The flow features over L/D = 2 cavity presented in Fig. 4.2 indicate that the bifurcated shock system, its associated shock train as well as the characteristics of the boundary layer both on top and bottom sides are very similar to the earlier case (L/D = 1). However, the boundary layer separation on bottom occurs early as compared to the earlier case (L/D = 1) because length of the cavity is increased. In this case, at P_{01}/P_0 = 0.52 (Fig.4.2c) onwards the transient starting shock interacts with the cavity shear layer.

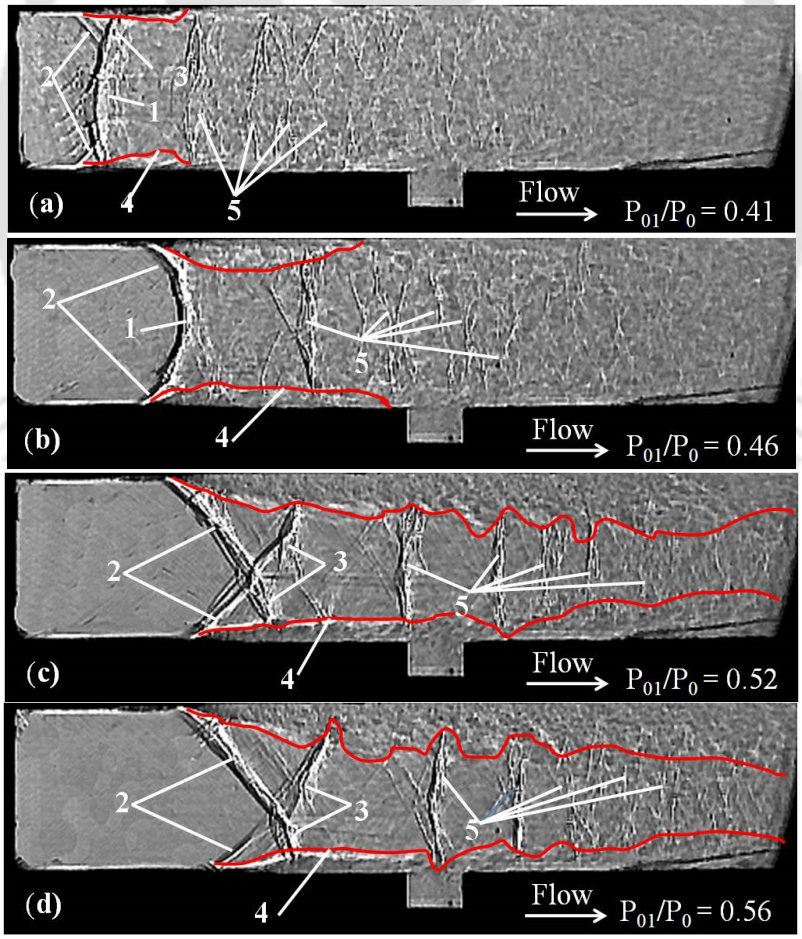

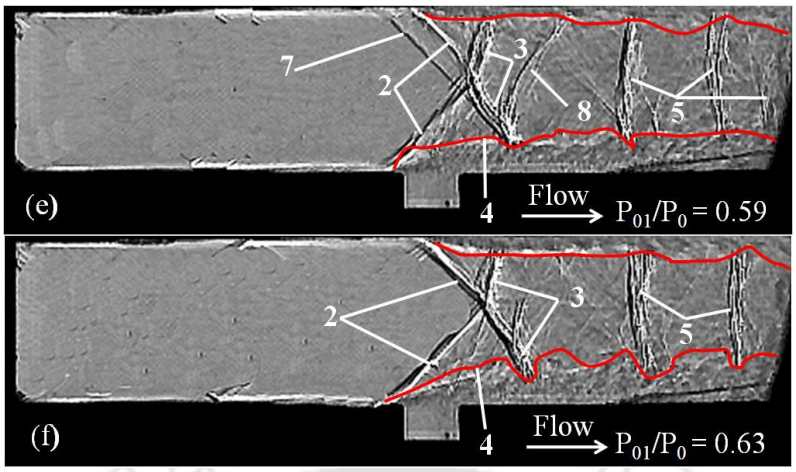

Fig. 4.2: Sequential images of transient starting shocks over L/D = 2 cavity

At this pressure, the first shock in the shock train stands at the leading edge of the cavity thereby produces fluctuations inside the cavity may lead to modes/tones. Further increase in pressure to $P_{01}/P_0 = 0.56$ (Fig.4.2d) the first shock in the shock train is at the middle of the cavity and interacts with cavity shear layer cause the fluid structure to experience the unsteadiness. Once the pressure is increased to $P_{01}/P_0 = 0.59$ (Fig.4.2e), the first shock in the shock train moves downstream of the cavity while the bifurcated shock system stands at the cavity front wall. This produces large shear layer separation over the cavity and part of it impinges at cavity aft wall, which in turn produces unsteadiness. The trailing shock of the bifurcated shock system is not strong enough to impinge at the shear layer and hence, a Mach reflection and its associated oblique shock (point 8) are seen. The same phenomena is observed at $P_{01}/P_0 = 0.63$ where, increased size of the shear layer over the cavity is witnessed. Since, partial impingement of the shear layer at cavity aft wall is observed for the pressures between $0.56 \leq P_{01}/P_0 \leq 0.63$; unsteady pressure measurements are carried out inside the cavity for these pressures. It will help to find out whether the transient starting phenomena

causes the cavity to experience modes/tones at discrete frequencies and is there any mode switching phenomena takes place or not.

The pressure spectra corresponds to various pressures $0.52 \leq P_{01}/P_0 \leq 0.63$ inside the cavity at three locations namely front, bottom and aft walls during starting process are presented in Figs.4.3 to 4.6. At $P_{01}/P_0 = 0.52$ (Fig.4.3), the front wall pressure spectrum shows broad band noise along with two peaks at 19.1 and 38.5 kHz. The bottom and aft walls show number of small amplitude modes/tones, which corresponds to the shadowgraph, image (Fig.4.2c). The image shows a normal shock of the shock train behind the bifurcated shock system, which is located at the cavity leading edge. Once this shock interacts with the cavity shear layer, a hump is seen downstream of the interaction point. Hence, the shear layer partially impinges at cavity aft wall which contains small scale eddies. This is reflected in the cavity aft wall pressure spectrum, which consists of small amplitude modes/tones at different frequencies ranging from 4.5 kHz to 17.5 kHz while a dominant mode/tone occur at 38.5 kHz. Similarly, at bottom wall, small amplitude modes/tones are seen at same frequencies, which are an indicative of nonexistence of mode/tone switching phenomena. However, initial portion of the spectra contains fluctuation due to small scale eddies.

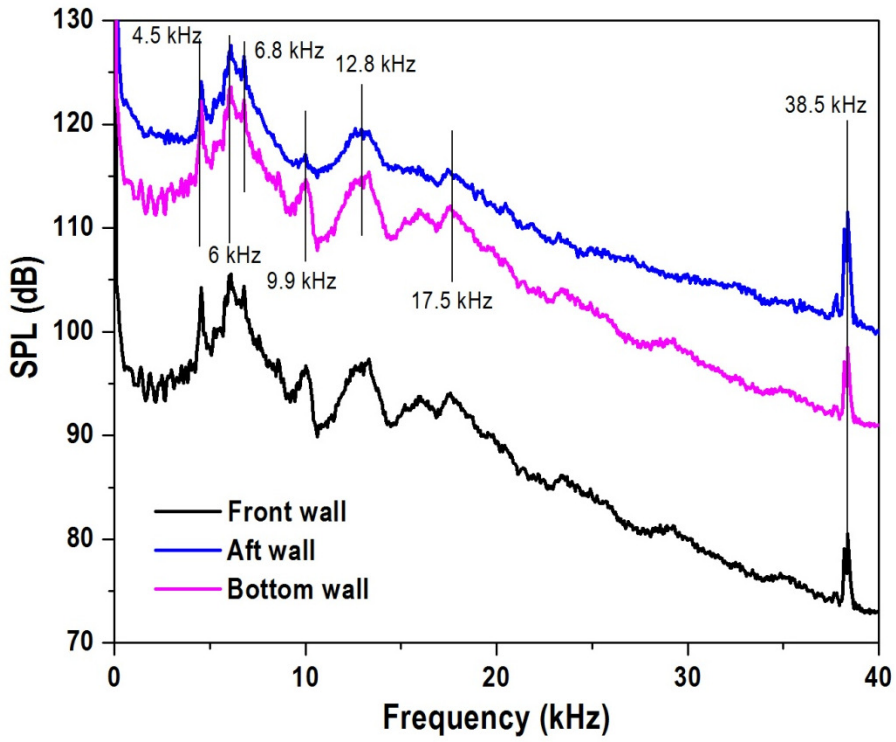

Fig. 4.3: Pressure spectra for P_{01}/P_0 = 0.52

Increasing the pressure to P_{01}/P_0 = 0.56 and 5.9 (Figs.4.4 and 4.5) similar small amplitude modes/tones are seen in the pressure spectra. In these cases, a smooth trend is seen as compared to the earlier case, which is due to relatively large scale eddies. At P_{01}/P_0 = 0.56, a normal shock in the shock train is at the middle of the cavity (Fig.4.2d) and hence its interaction with the shear layer leads to a hump in the shear layer. Therefore, the shear layer impinges at cavity aft wall that contains relatively large scale eddies. This is reflected in the pressure spectra where the spectra at cavity aft wall is smooth and the initial portion of the spectra contains less fluctuation as compared to the earlier case. With further increase in pressure (P_{01}/P_0 = 0.63), number of small-scale amplitudes is reduced (Fig.4.6) and the modes/tones are suppressed.

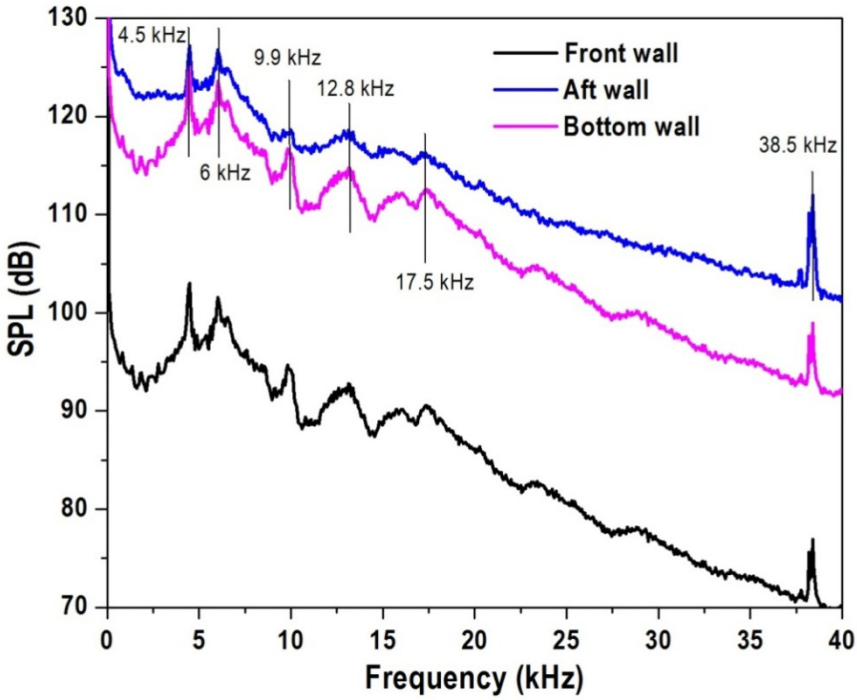

Fig. 4. 4: Pressure spectra for $P_{01}/P_0 = 0.56$

This can be explained through the shadowgraph images (Fig.4.2f) where the bifurcated shock system as well as the normal shock does not interact with the cavity shear layer. In this case, the cavity shear layer is not directly disturbed and hence, eddies are allowed to grow in size to form large-scale structures. These eddies due to impingement on cavity wall generates pressure pulses that moves upstream inside the cavity. A comparison of the oscillatory modes/tones for all the pressure ratios is presented in Fig. 4.7. It can be observed that the cavity of L/D = 2 does not exhibit mode switching phenomena during the transient starting process. However, at P_{01}/P_0 = 0.63, the unsteady pressure measurement shows that there is a possibility that the cavity may undergo mode switching phenomena. As the pressure ratio during transient starting process increases, the OASPL also increases (Fig.4.8). In this case, minimum value of

OASPL is 134dB occurs at cavity front wall for P_{01}/P_0 = 0.41 while the cavity aft wall experiences as high as 171dB at P_{01}/P_0 = 0.63.

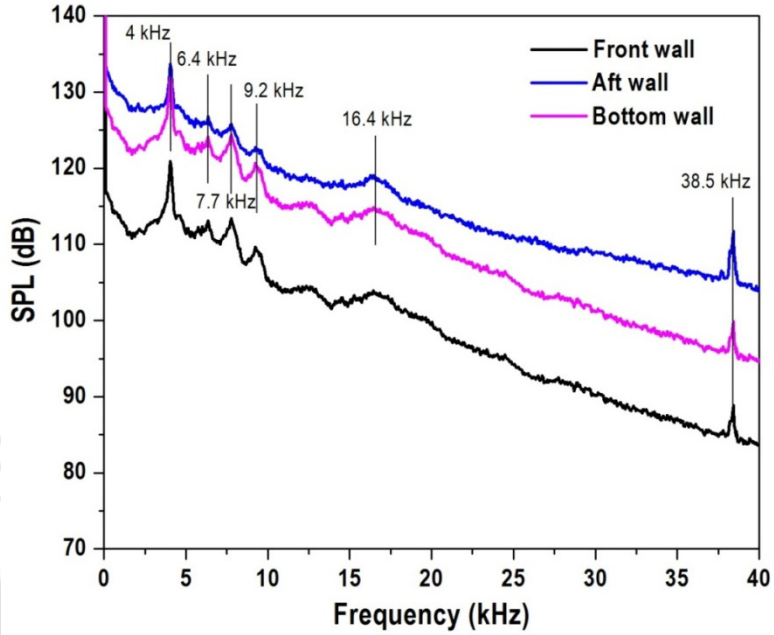

Fig. 4.5: Pressure spectra for P_{01}/P_0 = 0.59

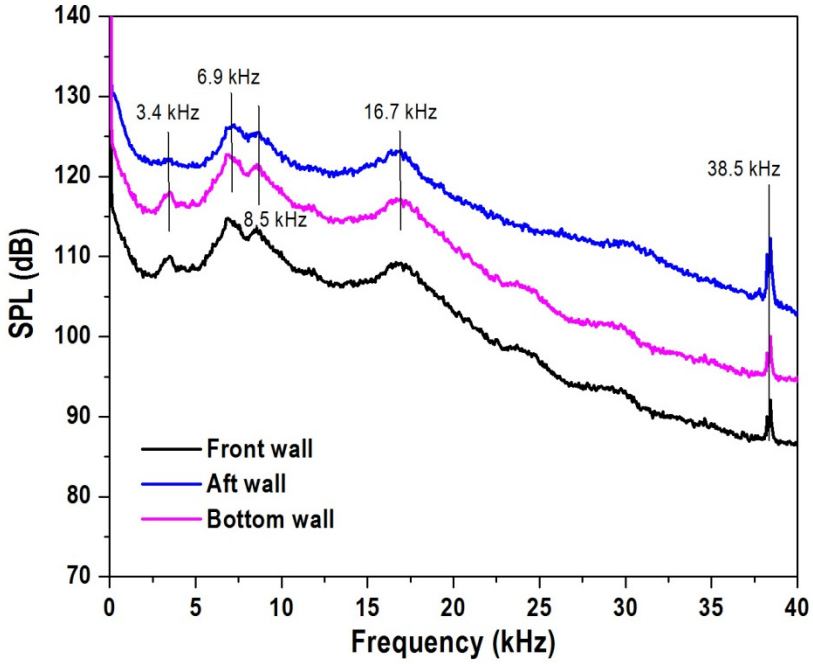

Fig. 4.6: Pressure spectra forP_{01}/P_0 = 0.63

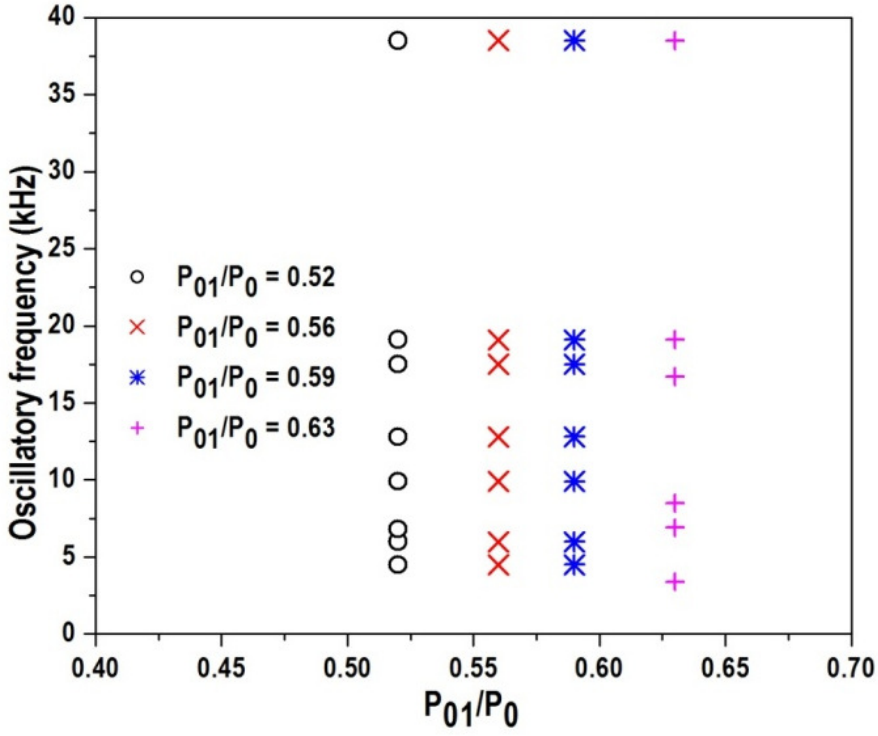

Fig. 4.7: Oscillatory modes for different transient starting pressures

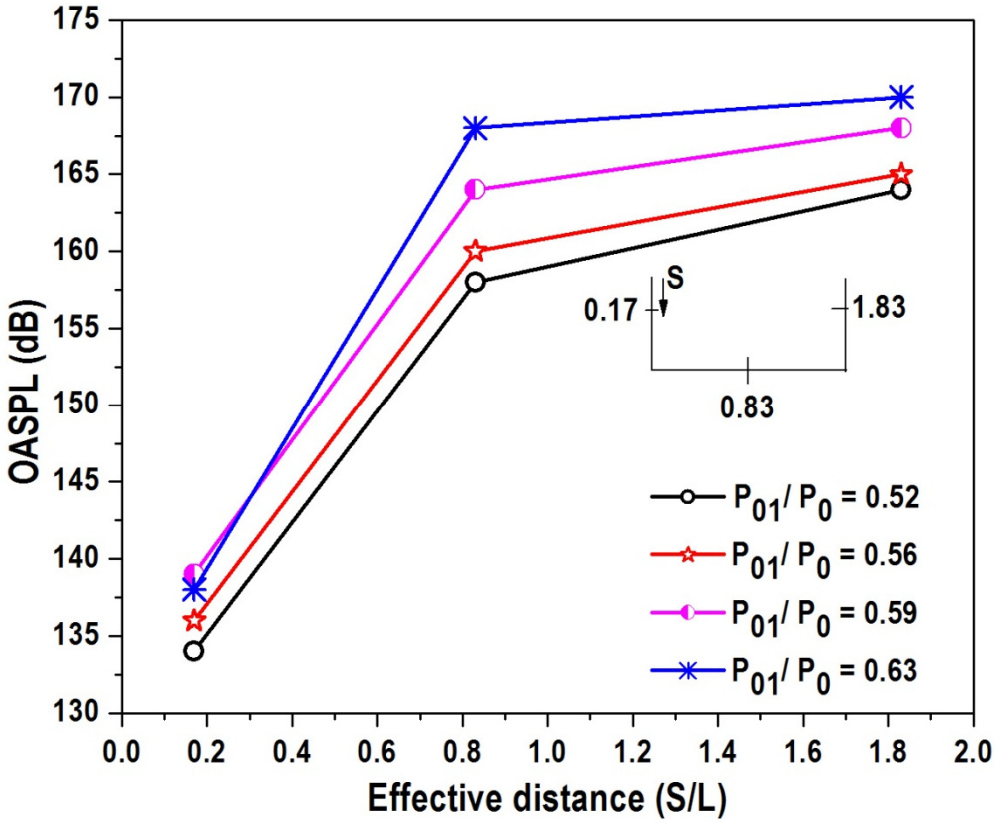

Fig. 4.8: OASPL levels during transient starting condition

4.2.1.1c **L/D = 3**

Up to P_{01}/P_0 = 0.46 (Figs.4.9a and 4.9b), the flow features for L/D = 3 during transient starting process is very similar to other L/D ratios. These figures explain the salient features of such as bifurcated shock system and its associated shock patterns. However at P_{01}/P_0 = 0.52 (Fig.4.9c) unlike L/D = 2 (Fig.4.2c) cavity, the normal shock of the bifurcated shock system stands right above the cavity shear layer. Due to increased cavity length, this phenomenon is occurred at low pressure. Hence, downstream of the interaction point the shear layer has got a hump which contains

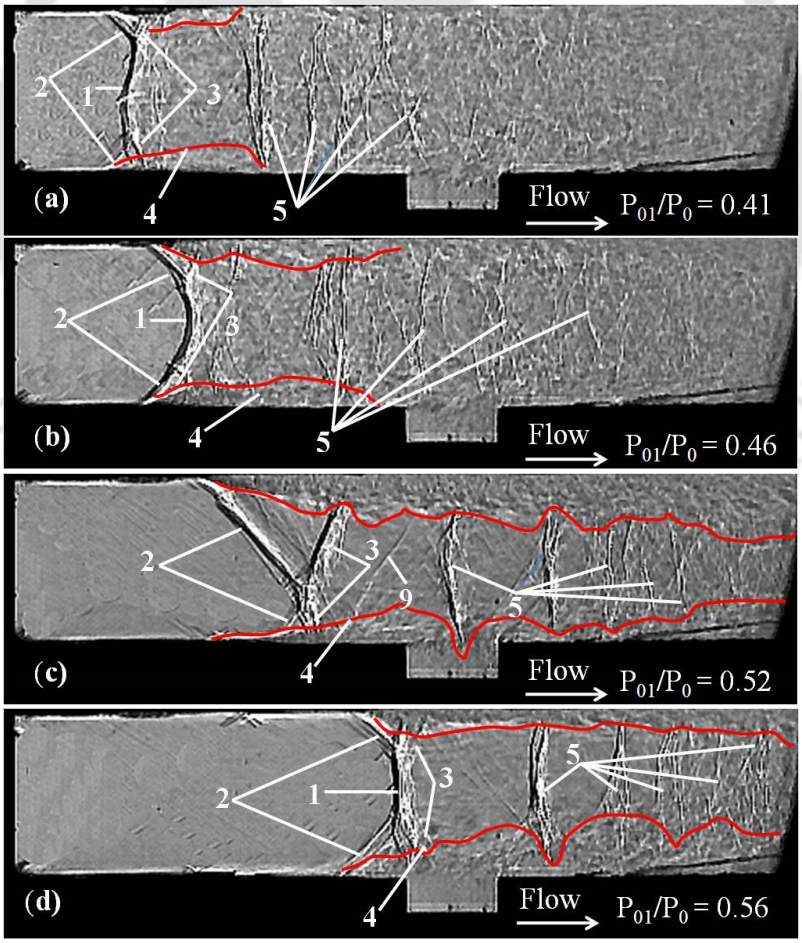

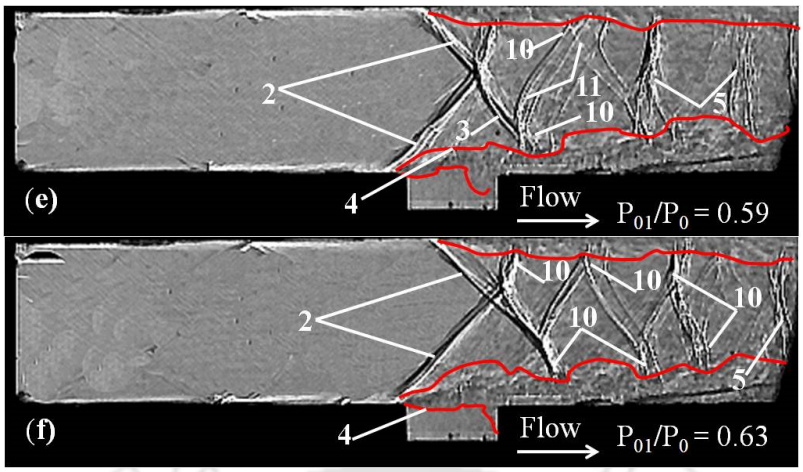

Fig. 4.9: Sequential images of transient starting shocks in a confined duct (L/D= 3)

small scale eddies that affects the cavity unsteadiness after partial impingement at cavity aft wall. At P_{01}/P_0 = 0.56 (Fig.4.9d), the bifurcated shock system is at the cavity leading edge and the normal shock in the shock train moves downstream of the cavity aft wall. In this case, large separation of cavity shear layer is observed and it impinges partially at cavity aft wall. Since the normal portion of the bifurcated shock is at the cavity leading edge, the initial portion of the shear layer may be affected and this interaction may cause the generation of small scale eddies which is explained in the unsteady pressure measurements. Further, increasing the pressure (P_{01}/P_0 = 0.59) causes the leading shock (point 2) of the bifurcated shock system positioned just upstream of the cavity (Fig.4.9e). In this case, large separation is seen on cavity side as compared to top wall and hence, the bifurcation of the shock system is large on cavity side. Also, the trailing shock (point 3) of the bifurcated shock system becomes a Mach reflection (point 10) near the shear layer due to the fact that this shock is not strong enough to cause a regular reflection. In order to equalize the back pressure/flow parallel to the wall, this Mach reflection takes place. Also, an associated shock (point 11) due to

Mach reflection is captured. This shock (point 11) once reaches the top wall becomes Mach reflection. However, downstream of this Mach reflection, the normal shock train (point 5) is formed. The shear layer growth for this pressure is continuously increased and it is expected that the shear layer contains relatively large scale eddies which is addressed in unsteady pressure measurements.

At P_{01}/P_0 = 0.63 (Fig.4.9f), the leading shock (point 2) is positioned exactly at the leading edge of the cavity and the bifurcation of the shock system is maximum at this pressure. In this case, to make the flow parallel to the wall or to match the backpressure, three Mach reflections and associated shock are formed which are marked by point 10 and 11 followed by normal shock train (point 5). The shear layer is unaffected due to the transient shock and downstream side it is continuously growing in size that contains large-scale structures. These structures impinge at cavity aft wall and produce pressure pulses, which move inside the cavity towards the front wall, and hence, it may be expected to have modes/tones, which are discussed in the unsteady pressure measurements.

The unsteady pressures inside the cavity at different locations are presented in Figs.4.10 to 4.13. At P_{01}/P_0 = 0.52, the front wall sensor shows fluctuation at low frequencies (Fig.4.10). This can be corroborated through the shadowgraph image (Fig.4.9c). The shear layer near the cavity leading edge contains small eddies and the sensor is located at 2mm from the cavity front wall and hence, it experiences small scale fluctuation which is reflected in the pressure spectrum in the initial portion. However, once the shear layer impinges partially at cavity aft wall, the pressure pulses

are generated which moves upstream inside the cavity are picked up by the sensor. Spectrum indicates that the energy level is more at low frequencies and reduces very fast at high frequencies. On the other hand, due to direct impingement of the shear layer at aft wall, the modes/tones detected by the sensor indicate smooth trend with moderate amplitude. The bottom wall sensor experiences the modes/tone which are generated due to the pressure pulses generated at cavity aft wall and hence, compared to aft wall sensor, the amplitude of modes/tones is high in bottom wall sensor. Nevertheless, all the sensors indicate modes/tones at the same frequencies.

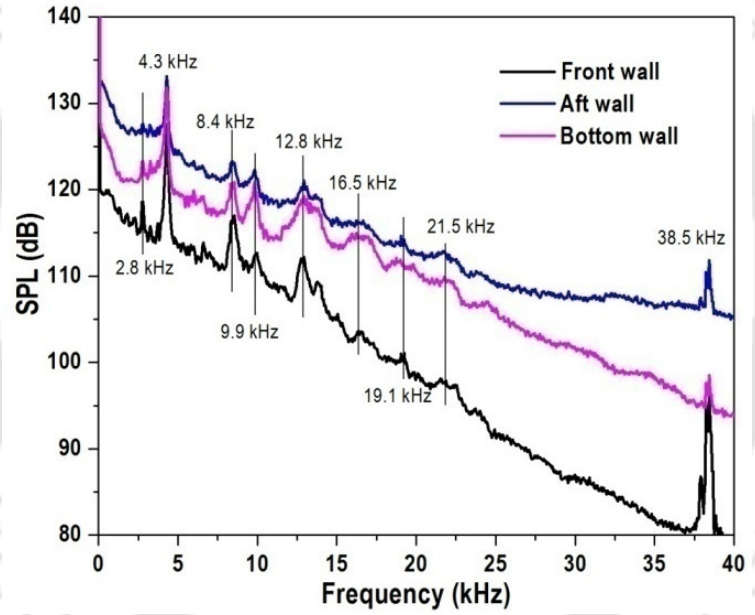

Fig. 4.10: Pressure spectra for P_{01}/P_0 = 0.52

As the pressure is increased (P_{01}/P_0 = 0.56), the number of modes/tones experienced by the sensors are decreased (Fig.4.11). From the shadow graph image (Fig.4.9d) it is understood that the shear layer is not disturbed by shocks in the free stream except a small region in the vicinity of cavity leading edge where the bifurcated shock system stands. Thus, eddies in the shear layer grows without much disturbances

and they may become relatively large scales. This is reflected in the aft wall sensor where a smooth variation in the pressure spectrum with small amplitude modes/tones. Similar to previous case, the pressure pulses due to the impingement of shear layer at cavity aft wall are sensed by the bottom wall sensor that produces modes/tones. The front wall sensor on the other hand shows a rapid slope change in the pressure spectrum contains modes/tones at different frequencies. It indicates that the

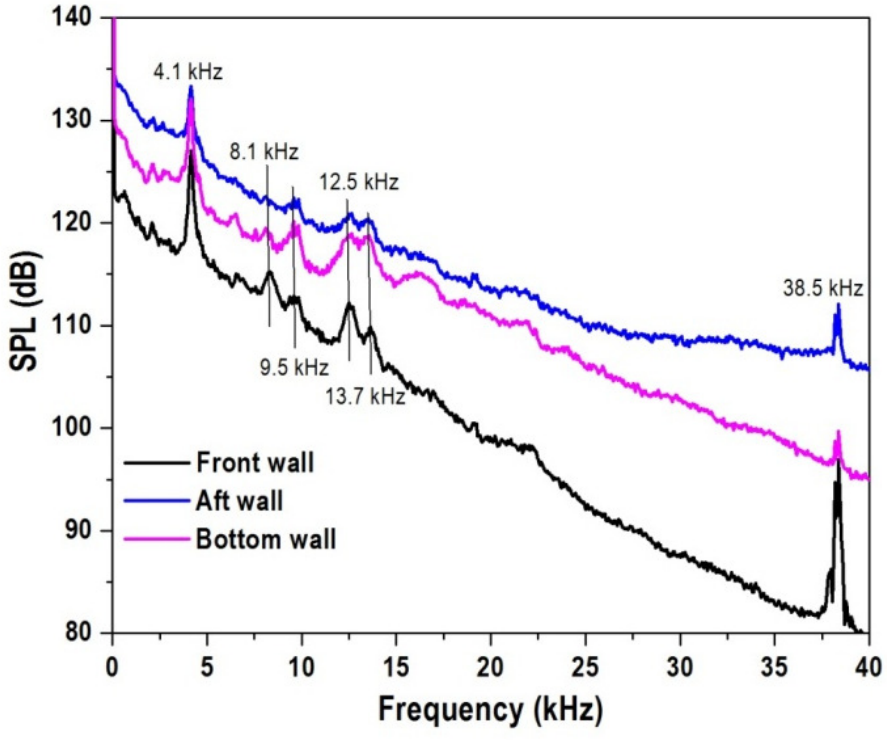

Fig. 4.11: Pressure spectra for $P_{01}/P_0 = 0.56$

impingement at the trailing edge and the pressure wave travel inside the cavity is having least influence at the leading edge sensor location; hence the energy reduces very fast. In this case, all the sensors show modes/tones at same frequencies, which are different from $P_{01}/P_0 = 0.52$ indicates a mode switching phenomena.

At P_{01}/P_0 = 0.59 and 0.63, the pressure spectra show multiple modes/tones and the unsteadiness are further reduced due to the fact that the shear layer contains large scale eddies. This is evident from the shadow graph images (Figs.4.9e and 4.9f) where the cavity leading edge experiences an oblique shock due to separation (point 2) and compare to earlier case, the shear layer is not disturbed much and hence, large growth in the eddies which is reflected in the pressure spectra. However at P_{01}/P_0 = 0.59, the trailing shock (point 3) of the bifurcated shock system is located just downstream of the cavity aft wall. This may cause upstream influence, which is observed from pressure spectra of all the sensors. At P_{01}/P_0 = 0.63, the trailing shock (point 3) of the bifurcated shock system is located much downstream and resulted in discrete modes/tones in the pressure spectrum. The slopes of SPL verses frequency for different locations are different. Wherever shear layer reattachment is there, the magnitude of pressure fluctuation is more at low frequencies and reduced as the frequency increases. The reason may be the pressure fluctuation levels cannot be same at all frequencies. When we move away from the reattachment location the magnitude of pressure fluctuation comes down at low frequencies and the fluctuation level reduced too much at higher frequencies.

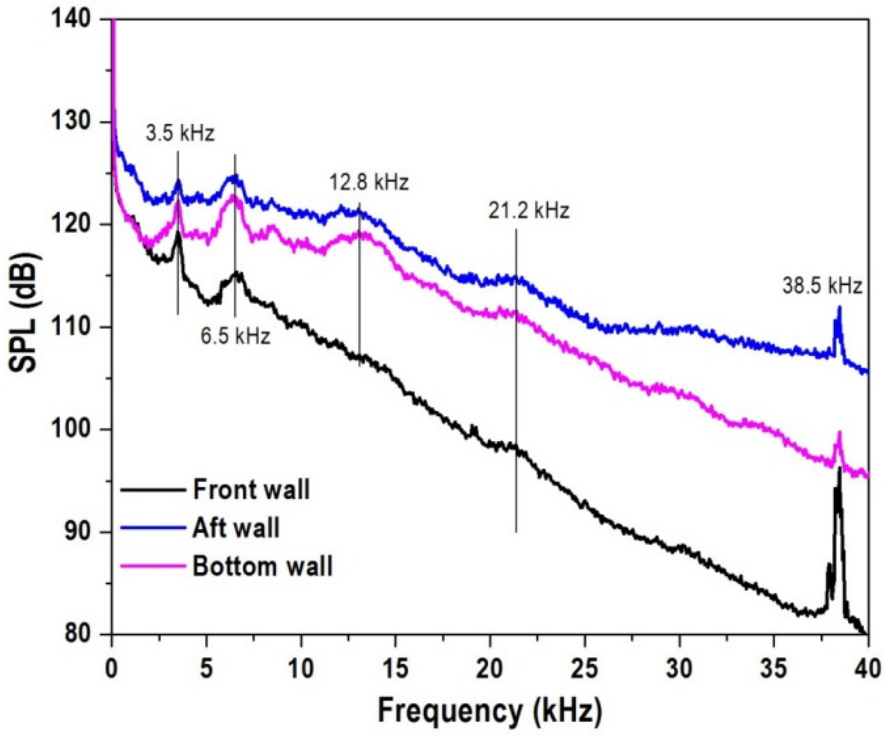

Fig.4.12: Pressure spectra for $P_{01}/P_0 = 0.59$

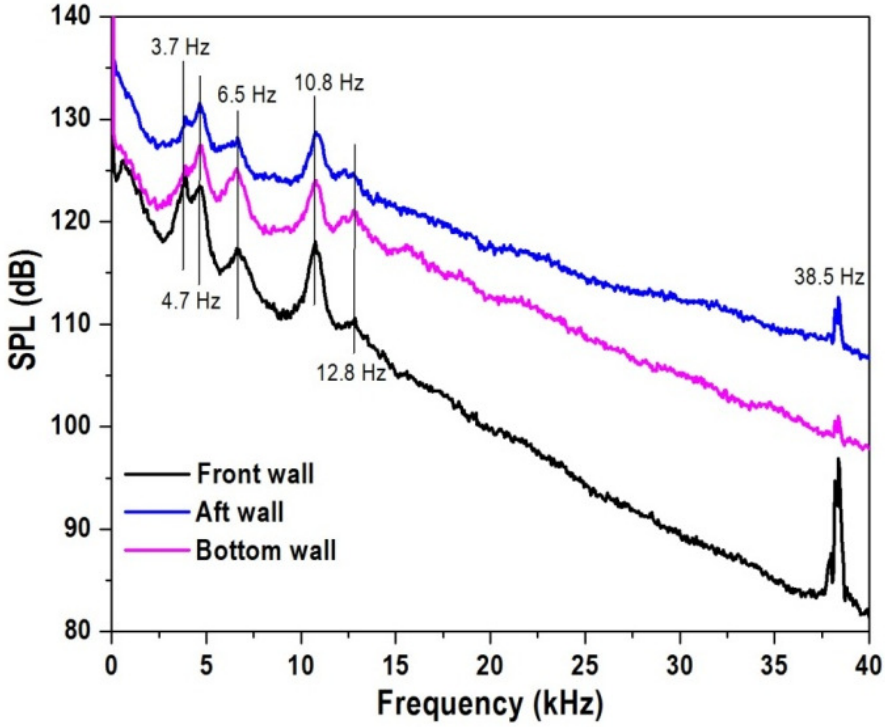

Fig.4.13: Pressure spectra for $P_{01}/P_0 = 0.63$

In order to see the mode/tone switching phenomena for L/D = 3 cavity due to transient starting process at different P_{01}/P_0, a summarized results are presented in Fig.4.14. It can be observed that the L/D = 3 cavity possess certainly the modes/tones at different frequencies depending upon the pressure. At pressures greater than P_{01}/P_0 = 0.56, number of modes/tones is decreased. A unique common feature is a mode/tone occurs at 38.5 kHz irrespective of the pressures. As the pressure ratio increased during transient starting process, the OASPL also increases (Fig.4.15). In this case, the minimum OASPL of 157dB occurs at cavity front wall for the pressure P01/P0 = 0.41 while the cavity aft wall experiences as high as 171dB at P01/P0 = 0.63.

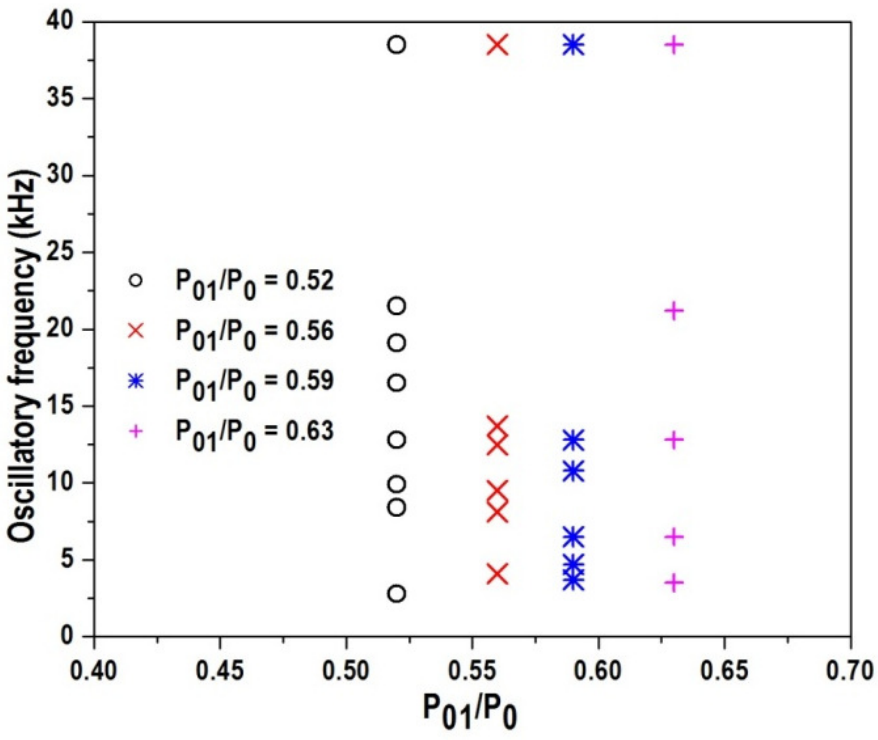

Fig.4.14: Oscillatory modes for different transient starting pressures

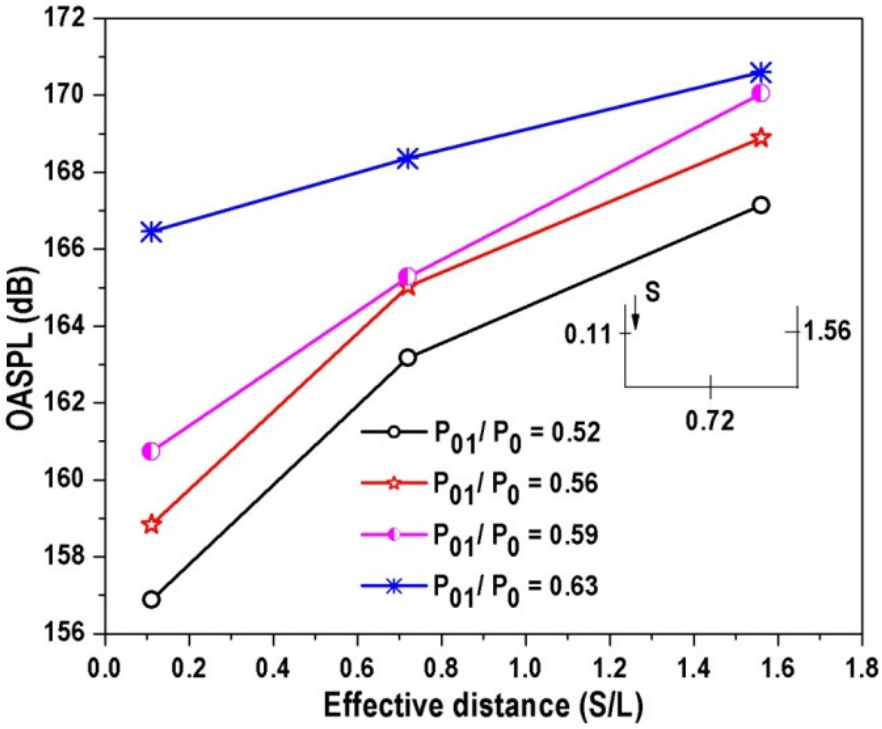

Fig. 4.15: OASPL levels during transient starting condition

4.2.1.2. *Case II Flow structures over shallow open cavities (L/D = 4 and 5)*

The transient starting process of transitional cavities from shallow to open is studied. In this case, the influence of different stagnation pressures during transient process, cavity unsteadiness and mode switching phenomena are studied. Also, continuously increasing stagnation pressure and its increasing rate or the time duration of the starting process is studied. The present section mainly intended to focus on rectangular open cavities namely L/D = 4 and 5 in terms of flow features as well as unsteadiness during transient starting process. Further, rate of increasing the stagnation pressure as well as the unsteady pressure measurement during the entire transient process by continuously varying stagnation pressure are addressed.

4.2.2. Effect of continuously increasing stagnation pressure (L/D = 4)

Figure 4.16 demonstrates the effect of rate at which the stagnation pressure varies continuously during entire transient process (from P_{01}/P_0 = 0 to 0.63) on cavity unsteadiness. In the present studies, the stagnation pressure $P_{01}/P_0$is increased from 0 to 0.63 in 2 s and in 4s is considered. The pressure spectra clearly show that a dominant mode/tone occurs at 3.7 kHz irrespective of the measured locations inside the cavity. The front wall sensor of cavity further demonstrates the presence of small amplitude modes/tone at various frequencies namely 4.5, 8.6, 10, 12.8, 17.6, 38.5 kHz and the slope decreases rapidly. Similarly, the bottom wall sensor also reveals small amplitude modes/tones at different frequencies. However, the aft wall pressure

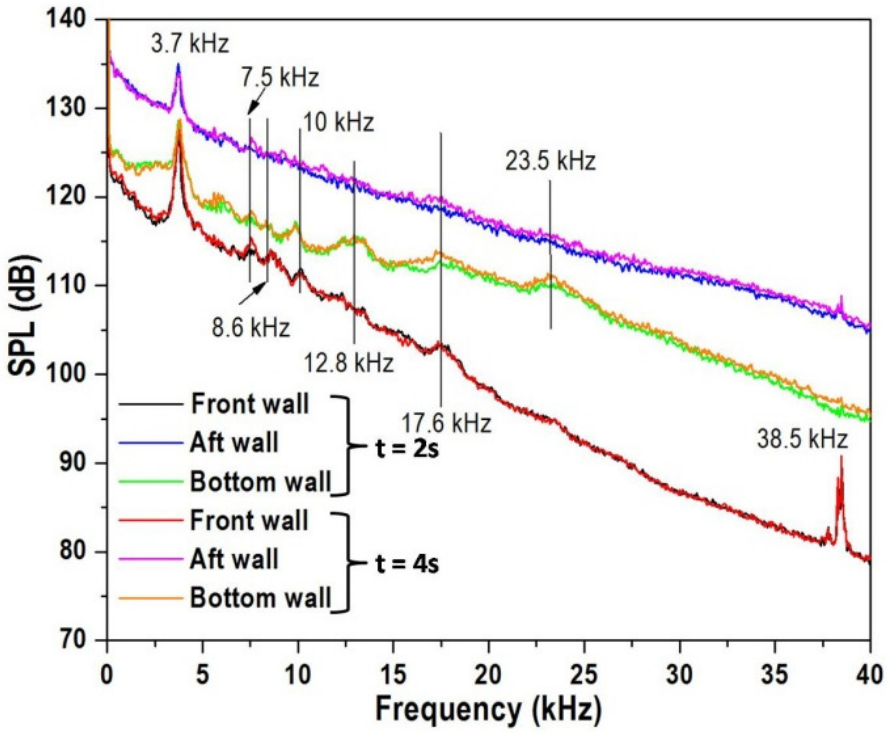

Fig. 4.16: Pressure spectra for continuously increasing stagnation pressure during transient starting process

spectrum contains a single mode/tone at 4.5 kHz. However, by increasing the stagnation pressures at different rates clearly indicate that the phenomena are hardly altered. Hence, the transient starting process is independent of rate at which the stagnation pressure is increased. In order to see this effect, the OASPL is plotted in Fig.4.17. This shows that the OASPL levels are very closely comparable with different rate at which the stagnation pressures are increased. The OASPL levels show the values between 177 to 181 dB which are significant during transient starting process hence the system design should take care of this issue. Thus, the cavity behavior during transient starting process at discrete stagnation pressures is studied to get insight into the flow physics.

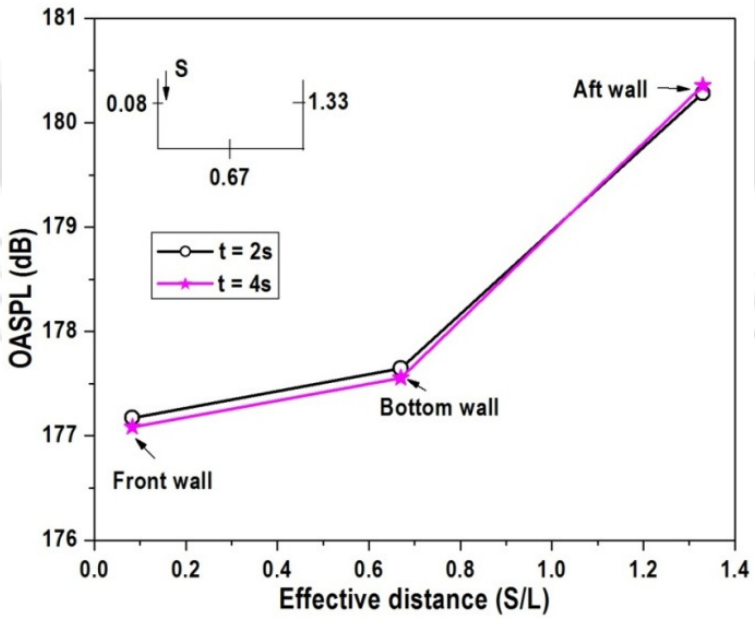

Fig. 4.17: OASPL levels continuously increasing stagnation pressure during transient starting process

4.2.3. Cavity flow features at discrete stagnation pressures (L/D = 4)

At stagnation pressure of P_{01}/P_0 = 0.41 (Fig.4.18-a), the starting shock (point 1) stands at the initial portion of the test section and its interaction with the boundary layer is observed to be minimum. Hence, a bifurcation (point 2 and 3) of this shock is seen both at the top and bottom wall (called bifurcated shock system). In this case, the boundary layer (point 4) is observed to be reattached (marked as red line). Immediately downstream of this bifurcated shock system, a normal shock train (point 5) is formed where the distance between the successive normal shocks is decreased. Further increase in pressure (P_{01}/P_0 = 0.46) produces strong interaction between the shock system and the boundary layer (Fig.4.18b). This is evident from gradual slope change in the shock, which is appeared to be concave in shape. Also, boundary layer is reattached downstream of the shock system. Similar to previous case, a system of normal shocks is formed behind the bifurcated shock system to form a shock train.

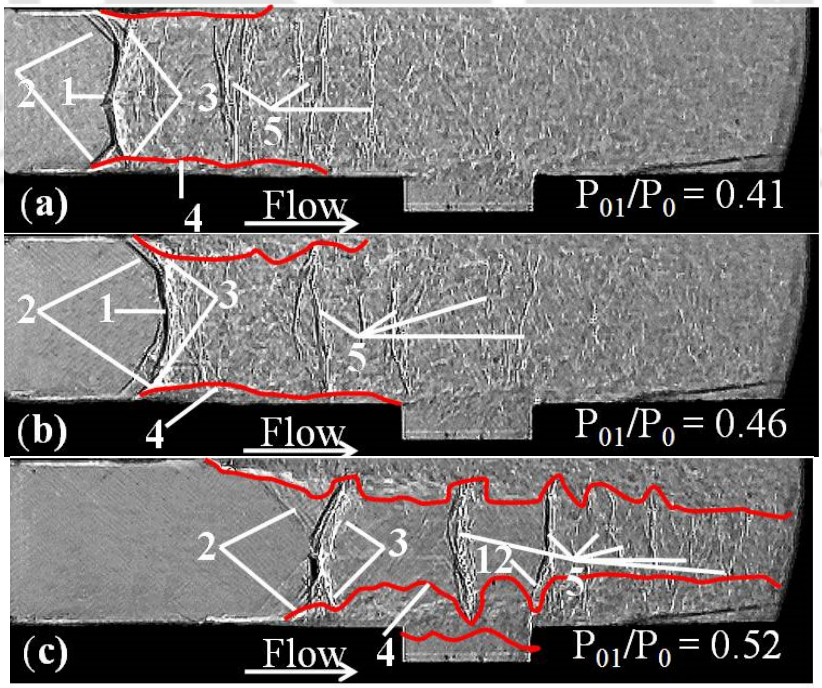

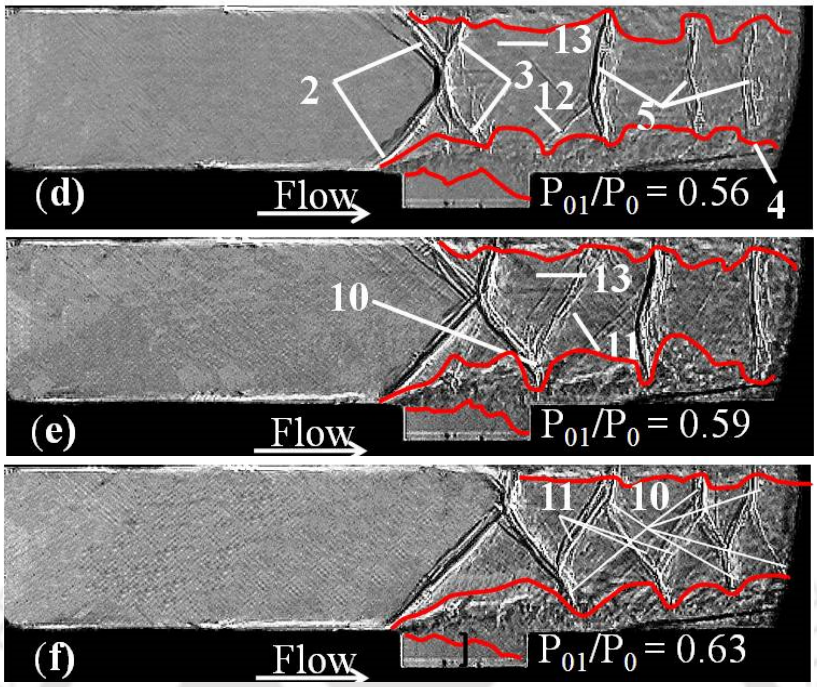

Fig. 4.18: Sequential images of transient starting shocks in a confined duct (L/D= 4)

At P_{01}/P_0 = 0.52 bar (Fig.4.18c), bifurcated shock system is well defined upstream of the cavity where strong interaction is seen both top as well as bottom wall and the separated boundary layer is not reattached. On top wall, due to large adverse pressure gradient, early separation is detected whereas on bottom wall due to cavity the area increase leads to flow expansion which delays the boundary layer separation and hence, an asymmetry is seen in the shock system. The shear layer over the cavity contains eddies of different scales and interacts with the cavity aft wall which in turn generates a cavity trailing edge shock (point 12). This shock upon incident on the normal shock in the shock train forms a lambda shock structure. Immediately downstream of the bifurcated shock system, number of shocks is formed in the shock train. It is observed that the normal shock in the shock train interacts with the cavity shear layer at the middle. Also, downstream of the cavity trailing edge, the shear

layer/boundary layer grows rapidly that can cause considerable changes in the structure of turbulence/eddies and its statistical properties. Hence, substantial changes in length scales may be expected due to interactions of shock wave with shear layer. This may affect the pressures inside the cavity that will be explained in the next section. Further increase in pressure (P_{01}/P_0 = 0.56) the shock system stands just downstream of the cavity leading edge (Fig.4.18-d) and the bifurcation is found to be large at cavity side. Also, a shock (point 12) due to shear layer impingement at cavity aft wall is seen followed by a shock train (point 5). In this case, the trailing shock (oblique shock) in the bifurcated shock system interacts with the cavity shear layer, which is evident from the growth of the shear layer. Similar to the previous pressure ratio case (Fig.4.18c), a shock (point 12) is originated at cavity trailing edge to forms a lambda shock structure.

At P_{01}/P_0 = 0.59 (Fig.4.18e), the bifurcated shock system is positioned at mid-way through the cavity where the leading shock (point 2) is located at cavity leading edge and the trailing shock (point 3) is at cavity aft wall. Similar to the previous pressure ratio (Fig.4.18d), the shear layer and the bifurcation is found to be large on cavity side. The trailing shock (point 3) after incident on top wall boundary layer reflects as an expansion wave (point 13). To make the flow parallel to the wall/ equalize the backpressure, an oblique shock (point 11) near the shear layer is formed. At this pressure, continuous growth in the shear layer is observed. When P_{01}/P_0 = 0.63 (Fig. 4.18-f), the flow features are entirely different where a series of oblique shocks (oblique shock train) is noted. The bifurcated shock system in this case is almost at the cavity trailing edge and the bifurcation is found to be large at cavity side as compared to top

wall. To make the flow parallel to the wall or equalize the backpressure, a Mach reflection (point 10) occurs. Similarly, a series of oblique shocks with corresponding Mach reflections (point 10) are observed.

Cavity unsteadiness due to interaction between transient shock system and shear layer is obtained through simultaneous acquisition of unsteady pressures at three locations inside the cavity and corresponding pressure spectra are shown in Figs. 4.19 - 4.22. Figure 4.19 shows the pressure spectra for $P_{01}/P_0 = 0.52$ where the cavity aft wall sensor shows smooth trend with number of small amplitude modes/tones (from 2.5 kHz to 13.4 kHz). This can be correlated to the shadowgraph image (Fig.4.19-c) where a normal shock in the transient shock system impinges at the cavity middle. This allows small scale eddies to grow and become relatively large scale structures which

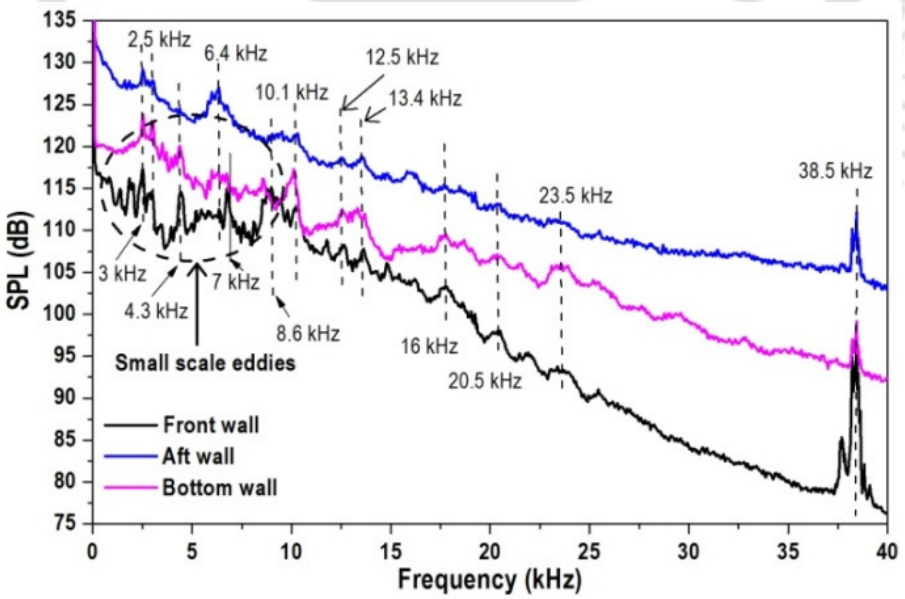

Fig. 4.19: Pressure spectra for $P_{01}/P_0 = 0.52$

are evident from shear layer hump (growth). When the shear layer with relatively large scale structures impinge at cavity aft wall generates a pressure pulse, which moves upstream inside the cavity. The shadowgraph image (Fig.4.18-c) indicates the existence of pressure waves inside the cavity. The tendency of this pressure pulse is periodic in nature and hence, the pressure sensor at cavity aft wall shows modes/tones at different frequencies. Similarly, cavity floor sensor exhibits small amplitude modes/tones. However, due to the dissipation effect, the strength of the pressure wave decreases and hence, small-scale fluctuations below 10 kHz are seen (marked as dotted circle). On the other hand, the cavity front wall sensor contains number of small-scale fluctuations (marked as a dotted circle) in its initial portion (<10 kHz). This may be due to the attenuation of the pressure waves inside the cavity towards front wall owing to dissipation as well as the interaction of the pressure waves with shear layer. Since the front wall sensor is positioned very close proximity to on-coming shear layer, this interaction may produce small scale eddies that decays fast which is evident from rapid decrease in the slope. Like other sensors, cavity front wall also shows modes/tones. All the sensors show small amplitude modes/tones at same frequencies indicate a global instability.

At P_{01}/P_0 = 0. 56 (Fig.4.20), the pressure spectra for all the sensors show similar results as compared to earlier case except reduced fluctuations in the initial portion (< 10 kHz). This can be corroborated through the optical images as shown in Fig.4.18-d where the interaction of transient shock system with the shear layer is found to be weak. In this case, the boundary layer is separated just upstream of the cavity where the

leading shock (point 2 – separation shock) is strong enough to generate a large separation.

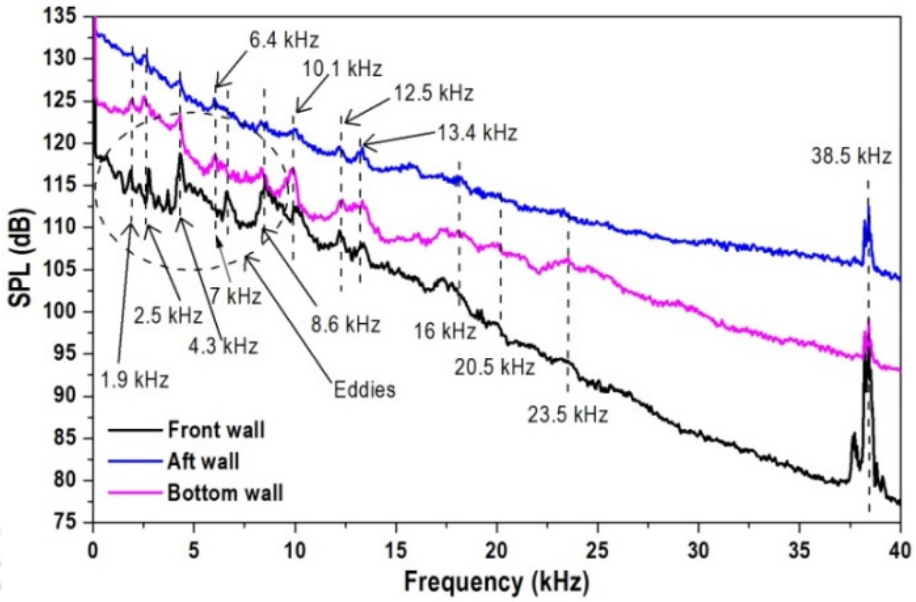

Fig. 4.20: Pressure spectra for $P_{01}/P_0 = 0.56$

Further, the normal shock in the shock system moves downstream of the cavity and only the trailing shock (point 3) of the bifurcated shock system is found to be on the shear layer along with a generation of shock (point - 12) from cavity aft wall due to shear layer impingement. Thus, eddies in the shear layer starts growing from the leading edge and are less affected by the trailing shock (point 3) interaction with the shear layer. Hence, downstream of the trailing shock, though the shear layer starts growing, contains moderate structures. This is reflected in the pressure spectra where, the aft wall has number of modes/tones with reduced amplitude as compared to the earlier case. Also, reduced fluctuations are seen in the front and bottom wall of the cavity sensors. Though the modes/tones irrespective of the sensor locations occur at

the same frequencies; its occurrence is found to be different from the earlier case (P_{01}/P_0 = 0.52).

At P_{01}/P_0 = 0.59 and 0.63 (Figs.4.21 and 4.22), unlike the earlier cases, the initial portion of the pressure spectrum does not contain eddies which is evident from the smooth trend. This shows the transition of small scale eddies in the cavity shear layer into large-scale structures. This can be corroborated through shadowgraph images as shown in Fig.4.18 (e-f). The optical images show large separation over the cavity due to leading shock (separation shock) where in both the cases, the bifurcation of the shock system is found to be large on cavity side. In these cases, the trailing shock (point 3) of the bifurcated shock system moves downstream of the cavity. Thus, the shear layer over the cavity is not influenced by the interaction and hence, eddies grow in size to become large scales and hence, a smooth trend in the pressure spectra is seen. Also, the shadowgraph images show the existence of the shock at the cavity aft wall owing to shear layer impingement. In these cases (P_{01}/P_0 = 0.59 and 0.63), irrespective of the measurement locations, two and four modes/tones are present respectively. In all the cases, during transient process, a mode/tone is seen at 38.5 kHz irrespective of measured locations.

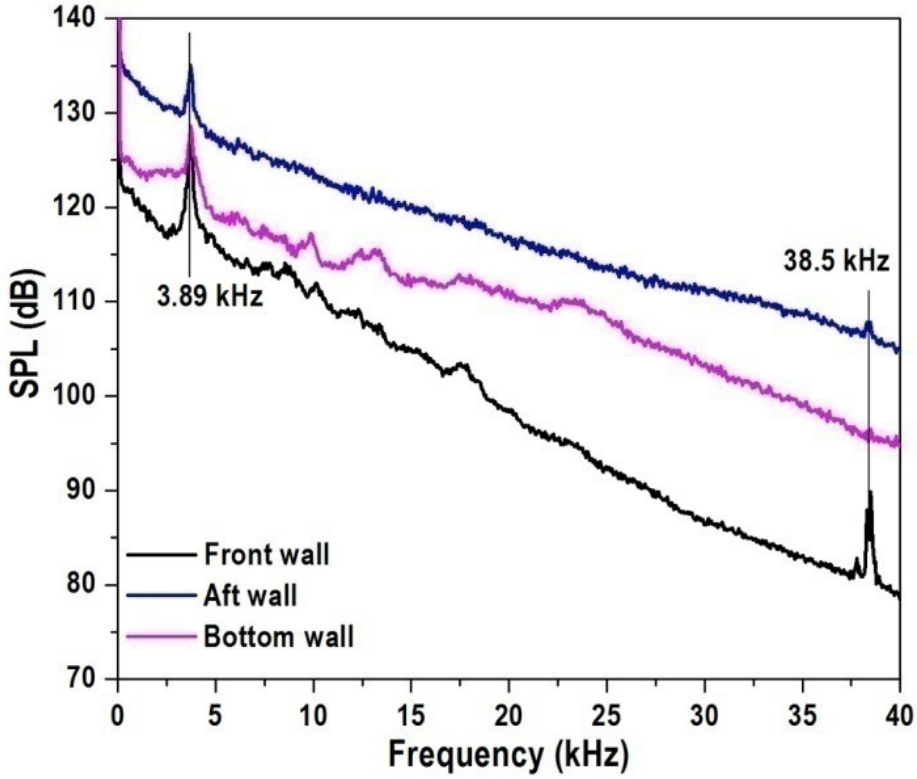

Fig. 4.21: Pressure spectra for $P_{01}/P_0 = 0.59$

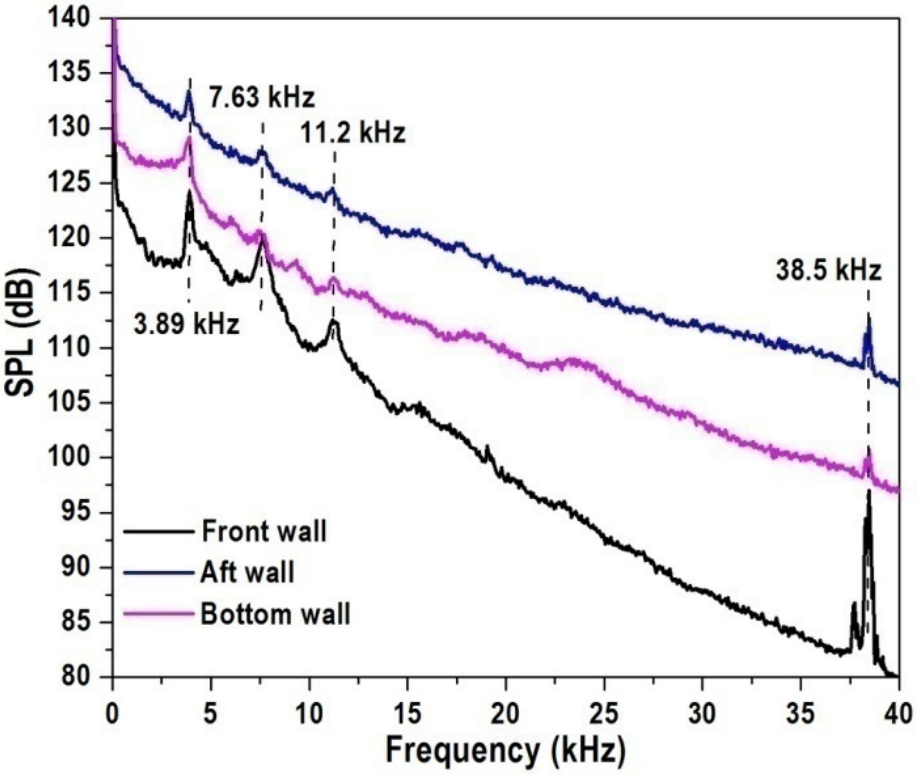

Fig. 4.22: Pressure spectra for $P_{01}/P_0 = 0.63$

In general, for different operating pressures during transient process, the pressure spectra of all the sensors contain small amplitude modes/tones. At a particular pressure, the frequencies at which the modes/tones occurred are independent of the measured locations. For example, at P_{01}/P_0 = 0.59, the front wall sensor shows mode/tone at 3.89 kHz whereas, at P_{01}/P_0 = 0.63, three modes/tones are observed at frequencies correspond to 3.89, 7.63 and 11.2 kHz respectively. Hence, the starting transient process produces small scale eddies as well as relatively large-scale structures in the shear layer that generates modes/tones which is not necessarily occur at the same frequency. Hence, there exists a mode/tone switching phenomena during transient process which is presented in Fig. 4.23.

The above results give insight into the interaction between the starting transient shocks and the shear layer. Hence, the cavity walls show unsteady fluctuations lead to the appearance of several modes/tones at different frequencies. To visualize this effect, the overall sound pressure level inside the cavity is presented in Fig.4.24. It shows that maximum OASPL occurs at cavity aft wall due to direct impingement of shear layer

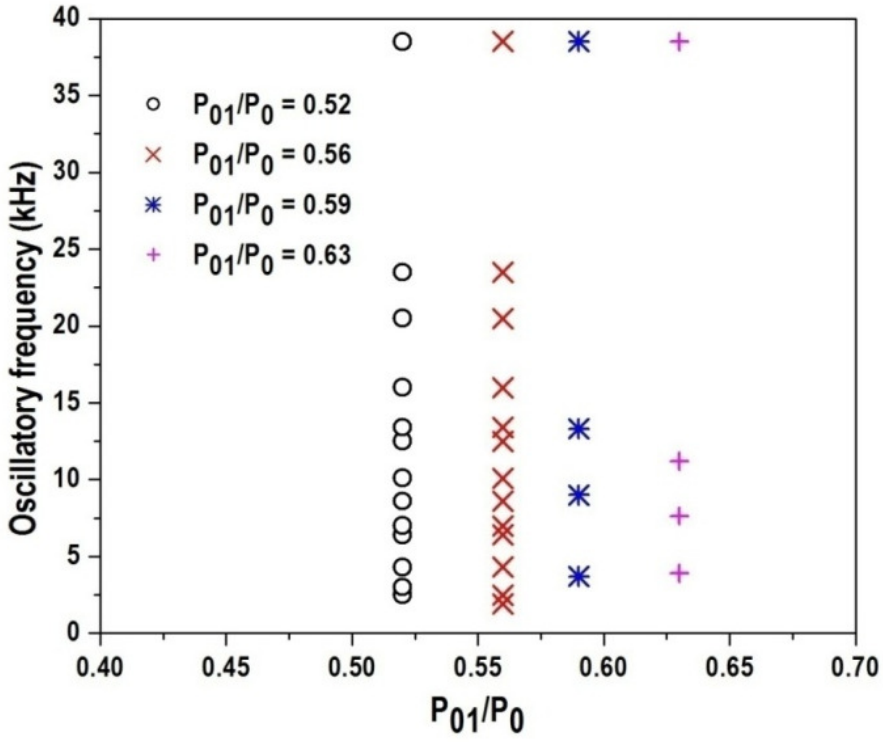

Fig. 4.23: Oscillatory modes for different transient starting pressures

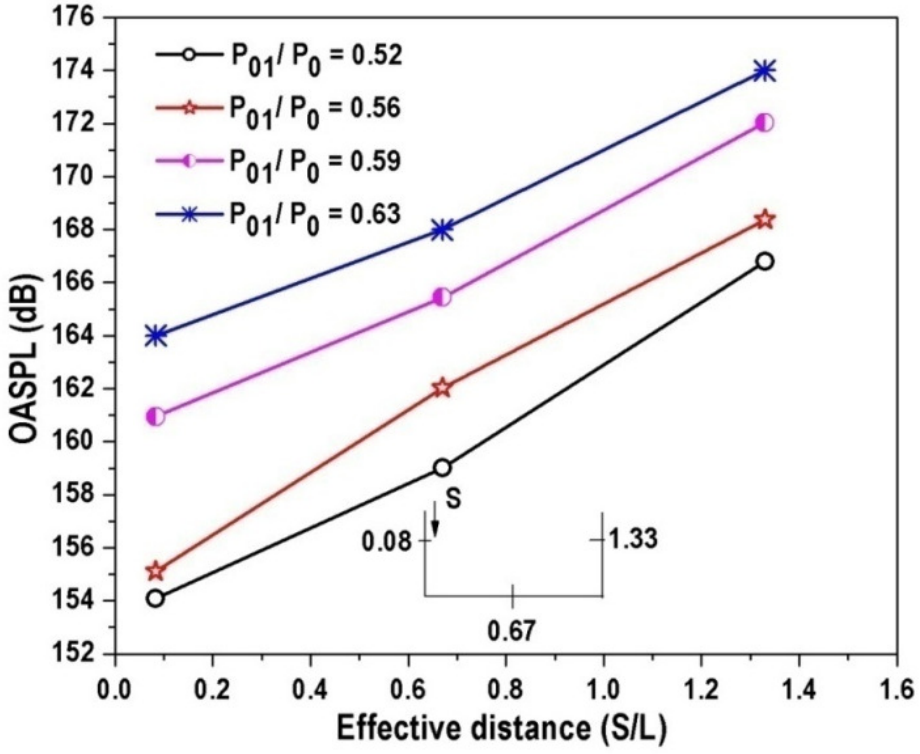

Fig. 4.24: OASPL levels during transient starting condition

whereas the cavity front wall encounters minimum OASPL. Inside the cavity, the OASPL values vary from 154 to 180 dB. Though the interaction of transient starting shock with shear layer exists for short time, its effects on the performance has to be taken care in the design.

4.2.4. Effect of continuously varying stagnation pressure (L/D = 5)

In ramjet to scramjet mode of operation, the transition may takes place at different rates depending upon the configuration, change over strategy and mission. Hence the test final stagnation pressure is achieved by different rate of opening of a pressure regulating valve which results in different timing. In order to study this effect, experiments are conducted on L/D = 5 cavity by continuously varying the stagnation pressure to a required value (in this case, stagnation pressure varies from 0 to 3.4 bar) at different time steps namely 3, 4, 5 and 6s. During these tests, unsteady pressure measurements are carried out at cavity front, bottom and aft walls and the pressure spectra are derived which are shown in Fig. 4.25 for cavity aft wall. The pressure spectra contains small amplitude modes/tones and each pressure spectrum corresponds to the rate (different time steps) at which the stagnation pressure varies from 0 to 3.4 bar. The pressure spectra clearly indicate that for different rate of reaching the final pressure has negligible influence. This may be studied through OASPL variation shown in Fig.4.26 where, different rate (from 3 to 6s time steps) of increasing the stagnation pressure during transient starting process can change the OASPL value of ±0.5 dB. Hence, irrespective of the rate at which the stagnation pressure increases to a required condition the transient starting process results are not altered.

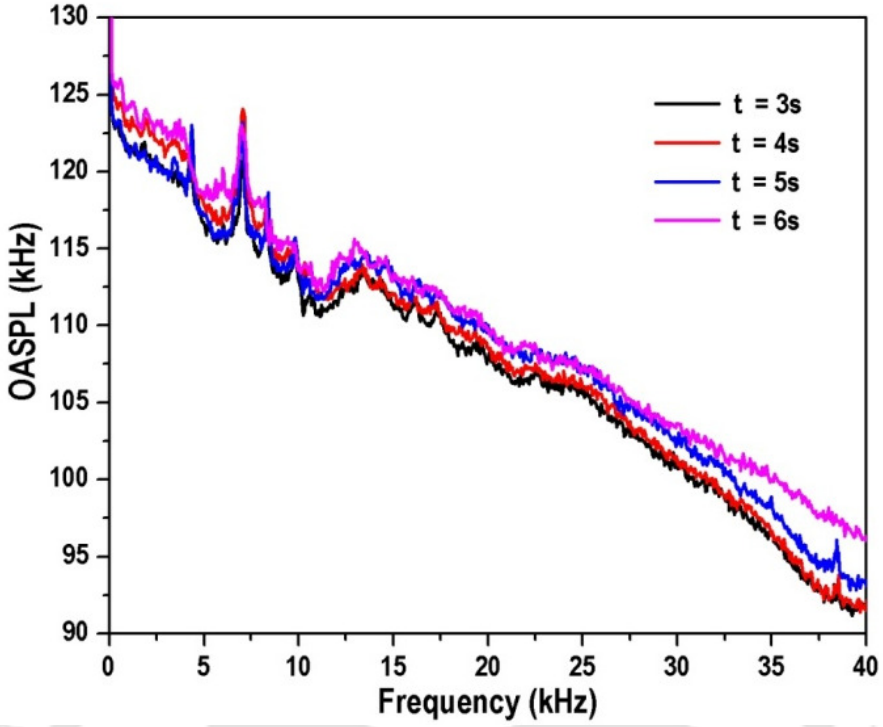

Fig. 4.25: Pressure spectra for continuously increasing stagnation pressure during transient starting process

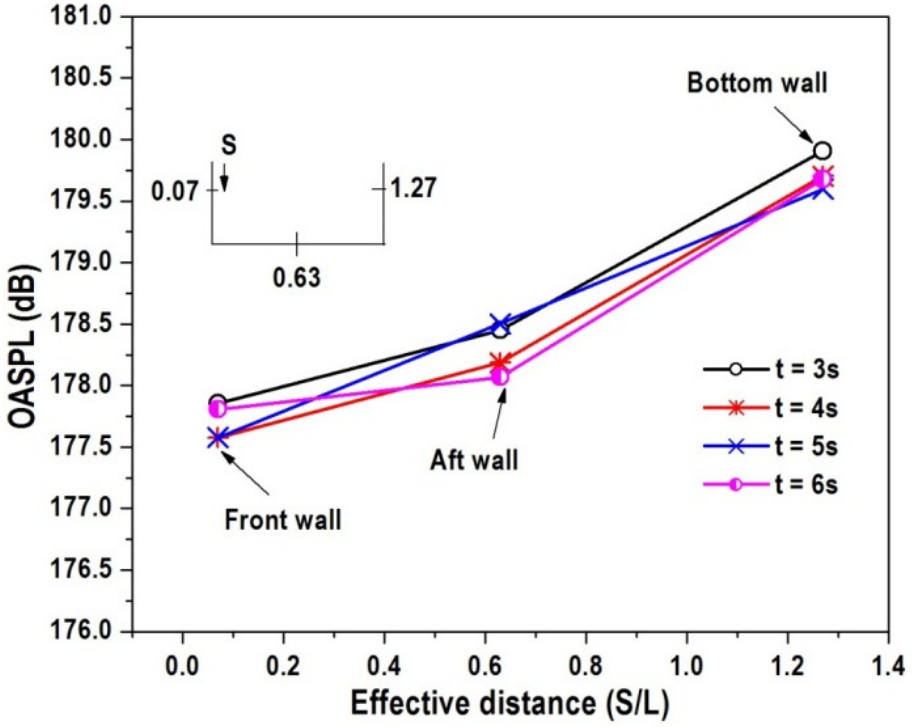

Fig. 4.26: OASPL levels continuously increasing stagnation pressure during transient starting process

4.2.5. Cavity flow features at discrete stagnation pressures (L/D = 5)

Upon starting the tunnel (P_{01}/P_0 = 0.41), a strong shock is generated just downstream of the nozzle followed by weak waves to form a shock train (Fig.4.27-a) and the distance between two successive waves decreases [48, 88]. For P_{01}/P_0 = 0.46 (Fig.4.27-b), change in the shape of the shock system is noticed where the upright shape of the bifurcated shock system becomes curved and the flow separates at the foot of the bifurcated shock system. Here, the normal shock train downstream of the bifurcated shock system is clearly visible and the shock train is located near the cavity. Once the stagnation pressure is increased further (P_{01}/P_0 = 0.52), the number of normal shocks in the shock train increases (Fig.4.27-c). In this, normal shocks in shock train are interacting with shear layer above the cavity and the remaining normal shocks are occurring downstream of the cavity. In the present case, large separation is observed both on top and bottom wall where, the size of the separation is found to be large on top wall as compared to the bottom wall. Generally, disturbances are communicated through boundary layer and propagate upstream. This leads to flow separation on account of adverse pressure gradient marked by the separation shock. This is observed in the present case where the flow on the top wall is separated earlier than the bottom wall, which is evident from the separation shock on the top wall, is much ahead of the bottom wall separation shock. This is due to the fact that the presence of cavity probably reduces the effect of adverse pressure gradient. Hence, the size of the bifurcation in the shock system is found to be large on the top wall as compared to the bottom wall. Once the bifurcated shock system stands above the cavity for P_{01}/P_0 = 0.56 (fig.4.27d), the size of the bifurcation is relatively large on the bottom wall as compared to top wall.

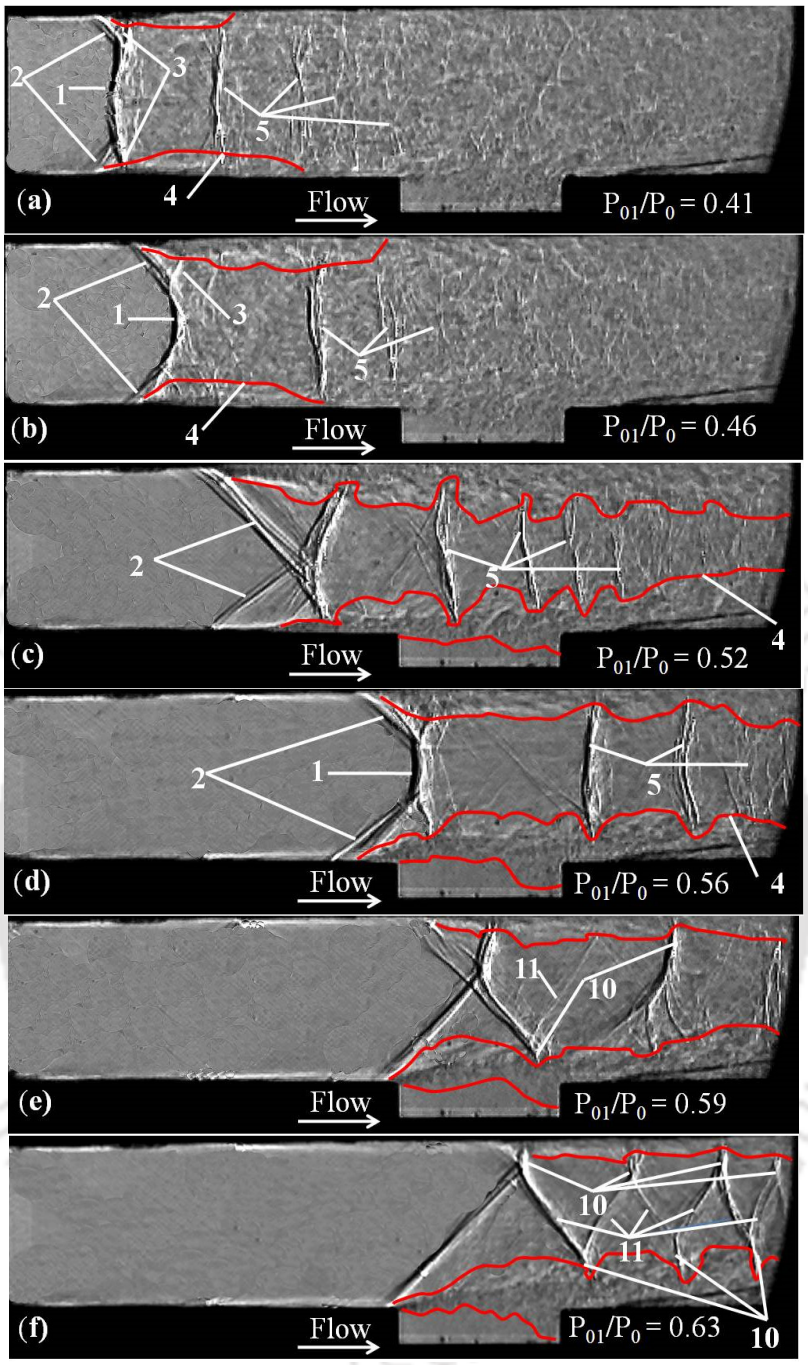

Fig. 4.27: Sequential images of transient starting shocks in a confined duct (L/D= 5)

Similarly, the growth of the shear layer over the cavity is large as compared to the top wall. Upon increasing the pressure to P_{01}/P_0 = 0.59 (Fig.4.27e), the flow structure is entirely different where the bifurcation of the shock system disappears on top wall. In this

case, the separation shock from top wall is not interacting with the shock system to form a bifurcation. On the other hand, the separation shock from the bottom wall interacts with the shock system to form a bifurcation. The top wall shock system appears to be a Mach reflection, terminates with a normal shock. It is seen that the trailing shock from the bifurcation shock system is reflected as an expansion wave from the shear layer. A system of such pattern is observed downstream of the first shock system where the compression waves coalesce to form a normal shock. In this case, the separated flow is found to be large on the cavity side compared to the top wall. By increasing the pressure (P_{01}/P_0 = 0.63), a number of shock systems is observed (Fig.4.27f) where the shocks are terminated with a Mach reflection. Also, downstream of the cavity, the growth of the separated flow is found to be large and the number of Mach reflection is found to be increased.

Figures 4.28 to 4.31 show the unsteady pressure measurements during transient starting process inside the cavity at two locations namely cavity aft as well as front walls at discrete stagnation pressures. For P_{01}/P_0 = 0.52 (Fig.4.28), many modes/tones of small amplitudes are observed in the pressure spectra at cavity aft wall and bottom wall which occur at the same frequencies indicate a global instability. This can be explained through the shadowgraph image (Fig.4.27c) where two normal shocks in the shock train interact with the cavity shear layer. Thus the interaction effect produces disturbances which lead to generate small scale eddies in the shear layer. When the first normal shock in the shock train interacts with the shear layer, the shear layer eddies breakup. Downstream of the interaction point, the shear layer starts growing up which is evident from hump of shear layer downstream of the first interaction point. Subsequently, a

second normal shock interacts just upstream of the cavity aft wall. Hence, the growth of eddies in the shear layer downstream of the first interaction point is affected and breakup may happen even further. This is captured by the pressure sensors at cavity aft and bottom wall, where sporadic modes/tones with small amplitudes are observed.

At P_{01}/P_0 = 0.56 and 0.59 (Figs.4.29and 4.30), the pressure spectra for the both cases are more or less similar that contains numerous modes/tones and only subtle differences are seen. From the flow visualization at P_{01}/P_0 = 0.56 (Fig.4.28d), the trailing shock (point 3) of bifurcated shock system interacts with the cavity shear layer just downstream of the cavity leading edge. Thus, eddies grow in size until the shear layer impinges at cavity aft wall which is evident from the enlargement of the shear layer. Hence modes/tones of small amplitudes along with the fluctuation observed in the pressure spectra. At P_{01}/P_0 = 0.59 (Fig.4.30e), the rear portion of the cavity shear layer is affected by the trailing shock (point 3). In this case, the size of eddies continuously increases until the region where the shock interacts with the cavity shear layer. However, the interaction effect is less pronounced because the trailing shock (point 3) is oblique in nature. Hence eddies have less break up possibility. Thus subtle difference in pressure spectra is seen with respect toP_{01}/P_0 = 0.56.

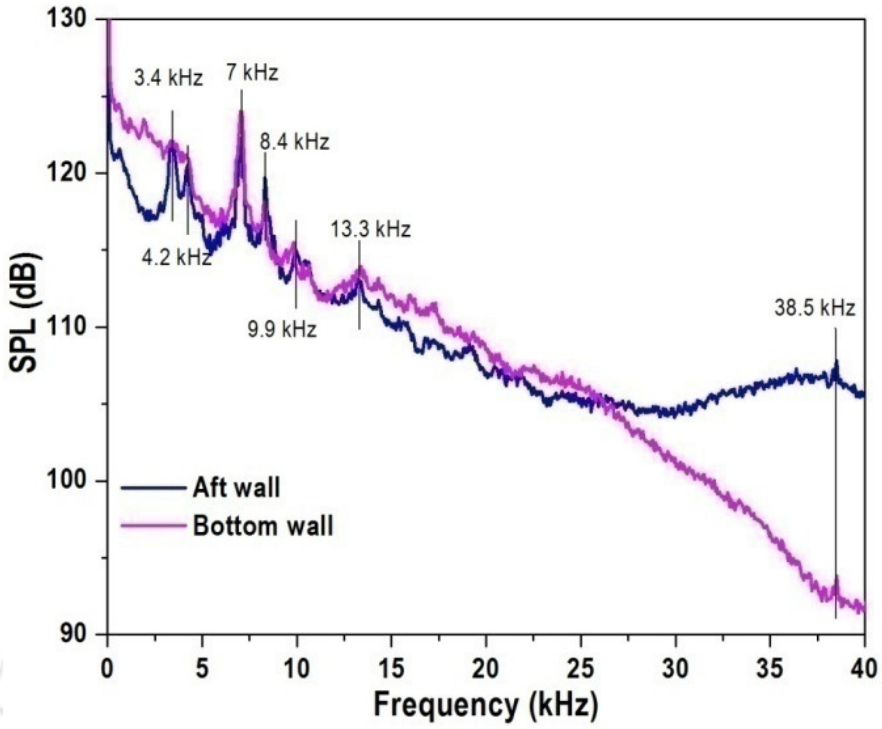

Fig. 4.28: Pressure spectra for $P_{01}/P_0 = 0.52$

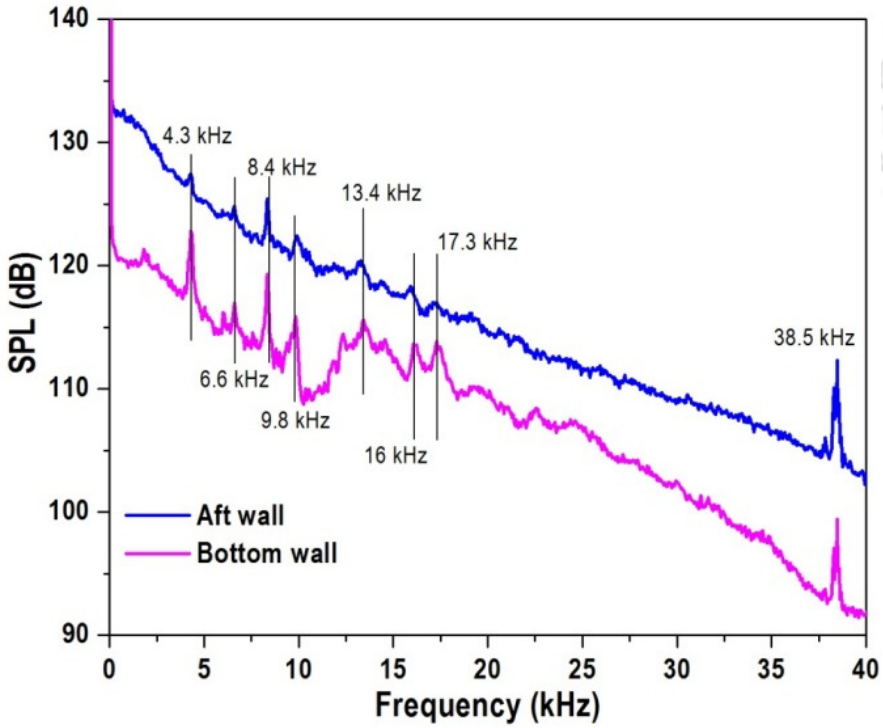

Fig. 4.29: Pressure spectra for $P_{01}/P_0 = 0.56$

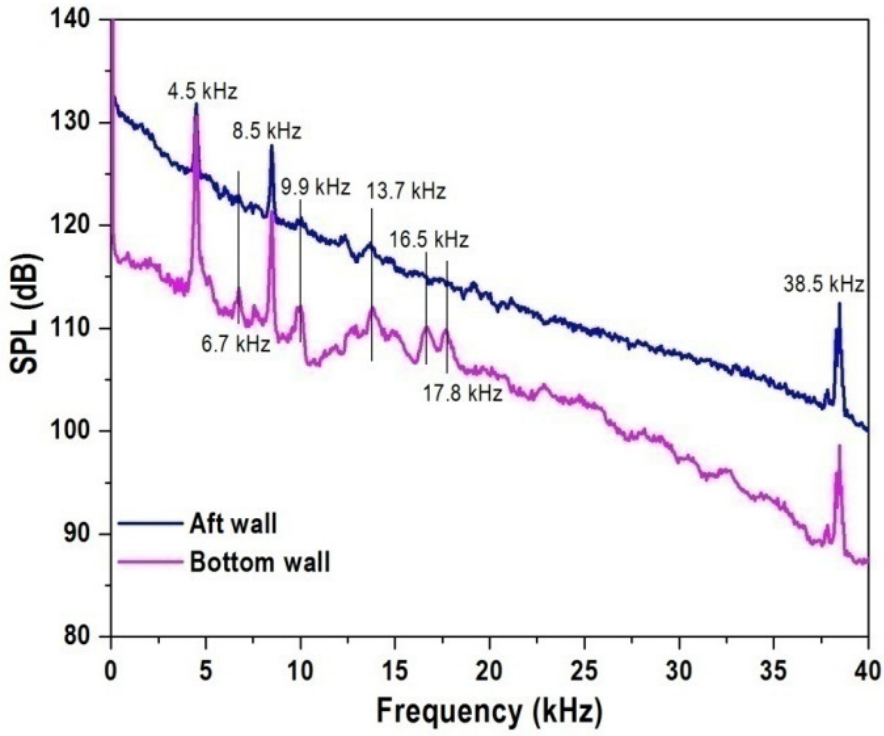

Fig. 4.30: Pressure spectra for $P_{01}/P_0 = 0.59$

Further increase in pressure ($P_{01}/P_0 = 0.63$) as presented in Fig.4.31, reveals that the pressure spectra has dominant modes/tone at discrete frequencies. This behavior can be explained through Fig.4.27 (f) where the cavity shear layer is not affected by the transient shock system. It allows the cavity shear layer to grow continuously and small scale eddies to become large-scale structures, which subsequently impinges at cavity aft wall. Thus, sharp amplitude modes/tones in the previous cases are disappeared instead, dominant modes/tones with flattened shapes at discrete frequencies are observed.

In order to examine whether any mode switching phenomena are present during transient starting process, modes/tones with different stagnation pressures are presented in Fig. 4.32. It is observed that undoubtedly there exists a mode-switching phenomenon.

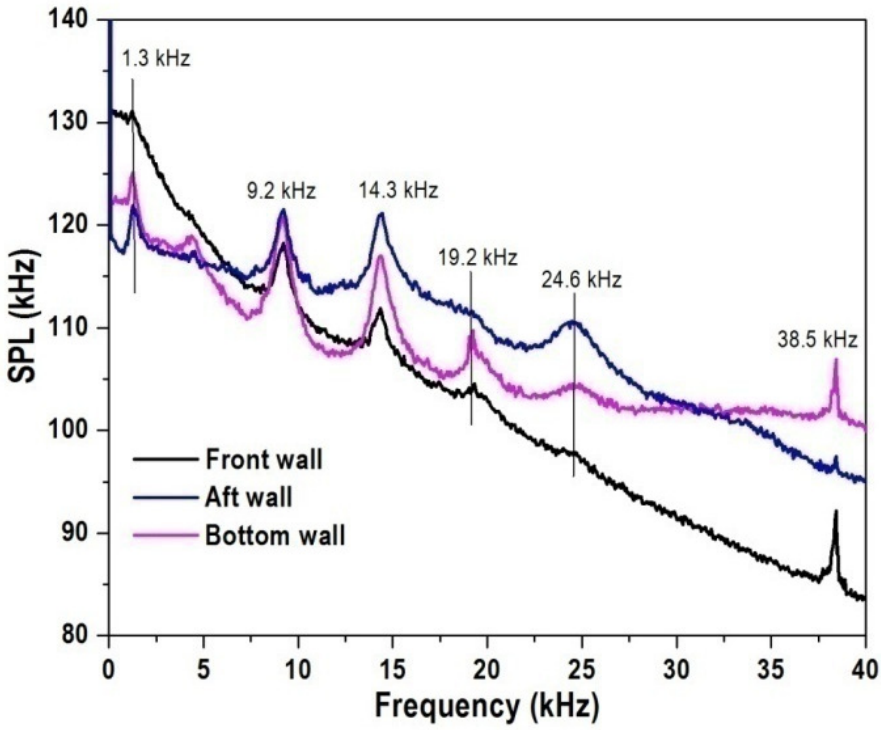

Fig. 4.31: Pressure spectra for $P_{01}/P_0 = 0.63$

At, stagnation pressures up to $P_{01}/P_0 = 0.59$, it is difficult to demark the mode switching phenomena but number modes/tones differ from various stagnation pressures. On the other hand, mode switching phenomena is seen from $P_{01}/P_0 = 0.59$ to $P_{01}/P_0 = 0.63$. The OASPL during transient starting process is shown in Fig.4.33.It is understood that the OASPL reaches to as high as 181 dB at cavity aft wall due to the stagnation pressure of $P_{01}/P_0 = 0.63$.

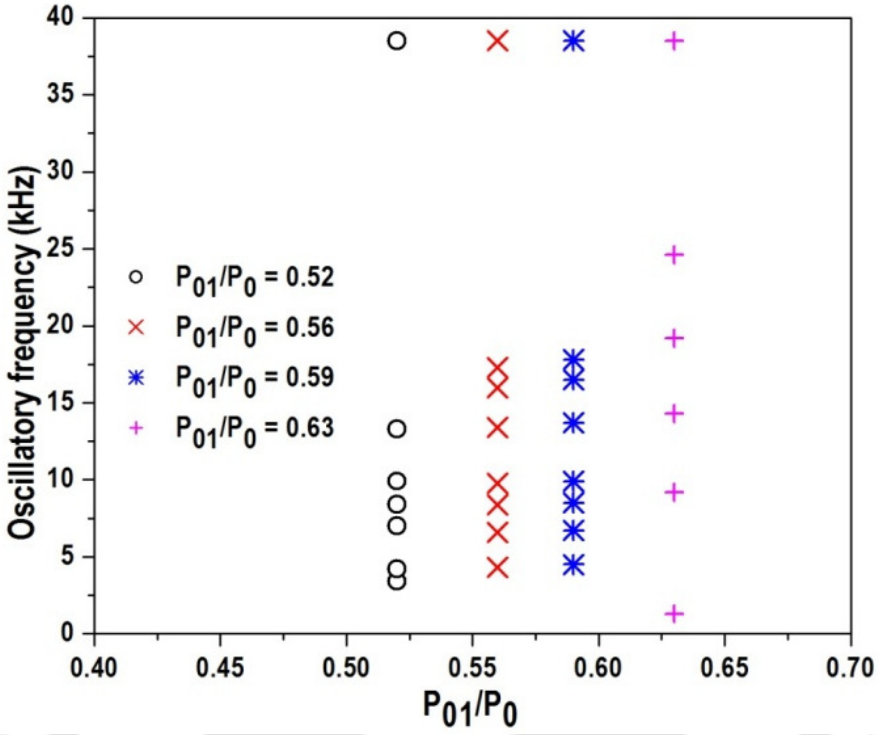

Fig. 4.32: Oscillatory modes for different transient starting pressures

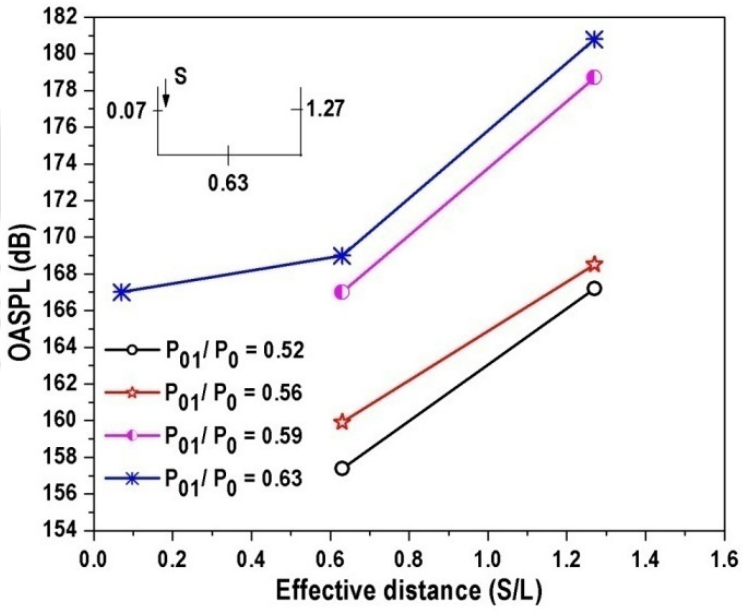

Fig. 4.33: OASPL levels during transient starting condition

4.2.1.3. *Case - III Transition flow from shallow open to shallow close cavities (6 ≤ L/D ≤ 10)*

Figures 4.34-4.36 show the transient starting characteristics of the cavities of L/D = 6, 7.5 and 10 respectively. These cavities are termed as transitional shallow cavities because the shear layer impinges at cavity floor under certain conditions and hence, it is inevitable to understand the flow features over such type of cavities. In the earlier cases, the cavity depth is kept constant and the length of the cavity is varied whereas, in the present studies, the length of the cavities remain unaltered (30mm) and the cavity depth is modified to achieve different L/D. Like all other cavities tested previously, these transitional shallow cavities also exhibit the flow features such as formation of bifurcated shock system, its interaction with boundary/shear layer, its associated shock train phenomena etc. Also, during transient starting process, the flow features evolved in the present studies (L/D = 6, 7.5 and 10) are quite similar to the earlier cases especially the structure of the bifurcated shock system, its propagation, boundary layer separation and shock train characteristics for different tunnel stagnation pressures (P_{01}/P_0 = 0.41 to 0.63). However, characteristics of cavity shear layer are different from the earlier cases. For L/D = 6, the shear layer is found to be attached at the aft portion of the cavity floor for P_{01}/P_0 = 0.52 and 0.59. Whereas, for other pressures (P_{01}/P_0 = 0.56 and 0.63), the shear layer impinges at cavity aft wall. Since, the transient process is highly unsteady, the chance of shear layer impinges the cavity floor is a random process due to the fact that the cavity (L/D = 6) posses the transition behavior. On the other hand, for L/D = 7.5, the shear layer impinges at cavity floor near the aft end corner for P_{01}/P_0 = 0.41 and 0.46. By increasing the pressure (P_{01}/P_0 = 0.52 to 0.63), the shear layer impinges on cavity floor at

halfway through the cavity length (increasing the pressure results in increase in length of separated region). In this case, the cavity experiences half closed due to partial impingement of the shear layer at cavity floor. For L/D = 10, the shear layer impinges on cavity floor near the leading edge for range of pressures (P_{01}/P_0 = 0.52 - 0.63).

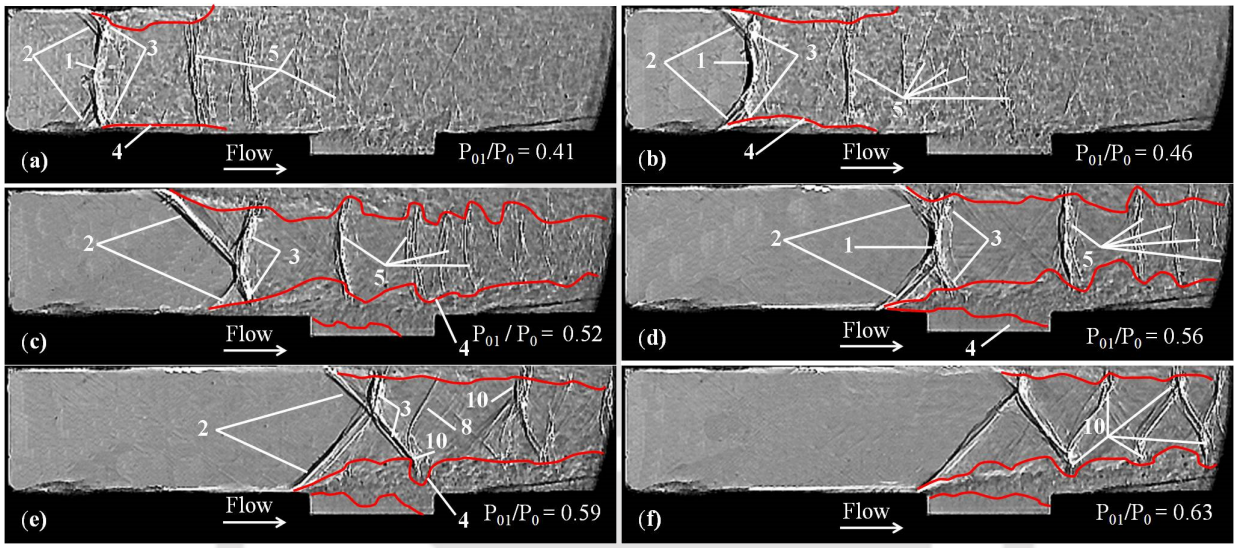

Fig. 4.34: Sequential images of transient starting shocks in a confined duct (L/D= 6)

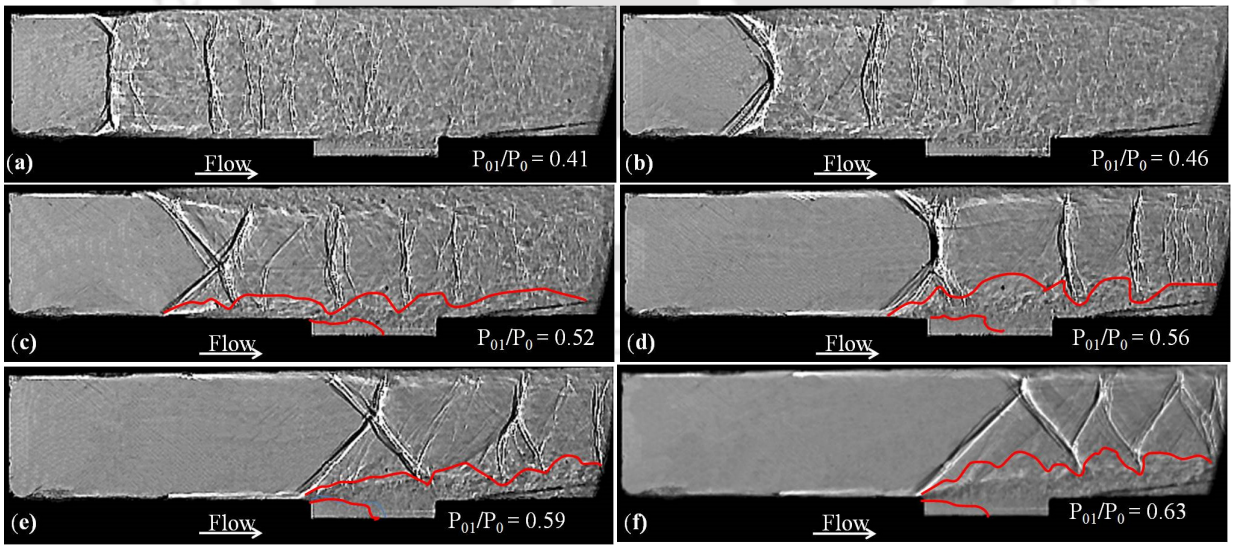

Fig. 4.35: Sequential images of transient starting shocks in a confined duct (L/D=7.5)

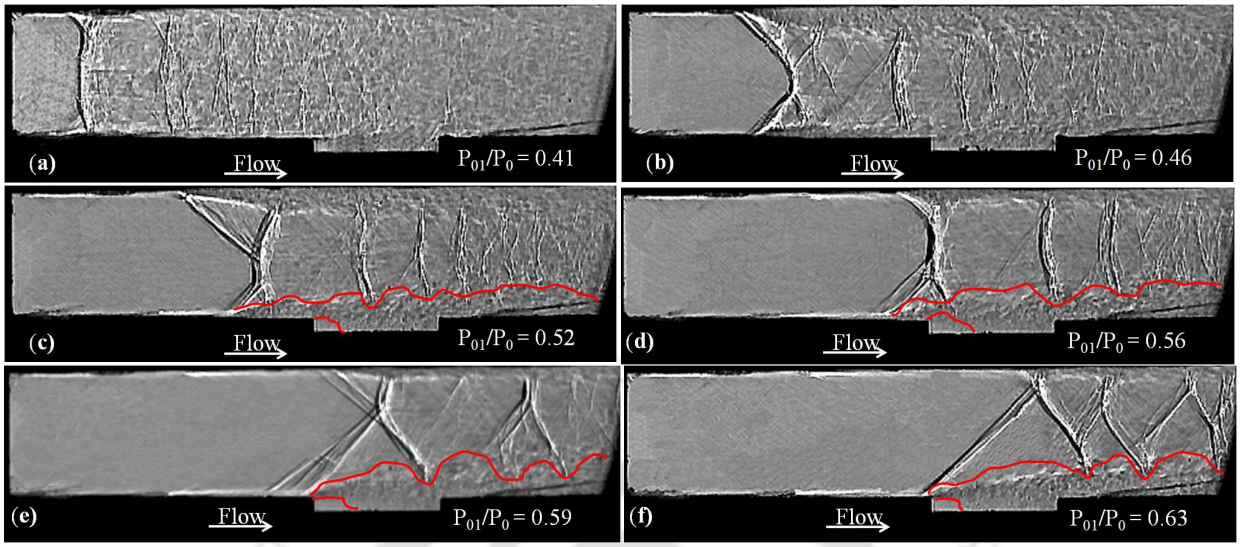

Fig. 4.36: Sequential images of transient starting shocks in a confined duct (L/D=10)

Thus, most of the cavity floor covered with shear layer, which amounts to a fully closed condition. In the case of cavities for transition from open to close, unsteady pressures are not measured which is be explained in chapter 7.

4.3 Summary

Experiments are carried out to bring out the effect of transient starting process for different cavities (L/D = 1 to 10) for the range of pressures (P_{01}/P_0 = 0.41 to 0.63) through high-speed shadowgraph images and unsteady pressure measurements. These cavities are categorized into three parts namely, transition from deep to shallow open cavities, shallow open cavities and transition from open to close cavities. The shadowgraph images revel the existence of bifurcated shock system and shock train phenomena. Also, the boundary/shear layer behavior is well captured during the transient starting process. Once the stagnation pressures are increased, the flowfield is getting evolved and the shock system along with the shock train interacts with cavity shear layer and produces modes/tones inside the cavity. The salient outcomes of the test results are summarized below.

1. The transient starting process test is carried out at discrete stagnation pressures. The rate at which the stagnation pressure increases continuously has negligible impact on the results.
2. For L/D = 2 to 5cavities, small amplitude modes/tones occur at different frequencies. Irrespective of the cavities, a mode/tone occurs at 38.5 kHz.
3. For L/D = 2, a mode switching phenomena is seen at pressure P_{01}/P_0 = 0.63. Whereas for L/D = 3, produces mode switching phenomena at P_{01}/P_0 = 0.41itself and continues the trend with increase in pressure ratio.
4. For L/D = 4, mode switching is seen beyond P_{01}/P_0 = 0.56 whereas, for L/D = 5, mode switching phenomena is observed at P_{01}/P_0 = 0.43.

5. During transient starting process, as the L/D ratio is increased, number of small amplitude modes/tones may also observed to be increased (Fig.4.37)
6. During transient starting process L/D =5 cavity experiences the OASPL as high as 181 dB. The transitional cavities (L/D = 2 and 3) shows the OASPL range from 134 to 170 dB while the shallow open cavities (L/D = 4 and 5) exhibit the OASPL of 155-181 dB (Fig.4.38).

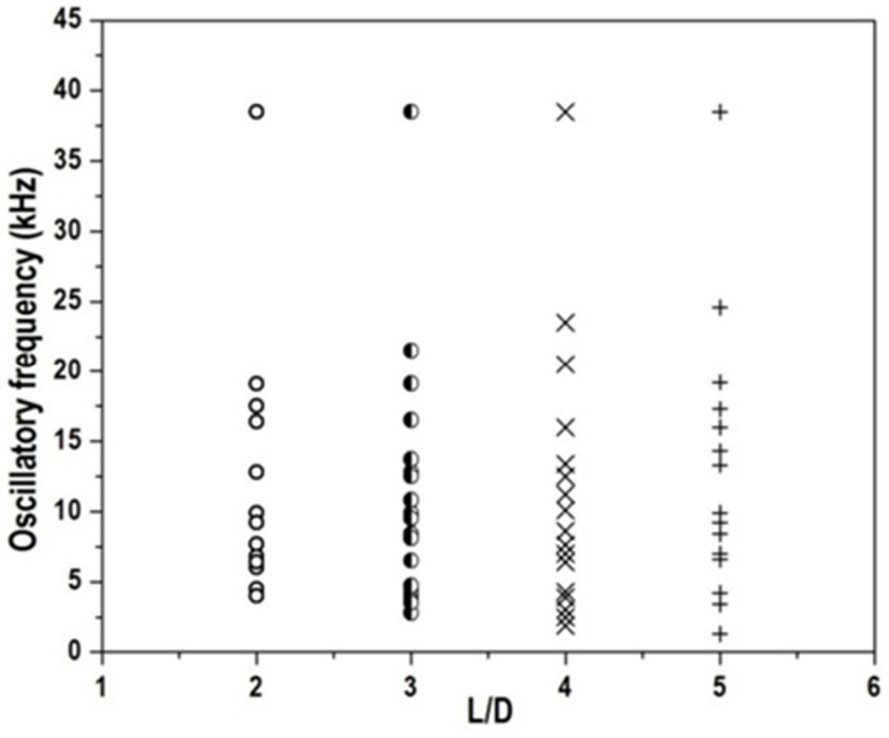

Fig. 4.37: Oscillatory modes during transient starting process for various L/D cavities

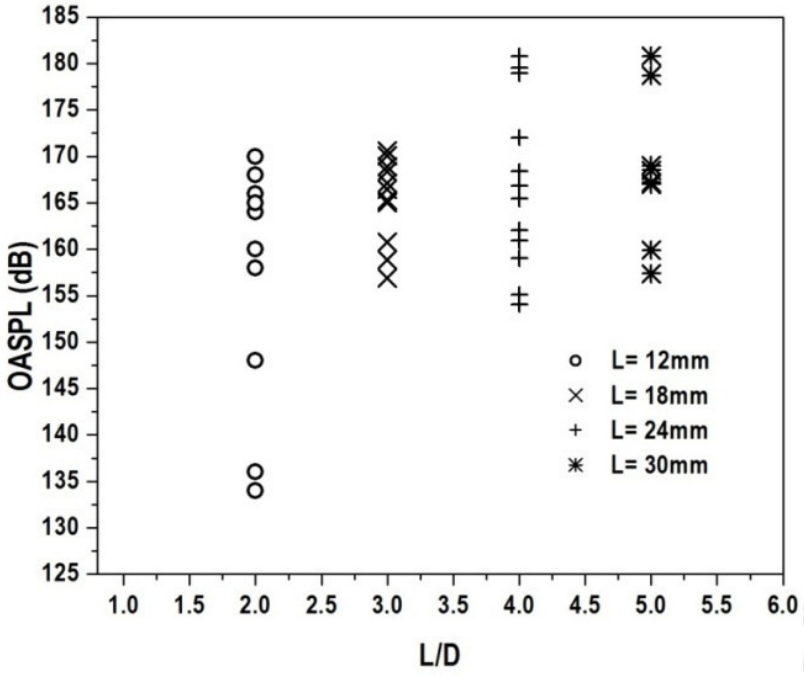

Fig. 4.38: OASPL values of various L/D cavities during transient starting process

CHAPTER 5

RESULTS AND DISCUSSIONS

ONSET OF CAVITY OSCILLATION FROM TRANSVERSE TO LONGITUDINAL MODE

5.1 Introduction

One of the pioneering works by Krishnamurthy [3] on supersonic flow over rectangular cutout demonstrates that the cavity oscillations may occur in any direction namely span wise, longitudinal and transverse depending upon L/D ratio. If L/D ≥ ~2, the cavity is expected to be dominated by longitudinal oscillation while, transverse oscillation becomes a dominant aspect of the cavity when L/D ≤ ~2. Hence, it is suggested that the transverse to longitudinal oscillation may occur at L/D ≈ 2. This is also observed by Chandra and Chakravarthy [102] for the range of L/D = 1.5 - 2 at supersonic flow where the Strouhal numbers (calculated based on the cavity length) are approximately constant. The transition of cavity oscillation from transverse to longitudinal direction is experimentally investigated by Zhang and Edwards [42] using interferogram and unsteady pressure measurements. It is indicated that the transition from transverse to longitudinal oscillation occurs between L/D = 1 and 2 at a free-stream Mach number of 1.5 and between L/D = 2 and 3 at a free-stream Mach number of 2.5. Recent experiments on transitional cavities [103] show changes in oscillation pattern from longitudinal mode to transverse mode when L/D ratio varies from 3.3 to 1.67 at supersonic flow, which is characterized by the presence of two oblique shocks at the trailing edge instead of one. The transition is found to occur between L/D of1.67 and 2, marked by a change in the feedback mechanism, resulting in a shift from the vortex

circulation driven transverse feedback mode to the oscillating shear layer driven longitudinal feedback mode.

In general, in spite of large amount of cavity flows are studied and addressed in supersonic flows, the transitional cavities are less explored. Hence, it is inevitable to understand the flow features of such transition from deep to shallow cavity in terms of their oscillatory modes. In this context, experiments are carried out for transitional cavities ranging from $1 \leq L/D \leq 3$. These cavities are characterized through time resolved schlieren images and unsteady pressure measurements. From time resolved schlieren images, dynamics of the vortex in the cavity shear layer and wave patterns around the cavity are studied. The extracted information from time resolved schlieren images are correlated to pressure spectra derived from unsteady pressure measurements. Further the modes/tones are compared with modified Rossiter empirical relation. In the present studies, the non-linear behavior of shear layer vortices is brought out and derived convective term. The pressure spectra and cross correlation between different pressure sensors inside the cavity are studied to understand the cause for the generation of modes/tones.

5.2 Flow features around cavity

Figure 5.1 depicts the flow features (schlieren pictures)around L/D = 1 cavity where Fig 5.1a represents 40000fps and rest of the images Fig. (5.1b-d) are taken at a rate of 125000fps. It may be seen that the cavity is driven by a thick shear layer marked in red color. and characterized by a single vortex, which has symmetry. However,

outside the cavity (Fig.5.1-b) two waves namely "type – *I* and *III"* are seen which are originated from cavity leading and trailing edges due to shear layer flapping and its impingement at cavity aft wall. The enlarged view of the cavity (Fig.5.1-c) reveals two waves and the shape is resembles like V- shape structure. It is a typical signature of a transverse mode of cavity oscillation, which has not been reported in literature, but only the schematic representation [42] is presented. The blown-up view in Fig.5.1-d indicates the trailing shock (type - *III*) is accompanied by two waves where one wave is due to shear layer re-attachment and the root cause for the existence of other wave may be presumed due to shear layer disturbances upstream of the cavity trailing edge. Hence, the L/D = 1 cavity is influenced by only the transverse mode of oscillation.

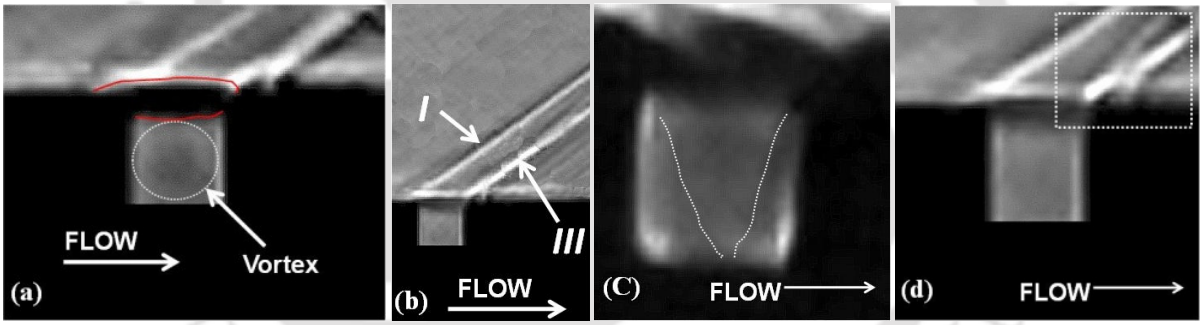

Fig. 5.1: Flow features of L/D =1 cavity: (a) 40000 fps; (b-d) 125000 fps.

The flow field inside the cavity for L/D = 2 and 3 are presented through schlieren pictures in Fig.5.2. These cavities are driven by a thick shear layer along with two vortices. In the former case (L/D =2), a large vortex is occupied immediately downstream of the cavity front wall whereas, near cavity aft wall, there exists a small vortex. This is a classical example of transitional cavities where both transverse as well as longitudinal modes are present in which longitudinal mode is expected to be

dominant. Conversely, though L/D = 3 cavity exhibits two vortices, unlike the L/D = 2 cavity, a large vortex is seen adjacent to the cavity aft wall while near the front wall, a small vortex is captured. This shows the L/D = 3 cavity possesses only the longitudinal mode of oscillation.

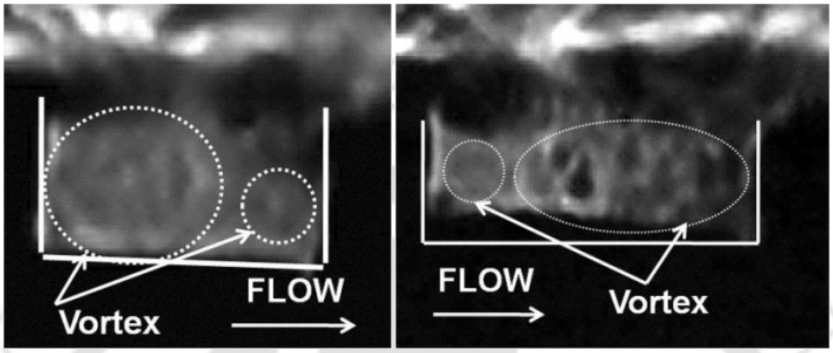

Fig. 5. 2: Flow structure inside L/D = 2 (left) and L/D = 3 (right) cavities – 40000fps

5.3 Non linear characteristics of cavity shear layer

The wave features and the flow characteristics of the cavities (L/D = 2 and 3) for one vortex shedding cycle captured through time resolved schlieren images at 125000 fps are shown in Figs. 5.3 and 5.4. All the schlieren images under fully established supersonic state are acquired for 4 seconds that leads to 500000 images. The definition of one vortex shedding cycle is the time taken by a shear layer vortex to travel from cavity leading edge to its trailing edge. To derive the timing from schlieren, enormous amount of effort is put in and confirmed the authenticity of the time. In Fig. 5.3, for L/D = 2 cavity, one vortex shedding cycle completes in a time period of 40 μs and each frame in a cycle has an elapsed time of 8 μs. In this case, number of vortex shedding cycles is approximately 83333. Figure 5.3 (a) shows the flow features at t = 0s where, a vortex (V_C) in the current shedding cycle is just initiated at cavity leading edge and at the same

time, another vortex (V_P) is observed at cavity trailing edge which is generated in the previous vortex shedding cycle. Based on number of schlieren images (100 averages), the core of the vortex (point V_C) is calculated to be 1.2 mm. The flow features outside the cavity show various wave structures due to flapping of shear layer and vortex convection in the shear layer. These waves are characterized into different types depending upon the characteristics of the cavity shear layer. Type - *I* wave is generated at cavity leading edge due to shear layer flapping. This can be either shock or expansion wave based on whether the shear layer is flapped up or down. In the present case (Fig. 5.3-a), the shear layer is flapped up and hence, a shock wave (type-*I*) is generated. Type - *II* wave is generated due to shear layer vortex that disturbs the supersonic free stream leads to formation of a shock wave. In the present case, two vortices namely V_C and V_P are prevailed in the shear layer and their associated shocks (type – *II* waves) are captured. Also, when type – *II* waves interact with type – *I* wave; a lambda (λ) type shock structure is formed. At cavity trailing edge, the shear layer impinges partially (partial clipping) and hence, type – *III* wave is generated. Finally, due to the reattachment of shear layer downstream of the cavity trailing edge produces a reattachment shock (point R). Inside the cavity, some waves are seen due to freestream entrainment between shear layer vortices designated as type – *V* waves which are responsible for the generation of number of modes/tones in the cavity.

At t = 8 μs (Fig. 5.3b), the vortex (V_C) in the current vortex shedding cycle is about to grow in size while the vortex (V_P) in the previous vortex shedding cycle is found to be partially covering the cavity trailing edge. Other flow features are similar to the

earlier case except the downward movement of type – *II* wave due to vortex convection where

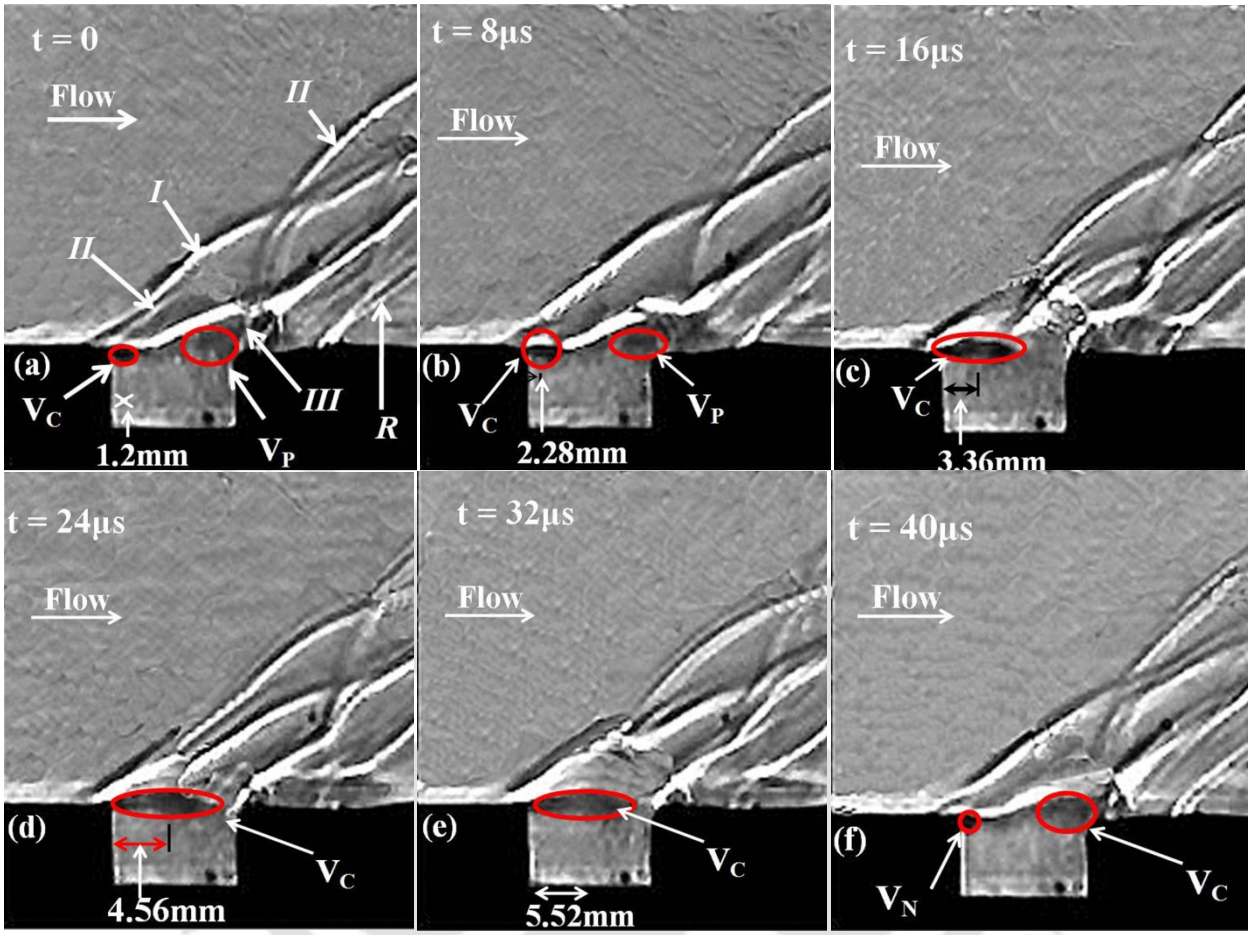

Fig. 5.3: Schlieren flow visualization around L/D = 2 cavity at 125000 fps

the core of the vortex (V_C) moves to 2.28 mm downstream of the cavity leading edge and the corresponding vortex speed is calculated to be 135 m/s. Similarly, at t = 16, 24 and 32 µs (Figs. 5.3c-e), the flow features are quite similar as discussed in the earlier cases except the vortex convection and the type – *I wave*. In these cases, the vortex core from cavity leading edge is measured as 3.36, 4.56 and 5.52mm respectively which corresponds to the vortex speed of 135, 150 and 129 m/s. Based on 100 vortex shedding cycles, the uncertainty in the vortex speed is calculated to be ± 40 m/s. At t =

40 µs (Fig. 5.3-f), shear layer is deflected upward leading to generation of a shock wave (type – *I*) at cavity leading edge. In this case, there are two vortices observed in the shear layer where the vortex (V_C) in the current vortex shedding cycle reaches the cavity aft wall while, a vortex (V_N) in the next vortex shedding cycle is just originated at the cavity leading edge. It may be concluded that the vortex convection in the cavity shear layer for one vortex shedding cycle is observed to be non-linear.

The cavity bearing L/D = 3, exhibits two vortices and the shear layer characteristics are different from earlier case as shown in Fig. 5.4. In this case, time taken by the vortex from cavity leading edge to trailing edge is 56µs. Figure 5.4a shows three vortices in the shear layer at t = 0 s, where vortex (V_C) in the current vortex shedding cycle is in the vicinity of cavity leading and the core of this vortex (V_C) is at a distance of 3.1 mm. The other two vortices (V_P) from the previous vortex shedding cycle are positioned downstream. At t = 8 µs (Fig. 5.4b), the vortex core (V_C) in the current vortex shedding cycle is at 5.27mm and the corresponding vortex speed calculated is ~271m/s based on time- distance method. It is noticed that one of the two vortices (V_P) in the previous vortex shedding cycle disappears due to convection and hence, one vortex (V_P) is seen. At t = 24 µs, the vortex (V_C) core in the current vortex shedding cycle is approximately at the centre of the cavity (9.22mm) and the vortex speed is ~247 m/s. At the same time, a new vortex (V_N) is formed just downstream of the cavity leading edge in the next vortex shedding cycle and the vortex (V_P) in the previous vortex shedding cycle is at the cavity trailing edge. At subsequent instants correspond to t = 40, 48 and 56 µs (Fig. 5.4d-f), the vortex (V_C) in the current vortex shedding cycle grows

in size and reaches cavity trailing edge. The distance of the vortex (V_C) core in the current vortex shedding cycle at t = 40and 48 µs, is observed to be 13.8and 15.9 mm from cavity leading edge and the vortex speed is ~305 and 263m/s respectively.

In general, shear layer impingement at cavity aft and generation of type – *V* waves due to entrainment of free stream flow inside the cavity between shear layer vortices produces cavity modes/tones. The type – *V* waves depend on number of vortices generated which are not necessarily always observed in the optical images due to its strength. If the strength of these waves are strong, it can be viewed in the images and vice versa.

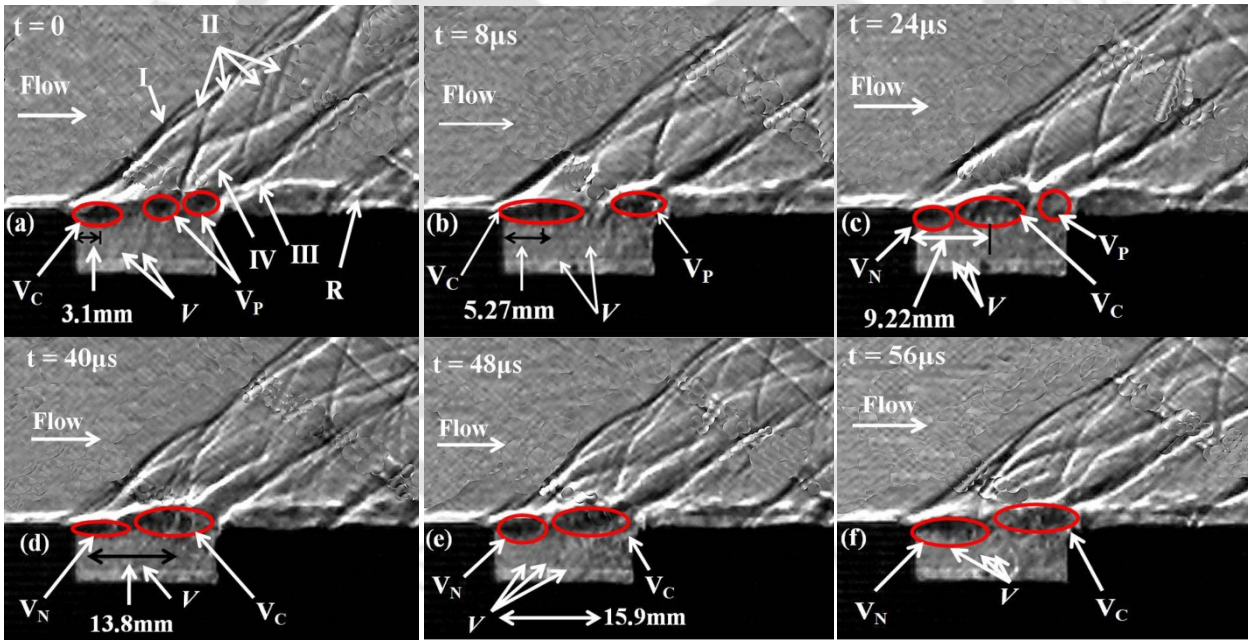

Fig. 5.4: Schlieren visualization around L/D = 3 cavity at 125000 fps

The vortex generation mechanism is due to perturbation generated by the interaction between shear layer and wave. This wave is generated because of shear layer impingement at cavity aft wall, which moves upstream inside the cavity and

perturbs the shear layer. The perturbation acts like a spoiler and trip the shear-layer flow to form small scale eddies. These eddies under the influence of clockwise rotational components produced by high-speed free stream, becomes a large-scale structure, which is a random process and accelerates under the action of centripetal force. The size and speed of these large-scale structures vary for different vortex shedding cycles resulting in a non-linear behavior. Based on above discussions, the vortex speed in the shear layer for L/D = 2 and 3 cavities presented in Fig. 5.5 reveals that the vortex speed is non-linear. In both cases, initially the vortex speed is decreased and then recovered to a maximum value followed by a decreasing trend. The initial decreasing trend is due to perturbation and the increasing trend is owing to the action of centripetal force. Once the large-scale vortex attains its maximum size of the order of shear layer thickness, the speed is affected due to its inertia, which is observed from the decreasing trend.

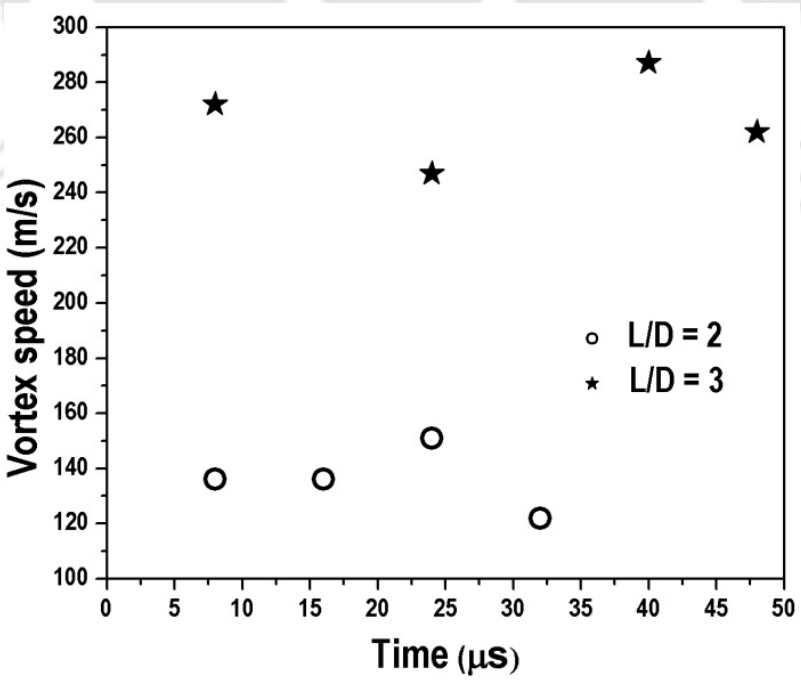

Fig. 5. 5: Vortex convection speed

5.4 Unsteady pressure spectra

Pressure spectra inside the cavities (L/D = 1, 2 and 3) at three locations namely front, bottom and aft walls using Fast Fourier Transform are presented in Figs.5.6-5.8. The pressure spectra for L/D = 1 cavity (Fig.5.6) shows small amplitude modes/tones less than 10 kHz frequency range. These modes/tones indicate the presence of both transverse as well as longitudinal oscillations which is supported by the schlieren shown in Fig.5.1. Here, a single vortex and a V shape wave structure is seen inside the cavity. On the other hand, a discrete mode/tone is seen at 19.1 kHz frequency. The pressure spectra at the bottom wall sensor shows higher magnitude as compared to other locations whereas, the aft wall sensor possesses low amplitude, which is contrary to the expected trend. This may be due to overriding of transverse oscillation as compared to longitudinal oscillation.

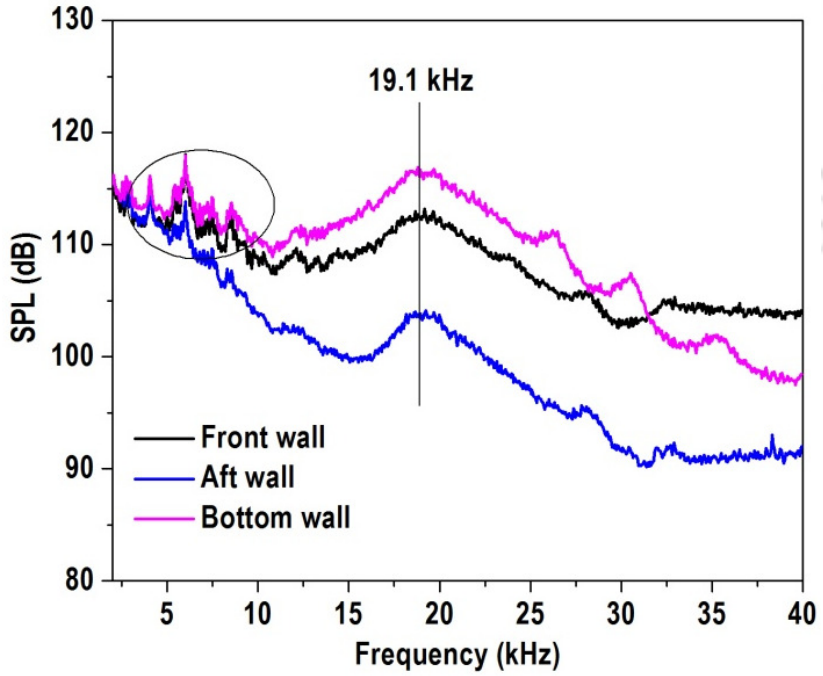

Fig. 5.6: Pressure spectra of L/D = 1 cavity

For L/D = 2 cavity (Fig.5.7), dominant mode/tone of large amplitude occurs at 21.8 kHz whereas, medium amplitude modes/tones prevail at frequencies 11.2 and 34 kHz for all sensors which indicate global instability. This may be due to shear layer impingement and wave generation at cavity aft wall as well as the type *V* wave due to free stream entrainment between shear layer vortices. However, around 3.9 and 7.6 kHz, low amplitude multiple peaks are seen at all the sensor locations which is due to transverse oscillation. By carefully analyzing the pressure spectra, one can conclusively ascertain that the cavity unsteadiness is primarily dominated by longitudinal oscillation accompanied by a subtle transverse oscillation. Based on the results, it can be concluded that the transition of oscillation from transverse to longitudinal direction occurs beyond L/D = 2.

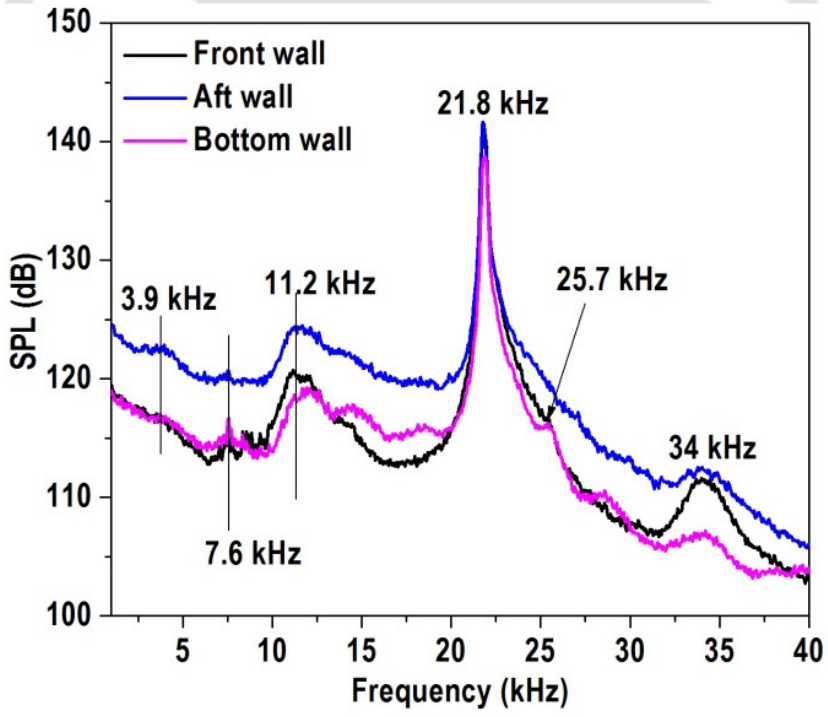

Fig. 5.7: Pressure spectra of L/D = 2 cavity

Figure 5.8 demonstrates five modes/tones for L/D = 3 cavity at discrete dominant frequencies irrespective of sensor locations. These modes/tones are mainly due to shear layer impingement at cavity aft wall, pressure wave generation as a consequence of shear layer impingement and waves generated inside the cavity due to freestream entrainment between the shear layer vortices. Since the pressure spectra does not contain any small scale fluctuation, it indicates that the cavity oscillation is purely longitudinal. Hence it may be concluded that the transition of oscillation from transverse to longitudinal mode occurs between L/D = 2 to L/D = 3 for the given length and depth of the cavity.

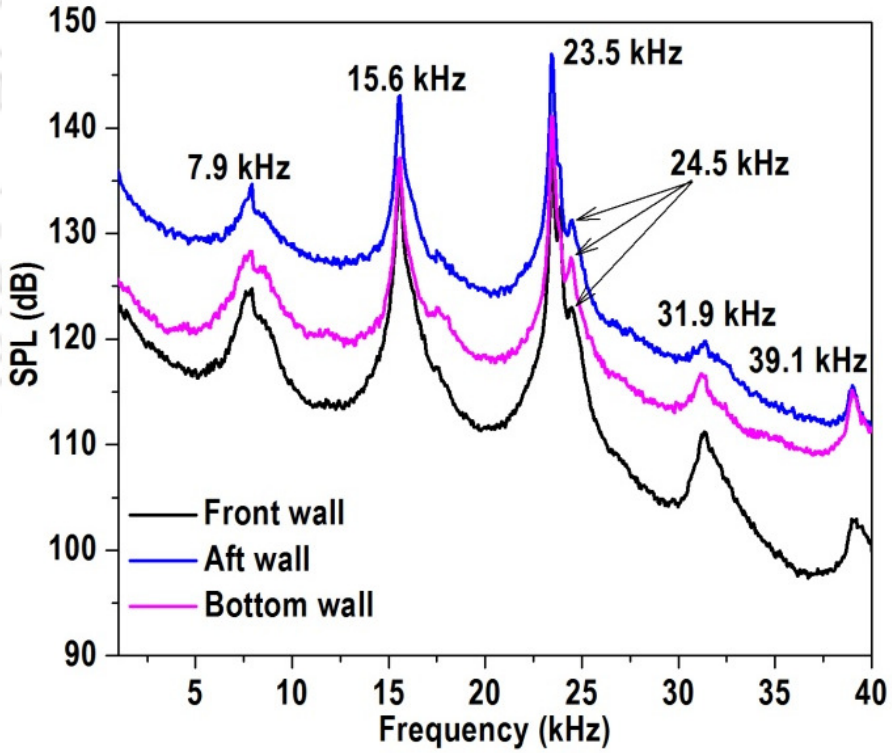

Fig. 5.8: Pressure spectra of L/D = 3 cavity

5.5 Characteristics of cavity oscillation from transverse to longitudinal mode

In order to explain the transition of cavity oscillation from transverse to longitudinal mode, pressure spectra at cavity bottom wall is presented for L/D = 1, 2 and 3 in Fig. 5.9. For L/D=1 cavity, multiple small amplitude peaks are observed below 10 kHz and hence, the cavity oscillations are determined by transverse oscillations. Similarly, for L/D = 2 cavity, dual oscillations (around 7 to 9 kHz) are observed along with a discrete mode/tone at 21.8 kHz. Though both the oscillation modes are stay alive in this case, transverse oscillation is suppressed by the longitudinal oscillation. Once L/D is increased to 3, dominant modes at discrete frequencies (without small amplitude fluctuations at low frequency) are seen.

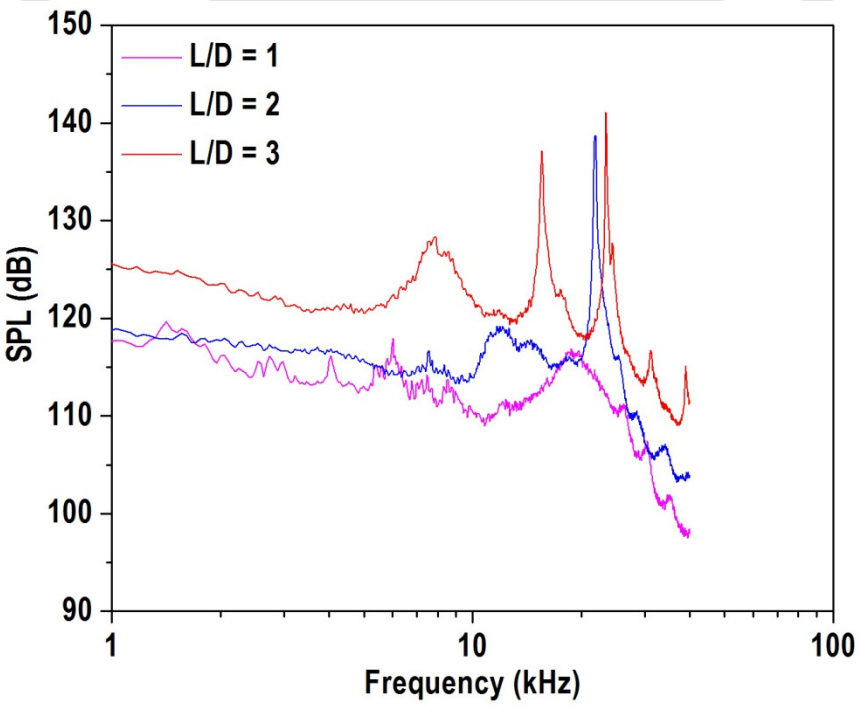

Fig. 5.9: Pressure spectra at bottom wall of the cavity

This indicates that the oscillation is purely in longitudinal direction. From bottom wall pressure spectra, it is clear that the transition of oscillation mode from transverse to longitudinal direction occurs between L/D = 2 to 3 at M = 1.8. Earlier studies [42 and 103] demonstrated that the mode transition occurs between L/D = 1 and 2 for M = 1.5 and 2.5 respectively while at M = 2.5, the transition occurs between L/D = 2 and 3. Thus the mode transition depends upon free stream Mach number, length and depth of the cavities, on coming boundary layer, etc.

The root mean square (rms) of the unsteady pressure for different cavities (L/D ratios) gives a measure of onset of transition from transverse to longitudinal oscillation. Earlier studies [42] revealed a sharp rise in the rms pressure during transition of oscillatory mode from transverse to longitudinal. In this context, the rms pressure for different cavities (L/D = 1 to 3) are plotted in Fig. 5.10 along with the literature results [42].

It is observed that the trend is exactly captured whereas; their values are different due to variation in the free stream Mach number. In the present case, free stream Mach number is 1.8 while in the literature [42], two Mach numbers namely 1.5 and 2.5 are used. The present results are in between these values suggesting that the generated results are trustworthy. From L/D = 1 to 2, a sharp increase in the fluctuating pressure is observed due to transverse mode of cavity oscillation. Between L/D = 2 to 3, the magnitude of the rms pressure decreases and at L/D = 3, the value is found to be low. This indicates that the L/D = 3 cavity experiences longitudinal mode of oscillation. Since

the studies are not covered for various L/D ratios between 2 and 3, the exact L/D ratio at which the transition occurs could not be pinpointed. Nevertheless, the transition occurs between L/D of 2 and 3 at a free stream Mach number of 1.8.The magnitude of rms pressure is expected to decrease continuously with increase in L/D ratio.

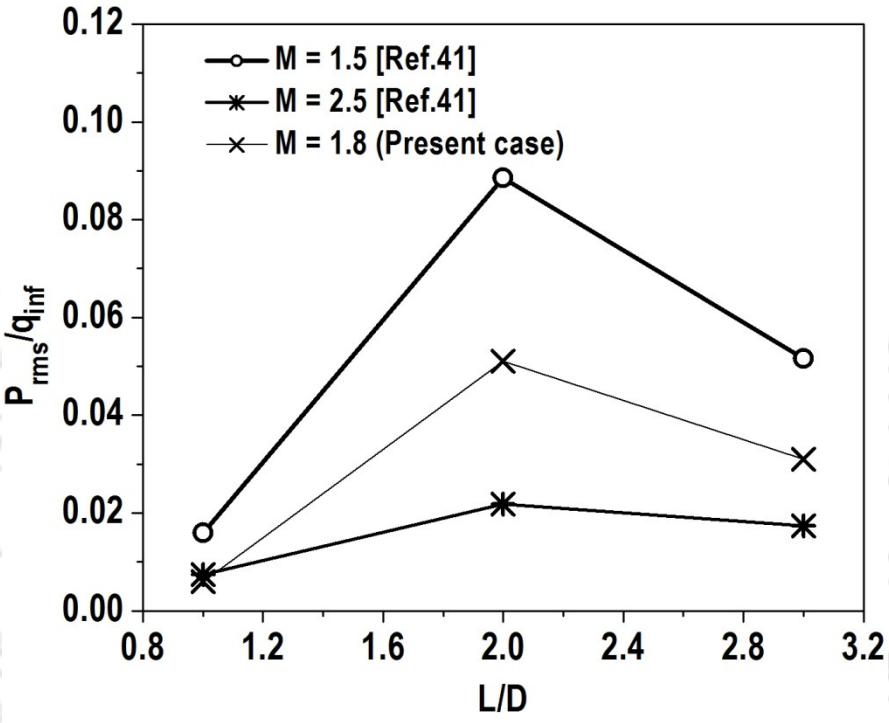

Fig. 5.10: Root mean square values at cavity bottom wall.

The drag may be calculated from pressure difference between front and aft wall of the cavity. The drag coefficients of the tested cavities are presented in Fig. 5.11 along with the literature results [42]. The results are closely matching with the literature values at M = 2.5. Since the transition occurs near L/D = 2, the drag coefficient is increased due to momentum as compared to L/D = 1 cavity. On the other hand, L/D = 3 cavity is in the early state of longitudinal oscillation that dictates the mass and momentum balance of the cavity. In this cavity, the front wall experiences low pressure due to momentum

diffusion whereas, the aft wall is in the state of high pressure due to direct impingement of the shear layer. Hence, recompression of the flow and large downward deflection of the shear layer near the aft wall causes an increased dynamic pressure towards the stagnation point which leads to increase in drag.

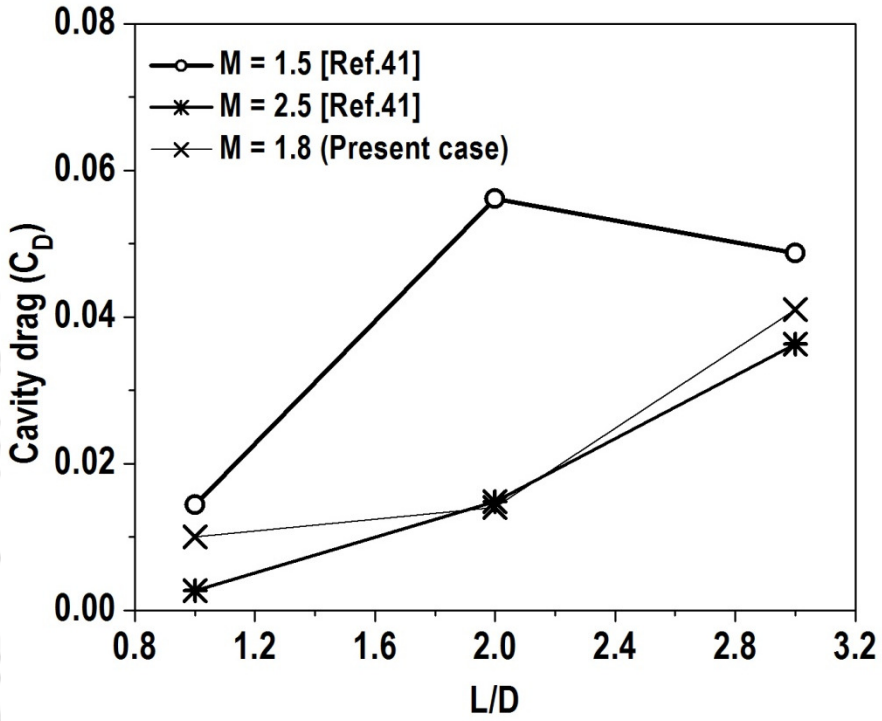

Fig. 5.11: Variation of cavity drag with respect to (L/D).

5.6 Oscillation modes/tones of cavities - a comparison with Modified Rossiter relation

Generally, cavity modes/tones are compared with modified Rossiter relation [31]. Rossiter made a basic assumption to predict cavity frequencies is that the vortex shedding phenomena is periodic. Based on time resolved schlieren images, it is ascertained that the vortex shedding is not periodic. At any instant of time, the vortex shedding appears to be random. However, generation of vortex due to several

hundreds of small-scale structures over the time appears to be a periodic. With this background, modes/tones of the cavities (L/D = 2 and 3) derived from unsteady pressure measurements and experimentally generated *k* value from schlieren images are compared with modified Rossiter [31] relation.

For one vortex shedding cycle, the convective speed of the vortices is calculated based on free stream velocity of 486 m/s. For L/D = 2, the values of *k* for one vortex shedding cycle are found to be 0.28, 0.28, 0.31 and 0.25 with an average value of 0.28 (Table.5.1). Similarly, the *k* values for L/D = 3 are calculated to be 0.56, 0.51, 0.59 and 0.54 with an average of 0.55 (Table.5.2).

Table.5.1 Comparison of Strouhal number for L/D = 2

Cavity modes (m)	Expt. Unsteady pressure	Modified Rossiter relation [31]	Experiment (From schlieren images)				
		K = 0.57	**K1 = 0.28**	**K2 = 0.28**	**K3 = 0.31**	**K4 = 0.25**	**K_{avg} = 0.28**
1	0.11	0.24	0.15	0.15	0.16	0.14	0.15
2	0.28	0.55	0.36	0.36	0.38	0.32	0.36
3	0.54	0.87	0.55	0.55	0.59	0.51	0.55
4	0.84	1.19	0.76	0.76	0.81	0.69	0.76

Table.5.2 Comparison of Strouhal number for L/D = 3

Cavity modes (m)	Expt. Unsteady pressure	Modified Rossiter relation [31]	Expt. (From schlieren images)				
		K = 0.57	**K1 = 0.56**	**K2 = 0.51**	**K3 = 0.59**	**K4 = 0.54**	**K_{avg} = 0.55**
1	0.29	0.24	0.24	0.22	0.24	0.23	0.23
2	0.58	0.56	0.55	0.52	0.57	0.54	0.54
3	0.87	0.87	0.87	0.82	0.89	0.85	0.86
4	1.18	1.19	1.18	1.12	1.21	1.15	1.17
5	1.45	1.51	1.50	1.41	1.53	1.46	1.48

For L/D = 2 cavity (Fig. 5.12), prediction based on modified Rossiter relation indicates a maximum deviation as high as 42% at higher mode/tone as compared to unsteady pressure measurements while, experimentally generated k_{avg}= 0.28 through schlieren images matches within 9.5%. The large deviation using modified Rossiter relation is attributed due to the fact that L/D = 2 cavity undergoes transition from transverse to longitudinal oscillation in addition to non-linear vortex convection phenomena. On the other hand, though non-linear vortex convection is captured in the schlieren images, the effect of mode transition from transverse to longitudinal oscillation is not precisely captured in the schlieren images which leads to the deviation of 9.5% against the unsteady pressure results. The comparison of modes/tones in terms of Strouhal number (St_n) for L/D = 3 cavity is presented in Fig.5.13. It is observed that both modified Rossiter relation as well as experimentally generated values through schlieren images are well within 4 and 2.5% respectively as compared unsteady pressures. In this case match is fairly good due to the fact that the cavity experiences only the longitudinal mode of oscillation. Since the non-linear vortex convection is not included in the modified Rossiter relation, its value is higher than the experimentally generated schlieren results where the non linearity is accounted.

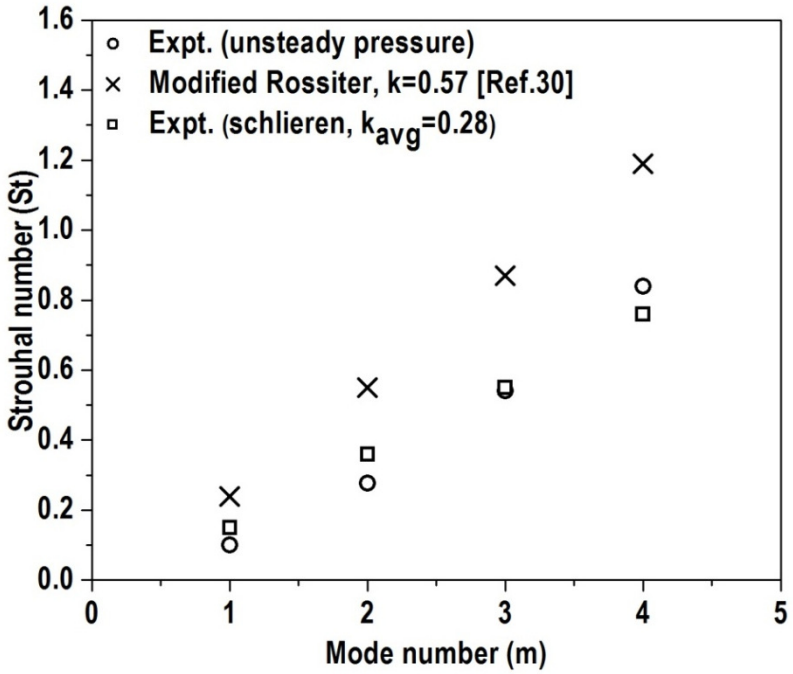

Fig. 5.12: Strouhal number comparison (L/D = 2)

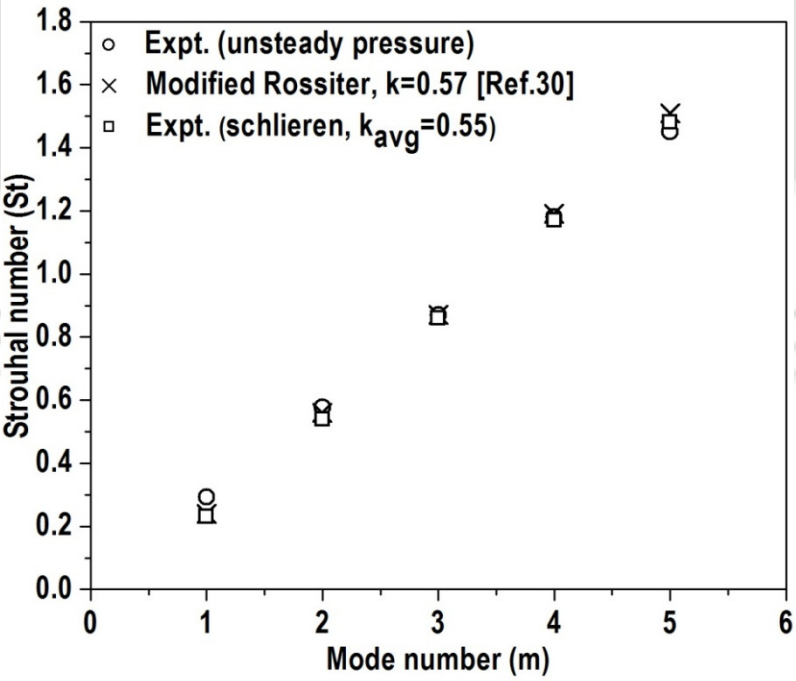

Fig. 5.13: Strouhal number comparison (L/D = 3)

5.7 Cross correlation of unsteady pressures

Inside the cavity, multiple sensors are kept and data acquired simultaneously to get the cavity oscillation. Thus, a relation among the sensors location may be established through cross correlation. Figures 5.14-5.16 show the normalized cross correlation plot of L/D = 1, 2 and 3 cavities against time lag. Cross correlation between two signals is the “time lag” between two measured peaks converted into frequency domain. For example, Fig 5.16, the time lag between second and third peak is 45 µs, which correspond to a frequency of 22.2 kHz. It represents 3rd mode/tone of the cavity oscillation. The plots contain auto correlation of aft wall sensor (correlation of aft wall sensor with itself) and cross correlation between aft and front wall sensors to get insight into the wave propagation inside the cavity as well as the cause for the generation of modes/tones. When cross-correlation is compared with autocorrelation, it gives the phase difference between waves from trailing edge and leading edge. The time (in µs) for cross-correlation may be chosen depending upon the information choice of scale in the processing software (MATLAB). Since, the source for cavity oscillation is due to shear layer impingement at cavity aft wall, the cavity aft wall sensor is taken as the reference (auto correlation of cavity aft wall). On the other hand, cavity front wall sensor certainly responds to the cavity oscillation and hence, it is cross-correlated with aft wall sensor.

The cross correlation plot for L/D = 1 cavity presented in Fig. 5.14 shows auto correlation of the aft wall sensor is maximum at time t = 0s followed by an attenuation in the signal. Similarly, the cross correlation between front and aft wall sensors are derived

which indicates that they are poorly correlated. On the other hand, L/D = 2 and 3 cavities show the existence of cross correlation. During entire duration, the signals are sinusoidal in nature and hence, a short time from -50μs to250μs in the correlation, is considered to explain the phenomena. For L/D = 2 as shown in Fig. 5.15, the auto correlation and the cross correlation clearly demonstrate that the wave generated and reflected from aft and front walls is almost in phase with each other. The time lag between two consecutive peaks in the cross correlation as well as in the auto

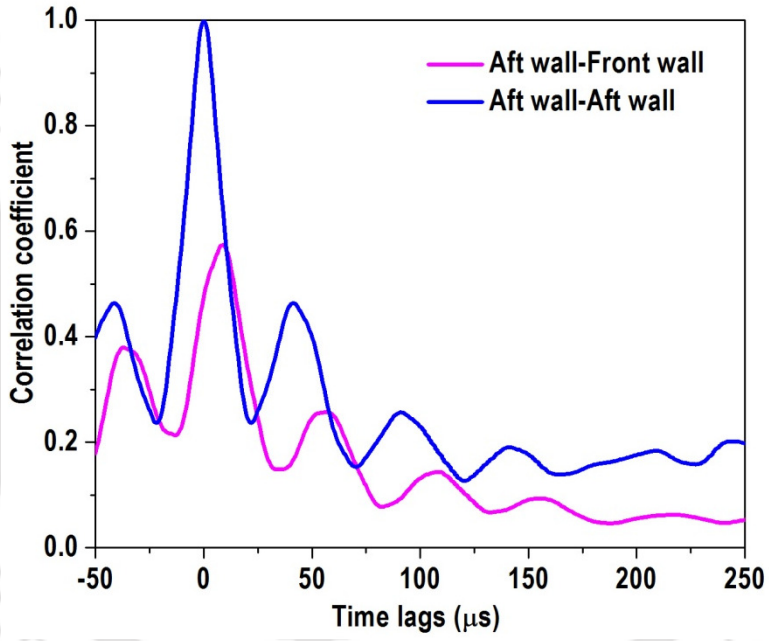

Fig. 5.14: Cross correlation for L/D = 1 cavity

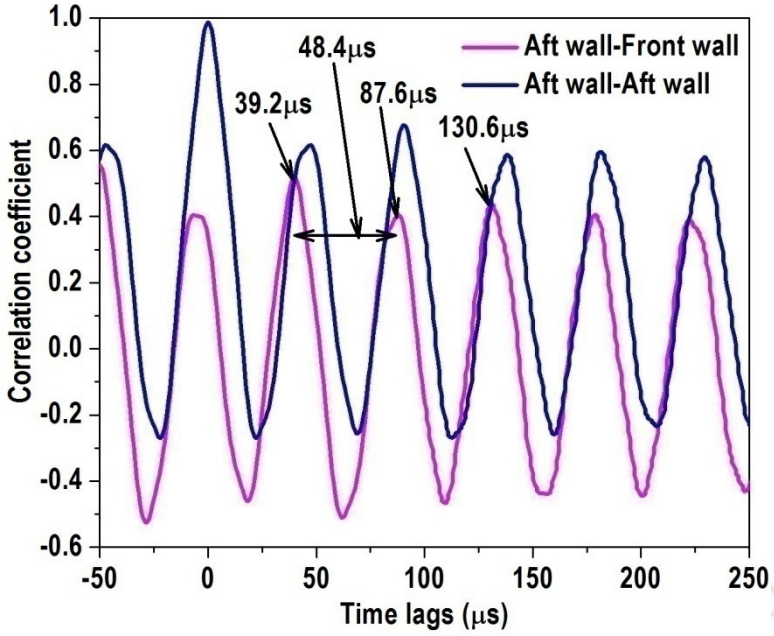

Fig. 5.15: Cross correlation for L/D = 2 cavity

correlation is found to be 48.4μs that corresponds to 20.7 kHz which is the dominant mode/tone of the cavity (i.e. 4th mode/tone of the cavity). In cross correlation, there are three peaks which are repeating during entire time. The 3rd peak occurs at a time lag of 130 μs which is the pressure pulse generated due to shear layer impingement at cavity aft wall. The corresponding frequency calculated through equn.5.1 is 3.85 kHz which is the 1st mode/tone of the cavity oscillation.

$$f = \frac{v}{\lambda} = \frac{v}{2L} \tag{5.1}$$

Where, f is the frequency (Hz), L is the cavity length (m) and λ is the wave length which is equal to 2L. Since the wave propagates back and forth inside the cavity, the wave length (λ) is equal to 2L. The 2nd peak in the cross correlation occurs with a time lag of 87.6 μs which correspond to the vortex impingement time at the cavity aft wall and the

corresponding frequency is 11.4 kHz (which is calculated through equn.5.2).This is the 3rd mode/tone of the cavity oscillation.

$$f = \frac{v}{\lambda} = \frac{v}{L} \tag{5.2}$$

The 1st peak in the cross correlation indicates a time lag of 39.2 μs which corresponds to the frequency of 25.5 kHz .This corresponds to the sub mode/tone of the cavity oscillation.

Examining L/D = 3 cavity (Fig. 5.16), the autocorrelation coefficient is maximum when the cross-correlation coefficient is minimum, and vice versa, which suggests that the wave generated at the trailing edge wall and the wave reflected from the front wall are out of phase by 180°. Here also, three peaks are seen which is repeating during entire time. The time lag between two peaks is 45 μs and the frequency calculated is 22.2 kHz which is the 3rd mode/tone of the cavity oscillation. The 3rd peak in the cross

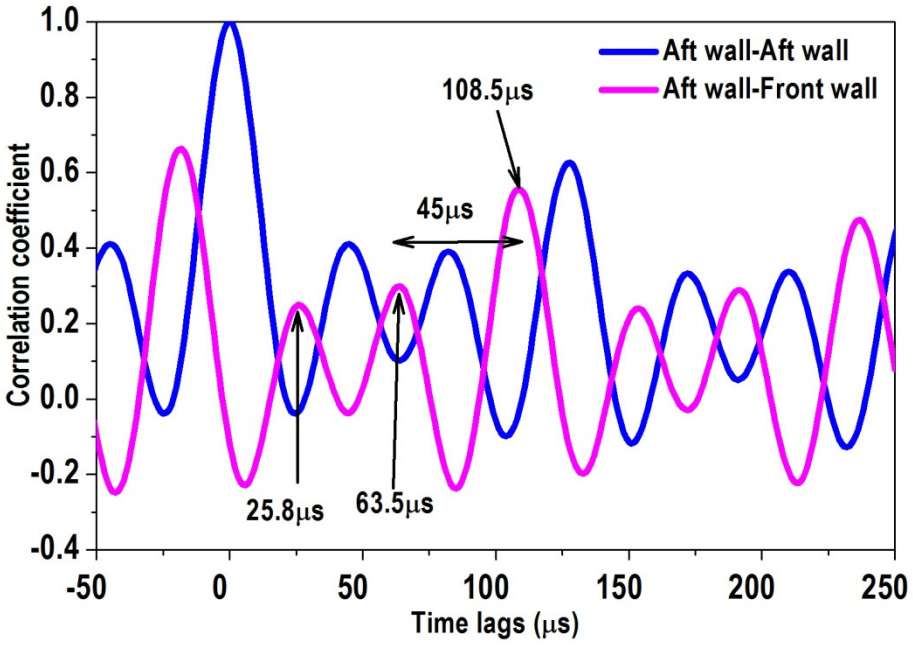

Fig. 5.16: Cross correlation parameter for L/D = 3 cavity

correlation occurs at a time lag of 108.5 μs and the corresponding frequency is 4.6 kHz which is close to the 1st mode/tone of the cavity. This first mode tone is due to wave propagation. The 1st and 2nd peaks correspond to a time lags of 25.8 and 63.5 μs lead to the frequencies of 38.6 and 15.7 kHz which are related to 5th modes/tone and 2ndmode (due to shear layer impingement) of the cavity oscillations respectively.

5.8 Coherence coefficient

Coherence of two signals gives an insight into the similarity between the signals in frequency domain. If the coherence coefficient between two signals is high, then common source/phenomena is responsible for both the signals. Figure 5.17 show the coherence coefficient of unsteady pressure signals between cavity front, bottom and aft walls for L/D = 1 cavity. In this case, the coherence coefficient doesn't have sharp peaks which indicate they are less cohesive.

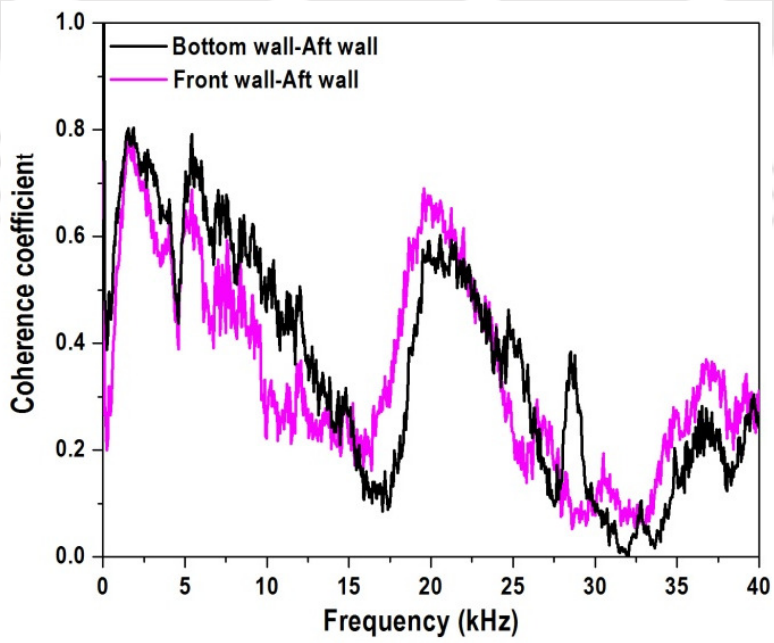

Fig. 5.17: Coherence coefficient between pressure signals (L/D = 1)

On the other hand, for L/D = 2 (Fig.5.18) moderate coherence coefficients exist at 1st and 2nd modes/tones. In the case of 2nd mode/tone a sharp feature is seen while the 1stmode/tone coherence coefficient is not as sharp as second mode. For L/D = 3, as shown in Fig.5.19 high values of coherence coefficients exists in dominant modes (2nd and 3rd modes/tones). Hence, it is believed that the source/phenomena for the pressure peak at a given location inside the cavity are also responsible for the pressure peak at other locations. This is mainly due to the generation and upstream movement of a wave (type – *V* wave). Hence, the sensors located at different locations inside the cavity pick up almost the same pressure signals due to the movement of these waves. Hence high values of coherence coefficients are observed in 2nd and 3rd modes/tones at dominant frequencies.

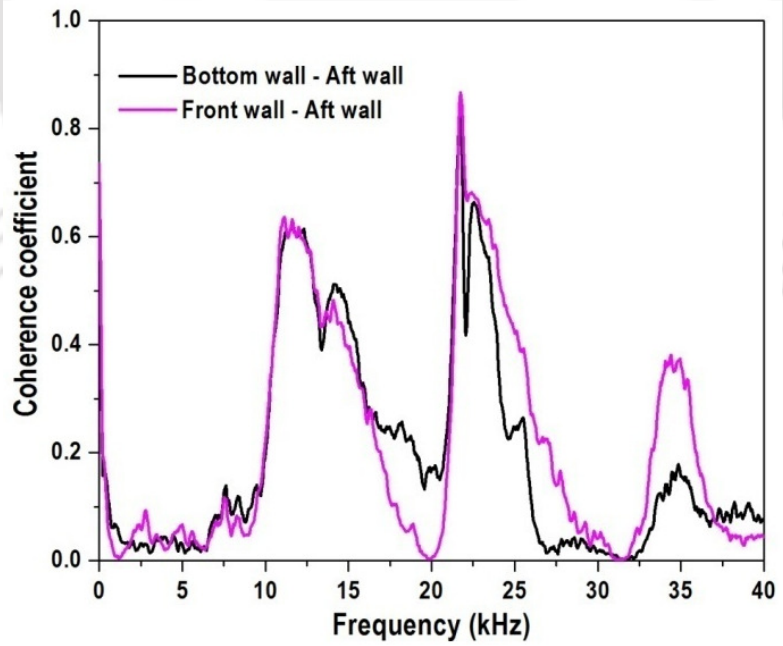

Fig. 5.18: Coherence coefficient between pressure signals (L/D = 2)

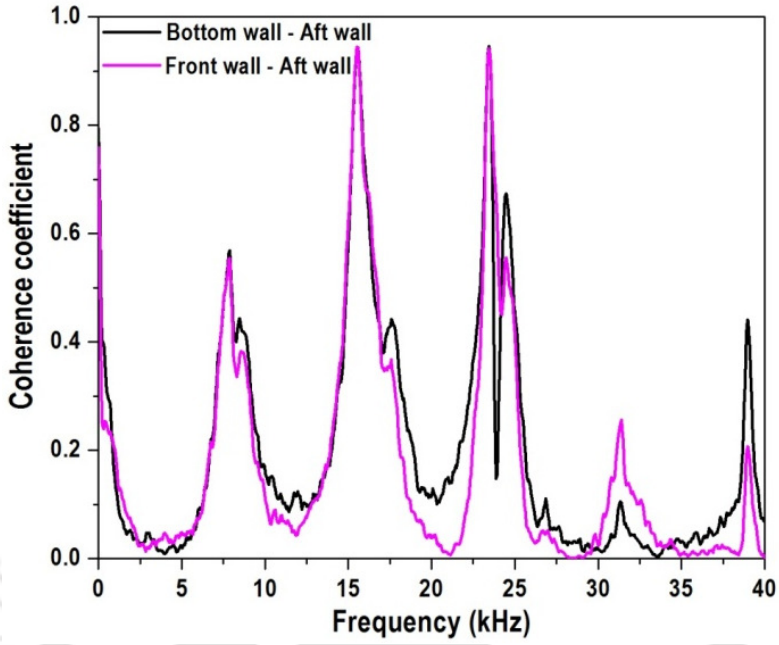

Fig. 5.19: Coherence coefficient between pressure signals (L/D = 3)

This corroborates the existence of feedback mechanism and resonance inside the cavity. The broadband oscillations in the coherence coefficients are due to vortices and mass entrainment inside the cavity.

5.9 Spectrogram

The plot of sound pressure level with frequency depicts the distribution of acoustic energy in terms of frequencies. In order to understand the temporal information of the acoustic energy such as existence of the dominant modes/tones for the entire time, spectrogram is derived from unsteady pressure signals using short time Fourier transformation. Figures 5.20-5.22 show the spectrogram images for L/D = 1, 2 and 3

cavities at three locations namely front, bottom and aft walls of the cavity which are represented by a, b and c respectively. For L/D = 1 (Fig.5.20), the spectrogram images for all locations show broad band for the entire duration of acquisition while dormant signature is observed at higher frequencies. Three modes/tone are captured for L/D = 2 (Fig.5.21) where, 3rd mode/tone is found to be more dominant which is indicated by a sharp and strong signal throughout the sampling time of 4s indicate that the energy content is high. Though, occurrence of 3rd mode/tone signal exists throughout the time, the strength is reduced intermittently and the signal level is close to noise. Whereas, other modes/tones are seem to be feeble and the strength of the signal is found to be weak. For L/D = 3 (Fig.5.22), spectrogram of front, bottom and aft walls show strong signals of the 1st, 2nd and 3rd modes/tones, among which 2nd and 3rd modes/tones exhibit sharp features. However, the 3rd mode/tone contains the sub-tone which is corroborated through pressure spectra as shown in Fig.5.8. In the present studies, though the signals indicate the existence of the mode/tone and their strength throughout the test time is same, it does not convey whether the mode switching mechanism is there or not.

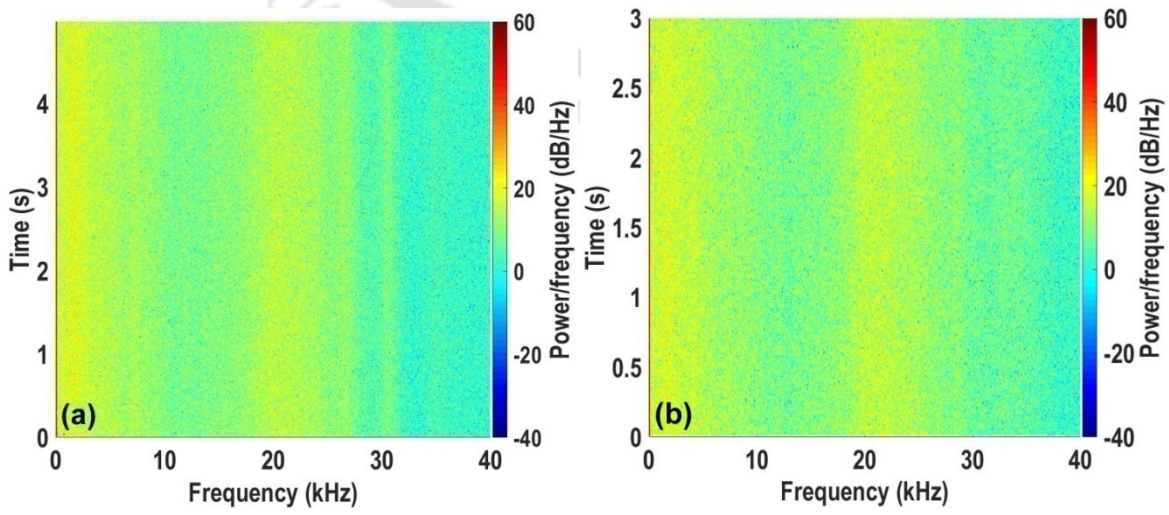

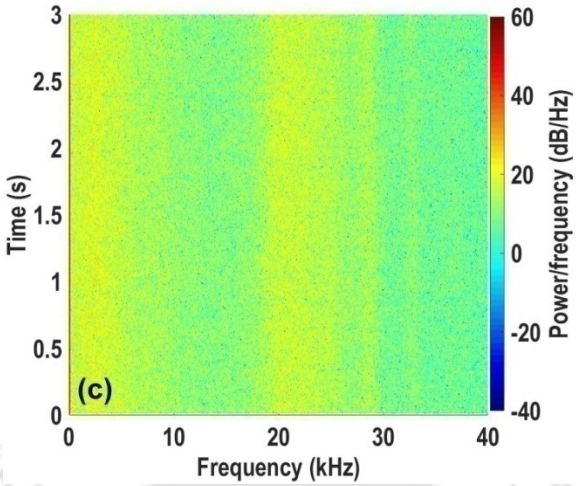

Fig. 5.20: Spectrogram for L/D = 1 (a-front wall, b-bottom wall, c-aft wall)

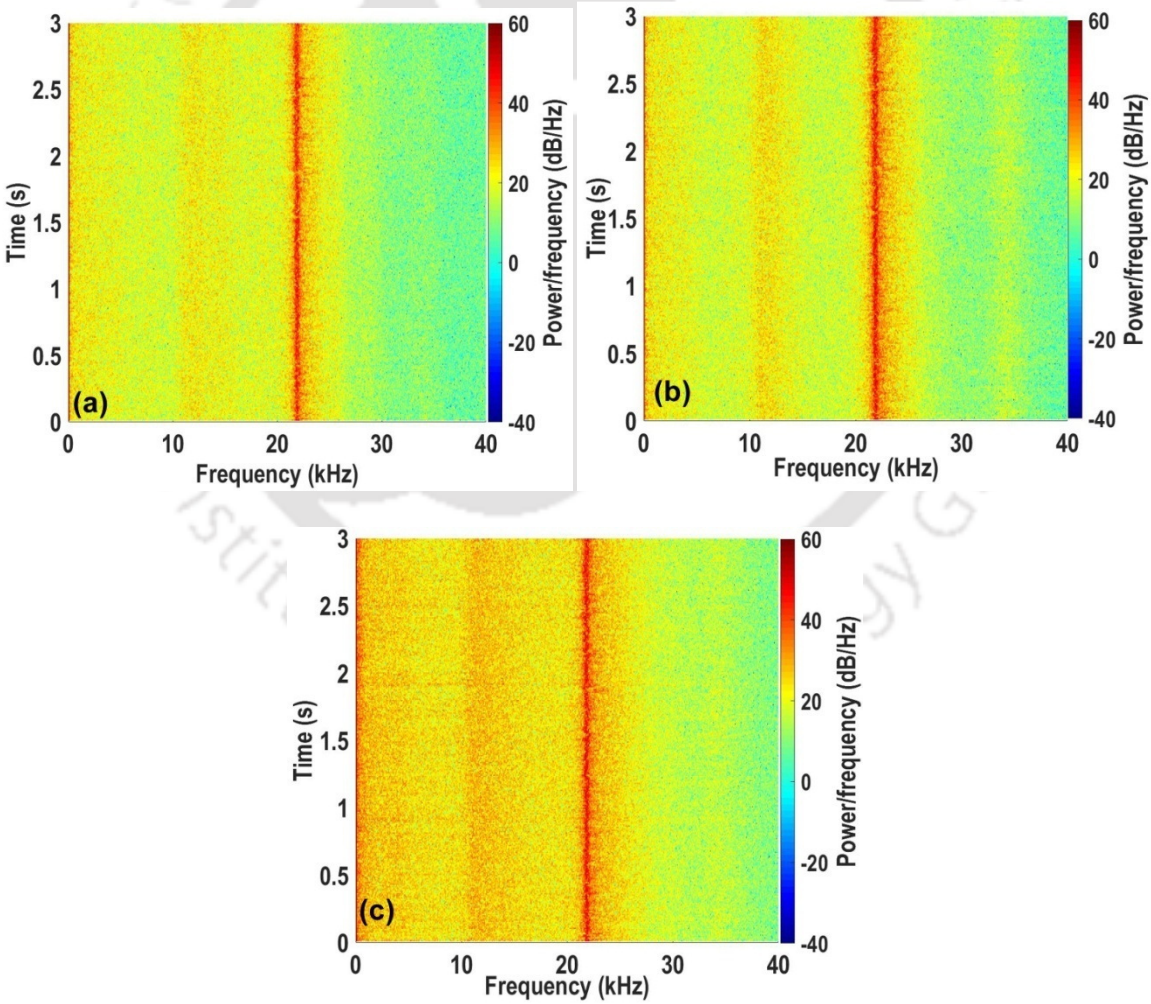

Fig. 5.21: Spectrogram for L/D = 2 (a-front wall, b-bottom wall, c-aft wall)

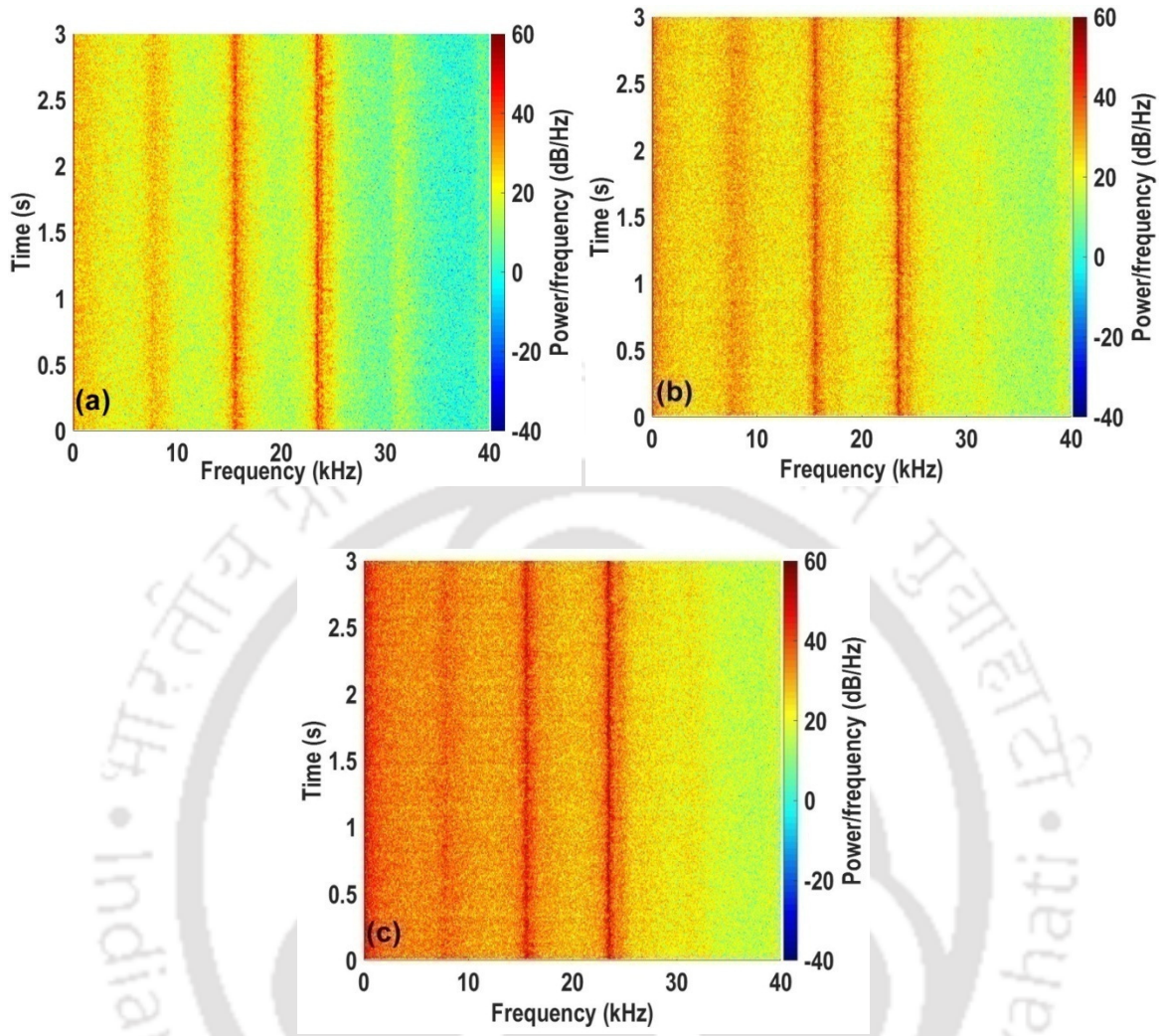

Fig. 5.22: Spectrogram for L/D = 3 (a-front wall, b-bottom wall, c-aft wall)

5.10 Wavelet transform

Figures 5.23-5.25 show the wavelet power spectra for L/D = 1, 2 and 3 cavities as a function of time and frequency at cavity aft wall for a sampling time of 0.1s. Since the cavity is driven by a thick shear layer that impinges at cavity aft wall, the same is used as a source. The Morlet wavelet coefficients corresponding to 81 scales (ranging from 1563 to 40,000 Hz) are considered in the present study where all the modes/tones experienced by the cavity are within this range. The x axis represents time in second

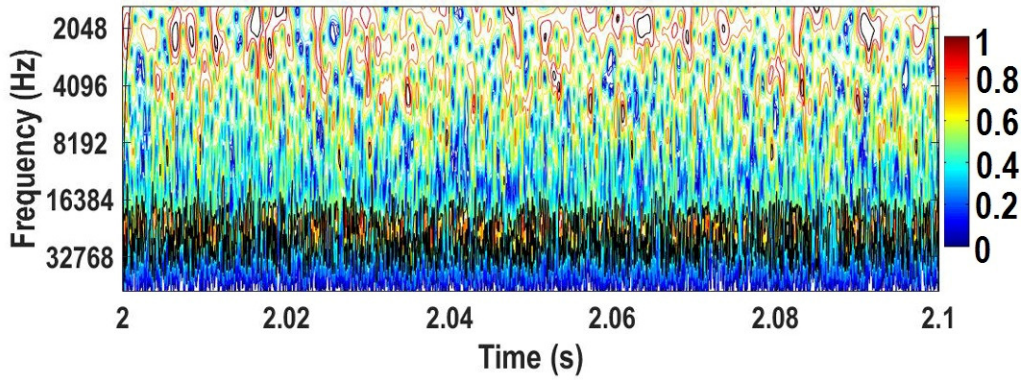

Fig. 5.23: Aft wall wavelet spectra for L/D = 1

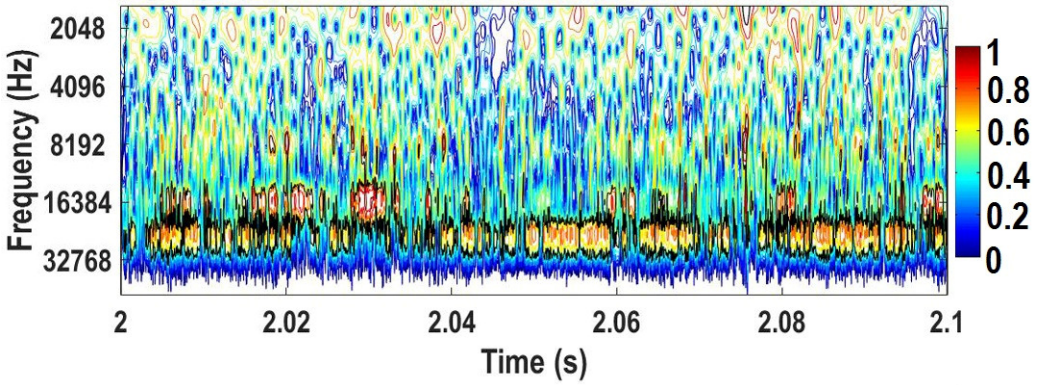

Fig. 5.24: Aft wall wavelet spectra for L/D = 2

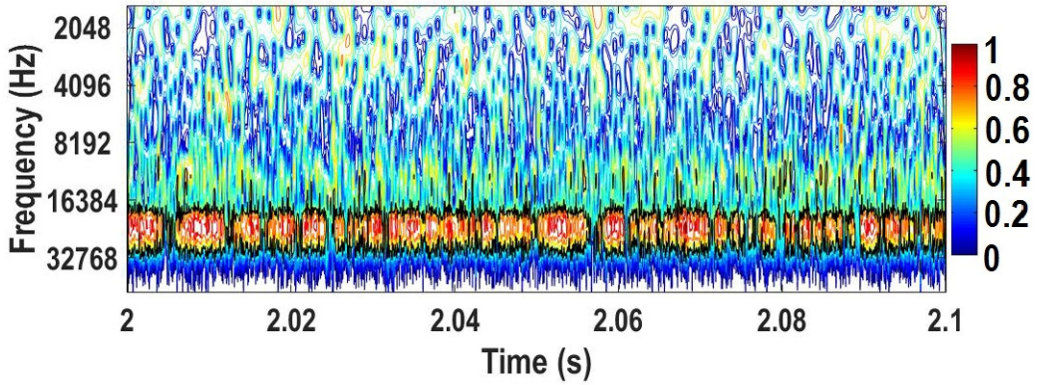

Fig.5.25: Aft wall wavelet spectra for L/D = 3

whereas the y axis represents frequency in Hz. The color bar represents the magnitude of the wavelet coefficients. Wavelet coefficient is nonzero if there is a fluctuation at given scale (frequency band) in the associated time window and the value is zero if

there is no fluctuation. For L/D = 1 (Fig..5.23), only at high frequencies (19.1 kHz) the wavelet coefficient shows a sporadic distribution of energy events. For L/D = 2 cavity (Fig. 5..24), wavelet spectra indicate a mode/tone switching phenomena between 2nd and 3rd mode/tone due to dual nature of transverse as well as longitudinal modes . At certain incidences, when 3rd mode/tone is present, 2nd mode/tone is absent and vice versa. Alternatively, both the modes/tones are either present or absent at other definite periods. In the present case, the cavity experiences cyclic oscillation of unsteady pressures during most of the time while it is reasonably quiet at other periods in terms of mode/tone switching is concerned. For L/D = 3 cavity (Fig. 5.25), the mode/tone corresponds to 23.5 kHz is seen in the wavelet spectrum whereas feeble information is observed at 11.2 kHz. In most of the time, the spectrum at 23.5 kHz shows high-energy events with intermittent distribution of low energy events.

5.11 Summary

Experimental investigations are carried on supersonic flow (M = 1.8) past cavities (L/D = 1, 2 and 3) with a fixed depth (D = 6mm) and varying lengths (L = 6, 12 and 18mm) to study their oscillation characteristics from transitional to longitudinal mode. The flow features are obtained by time resolved schlieren images and unsteady pressure measurements. The cavity modes/tones are compared with modified Rossiter relation. In-depth analyses are carried out in terms of instantaneous images, FFT, cross correlation and wavelet transform. The conclusions based on tested cavities are presented here.

1. For short cavity (L/D = 1), the oscillation mode is primarily in the transverse direction which is marked by the presence of a single vortex and ascertained through a typical V- shape wave signature inside the cavity.
2. As the cavity length is increased (L/D = 2 and 3), two vortices are observed. For L/D = 2 cavity, a large vortex as well as a small vortex is observed near front and aft walls respectively and the pressure spectra shows dual mode of oscillations around 7 to 9 kHz along with discrete modes/tones at 11.2 and 21.8 kHz. This indicates the existence of both transverse and longitudinal mode of oscillations which is evident from rapid increase in the rms pressure value between L/D = 1 and 2. For L/D = 3, the flow features inside the cavity are marked by a large vortex near cavity aft wall and a small vortex adjacent to the front wall. The pressure spectra reveal only dominant modes/tones at discrete frequencies. This shows that L/D = 3 cavity is driven by longitudinal mode of oscillation which is corroborated to low rms pressure. It can be concluded that the transition of cavity oscillation from transverse to longitudinal mode occurs between $2 \leq L/D \leq 3$.
3. The discrete frequencies correspond to dominant modes/tones for L/D = 2 cavity derived through modified Rossiter relation show a large deviation as high as 42% compared to unsteady pressure results. This indicates the periodic assumption in modified Rossiter relation is not valid for transitional cavity. On the other hand, the convective speed of shear layer vortices (non-periodic) for L/D = 2 when incorporated in the modified Rossiter relation, the derived discrete frequencies are well within 9.5% as compared to unsteady pressure results. This difference is still high due to the fact that the L/D = 2 cavity is transitional.

4. For L/D = 3 cavity, the oscillation mode is only in the longitudinal direction and hence, both modified Rossiter relation and experimentally generated vortex speed substituted in the same relation agreeing within 4.5 and 2.5% respectively as compared to unsteady pressure results. This shows that when the non-linearity is accounted, the results are closely matching with the unsteady pressure results.
5. The cavity drag is found to be low for L/D = 1 cavity whereas due to momentum, increased drag is seen for L/D = 2 cavity. Since oscillation of L/D = 3 cavity is in longitudinal mode, further increase in the drag is seen due to rise in the dynamic pressure on account of direct impingement of the shear layer at cavity aft wall.
6. From cross correlation, it is established that the 1^{st} and 2^{nd} modes/tones of cavity oscillation are due to wave propagation inside the cavity and shear layer impingement at cavity aft wall respectively.
7. Wavelet transform indicates mode/tone switching phenomena for L/D =2 where as L/D =3 does not exhibit mode/tone switching phenomena.

CHAPTER 6

RESULTS AND DISCUSSIONS

NON LINEAR CHARACTERISTICS OF SHALLOW OPEN CAVITIES

6.1 Introduction

In this chapter, the characteristics of shallow open cavities L/D = 4 and 5 are studied. The shear layer dynamics and its associated flow field information are presented in detail to understand its behavior along with unsteady pressure measurements. An in-depth analyzes are carried out and related the findings from the schlieren images, cross correlation from unsteady pressures and modified Rossiter relation. These analyzes are aimed to show the cause for generation of acoustic field inside the cavity and the correctness of data. Further, wave features around the cavity and its behavior are also discussed in this chapter.

6.2 Shear layer vortex dynamics

The approaching flow to the cavity is turbulent and hence significant growth in shear/boundary layer is expected. Due to nonexistence of no-slip condition, a velocity/pressure gradient occurs between subsonic flow inside the cavity and shear/boundary layer. If this velocity/pressure gradient does not disturb the shear/boundary layer, a natural instability is created [98] which leads to production of two dimensional vortices. On the other hand, forced shear/boundary instability is also present due to upstream propagating wave inside the cavity upon impinging on cavity

front wall [10]. It is reported that nearly 20% of the vortices in the shear layer are due to natural instability [52] and remaining 80% are owing to upstream movement of a wave inside the cavity.

The modified Rossiter [31] empirical relation used to calculate the dominant modes/tones in resonated cavities ($2 \leq L/D \leq 10$) assumes that the vortex shedding in the shear layer is periodic. However, the study [52] reveals that the vortex shedding mechanism is not periodic where, it is believed that the number of large-scale vortices differ at any given instant of time between cycles which means the vortex shedding mechanism is semi-periodic. The large scale vortices are produced due to coalesces of many small scale vortices over the time which is a random process. Thus in average, a standard pattern of large-scale vortices is produced and its shedding is appeared to be periodic.

In light of the above arguments, instantaneous schlieren images are acquired and presented for two vortex shedding cycles as shown in Figs. 6.1 and 6.2, for L/D = 4 cavity. In the present case, one vortex shedding oscillation cycle completes in 64 μs. These two vortex shedding cycles are arbitrarily considered where the shedding cycle starts when the vortex is at cavity leading edge and completes when it reaches the trailing edge. To explain the vortex shedding mechanism, selective frames of t = 0, 16, 32, 48, 56 and 64 μs are presented. In Fig.6.1-a, at t = 0, the vortex (V_C) in the current shedding cycle is just originated at the cavity leading edge. Immediately downstream of

this vortex (V_C), there exists a compression (pressure) wave inside the cavity which after incident on cavity front wall becomes a right running wave that trigger the cavity shear layer to form this vortex (V_C). A large scale vortex (V_P) produced in the previous vortex shedding cycle is seen close to middle of the cavity. These two vortices are seen as dark black pixels (marked by dotted lines) in the shear layer. It is seen that the shear layer thickness is increased due to disturbance in the form of compression wave, which acts like a spoiler and trips the shear layer [52]. As the time progresses (t = 16 and 32 μs) shown in Fig.6.1 (b-c), the vortices (V_C and V_P) grow and convectdownstream.

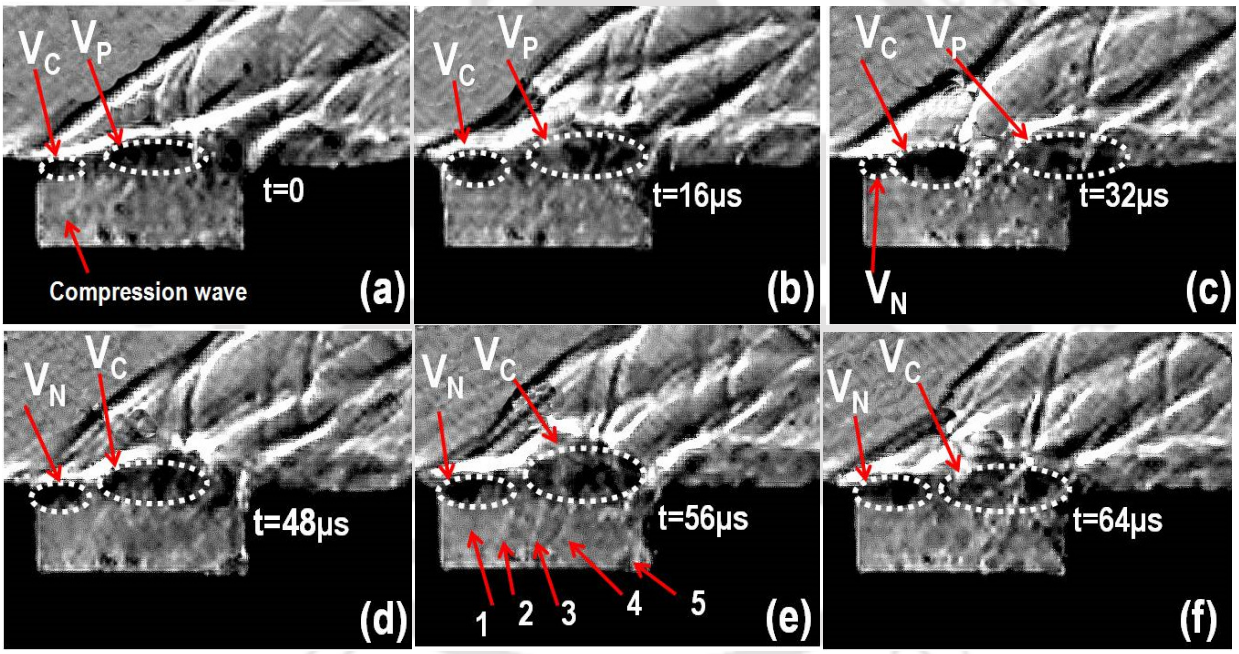

Fig. 6.1: Vortex shedding phenomena for first oscillation cycle (L/D = 4)

At t = 32 μs, the vortex (V_C) in the current cycle occupies just upstream of the cavity middle and the vortex (V_P) from the previous shedding cycle impinges partially at cavity aft wall, produces a wave which is seen. Also, a vortex (V_N) is just about to start at cavity leading edge in the next shedding cycle. Generally, the free stream flow is faster

than disturbed shear layer and hence, a clockwise rotational component is generated in the shear layer. This rotational component is accelerated by the free stream to form a vortex and allow growing in size under the influence of centripetal force. This is seen in Fig.6.1 (b-f), where the vortex (V_C) in the current cycle continuously increases in size until its size becomes thicker than the shear layer (Fig.6.1-d). At t = 56 μs (Fig.6.1-e), the vortex (V_C) in the current cycle is just arrived at the cavity aft wall whereas, the vortex (V_N) in the next cycle is about to grow. The vortex shedding cycle completes once the vortex impinges partially (or fully) at cavity aft wall or even escapes from it. In the present case, partial impingement is observed at t = 64 μs with this one cycle is getting completed. For each vortex cycle, numerous waves are formed inside the cavity, which is moving back and forth inside the cavity. Sometimes all these waves are either fully or partially visible. For example, Fig.6.1 (e) shows maximum number of waves inside the cavity. These waves are generated due to freestream entrainment between the vortices inside the shear layer. For resonant cavities, the dominant frequencies are determined by the number of vortices and waves associated in the process. Similarly, the growth and the convection of vortices in the second vortex shedding cycle are presented in Fig.6.2. It is noticed that a similar pattern of vortices (V_C, V_P and V_N) and wave signatures are observed. The movement of the current cycle vortex (V_C) is also marked in Fig.6.2 (a-e) from which, the vortex shedding speed (convection velocity) may be calculated which will be discussed in the next section. However, the size and the growth are found to be different which indicates coalescing of small scale vortices over the time to form a large scale vortex structure which is a random process and hence, the vortex shedding phenomena is not a periodic rather, it is a semi-periodic

process. Hence, the convective velocity of the vortical structure in general, taken to be a constant integer (0.57Ue) in modified Rossiter relation [31] which is not accurate at supersonic speeds [12, 42]. Thus, the dominant modes/tones in the resonated cavities vary based on periodic assumption of vortex shedding phenomena compared to semi-periodic process.

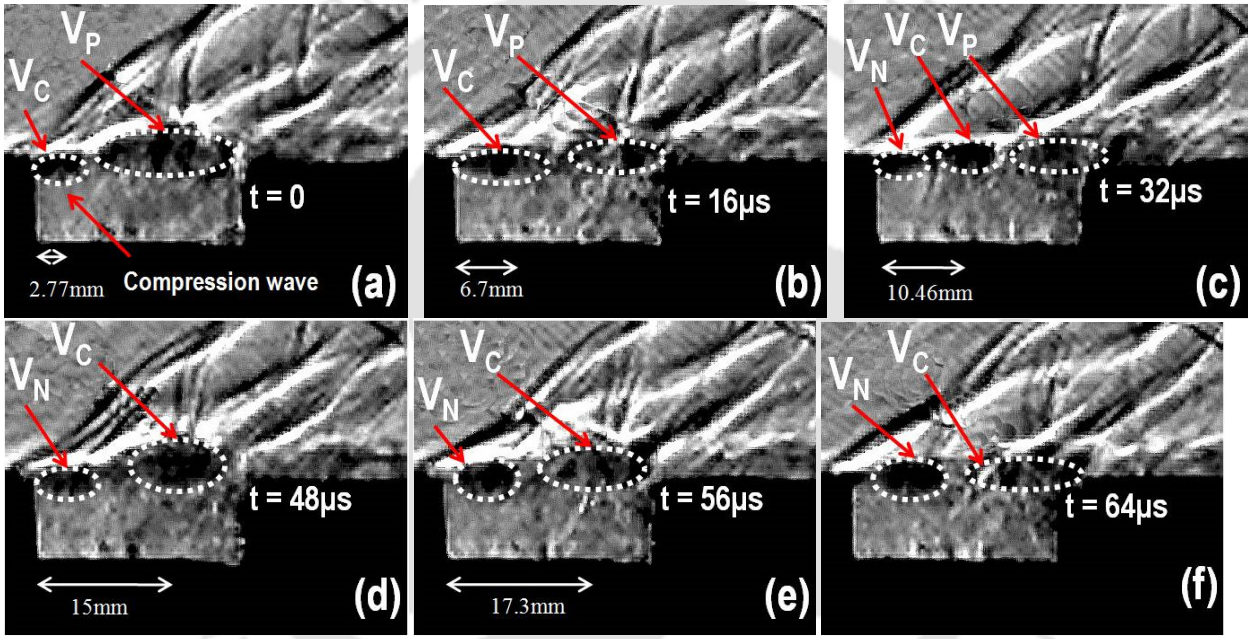

Fig. 6.2: Vortex shedding phenomena for second oscillation cycle (L/D = 4)

The shear layer characteristics for L/D = 5 cavity is presented in Fig.6.3 for one oscillation cycle. Unlike L/D = 4 cavity, the shear layer at t = 0 (Fig.6.2-a) consists of four vortices. The vortex (V_C) near the cavity leading edge is generated in the current oscillation cycle whereas; the remaining vortices (V_P) are generated in the previous oscillation cycle. The vortex (V_C) core in the current oscillation cycle is located at a distance 2.26mm from the cavity leading edge. Whereas, the vortices (V_P) in the

previous oscillation cycle occupy different locations in which the last vortex (V_P) is very close to the cavity trailing edge. At t = 8μs as shown in Fig.6.2-b, the core of the vortex (V_C) moves away from cavity leading edge and located at 4.25mm. Hence, the velocity of this vortex (V_C) is calculated to be 249 m/s by time- distance method. The last vortex (V_P) in the previous oscillation cycle is partially crossed over the cavity trailing edge. At t = 24 μs (Fig.6.3-c), a new vortex (V_N) of the next oscillation cycle is about to form whereas, the current vortex (V_C) grows in size and moves further downstream (9.1mm) at a velocity of 303 m/s. Further increase in time (t = 48 μs) as shown in Fig.6.3-d, the vortex (V_C) moves and occupy at the middle (15.9mm downstream of the cavity leading edge) of the cavity with a speed of 283 m/s. In the course of vortex movement in the shear layer, the size of vortex (V_N) grows up in size while, two of the vortices (V_P)from the previous oscillation cycle are moved away from cavity trailing edge.

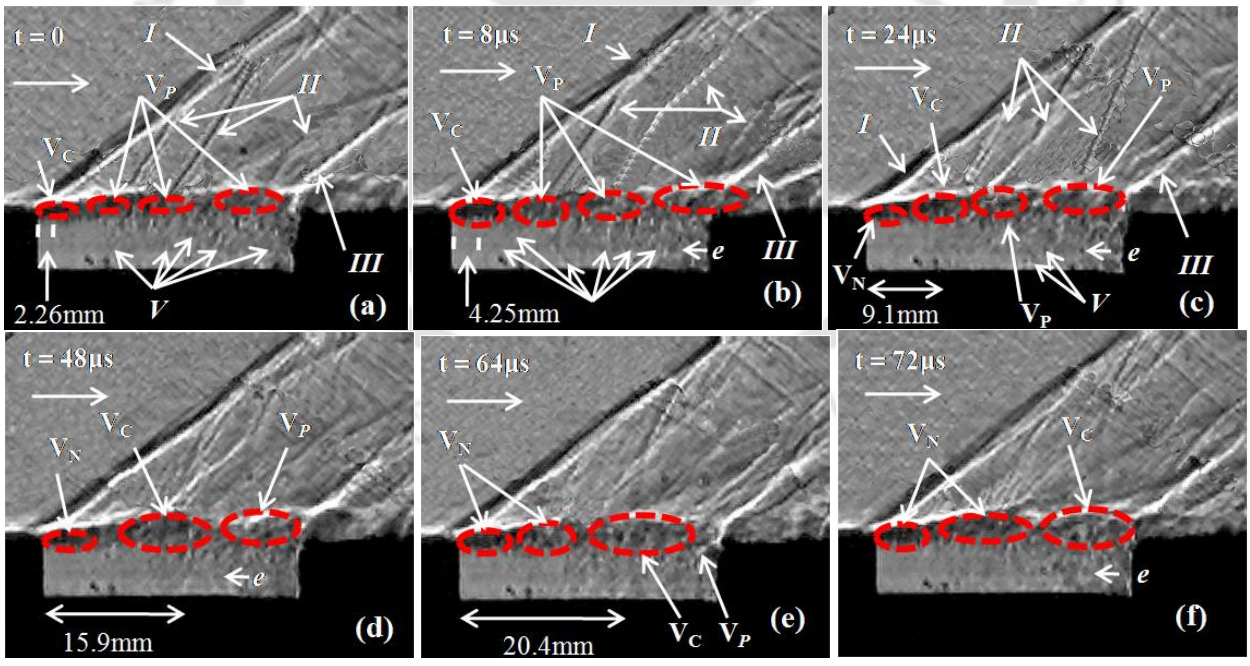

Fig. 6.3: Vortex shedding phenomena for one oscillation cycle (L/D = 5)

At t = 64 μs shown in Fig.6.3-e, the current oscillation cycle vortex (V_C) is approaching the cavity trailing edge at a speed of 281 m/s. At the same time, another vortex (V_N) of the next oscillation cycle is initiated at cavity leading edge whereas; the previous oscillation cycle vortex is vanished. The vortex shedding cycle is completed in 72 μs, which is evident from the vortex (V_C) at cavity trailing edge. The waves (type - *V*) inside the cavity are generated due to free stream entrainment between the vortices. The number of waves (type - *V*) indicates roughly the number of modes/tones experienced by the cavity. The flow features outside as well as inside the cavity will be explained later. It may be observed from the time resolved schlieren images that the characteristics of the vortex growth, its propagation in the shear layer is presented up to 72μs. The vortex speed inside the shear layer is also approximately calculated by time-distance method which gives the data on the propagation of the vortices in the shear layer. The distribution of vortex speed for open cavities namely L/D = 4 and 5 are presented in Fig.6.4. For both the cavities, vortex speed at initial time is low due to the fact that the vortex is just started to grow in size. However, in the evolution process of large-scale vortex structure, the supersonic external main stream causes the vortices to accelerate due to shearing action, which is evident from increase in vortex speed. On the other hand, when the vortex approaches the cavity trailing edge, the vortex speed is getting affected owing to obstruction in the form of cavity trailing edge and the associated shock.

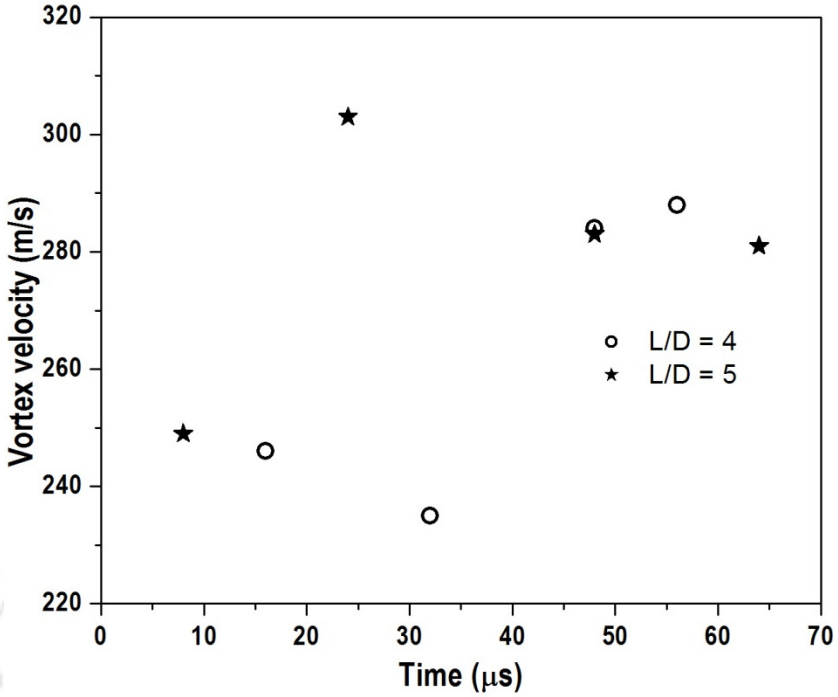

Fig. 6.4: Vortex velocities in the open cavities.

6.3 Wave propagation around the cavity

The vortex shedding cycle has already demonstrated in the previous discussion (Fig. 6.2) for L/D = 4. The flow features around the cavity for one vortex shedding cycle (64μs) is shown in Fig. 6.5. At t = 0 (Fig. 6.5-A), a vortex (point V_C) is positioned at the cavity leading edge whereas, another vortex (V_P) from the previous shedding cycle is positioned half way through the cavity. The flow feature outside the cavity indicates type-*I* wave at cavity leading edge. Since the shear layer vortices (V_C and V_P) act as an obstruction to the supersonic flow, type-*II* waves are formed in the free stream and move towards cavity trailing edge due to vortex convection, which are evident from subsequent schlieren images (Fig.6.5B-D). The type-*II* waves upon interact with type-*I* wave forms a λ-shock and the point "a" shows the foot of this λ-shock. Inside the cavity,

a wave (point d) moves towards the cavity aft wall which is responsible for the shear layer to excite and produce a vortex (V_C) and disturb the shear layer to generate a wave (type-*II*) in the free stream. On examining the flow features inside the cavity, there are many waves, which are marked by type-*V* waves in the previous vortex shedding cycle. Sometimes, the number of waves may vary from time to time and the appearance of these waves depends on the strength of the waves. These waves (type-*V*) may be responsible for production of number of vortices (V_P) in the previous vortex shedding cycle and disturb the shear layer to produce type-*II* waves in the freestream. On partial impingement of the vortex (V_P) at cavity trailing edge, a shock is formed at trailing edge marked as type-*III* wave and also, partial clipping (PC) in shear layer is seen. As a consequence, a wave is generated (point e) due to impingement of shear layer at cavity aft wall which disturb the shear layer to produce type *IV* wave. Also, in the freestream much downstream of the cavity aft wall, transient waves (point b and c) are observed. In the present case, all types of wave especially type-*I* to *IV* as well as wave front inside the cavity are captured. Hence, it is apparent that the flow features inside the cavity is more complex than reported in the literature wherein; a wave front travels upstream inside the cavity because of shear layer impingement, incident on the cavity front wall and reflect back towards cavity aft wall.

At time t = 16μs (Fig. 6.5B), the vortex (V_C) in the current shedding cycle grows and well developed whereas, the vortex (V_P) in the previous shedding cycle covers the most of the cavity length and deflect the shear layer. The wave features outside the cavity show typical wave patterns as discussed in the previous time step except the

downstream movement of type-*II* waves. Inside the cavity, the reflected wave (point d) which is responsible for the generation of vortex in the shear layer, moves downward (right running wave) that disturb the shear layer to produce type-*II*. In this case, type-*V* waves inside the cavity interact with each other, which are marked as a dotted circle and disturb the shear layer and produces type-*II* wave. Also, the wave (point e) as a consequence of shear layer impingement at cavity aft wall moves upstream and influence the shear layer to produce a left running wave (type-*IV*).

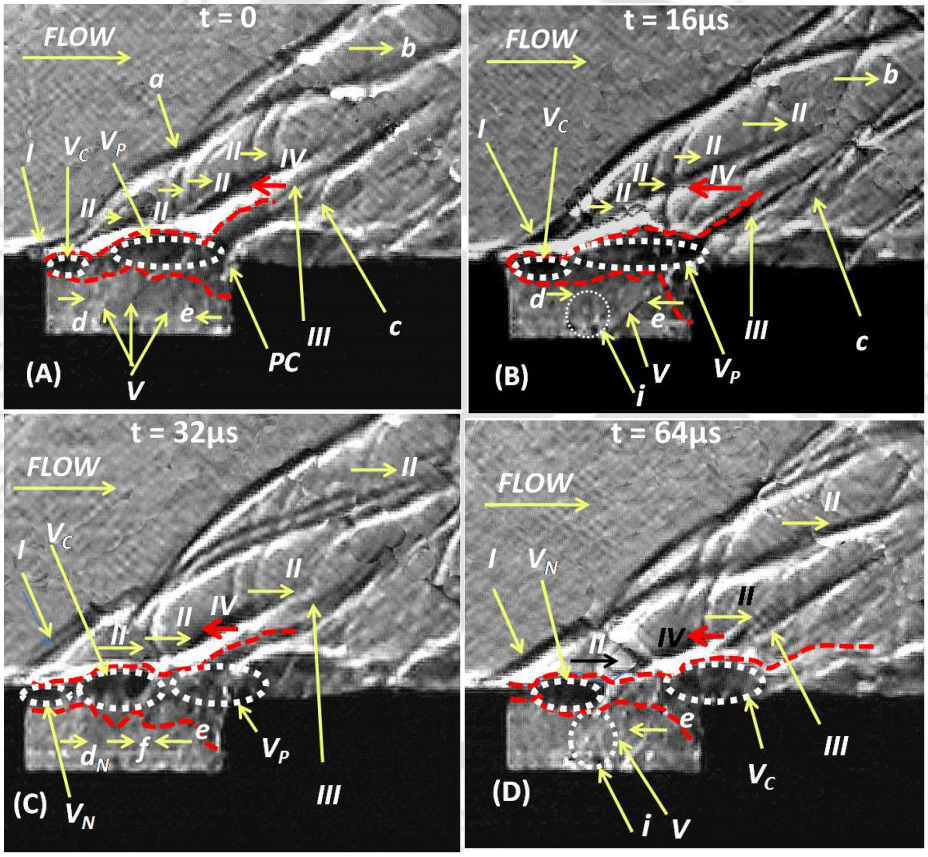

Fig. 6.5: Flow features around L/D = 4 cavity

In the next frame depicted in Fig. 6.5C, at t = 32µs, the vortex (V_C) in the current cycle is located at the centre of the cavity whereas, at the same time, the previous shedding cycle vortex (V_P) reaches aft wall of the cavity and a new vortex (V_N) in the

next shedding cycle is formed. All the wave types outside the cavity are captured whereas inside the cavity, a reflected wave (d_N) responsible for the next vortex shedding cycle is also captured. This wave (d_N) produces a type-*II* wave in the free stream due to shear layer disturbance which lags behind type-*II* wave produced by the current cycle vortex (V_C). Inside the cavity, type-*V* waves coalesce together to form a single wave (point f) that moves downward whereas the left running wave (point e) move towards the cavity front wall which generates a type-*IV* wave.

At time t = 64μs (Fig. 6.5D) the vortex (V_C) in the current shedding cycle just crosses over the cavity trailing edge whereas the vortex (V_N) in the next shedding cycle is developed and positioned upstream of the cavity middle. Inside the cavity, the wave d_N of the next shedding cycle (after reflection from the cavity front wall) and the wave (point e) of the previous time step (t = 32μs, generated from the cavity aft wall) interacts with each other (marked as dotted circle) and disturb the shear layer to form a type-*II* wave. On examining further, the right running wave (point f) moves towards the cavity aft wall with that completes one vortex shedding cycle.

The flow field outside L/D = 5 cavity (Fig.6.6) shows complex wave features for one vortex shedding cycle. It includes cavity leading edge shock (type *I*), cavity trailing edge shock (type *III* - due to reattachment of shear layer), shock (type *II*- due to vortex roll-up, partial clipping upstream propagating wave (type *IV*- due to periodic interaction of shear layer with cavity trailing edge) and compression waves downstream of the cavity in the free stream. In one vortex shedding cycle, the shock (type - *II*) due to vortex rolls-up,

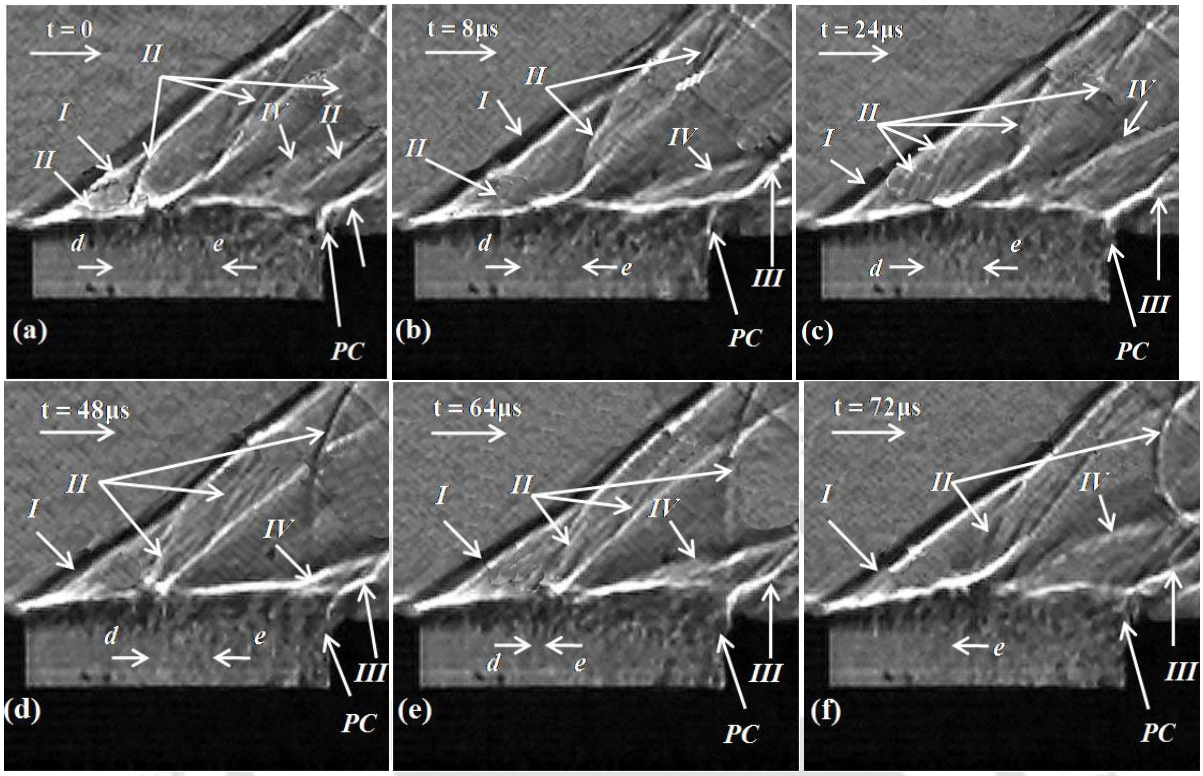

Fig. 6.6: Flow features around L/D = 5 cavity

Interacts with the cavity leading edge shock (type - *I*) and becomes a λ-shock. During the course of vortex convection, the front leg of the λ-shock moves downstream (Figs.6.6a-e) which is evident from the schlieren images. The shape of this shock (type - *II*) is oblique till the foot is attached to the cavity leading edge shock (Figs.6.6a-e) beyond which the shape becomes concave (Fig.6.6-f). Also, a partial clipping is observed at the cavity trailing edge which is responsible for mass addition and removal from the cavity. Another important flow feature during one vortex shedding cycle is the generation of a shockwave (type - *IV*) and its upstream movement (left running) due to periodic interaction of the shear layer with the cavity trailing edge (Figs.6.6a-f). At the same time, inside the cavity, a wave (point e) moves upstream towards cavity leading edge (ahead of shock wave type - *IV*). It is also observed that a reflected compression wave (point d) from cavity leading

edge (which is generated in the previous vortex shedding cycle) moves downstream inside the cavity. The arrows in Figs.6.6 (a-e) represent the upstream and downstream movement of the compression waves (point e and d). Figure 6.6 (f) show the flow features inside the cavity once these two compression waves (point d and e) interact each other. In this case, after interaction, only left running compression wave is seen. Hence, there exists a relation between propagation of waves both outside and inside the cavity.

6.4 Unsteady pressure measurements - Sound pressure levels

The cavity oscillations as a consequence of vortex convection and impingement at cavity aft end are obtained through simultaneous measurement of unsteady pressures. The pressure spectra derived from unsteady pressure signals using Fast Fourier Transform at three locations inside the cavity show discrete large amplitude peaks corresponding to cavity modes/tones. This may be correlated to shear layer vortices or waves inside the cavity. For L/D = 4, the cavity experiences six dominant modes/tones as shown in Fig.6.7 due to resonance, caused by shear layer impingement at cavity aft wall. Irrespective of measurement locations, cavity modes/tones occur at the same frequency, which is a sign of global instability. In the present case, 3rd mode/tone is very prominent with large amplitude. Though the 1st and 5th modes/tones are observed to be distinct, they do not have sharp features as compared to other modes/tones due to the fact that the thick shear layer tends the flow to become smooth. On the other hand, 2nd, 4th and 6th modes/tones are appeared to have more distinct sharp features with suppression in the sound pressure level. It may be seen from

fig.6.1e that there exists number of waves inside the cavity where some of the waves are very prominent and other waves are feeble which are picked up by the sensors.

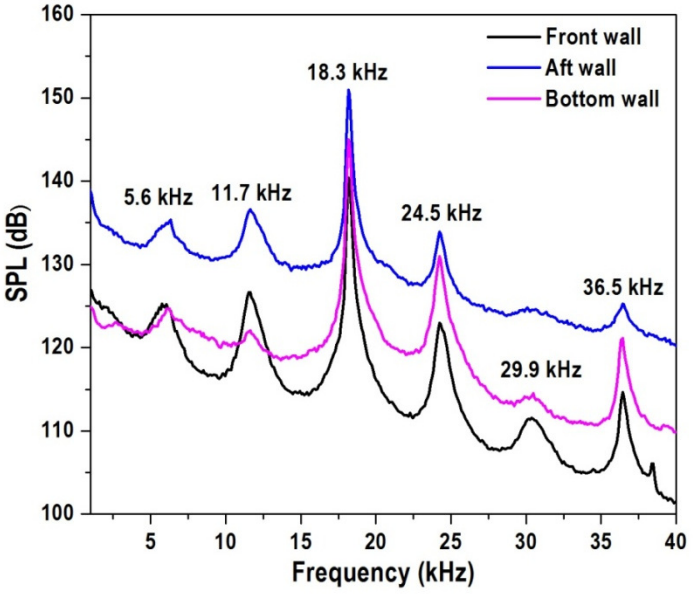

Fig. 6.7: SPL distribution for cavity L/D = 4

The cavity modes/tones, which are experimentally generated, are compared with modified Rossiter relation [31]. The comparison of experimental results exhibit fairly good match with the modified Rossiter relation and the maximum difference is found to be 14% (Table.6.1). It is observed that a maximum difference is at 1st mode whereas, as the mode/tone is increased, the difference is found to be small. The time resolved schlieren images (Fig.6.2) reveal that the vortex convection is semi-periodic and hence, the frequencies at which the modes/tones derived from modified Rossiter relation are found to be departed from experimental results (Fig.6.8) in terms of Strouhal number. But, an average K value calculated is found to be very close match with the Rossiter relation. In order to gain confidence, five tests are carried out at identical conditions to establish the repeatability of the test results which are presented in Fig.6.9 for cavity aft

wall sensor where the shear layer impinges directly. The uncertainty in the frequency calculated is±130 Hz. The OASPL is also given in Fig.6.10 where the maximum OASPL occurs at cavity aft wall due to direct impingement of shear layer. The lowest value is seen at front wall. From aft wall to front wall, the OASPL is found to be decreased continuously due to entrained vortices and reduction in turbulent fluctuations.

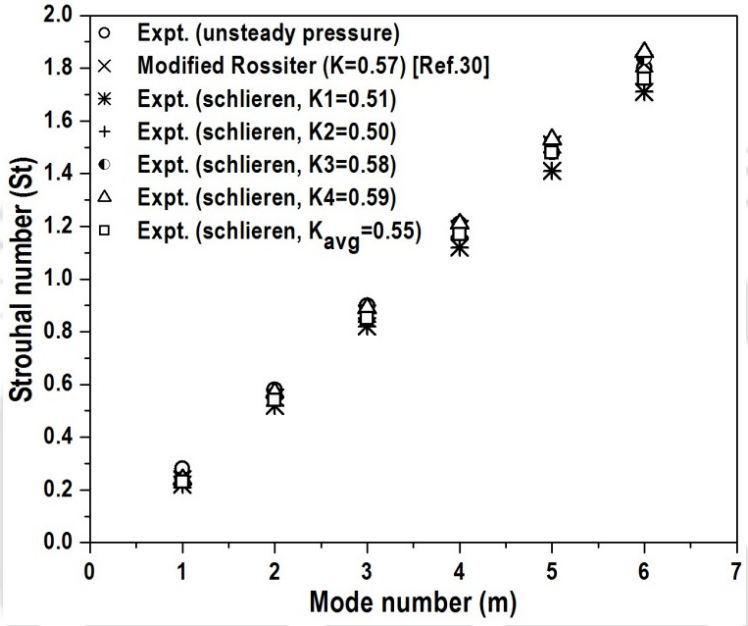

Fig. 6.8: Comparison of Strouhal number for L/D = 4

Table.6. 1 Comparison of Strouhal number for L/D = 4

Cavity modes (m)	Expt. Unsteady pressure	Rossiter relation [31]	Expt. (From schlieren images)				
		K = 0.57	K1 = 0.51	K2 = 0.5	K3 = 0.58	K4 = 0.59	K_{avg} = 0.55
1	0.28	0.24	0.22	0.22	0.24	0.24	0.23
2	0.58	0.55	0.52	0.52	0.56	0.57	0.54
3	0.90	0.87	0.82	0.82	0.88	0.89	0.85
4	1.21	1.19	1.12	1.12	1.20	1.21	1.17
5	1.48	1.51	1.41	1.41	1.52	1.53	1.48
6	1.80	1.82	1.71	1.71	1.84	1.86	1.76

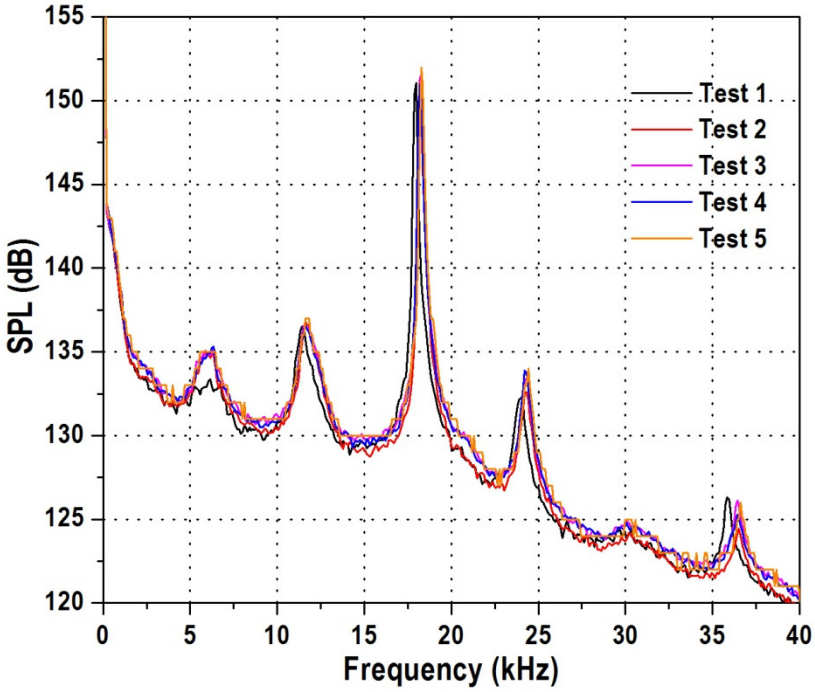

Fig. 6.9: Measurement uncertainty

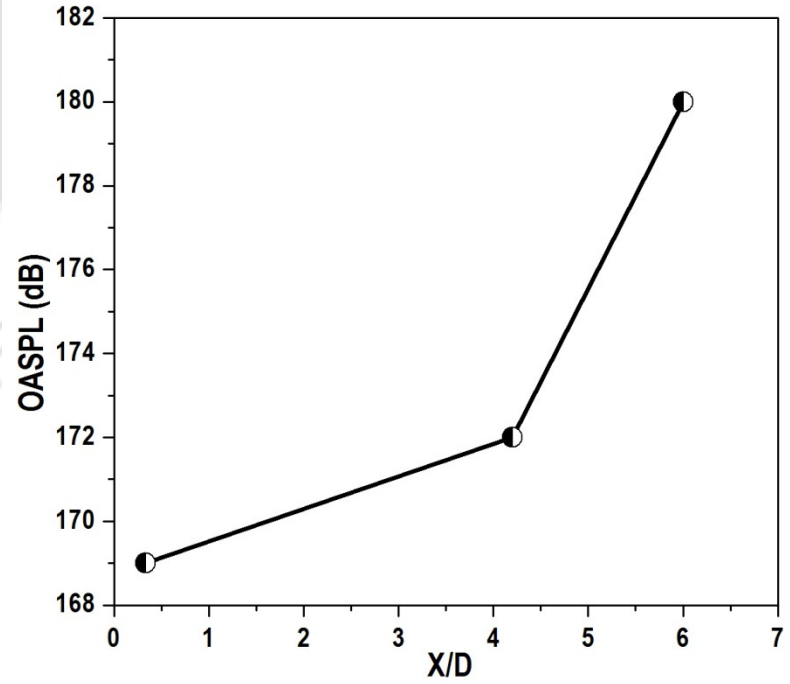

Fig. 6.10: Distribution of OASPL

Figure 6.11 shows the sound pressure level of L/D = 5 cavity at front wall, aft wall and bottom wall. The resonance occurs when the shear layer impinges at the cavity

trailing edge, which is marked by peaks (modes/tones) in the power spectrum. It is noted that irrespective of the sensor location, the peak occurs at the same frequency, with different magnitudes indicate the global instability of the flow. In the present case, seven modes/tones are seen and a broadband spectrum is observed in the 1st mode/tone at cavity aft as well as bottom walls due to the fact that the shear layer impinges on the floor of the cavity. Whereas, small amplitude peaks in 1st, 6th and 7th modes/tones are seen at cavity front wall. The sharp distinct features are observed in 2nd to 5th modes/tones at all the locations.

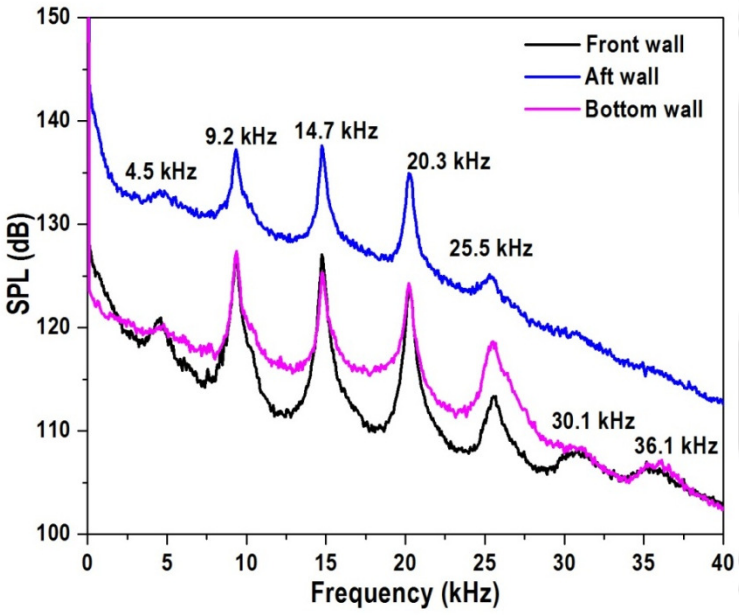

Fig. 6.11: SPL distribution for L/D = 5

The comparison of experimental results with modified Rossiter relation [31] match fairly and the maximum difference is 14% in the 1st mode. However, the other modes/tones are well within 5% compared to modified Rossiter relation. Based on time resolved schlieren images, the vortex speed is calculated and applied to modified Rossiter

relation. The K - value in the relation varies from 0.49 to 0.42 with the average value of 0.57.

Table.6.2 Comparison of Strouhal number for L/D = 5

Cavity modes (m)	Expt. Unsteady pressure	Rossiter relation [31]	Expt. (From schlieren images)				
		K = 0.57	K1 = 0.49	K2 = 0.62	K3 = 0.58	K4 = 0.58	K_{avg} = 0.57
1	0.28	0.24	0.22	0.25	0.24	0.24	0.24
2	0.57	0.55	0.51	0.58	0.56	0.56	0.55
3	0.91	0.87	0.80	0.91	0.88	0.88	0.87
4	1.25	1.19	1.09	1.24	1.20	1.20	1.19
5	1.57	1.51	1.38	1.58	1.52	1.52	1.51
6	1.86	1.82	1.71	1.91	1.84	1.84	1.82
7	2.23	2.14	1.96	2.24	2.16	2.16	2.14

The results are compared with the unsteady pressures and the Rossiter relation which are plotted in Fig.6.12 and presented in Table.6.2. The comparison shows that the results obtained from schlieren images exhibit very good match with K = 0.62 while deviations are seen with other K- values indicate that the L/D = 5 possess non-linear characteristics.

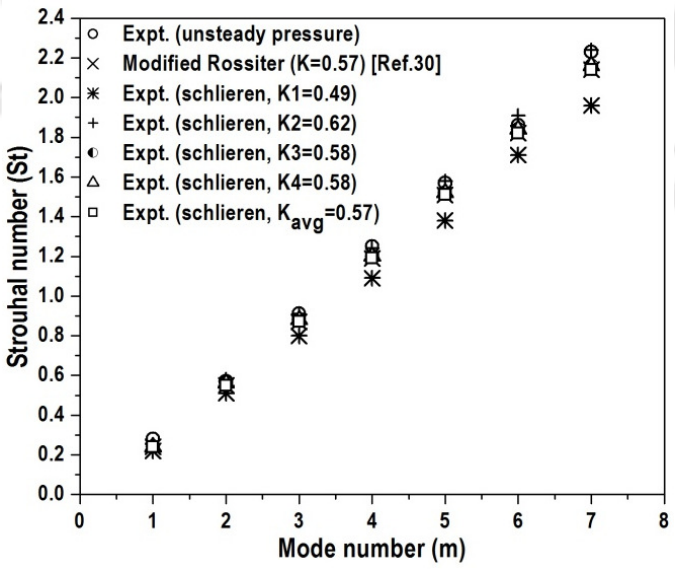

Fig. 6.12: Comparison of Strouhal number for L/D = 5

6.5 Relation between modes/tones and the waves/vortex

The 1st and 2nd modes/tones may be extracted from high speed schlieren images (which are approximate) and the 3rd mode/tone is also may be possible from schlieren images using immobilization technique [54] which is beyond the scope of this thesis. On the other hand, detection of higher modes/tones are not possible from schlieren images due to interaction of waves with lower modes/tones at certain location inside the cavity. The 1st mode/tone is related to the wave propagation inside the cavity from front wall to aft wall and back to front wall [54, 55]. In order to study this, the wave propagation inside the cavity at time t = 32 and 48 μs is presented in Fig.6.13 for L/D = 4.

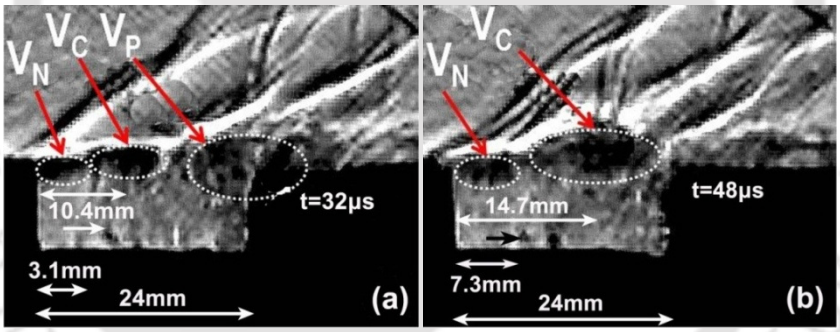

Fig.6.13: Wave speed inside the cavity (L/D = 4)

The speed of the wave inside the cavity is calculated from the average of 100 schlieren images using time distance method (Δx/ Δt) which is approximate. The distance travel by the wave from one position to another position is denoted as Δx and the time taken to cover this distance is Δt. It is found that the wave moves at a speed of approximately 262.5 ± 40 m/s. Based on this, the wave frequency can be calculated using the following relation (equ.6.1).

$$f = \frac{v}{\lambda} = \frac{v}{2L} \quad (6.1)$$

Where, f is the frequency (Hz), L is the cavity length (m) and λ is the wave length which is equal to 2L. Based on the above relation, the frequency of the wave propagation inside the cavity is calculated as 5468 Hz. It is observed that the 1st mode/tone from unsteady pressure measurements as shown in Fig.6.7 exhibit the value of 5600 Hz which is matching with the wave frequency inside the cavity. Hence, it is ascertained that the wave frequency inside the cavity is approximately equal to the 1st mode/tone. Since, the identification of the waves inside the cavity is very complex [92], the present calculations may be considered as approximate. The 2nd mode/tone is due to vortex shedding which may be approximately calculated from schlieren images (average of 100 images). The average distance travelled by the vortex in the shear layer is shown in Fig. 6.11 (a-b) between two frames (t = 32 and 48 μs) explain the 2nd mode/tone is generated due to vortex shedding. The average velocity of the vortex is obtained by distance-time method is approximately 265 ± 22 m/s which is much lower than the free stream velocity (U_∞ = 487 m/s). In the present case, the value of k = $\frac{U_C}{U_\infty}$, calculated is0.55 (average of 100 images) and the corresponding frequency calculated is 11.03 ± 0.6 kHz which is the 2nd mode/tone produced by the cavity . Also, based on the relation (eqn. 6.2), the mode/tone can be calculated.

$$f = \frac{v}{\lambda} = \frac{v}{L} \quad (6.2)$$

Where, f is the frequency (Hz), L is the cavity length (m) and λ is the wave length Based on the above relation, the frequency of the vortex convection is calculated to be 11.13 kHz. The 2nd mode/tone derived from unsteady pressure measurement is shown in

Fig.6.7 exhibits 11.7Hz which is fairly close to the vortex shedding frequency. The above methodology and the calculation show that the 2nd mode/tone is generated due to vortex shedding phenomena.

Similar studies are carried out for L/D = 5 and are presented in Fig.6.14 where wave propagation inside the cavity at time t = 0 and 8 μs is considered. Based on time-distance method, the velocity of the wave (right running) calculated inside the cavity is 268 m/s. From eqn. 6.1, the frequency of wave propagation calculated is 4458 Hz which is the 1st mode/tone of the cavity. From the unsteady pressure measurement the frequency calculated is 4500 Hz which is shown in Fig.6.11. Likewise, same methodology as discussed in L/D = 4 cavity is followed to determine average vortex speed in the present case also. The results indicate that the schlieren images show the vortex velocity of 258 m/s and the corresponding vortex frequency of 8617 Hz which is close to the 2nd mode/tone of the cavity (Fig.6.11).

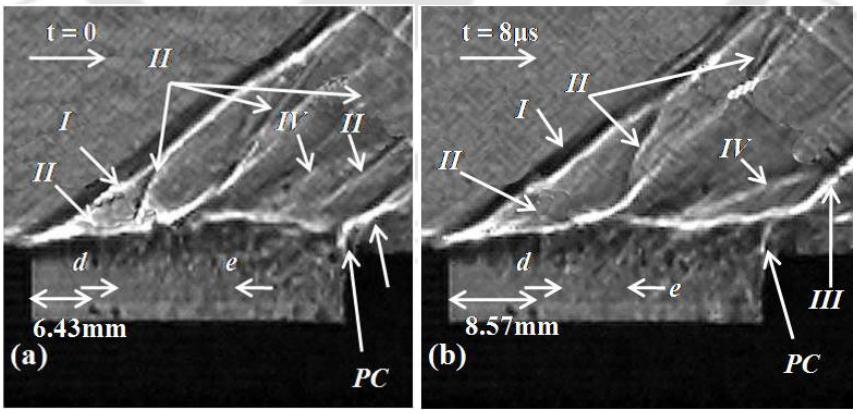

Fig. 6.14: Wave speed inside the cavity (L/D = 5)

6.6 Cross correlation

Figure 6.15 shows the cross correlation between aft and front wall sensors of L/D = 4 cavity. It is seen that the cross correlation is sinusoidal in nature. From the cross correlation, for one period, two peaks are found which is repeating for the entire acquisition time of 5s. However, the cross correlation is shown only for a short time from - 50μs to + 250μs.Auto correlation of the aft wall sensor (aft wall * aft wall - curve A) shows a maximum value of 1 at time t = 0s whereas, the cross correlation of the aft wall * bottom wall sensors (curve - B) has a time delay.

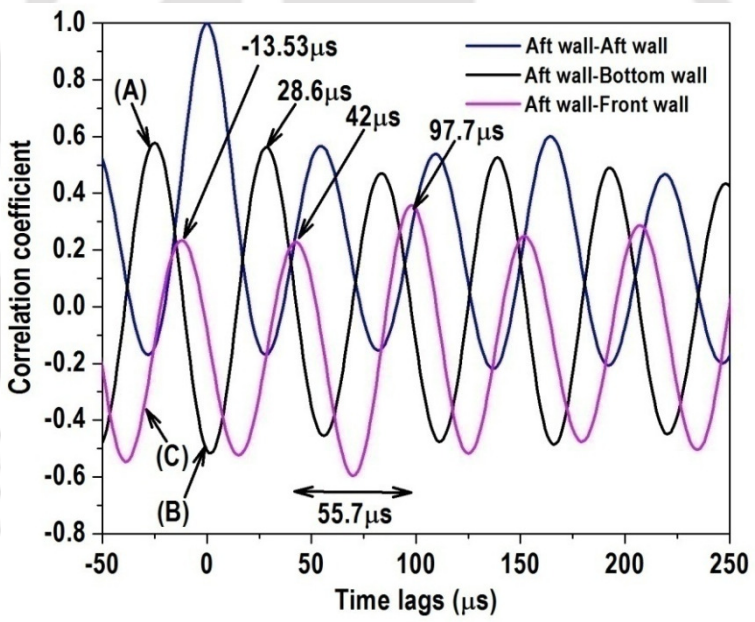

Fig. 6.15: Cross correlation for L/D = 4

It is seen that a phase shift is observed between the aft wall * bottom wall sensors (curve - B) whereas, out of phase is observed between aft wall * front wall sensor (curve -C). It may be explained as follows :if the cavity is considered to be a two dimensional one, the front and the bottom wall sensors would have resulted in a similar results as

compared to aft wall sensor due to the fact that the flow inside the cavity is along the bottom wall and reaches the front wall. However, in the present case, the flow is not two-dimensional rather it is three-dimensional. Inside the cavity, there exists two recirculation zones so called trapped vortices near the cavity front wall as well as the cavity aft wall. Due to mass entrainment or pumping action generated in the previous vortex shedding cycle owing to shear layer impingement at cavity aft wall, the fluid from the cavity aft wall moves upstream towards cavity front wall. In the presence of trapped vortex near the cavity aft wall, the flow gets turned along the side walls of the cavity and move forward in the recirculation zone towards the middle of the cavity [52]. This is seen in the cross correlation plot (Fig.6.15) that the phase difference is around 142°between bottom wall and front wall sensors whereas the aft wall and front wall sensors show almost in out of phase with each other.

Earlier studies [81, 85] show the wave speed inside the cavity through cross correlation, which is equal to the speed of sound (347 m/s) by assuming that the air temperature inside the cavity is equal to the free stream stagnation condition. On the other hand, from digital streak method [54, 55], the wave speed calculated is 240 ± 25 and 300 m/s respectively. Thus, from cross correlation (aft wall * front wall - curve C) it is possible to establish the wave propagation speed inside the cavity because of shear layer impingement and the resonating frequencies. The cross correlation shows the period of one oscillation cycle as 55.7 μs (peak to peak) and hence, the frequency of one cycle is 17.95 kHz which corresponds to the 3rd mode/tone as shown in Fig.6.7. Hence, it may be concluded that the period may be correlated to the frequency, which

corresponds to the dominant mode/tone (with maximum amplitude) of the cavity. It is seen that in one cycle (Fig.6.15), there are two peaks and thus, these peaks may be correlated to the vortex frequencies and wave speed inside the cavity.

In the present investigation, the cross correlation (aft wall * front wall - curve C) shows the pressure peak at front wall takes a time of 97.7μs to reach aft wall. This is the time taken by an acoustic wave to travel from the aft wall to front wall, thus confirming the presence of acoustic wave and Rossiter's feedback mode of communication inside the cavity. The velocity of this pressure wave based on cavity length (L = 24mm) calculated is 246 m/s which is in line with the literature value [54, 40]. Based on this, it is possible to calculate the wave frequency using eqn.6.1 results in 5118 Hz which is observed to be the 1st mode/tone of the resonating cavity. The cross correlation results also indicate the 1st mode of cavity oscillations (which is due to wave propagation inside the cavity).

Further analysis shows that the 1st peak in one cycle occurs at t = 42μs. It is a fact that the shear layer vortex impinges at the cavity aft wall and therefore, a pressure wave is generated. Hence, the 1st peak in the cycle is due to the direct impingement of shear layer vortex and the 2nd peak is due to wave generation. It may be argued that the vortex shedding in the shear layer impinges on the cavity wall ahead of the formation of pressure wave. Hence, the cavity aft wall sensor responds to this shedding vortex before the pressure wave is generated. The time delay of 2nd peak with respect to 1st peak is 55.7μs. Similar exercise is carried out and the frequency calculated based on 1st

peak is 11905 Hz. The frequency in this case is very close to 2nd mode/tone of the cavity oscillation (11700 Hz). On the other hand, the 1st peak behind the auto correlation at t = 0; curve C(for aft wall * front wall) lags by 13.53 µs which is presumed to be due to the wave generation in the previous time period. Based on cross correlation between cavity aft wall * front wall (curve - C), it is possible to derive first three modes/tones and 6th mode/tone. However, other modes/tones are not captured in the cross correlation.

On the other hand, cross correlation between aft wall * bottom wall (curve - B) shows a time lag of 28.6 µs to reach the pressure peak from cavity front wall to cavity bottom wall. The bottom wall sensor is located 8mm ahead of the aft wall of the cavity. Hence, based on this time delay and distance, wave speed calculated is 280m/s and the corresponding frequency calculated is 5828 Hz (eqn. 6.2) which is the 1st mode/tone of the cavity oscillation. A comparison of wave speed inside the cavity corresponding to 1st mode/tone against the literature value [54, 81, 49, 101] is presented in Table.6.3. It is observed that the present results are very well comparable with other data [54, 55] and gives confidence on the data. Also, the resonance frequencies correspond to 1st, 2nd, 3rd and 6th modes/tones are presented in Table. 6.4 reveal that the different techniques used to derive the dominant modes/tones are agreeing very well.

Table 6.3: Comparison of wave speed corresponds to 1st mode/tone (L/D = 4)

S.No.	Techniques	Wave speed (m/s)
1	Schlieren image	263±40
2	Cross correlation	246
3	Digital streak schlieren [54]	240±25
4	Schlieren images [55]	300
5	Cross correlation [81, 85]	347
6	Cross correlation [101]	333

Table 6.4: Comparison of dominant mode/tone frequencies (L/D = 4)

S. No.	Techniques	Frequency (kHz)			
		1st mode	2nd mode	3nd mode	6th mode
1	Schlieren	5.47	11.21	-	-
2	Cross correlation (curve A*C)	5.12	11.91	17.95	36.95
3	Unsteady pressures	5.60	11.70	18.30	36.50
4	Modified Rossiter [31]	5.13	11.97	18.87	39.57
5	Cross correlation (curve A*B)	5.83	-	-	-

The cross correlation along with auto correlation between aft and front wall pressure signals for L/D = 5 cavity is shown in Fig.6.16. Moderate correlation between these two sensors inside the cavity is observed. The cross correlation (aft wall-front wall) shows that the pressure peak at front wall takes a time of 132μs to reach aft wall and hence, confirming the existence of acoustic wave and Rossiter's feedback mode of communication inside the cavity.

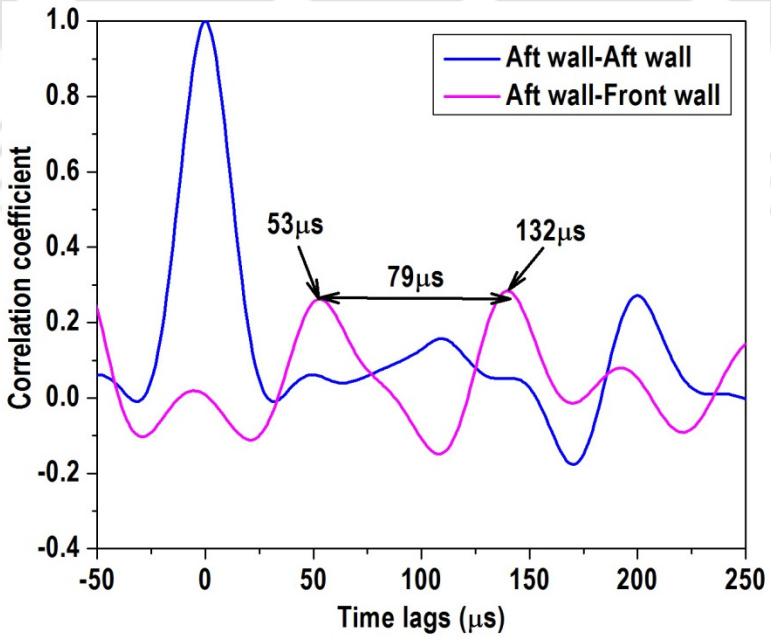

Fig. 6.16: Cross correlation parameter for L/D = 5

The speed of this wave for the cavity length of 30mm is calculated as 227 m/s and the corresponding frequency is 3783 Hz which is close to the 1st mode/tone from unsteady pressures. Similarly, the 1st peak in the correlation is at 53 μs and the corresponding velocity of the wave is 566 m/s leads to the frequency of 9434 Hz indicating the 2nd mode/tone of cavity oscillation. Further, one period of the cavity oscillation is 79 μs which leads to a frequency of 12658 Hz and fairly matching with peak mode/tone of cavity oscillation (3rd mode/tone). The comparison of dominant modes/tones at discrete frequencies is presented in Table6.5 using different analyzes. It shows that they are fairly matching.

Table 6.5: Comparison of dominant mode/tone frequencies (L/D = 5)

S. No.	Techniques	Frequency (kHz)		
		1st mode	2nd mode	3rd mode
1	Schlieren	4.46	8.60	-
2	Cross correlation	3.78	9.43	12.66
3	Unsteady pressures	4.50	9.20	14.70
4	Modified Rossiter [31]	3.89	8.90	14.10

6.7 Coherence

The coherence between unsteady pressures at different locations exists at all frequencies up to 25 kHz for L/D = 4 cavity is fair enough as shown in Fig. 6.17. The magnitude of the coherence coefficient at 1st mode between aft and front walls is moderate. This is due to the fact that the pressure pulses generated on account of shear layer impingement moves upstream and interact with the waves which already exist in the previous oscillation. Thus, due to dissipation effect, the strength of the signal

is getting reduced which leads to reduced magnitude in the coherence coefficient at 1st mode. However, the other modes/tones have higher coherence coefficient. Hence, the phenomenon, which is responsible at one location, is also responsible for other location, which leads to the presence of a feedback loop and global instability similar to that derived from correlation analysis. Similar behavior is seen for L/D = 5 cavity. In both cases, high coherence at frequencies corresponding to SPL peaks is observed between pressure signals of front and bottom wall. The pressure signal of aft wall has poor coherence at other frequencies. It is understood that the feedback and global instability exist for both the cavities at all dominant modes/tones.

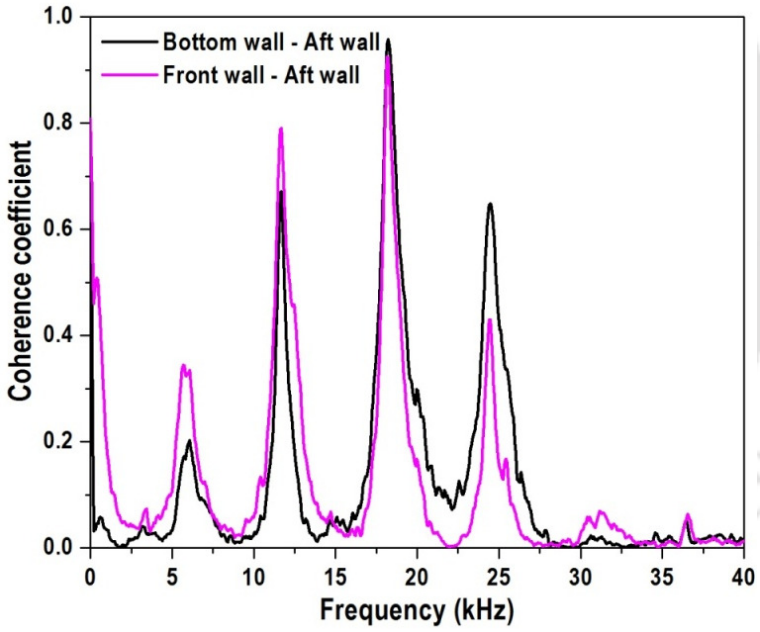

Fig. 6.17: Coherence parameter for L/D = 4

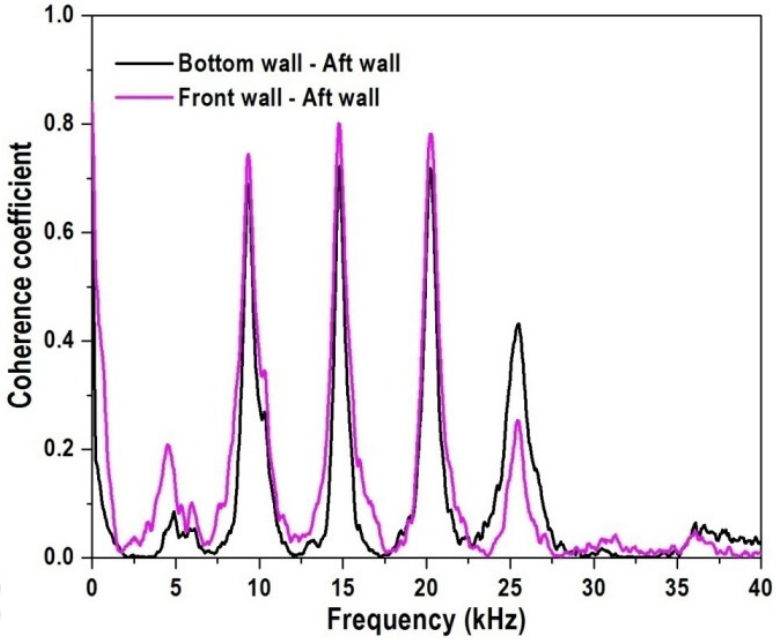

Fig. 6.18: Coherence parameter for L/D = 5

6.8 Spectrogram

On examining the spectrogram (Fig.6.19) for L/D = 4 cavity, it is noted that there are maximum of six modes/tones present. The 3rd mode/tone is dominating during the entire duration of the test. The spectrogram of cavity front wall (Fig.6.19-a) indicates the existence of 2nd and 3rd modes/tones during the entire acquisition period while the 4th mode/tone is randomly spread over the time period. Other modes/tones are still visible with reduced power/energy throughout the period considered. At cavity bottom wall (Fig.6.19b), the dominancy of the 3rd mode/tone is observed while 5th and 6th modes/tones exist intermittently during the test period. The 2nd mode/tone is feeble and intermittent; the other modes/tones (1st and 5th) are almost dormant. Cavity aft wall spectrogram (Fig.6.19c) shows strong signal due to direct impingement of shear layer where the back ground energy content at this location is large as compared to other locations. In this case, similar to other locations, the 3rd mode/tone is very dominant

whereas, 2nd and 4th modes/tones continuously persist throughout the time. Other modes/tones are found to be feeble. The spectrogram of L/D = 5 cavity presented in Fig.6.20 explains irrespective of the measurement locations, 2nd to 4th modes/tones contain equal energy which is intermittent. Also, the 1st, 6th and 7th modes/tones are dormant in nature and posses weak signal throughout the test duration. Similar to earlier case, the cavity aft wall contains higher strength over different frequencies.

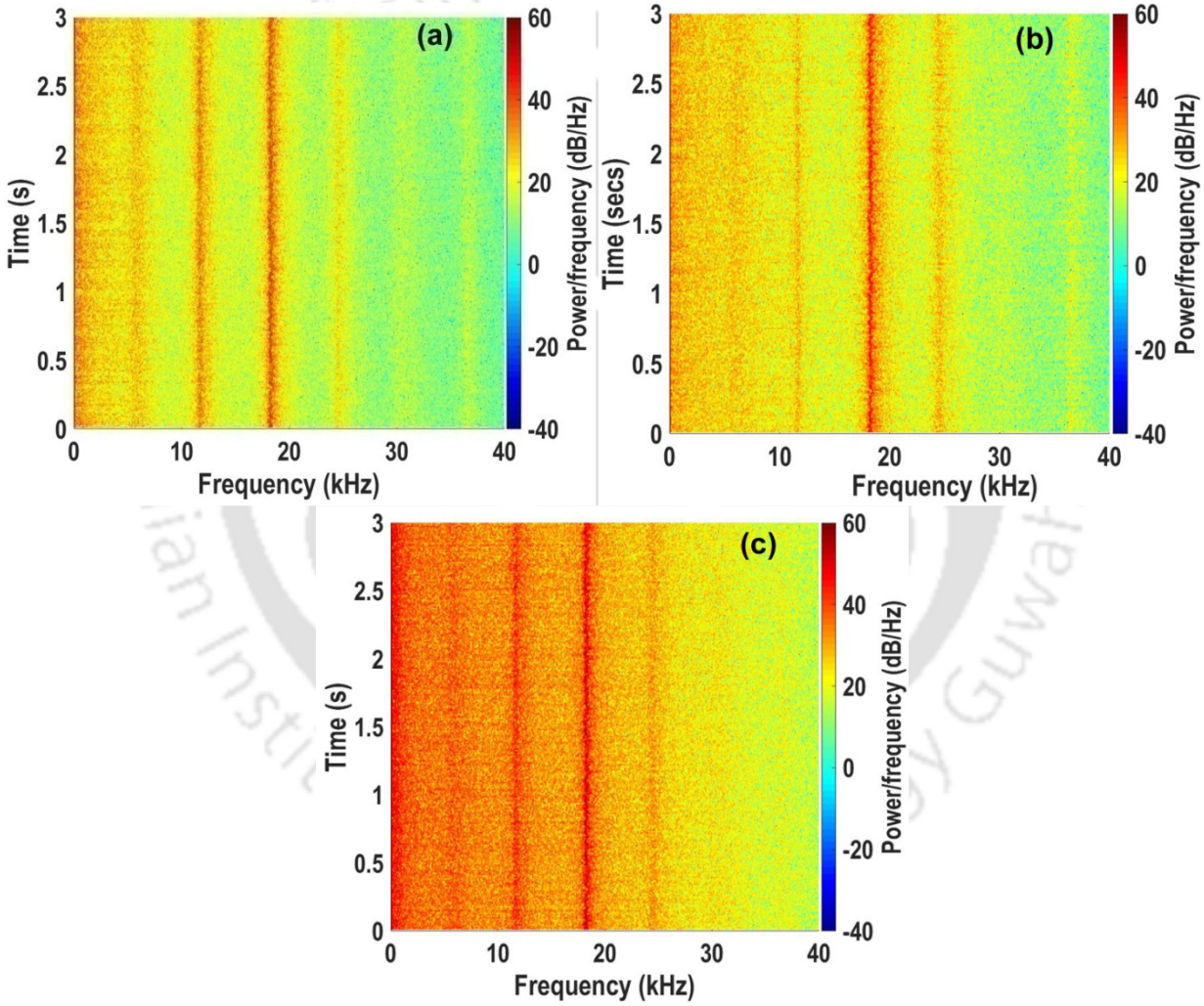

Fig. 6.19: Spectrogram for L/D = 4 (a-front wall, b-bottom wall, c-aft wall)

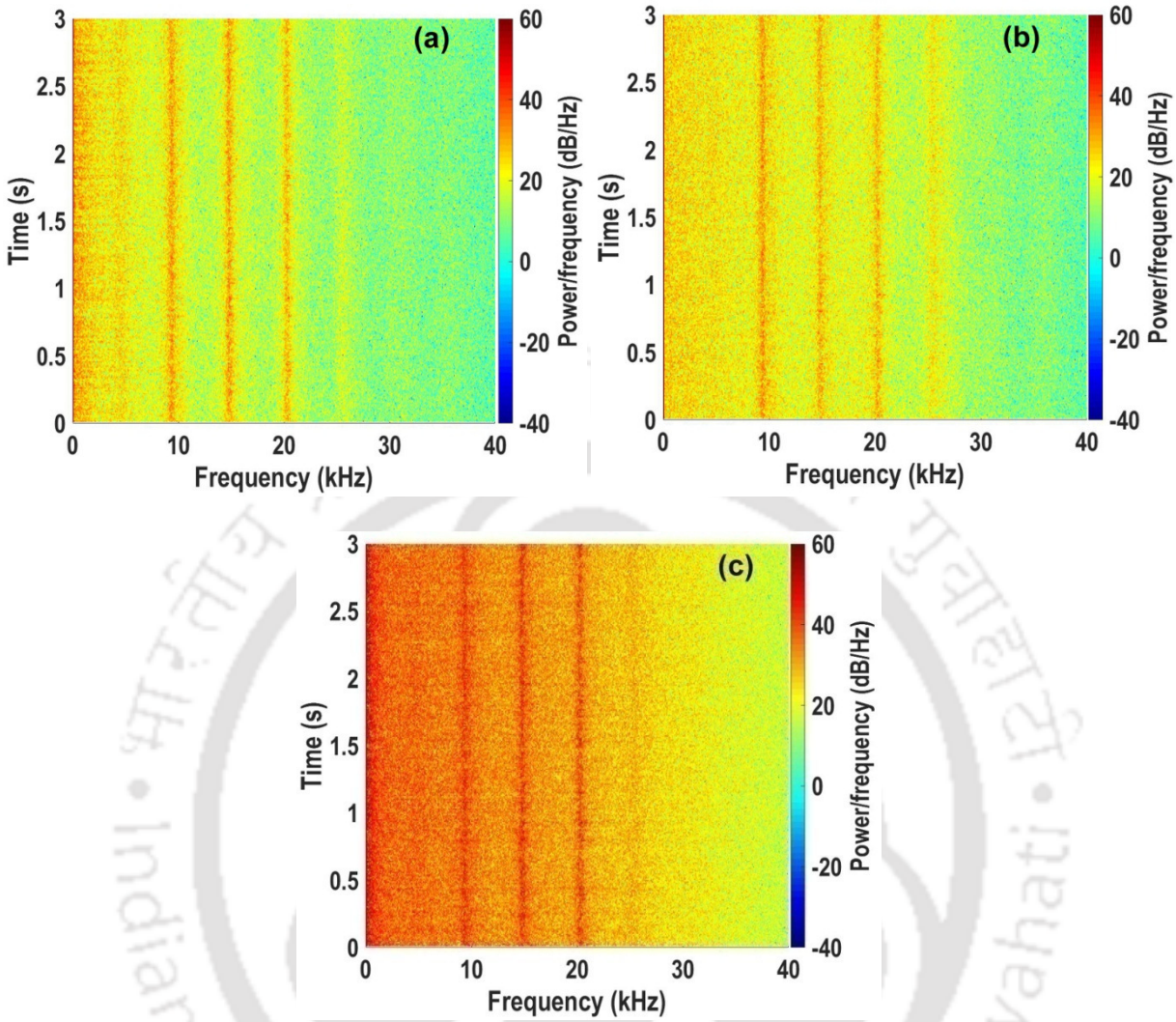

Fig. 6.20: Spectrogram for L/D = 5 (a-front wall, b-bottom wall, c-aft wall)

6.9 Wavelet analysis

Figures 6.21 and 6.22 show the plots of magnitude of the wavelet coefficients of the pressure signals obtained from the front, bottom and aft walls of the cavities L/D = 4 and 5 respectively. The magnitude of the wavelet coefficients are plotted as a function of time and frequency. The four cavity modes lie within this frequency range. The wavelet coefficients are obtained for the entire duration of the test. It is seen from

Fig.6.21 (a)that the front wall exhibit four modes at 5.6, 11.7, 18.3 and 24.5 kHz. It is observed that the cavity modes are amplitude modulated in time. This modulation is noticed due to better time resolution of wavelet transform. At 3rd mode, high energy event along with intermittent low and medium energy events is observed while, 2nd mode consists of generally a medium energy event with sporadic distribution of mixed low as well as high energy events. At cavity bottom wall (Fig.6.21-b), 2nd tone is not prominent. Here, high energy events are generally distributed over entire range of frequencies in the total time interval, whereas the medium energy events occur at a given time instant for a wide range of frequencies. At cavity aft wall (Fig.6.21-c), four modes are seen where the 3rd mode mostly covered with high energy content due to direct impingement of cavity shear layer. Whereas, medium and low energy events occur at 1st and 2nd mode respectively and they are sporadically distributed.

The wavelet analyzes for L/D = 5 shows in general, the amplitude of the modes more or less similar to L/D = 4 cavity. Here, clear demarcation is not seen at each mode/tone. At cavity front wall as represented in Fig.6.22 (a) the wavelet spectrum shows mostly low energy events with intermittent medium energy events occur. Whereas, at cavity bottom wall (Fig.6.22-b), 2nd to 4th modes are seen in which the 3rd mode contains large amplitude modulations along with high energy events distributed. The 2nd mode contains small amplitude modulation with randomly distributed high energy event. Similar behavior is shown (Fig.6.22-c) for aft wall.

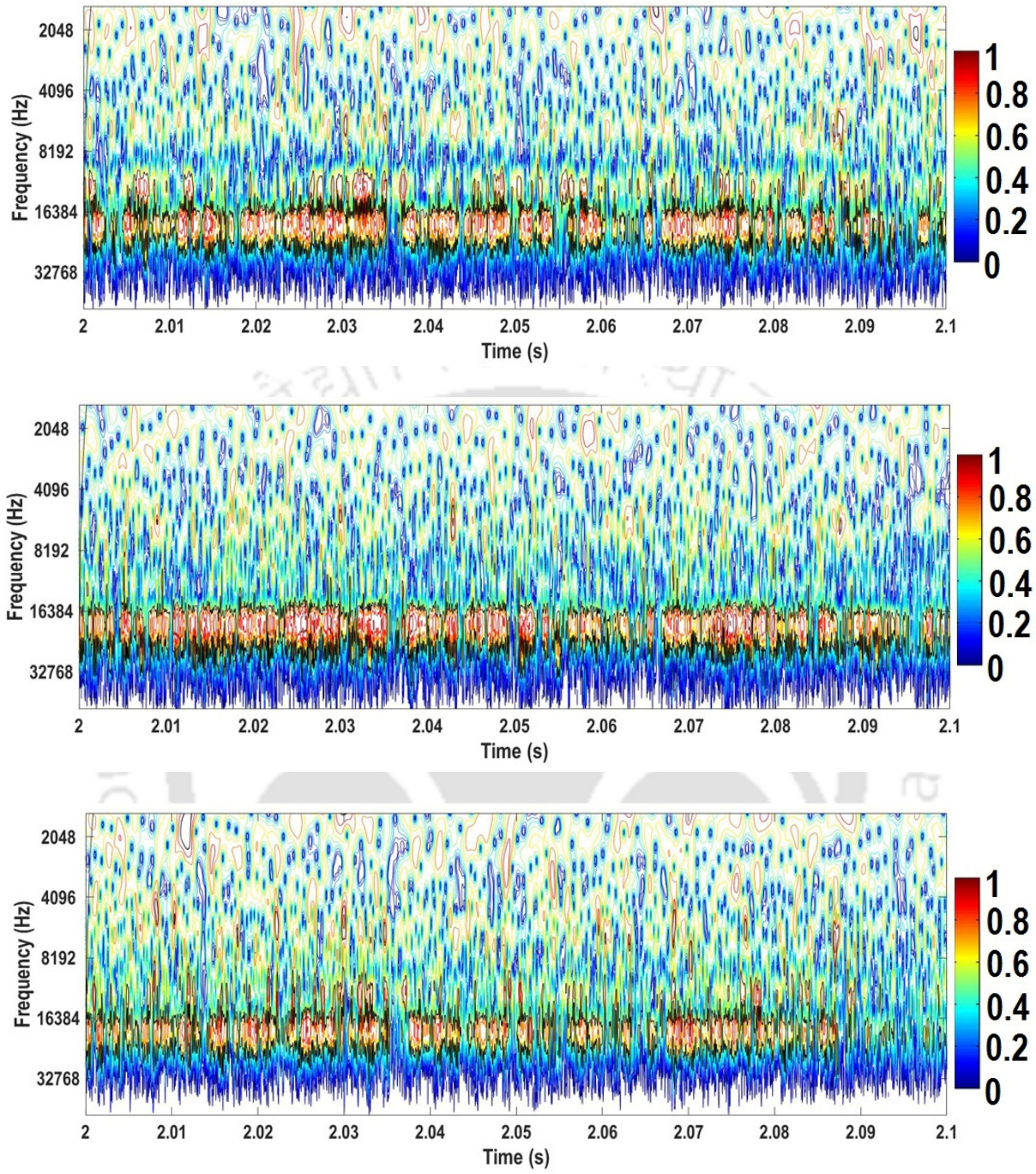

Fig. 6.21: Wavelet coefficient for L/D = 4 (a-front wall, b-bottom wall, c-aft wall)

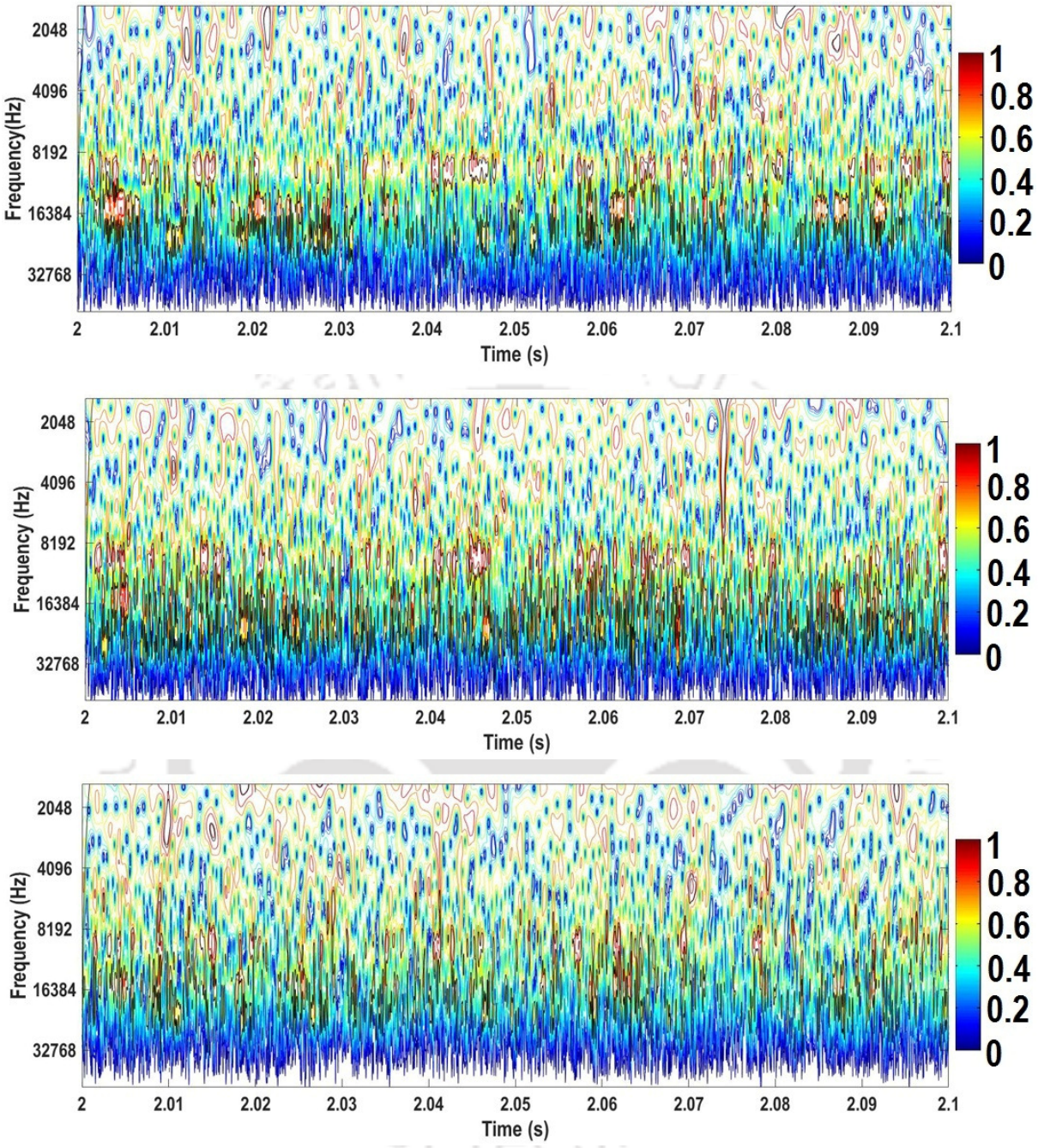

Fig. 6.22: Wavelet coefficient for L/D = 5 (a-front wall, b-bottom wall, c-aft wall)

6.10 Summary

Experiments on shallow open cavities (L/D = 4 and 5) using time resolved schlieren images and unsteady pressure measurements at supersonic speed brings out their characteristics as given below.

1. As the length of the cavity is increased (L/D = 4 to 5) number of modes/tones are also increased.
2. The dominant modes/tones for L/D = 4 cavity is more significant as compared to L/D = 5 cavity.
3. The vortex convection inside the cavity shear layer is non linear. In both the cavities, the vortex speed is found to be increased downstream of the cavity leading edge and is observed to be decreased near the cavity trailing edge.
4. The average vortex speed in the shear layer is in the range of 230 to 305 m/s.
5. The cross correlation analyzes reveal that the 1st mode/tone is due to wave propagation inside the cavity, 2nd mode/tone is due to vortex shedding and one cycle indicates the maximum mode/tone.
6. The cavity (L/D = 4) exhibits very good cross correlation between the pressure signals whereas, L/D = 5 cavity shows the cross correlation is very moderate.
7. The cavity (L/D = 5) clearly brought out the wave propagation mechanism.
8. In both cavities, the wavelet analysis shows no mode switching phenomena.

CHAPTER 7

RESULTS AND DISCUSSIONS

CHARACTERISTICS OF OPEN TO CLOSE RECTANGULAR CAVITIES

7.1 Introduction

In this chapter, the characteristics of L/D = 6 to 10 cavities are studied and discussed. For all the cavities, the length is kept constant and the depth is varied to achieve the required L/D ratios. The flow field outside the cavity is very similar to L/D 4 and 5 and hence, it is not discussed. However, the shear layer characteristics and associated vortex phenomena along with unsteady pressure measurements are presented. Further, the same methodologies such as SPL, coherence coefficients, spectrogram, cross correlation and wavelet spectrum are also presented to understand the cavity behavior.

7.2 Shear layer vortex dynamics

Figures 7.1 to 7.3 show the shear layer characteristics and associated vortex behavior. For L/D = 6 (Fig.7.1), the vortex dynamics at two time instances namely t = 0 and 8μs are shown in Fig.7.1 (a-b). In this case, the depth of the cavity is 5mm. At t = 0, it is observed that there are six vortices present in the shear layer which are marked by red circle and the shear layer is attached to the cavity floor just upstream of the cavity aft wall. At time t = 0, near the cavity leading edge, a vortex (V_C) in the current shedding

cycle is seen whereas, the remaining vortices (V_P) are generated in the previous shedding cycle.

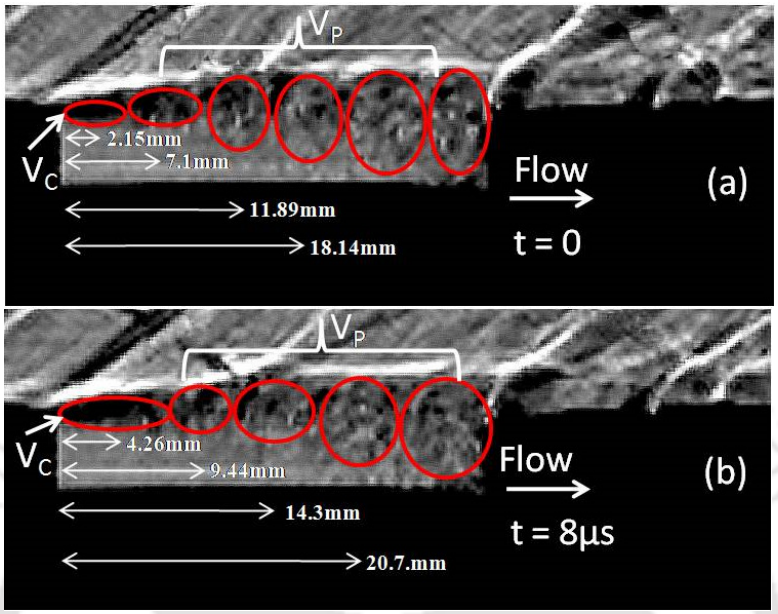

Fig. 7.1: Shear layer vortex dynamics for L/D = 6

These vortices are identified by the dark pixels in the schlieren images and the core distance of the vortices from cavity leading edge is measured by scaling the schlieren image. The schlieren images at t = 0 (Fig. 7.1a) indicate that the vortex shedding is not uniform which means the rate at which the growth of the shear layer vortices is not constant. At t = 8 µs, the vortex (V_C) in the current shedding cycle grows in size while one of the vortices (V_P) in the previous shedding cycle gone beyond the cavity due to convection. Similar to the earlier case, the shear layer is attached at cavity floor upstream of the cavity aft wall. The distance moved by the vortices in the shear layer for both t = 0 and 8 µs reveal that the velocity at which the vortices convect in the shear layer is not constant. The speed of different vortices in the shear layer is 264, 293, 301

and 320 m/s. and this indicates that the vortices are continuously accelerated by the free stream supersonic flow under the influence of centripetal force.

For L/D = 7.5, the cavity depth is 4mm and its vortex dynamics fortwo time instances 0 and 8 μs are presented in Fig.7.2 (a-b). It is observed that at t = 0 (Fig.7.2-a), there are five vortices among which the 1st vortex (V_C) is generated in the current shedding cycle while remaining four vortices (V_P) are generated in the previous shedding cycle. In this case, the shear layer is attached on the cavity floor upstream of the cavity aft wall. The speed of the vortices in this case is observed to be 256, 294, 338 and 344 m/s and the vortex dynamics show the behavior is non-linear. On the other hand, at L/D = 10, where the depth of the cavity is 3mm, the shear layer is attached at cavity floor approximately half the portion. Hence, it is very difficult to identify the vortices in the shear layer which is very coherent. The vortex speed for the two cases namely L/D = 6 and 7.5 presented in Fig.7.4 clearly indicates the transitional cavities from open to close is non-linear.

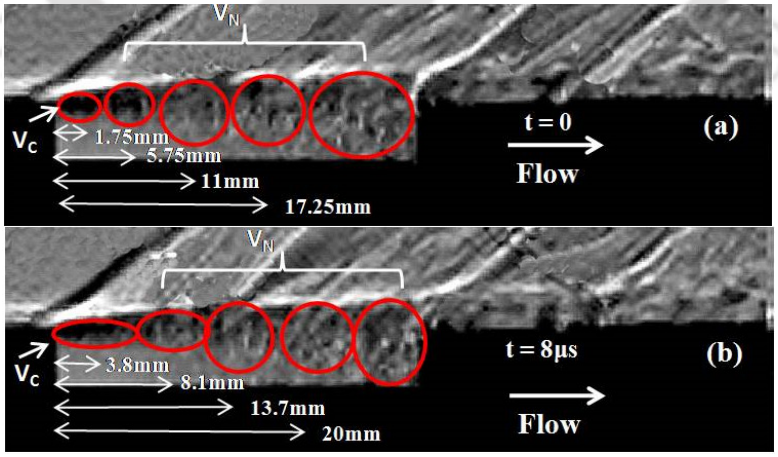

Fig. 7.2: Shear layer vortex dynamics for L/D = 7.5

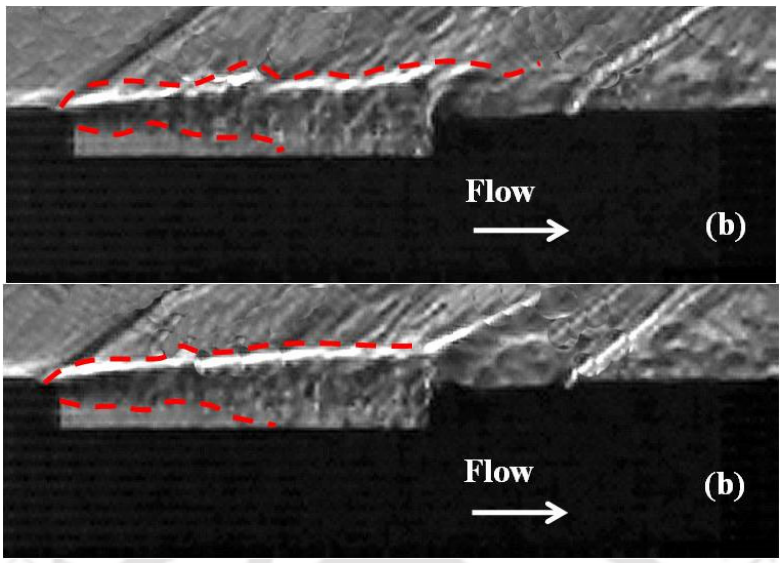

Fig. 7.3: Shear layer vortex dynamics for L/D = 10

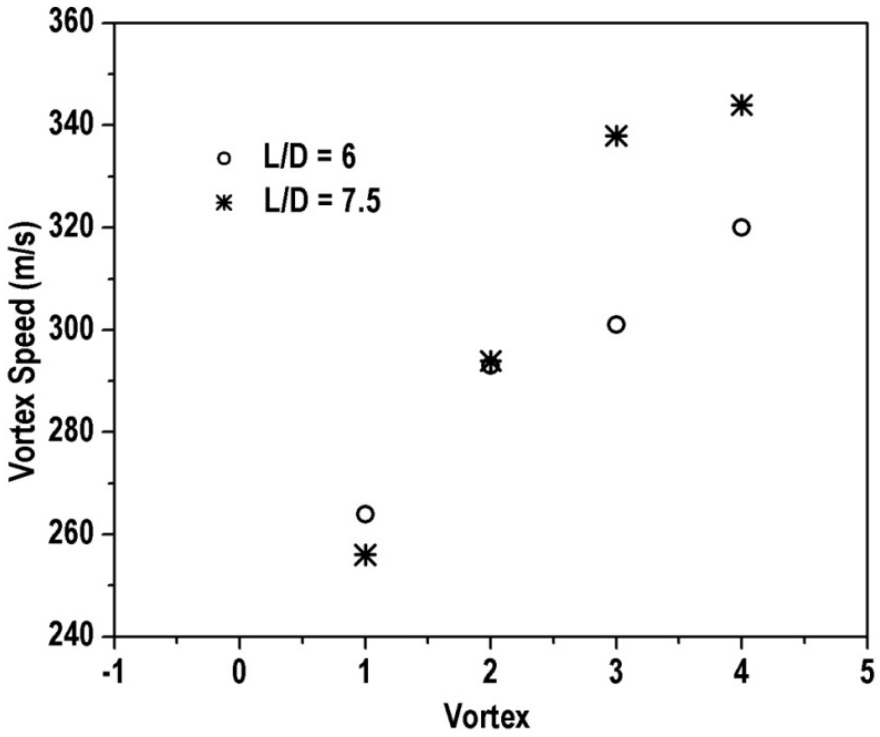

Fig. 7.4: Non-linearity of the vortex speed

7.3 Modes/tones of the transitional cavities

Figures 7.5-7.7 show the pressure spectra of modes/tones in terms of sound pressure levels (SPL). In can be correlated to the schlieren images presented in Figs.7.1-7.3. As the cavity L/D ratio is increased, the amplitude of the modes/tones is decreased irrespective of the locations. This is due to the fact that the shear layer is attached on cavity bottom wall and the length of re attachment location increases with increasing L/D ratio. In other words, as the L/D increases, the encroachment of the shear layer on to the cavity bottom wall is more pronounced. For L/D = 6 (Fig.7.5), five modes/tomes are seen at bottom and front wall. The cavity aft wall contains low amplitude 1st and 2nd modes/tones whereas the other region of spectra shows smooth variation without noticeable changes due to direct impingement of shear layer on bottom wall (Fig.7.1).

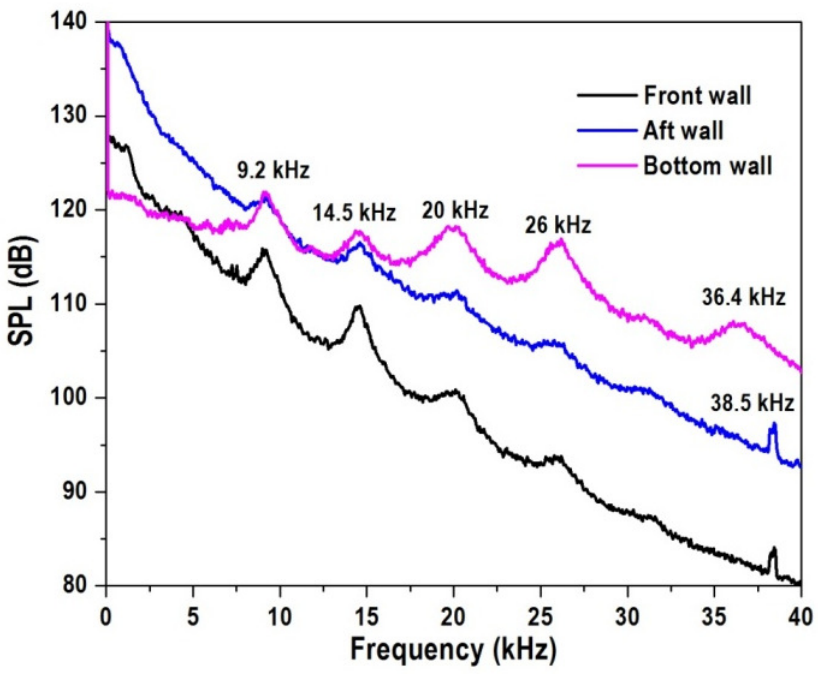

Fig. 7.5: SPL behavior for cavity (L/D = 6)

The cavity bottom wall exhibits five distinct modes/tones due to direct impingement of shear layer on bottom wall as well as the waves generated owing to free stream entrainment between the shear layer vortices. This impingement of shear layer and the waves (inside the cavity) are periodically encountered and hence, the modes/tones are distinctly visible. However, cavity front wall pressure spectrum shows two modes/tones whereas other modes/tones are found to be weak. In this case, the waves generated by free stream entrainment between the shear layer vortices may become weak due to dissipation effect on the course of their travel towards cavity front wall and hence, distinct modes/tones are seen beyond 2nd mode/tone. The pressure spectra for L/D = 7.5 as shown in Fig.7.6 further indicates the effect of shear layer impingement at cavity bottom wall on modes/tones.

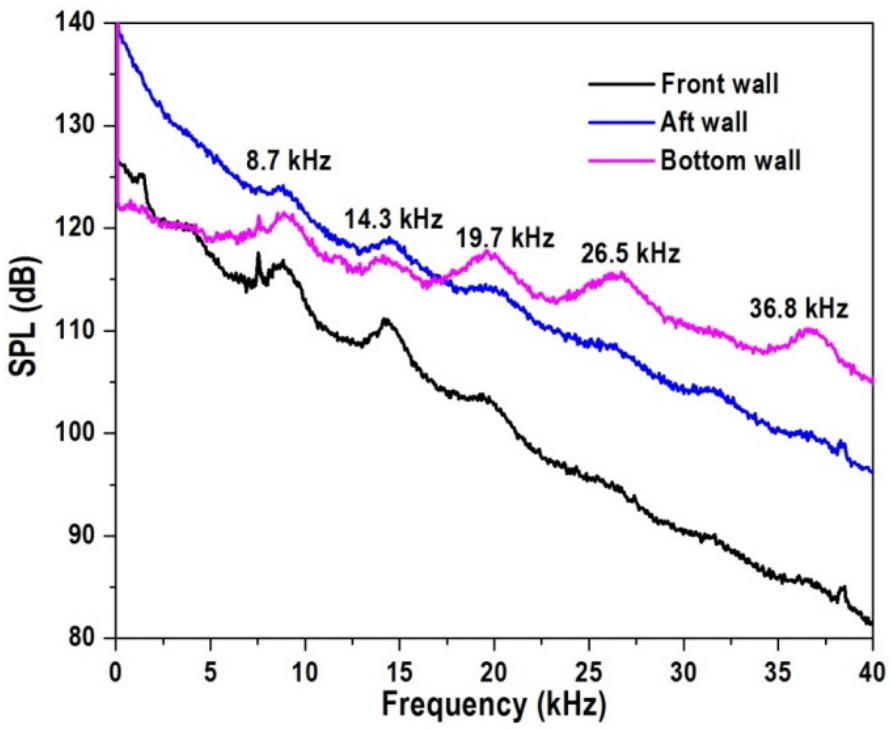

Fig. 7.6: SPL behavior for cavity (L/D = 7.5).

In this case from schlieren image (Fig.7.2), the impingement location of the shear layer on cavity bottom wall shifts upstream resulted in increased region of shear layer dominance. This is seen in the pressure spectra where the cavity aft wall shows smooth trend with less perceptible modes/tones. Though the length of the re attachment zone is increased, the cavity bottom wall experiences noticeable modes/tones with reduced amplitude due to the fact that the bottom wall sensor is away from the shear layer impingement location. Similar to the earlier case, the front wall exhibits two modes/tones with decreased amplitude. Once L/D = 10 (Fig.7.7), thick shear layer is formed and impinges on cavity bottom wall results in large region shear layer dominance on cavity bottom wall (Fig.7.3). Hence, the cavity aft wall spectrum is free from modes/tones whereas, the bottom and front walls have very low traceable modes/tones.

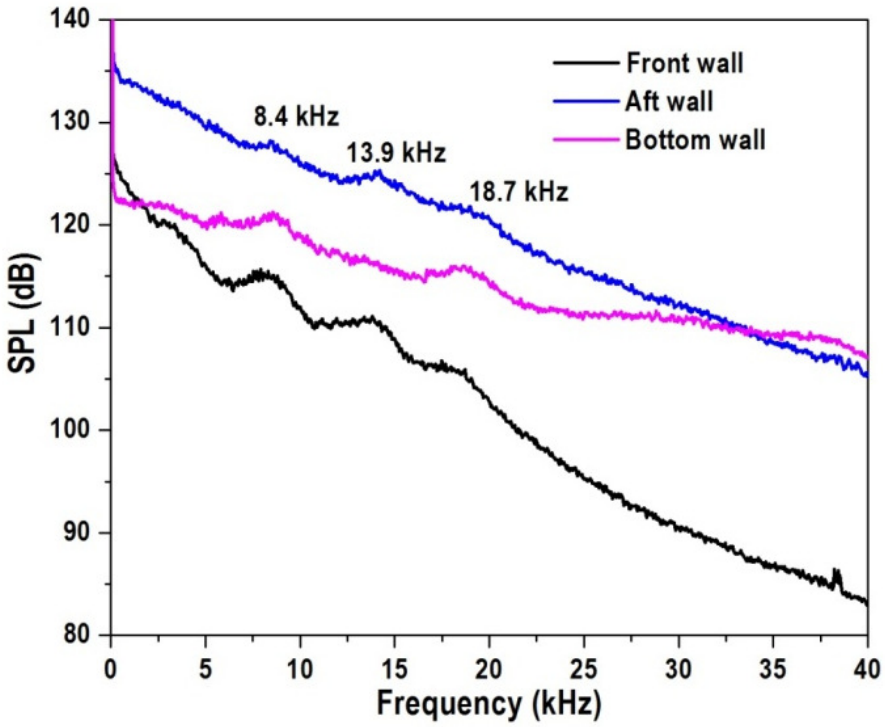

Fig. 7.7: SPL behavior for cavity (L/D = 10).

In general, as the L/D increases the spectrum slope is reduced. The cavities with lower L/D ratios, have more oscillations at various frequencies in terms of different modes. The oscillation levels at different frequencies are less for higher L/D ratio and hence the overall levels tending to become close to flat. It implies for higher L/D ratios, the mode switching and resonance may not happen.

7.4. Coherence Parameter

Poor coherence between different locations exists at all frequencies for cavities with L/D = 6, 7.5 and 10 as shown in Figs. 7.8 to 7.10. This is due to the shear layer attachment at cavity bottom wall as observed from the schlieren images. Hence, these cavities show the probability of nonexistence of a feedback mechanism as well as global instability.

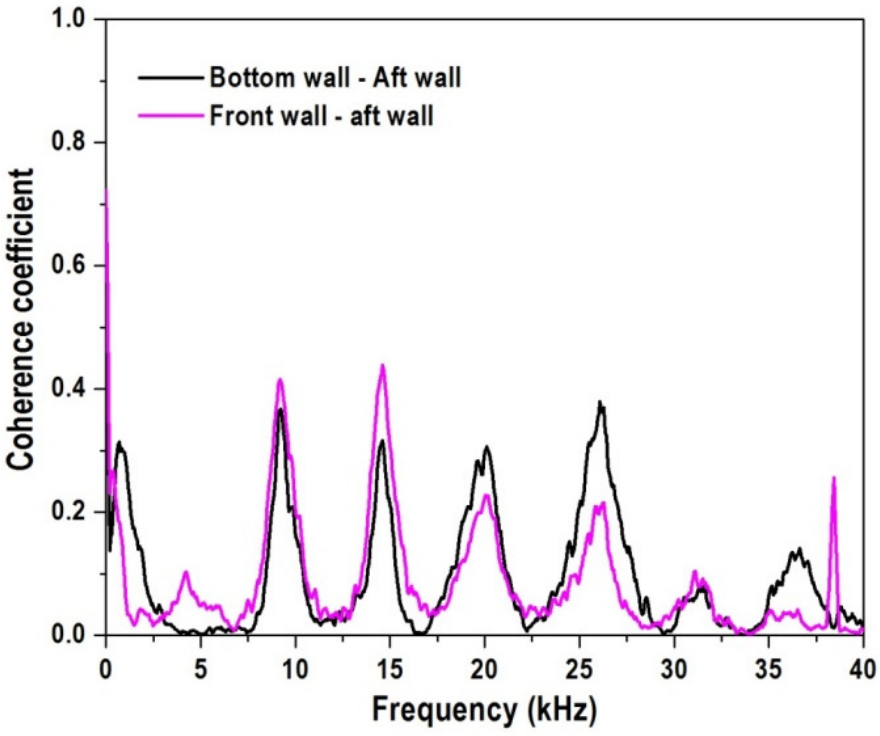

Fig. 7.8: Coherence parameter for L/D = 6

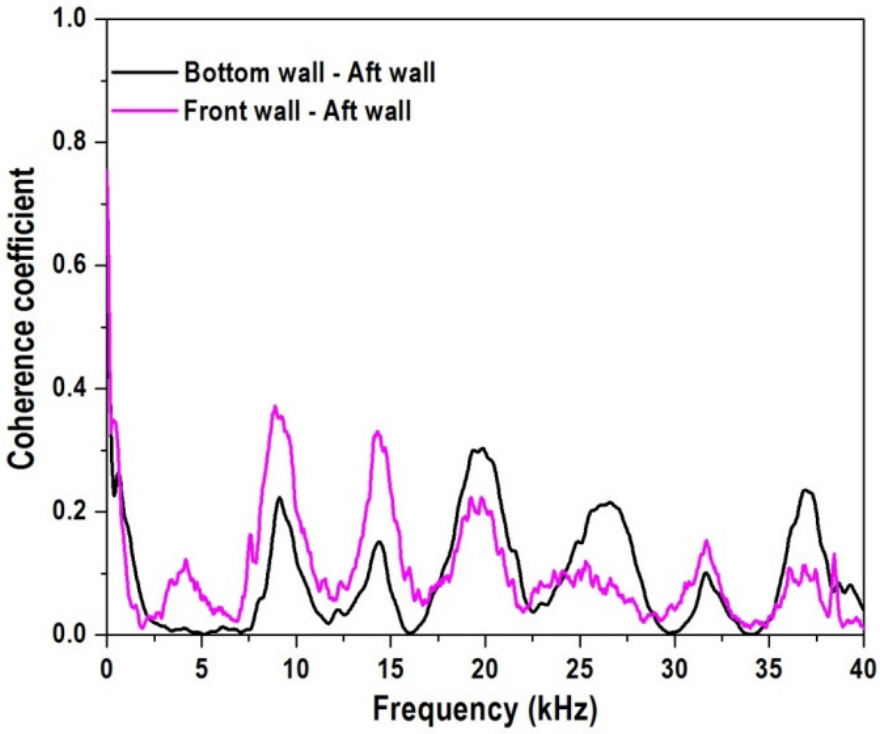

Fig. 7.9: Coherence parameter for L/D = 7.5

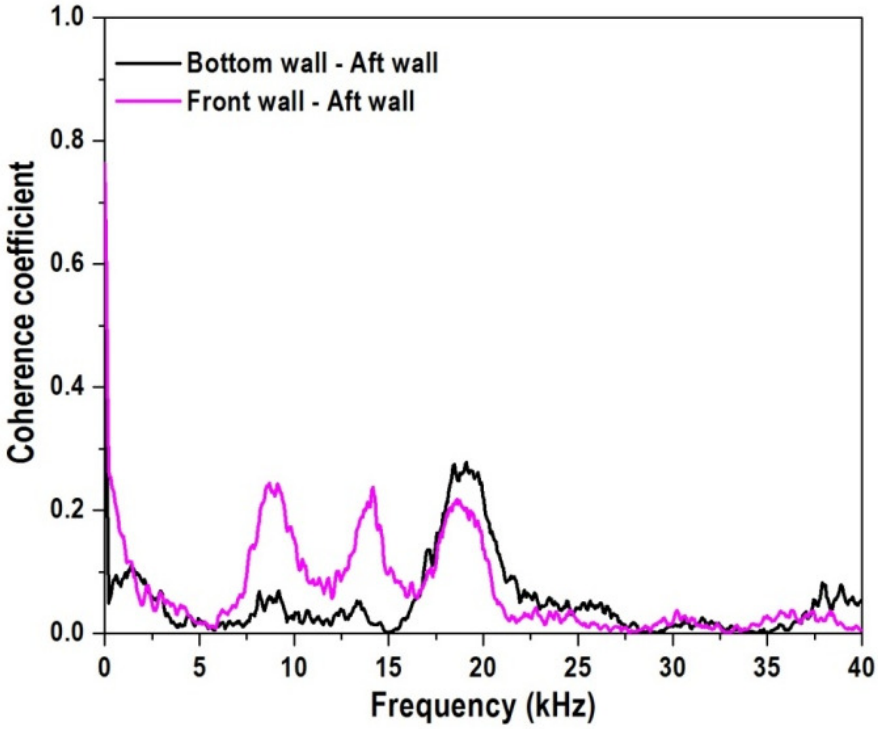

Fig. 7.10: Coherence parameter for L/D = 10

7.5 Cross correlation

The cross correlation between the pressures signals are presented for L/D =6, 7.5, and 10 in Figs. 7.11 to 7.13 respectively. Poor correlation between different locations inside the cavity is observed. Moreover, the periodicity is absent in the cross correlation coefficient variation due to broadband spectrum as shown in pressure spectra. This implies the absence of any feedback loop inside the cavity among various locations.

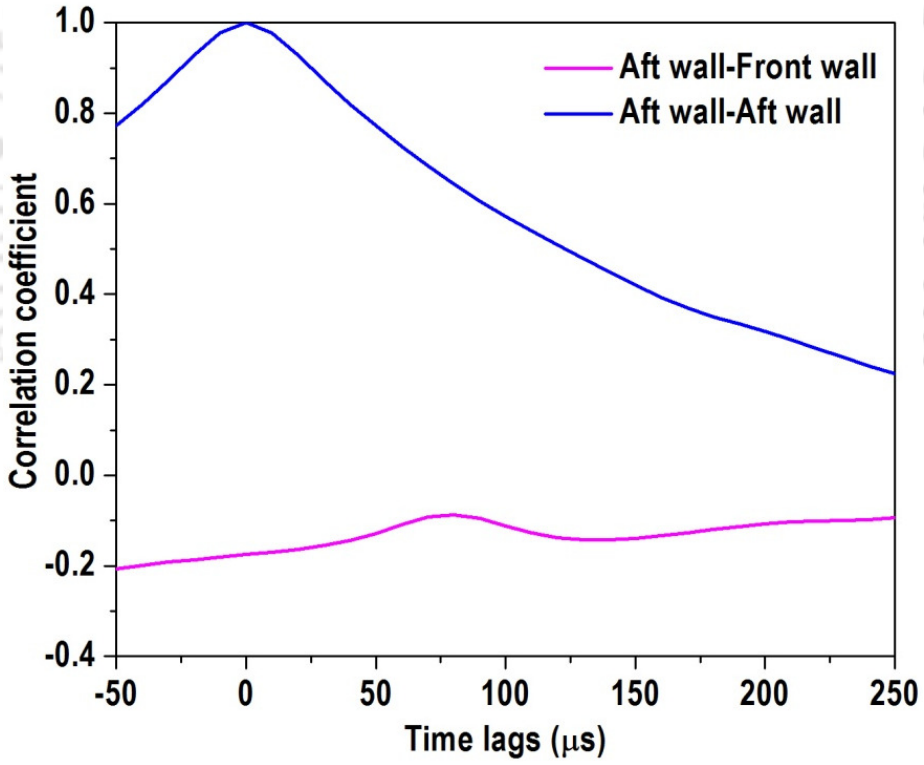

Fig. 7.11: Cross correlation parameter for L/D = 6

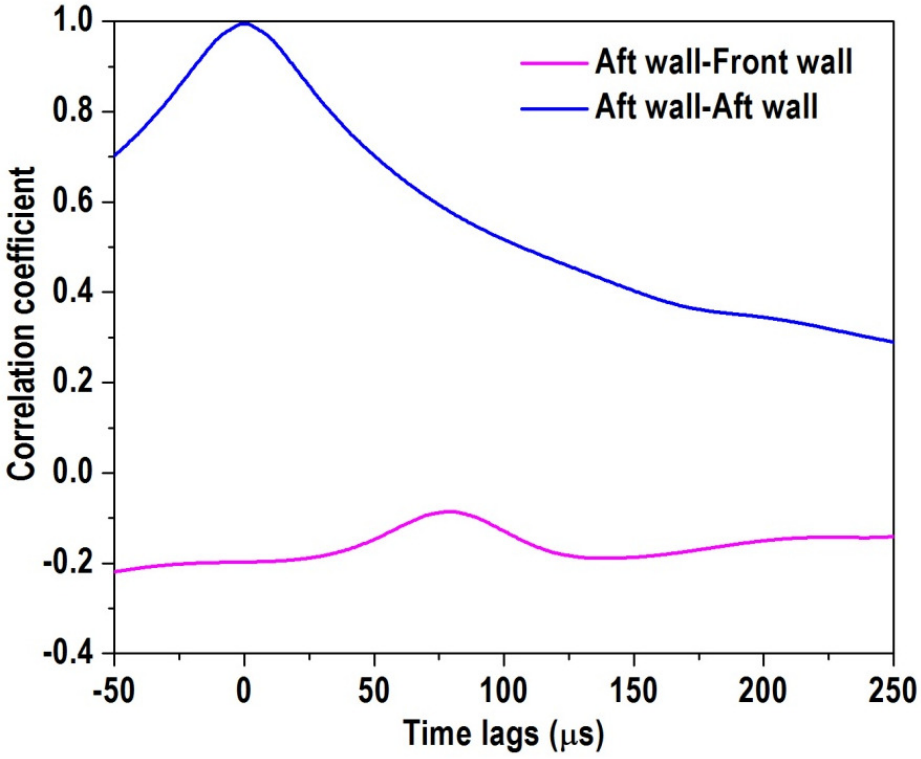

Fig. 7.12: Cross correlation parameter for L/D = 7.5

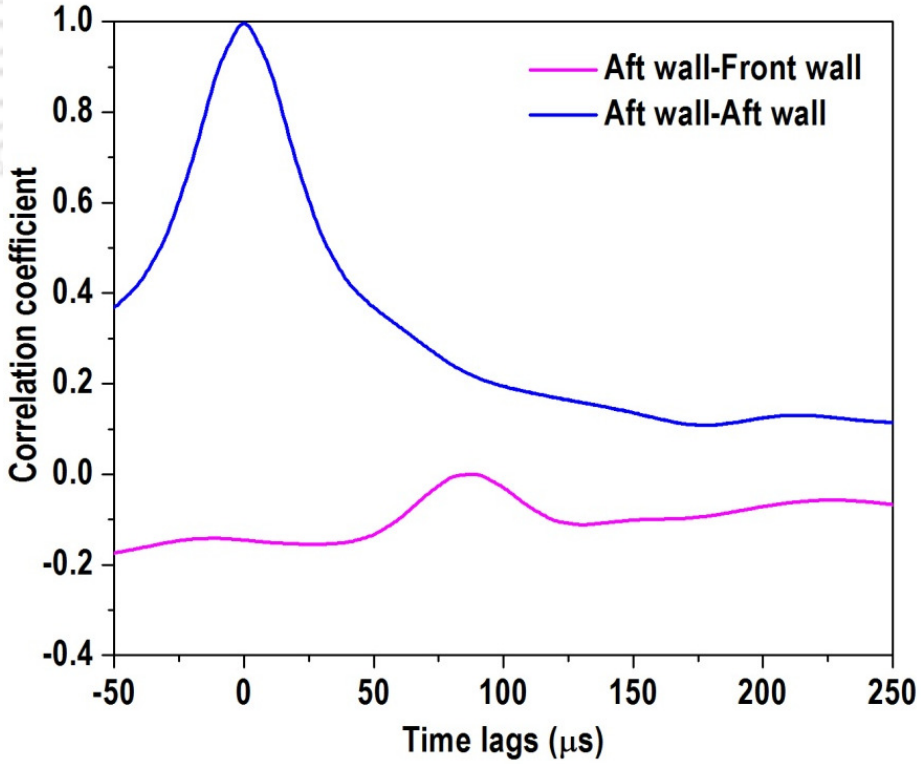

Fig. 7.13: Cross correlation parameter for L/D = 10.

7.6 Summary

Experimental results for cavities with L/D = 6, 7.5 and 10 using time resolved schlieren images and unsteady pressure measurements show the characteristics as given below.

1. Time resolved schlieren images show that the cavity shear layer impinges at cavity floor and hence, modes/tones of the cavity are affected.
2. As the cavity L/D increases, shear layer impingement inside the cavity is seen and more attached flow region in the cavity is observed.
3. The aft wall sensor for all the cavities show a broad band noise whereas, the other sensors in bottom and front walls exhibit low amplitude modes/tones which are decreasing with increasing L/D ratio.
4. The velocity of the vortex convection for L/D = 6 and 7.5 varies from 256 to 344 m/s indicate the non-linear behavior of the cavity.
5. Poor Coherence coefficients value show non-existence of feedback mechanism.
6. The absence of feedback mechanism is also confirmed through cross correlation.

CHAPTER 8

RESULTS AND DISCUSSIONS

EFFECT OF L/D RATIO ON CAVITY OSCILLATOTY MODES AND DRAG

8.1 Introduction

The overall performance of a scramjet engine depends on drag experienced by the components, which are located in the flow passage. The drag associated with other mixing and flame holding devices such as strut, pylon, etc is large. Hence, cavity is being considered as an alternate device that can aid positive thrust. Based on results presented in the earlier chapters for the range of L/D ratios, the drag experienced by various cavities are discussed in this chapter.

8.2 Oscillatory mode of cavities

Figure 8.1 shows the root mean square (rms) values of the pressure fluctuation on the floor of the cavity. It can be seen that from L/D = 1 to 2, a sudden rise in the oscillation is observed. Beyond L/D = 2 up to L/D = 5, decreasing trend is noticed. Subsequently, almost a constant value of rms of the order L/D =1value is seen. The sharp rise in the fluctuating pressure between L/D = 1 and 2 indicates transition of cavity oscillation from transverse to longitudinal mode and is dominated by the transverse mode of oscillation. Conversely, the low value of fluctuating pressure at L/D = 1 confirms the cavity oscillation is driven by a transverse mode which is substantiated

through schlieren images (Fig.5.1) where the cavity experiences a single vortex. When oscillation is driven by the longitudinal mode, the magnitude of fluctuating pressure is decreased which is seen beyond L/D = 2 and gradually decreases to the value corresponds to the level attained prior to the onset of the longitudinal oscillation due to change in the behavior of shear layer. From schlieren images (Figs.7.1-7.3) the thickness of the shear layer is increased towards approaching the cavity aft wall that affects the cavity oscillation. Due to this effect, the decrement in magnitude of the modes /tones is seen in SPL plots (Figs.7.5-7.7). The fluctuations are damped out beyond L/D = 5. The current experimental results show the captured trend is in line with the available evidence in the literature [42]. However, the magnitude of the pressure fluctuations could not be compared, because the free stream Mach numbers are different.

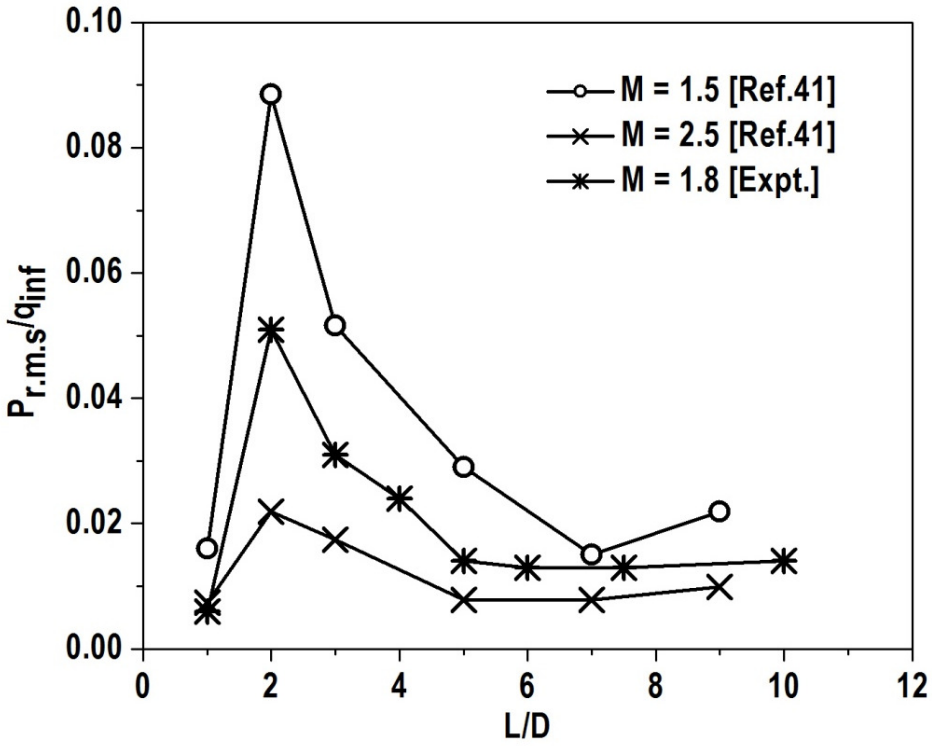

Fig. 8.1: Root-mean-square values of the pressure fluctuation.

8.3 Cavity drag

The drag coefficient of the tested cavities is derived from cavity front and aft wall pressures as shown in Fig.8.2. It is observed that rapid rise in the drag beyond L/D ≥ 5, is explained through the pressure spectra and the schlieren images. The pressure spectra (Figs.7.5-7.7) for these cavities reveal that the oscillatory magnitude becomes weak and the shear layer becomes very thick (Figs.7.1-7.3) with increasing L/D ratio.

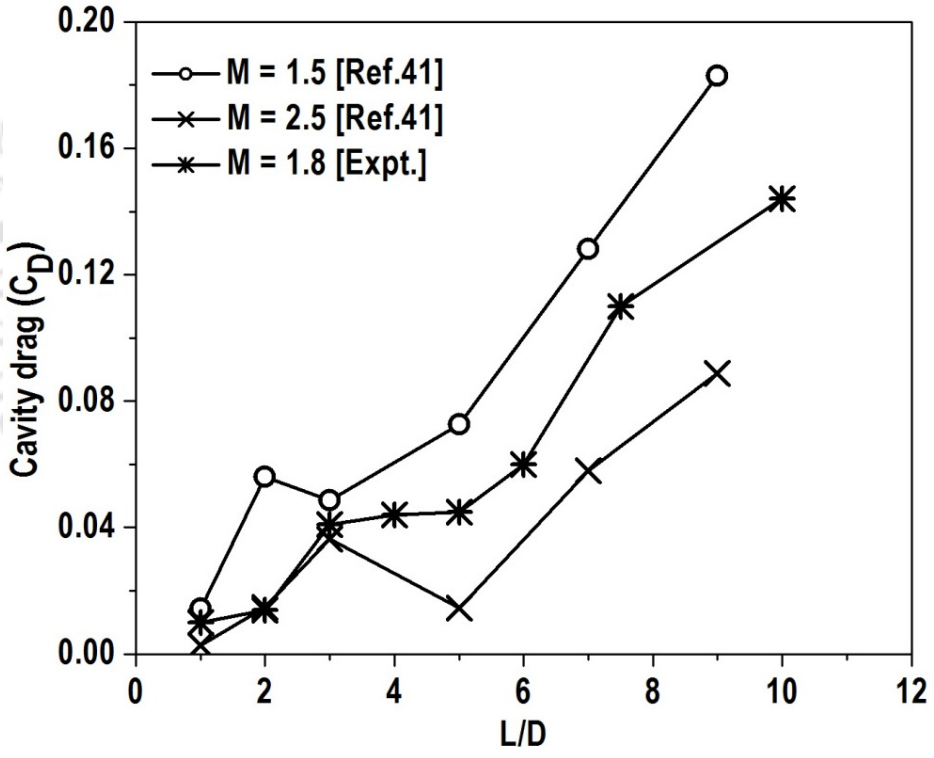

Fig. 8.2: Cavity drag for various (L/D) ratio.

Hence, it is expected that the front wall would experience a pressure drop due to momentum diffusion across the shear layer. Whereas, large rise in the pressure on cavity aft wall face is expected due to shear layer deflection and reattachment of the

flow. When the shear layer is attached to the cavity bottom wall, the dividing streamlines move towards the aft wall with higher dynamic pressure. The flow with increased dynamic pressure when impinges on cavity aft wall leads to a stagnation state resulted in rise in pressure. Thus, the combined impact would lead to increase the drag for $L/D \geq 5$. In the range, $3 \leq L/D \leq 5$, the cavity oscillation is determined by the longitudinal mode. Hence, it plays an important role in balancing the momentum as well as the mass resulted in almost same drag. The increase in drag is seen for $1 \leq L/D \leq 3$,. This is due to transition of cavity oscillation from transverse to longitudinal mode that brings additional momentum and hence, drag is increased. Figure 8.2 shows the comparison of cavity drag for the range of L/D ratios with the literature results [42]. It is understood that the trend of the drag is in line with the literature values. However, the magnitude differs due to the difference in Mach number. In the literature [42], the cavity drag is calculated for two Mach numbers namely M = 1.5 and 2.5, respectively. In the present studies, experiments are carried out at M = 1.8 and hence, the drag is found to be between these two Mach numbers which is in line with the trend.

8.4 Summary

In this chapter, the cavities oscillatory modes and the drag are studied to understand their behavior. Following are the observation from the experiments.

1. At L/D = 1, cavity oscillation is driven by a transverse mode where a single vortex is present in the cavity.
2. It may be seen that from L/D = 1 to 2, a sudden rise in the oscillation is observed due to transition of cavity oscillation from transverse to longitudinal mode. In this case, there is additional momentum due to transition of cavity oscillation from transverse to longitudinal mode for which the drag is increased.
3. From $3 \leq L/D \leq 5$, decreasing trend is noticed in pressure fluctuation due to the fact that the cavities in this range are driven by longitudinal mode of oscillation. Hence, mass and momentum balance takes place inside the cavity resulting in almost same drag.
4. Beyond $L/D \geq 5$, the fluctuating pressure gradually reduces and reaches to a value corresponds to L/D =1 due to shear layer impingement at cavity bottom wall. In these cases, rapid rise in the drag is observed because the aft wall faces the stagnation flow conditions and the approach flow dynamic pressure to the aft wall increases with increasing L/D. This in turn produces large pressure difference between cavity front and aft wall, which leads to increased drag.

CHAPTER 9

CONCLUSIONS AND FUTURE SCOPE

Experiments are carried out to study the cavity flow physics for a range of L/D ratios at supersonic condition in a confined duct. The range of L/D ratios used in the cavity is 1, 2, 3, 4, 5, 6, 7.5 and 10. These cavities are categorized into three main category namely transition from deep to shallow open cavities ($1 \leq L/D \leq 3$), shallow open cavities (L/D = 4 and 5) and transition from shallow open to shallow close cavities ($6 \leq L/D \leq 10$). Further, transient starting characteristics of all the cavities are experimentally studied for the range of stagnation pressures varying from $P_{01}/P_0 = 0.41$ to 0.63 to comprehend the transient shocks interaction with the cavity shear layer. The transient shock interaction with the cavity shear layer is captured through shadowgraph images while time resolved schlieren images are acquired to study shear layer vortex dynamics and wave features around the cavity. Further, the unsteady pressure measurements are carried out to explain the origin of the modes/tones generated by the cavities along with time resolved schlieren images. The modes/tones of cavity oscillations are derived from the unsteady pressure signals through FFT and the mode switching phenomena as well as the energy content of the modes/tones are elucidated through wavelet transform. In addition, cross correlation, coherence coefficients and the spectrogram derived from unsteady pressures are utilized to explain the characteristics of the cavities. Following are the conclusions from the present studies.

9.1. Onset of transient shock interaction with cavity shear layer and their characteristics

In the present studies, transient processes are achieved at discrete stagnation pressures. The ratio (P_{01}/P_0) continuously varied at different rates to reach the maximum pressure ratio. The shadowgraph images of transient starting characteristics show the existence of bifurcated shock system associated with shock train phenomena. Once the stagnation pressure is increased during transient starting process, bifurcated shock system along with shock train is observed in the flow. When these shocks interact with the cavity shear layer, they produce number of modes/tones inside the cavity. The studies demonstrate that the rate (2s and 4s) at which the stagnation pressure varied has negligible change on the results. For L/D ratios of 2 to 5, the pressure spectra exhibit small amplitude modes/tones at different frequencies, and a mode/tone occurs at 38.5 kHz. In all the cases, a mode switching phenomena is observed during the starting process. The overall sound pressure levels (OASPL) during starting process is as high as 181 dB and the range of OASPL for L/D = 2 and 3 cavities vary from 134 to 170 dB while shallow open cavities (L/D = 4 and 5) exhibit the OASPL of 155-181 dB. The experimental results clearly demonstrate the existence of shock interaction with the shear layer leads to high OASPL and hence, the acoustic effect of this magnitude has to be accounted in the airframe structure design.

9.2 Onset of cavity oscillation from transverse to longitudinal mode in a supersonic flow (1 ≤ L/D ≤ 3)

For short cavity (L/D = 1), the oscillation mode is primarily in the transverse direction which is marked by the presence of a single vortex and ascertained through a typical V- shape wave signature inside the cavity. As the cavity length is increased (L/D = 2 and 3), two vortices are observed. For L/D = 2 cavity, a large vortex as well as a small vortex are observed near front and aft walls respectively and the pressure spectra shows small amplitude oscillations around 7 to 9 kHz along with discrete modes/tones at 11.2 and 21.8 kHz. This indicates the existence of both transverse and longitudinal mode of oscillations which is evident from rapid increase in the rms pressure value between L/D = 1 and 2. In the case of L/D = 3, the flow features inside the cavity are marked by a large vortex near cavity aft wall and a small vortex adjacent to the front wall. The pressure spectrum reveals only dominant modes/tones at discrete frequencies. This shows that L/D = 3 cavity is driven by longitudinal mode of oscillation which is corroborated through rms pressure where the value becomes low. It may be concluded that the transition of cavity oscillation from transverse to longitudinal mode occurs between 2 ≤ L/D ≤ 3. The discrete frequencies correspond to dominant modes/tones for L/D = 2 cavity derived through modified Rossiter relation show a large deviation as high as 42% compared to unsteady pressure results. This indicates the periodic assumption in modified Rossiter relation is not valid for transitional cavity. For L/D=2, the Strouhal number derived from vortices convective speed (from schlieren video),the unsteady pressure measurements and the modified Rossiter relation match within 9.5%. This difference is still high due to the fact that the L/D = 2 cavity is

transitional. For L/D = 3 cavity, the oscillation mode is only in the longitudinal direction and hence, both modified Rossiter relation and experimentally generated vortex speed substituted in the same relation agreeing within 4.5 % and 2.5%, respectively, as compared to unsteady pressure results. This shows that when the non-linearity is accounted, the results are closely matching with the unsteady pressure results. The cavity drag is found to be low for L/D = 1 cavity whereas due to shear layer reattachment and associated flow conditions lead to increase in drag for L/D = 2 cavity. From cross correlation, it is established that the 1st and 2nd modes/tones of cavity oscillation are due to wave propagation inside the cavity and shear layer impingement at cavity aft wall. Wavelet transform indicates nonexistence of mode/tone switching phenomena for L/D = 2 cavity whereas, mode/tone switching phenomena is observed in L/D = 3 cavity which is not expected and the reason need to be explored.

9.3 Nonlinear characteristics of shallow open cavities (L/D = 4 and 5)

As the length of the cavity is increased (L/D = 4 and 5) number of modes/tones are also increased. The dominant modes/tones for L/D = 4 cavity is more significant as compared to L/D = 5 cavity. The vortex convection inside the cavity shear layer is nonlinear. In both cavities, the vortex speed is found to be increased downstream of the cavity leading edge and is observed to be decreased near the cavity trailing edge. The average vortex speed in the shear layer is in the range of 230 to 305 m/s. The cross correlation analyzes reveal that the 1st mode/tone is due to wave propagation inside the cavity, 2nd mode/tone is due to vortex shedding and one time period indicates the maximum mode/tone. The cavity with L/D = 4, exhibits very good cross correlation

between the pressure signals whereas, L/D = 5 cavity shows the cross correlation is very moderate. In both the cavities, wavelet analysis shows no mode switching phenomena.

9.4. Transition from shallow open cavities to closed cavities

Time resolved schlieren images show that the cavity shear layer impinges at cavity floor and hence, modes/tones of the cavity are affected. As the cavity L/D increases, shear layer impingement location moves upstream with respect to the trailing Edge of the cavity leads to more and more attached flow region within the cavity. The aft wall sensor for all cavities show a broad band noise whereas, the other sensors in bottom and front walls exhibit low amplitude modes/tones that decreases with increase in (L/D) ratio. The velocity of the vortex convection for L/D = 6 and 7.5 varies from 256 to 344 m/s, indicated the non-linear behavior of the cavity. Coherence coefficients show a poor value, which indicates the non-existence of a feedback mechanism. The absence of feedback mechanism is also confirmed through cross correlation for the cavities.

9.5. Effect of L/D ratio on cavity oscillatory modes and drag

At L/D = 1, cavity oscillation is driven by a transverse mode where a single vortex is present in the cavity. From L/D = 1 to 2, a sudden rise in the oscillation is observed due to transition of cavity oscillation from transverse to longitudinal mode that brings additional momentum and drag. In the range, $3 \leq L/D \leq 5$, decreasing trend is seen in pressure fluctuation due to longitudinal mode of oscillation which results in almost same drag. Beyond $L/D \geq 5$, the fluctuating pressure gradually reduces and reaches a value

corresponds to L/D =1 due to shear layer impingement at cavity bottom wall. In these cases, rapid rise in the drag is observed because the aft wall faces the stagnation flow conditions and the approach flow dynamic pressure to the aft wall increases with increasing L/D. This in turn produces large pressure difference between cavity front and aft wall which leads to increase in drag.

9.6. Scope of future work

In view of the limitations of timelines and proposed research themes, there is always a scope for future direction of research. Some of them are listed here:

- **Fuel injection and mixing:** The primary issue of supersonic combustion is the combined effect of fuel injection and its mixing with freestream. In a typical scramjet engine, the vorticities and turbulence promote mixing. Cavities are used for supersonic mixing primarily due to acoustic instabilities to drive large-scale structures. The studies on large-scale structures still need to be understood.
- **Shear layer stability**: The shear layers are generally stable and hence, prime reason for the poor mixing rate. The presence of a cavity, provides a subsonic path for feedback mechanism which in turn affects the local and global spatial-temporal stability characteristics of the cavity shear layer. This needs to be studied further.
- **Choice of methods for processing of time-series data**: The detection of flow structures using time series, frequency domain and wavelet domain have been practiced in different fluid mechanics areas. However, other methods such as POD (proper Orthogonal Decomposition), PIV, Hot wire anemometry, etc, need to be carried out for better understanding of the flow physics over cavity.
- **Supersonic combustion:** Finally, the supersonic combustion to be carried out for the cavities with temperature and pressure measurements. Also, the laser based techniques need to be studied in order to assess the mixing efficiency of the cavities.

REFERENCES

[1] Dipankar Das, "ISRO's scramjet experiment and way forward,"21st AeSI CFD symposium,August 9-10,National Aerospace Laboratories,Bangalore,India(2019).

[2] V. Sridhar, S.L. Gai, H. Kleine, H, “Oscillatory characteristics of shallow open cavities in supersonic flow,” AIAA.J, 54 (11) 3495-3508(2016).

[3] K. Krishnamurthy, “Acoustic radiation from two-dimensional rectangular cutouts in aerodynamic surfaces,” NACA Tech. Note 3487, (1955).

[4] L.W. Huellmantel, R.W. Ziemer, A.B. Cambel, “Stabilization of premixed propane–air flames in recessed ducts,” Jet Propulsion 31–43 (1957).

[5] A. Roshko, “Some measurements of flow in a rectangular cutout,” NACA TN 3488 (1955).

[6] A. Ben-Yakar, R. Hanson, “Cavity flame-holders for ignition and flame stabilization in scramjets: review and experimental study,” AIAA Paper 98-3122 (1998).

[7] B.K. McMillan, J.M. Seitzman, R.K. Hanson,” Comparison of NO and OH planar fluorescence temperature measurements in scramjet model flow fields,” AIAA.J, 32 (10) 1945–1952 (1994).

[8] J. Rossiter, “Wind-tunnel experiments on the flow over rectangular cavities at subsonic and transonic speeds,” Aeronautical Research Council Rept. 3438 (1964).

[9] H.E. Plumblee, J.S. Gibson, L.W. Lassiter, “A theoretical and experimental investigation of the acoustic response of cavities in an aerodynamic flow,” WADD-TR- 61–75 (1962).

[10] H.H. Heller, D.B. Bliss, “The physical mechanism of flow-induced pressure fluctuations in cavities and concepts for their suppression,” AIAA Paper 75-491 (1975).

[11] N.M. Komerath, K.K. Ahuja, F.W. Chambers, “Prediction and measurement of flows over cavities - A survey,” AIAA Paper 87-0166 (1987).

[12] X. Zhang, J.A. Edwards, “Computational analysis of unsteady supersonic cavity flows driven by thick shear layers,” Aeronautical Journal 92 (919) 365–374(1988).

[13] E.B. Plentovich, R.L. Stallings, “M.B. Tracy, Experimental cavity pressure measurements at subsonic and transonic speeds,” NASA Technical Paper 3358 (1993).

[14] D. Rockwell, E. Naudascher, E, Review: “Self–sustaining oscillations of flow past cavities,” Journal of Fluids Engineering, 100 (2) 152-165(1978).

[15] H.E. Plumblee, J.S. Gibson, L.W. Lassiter, “A theoretical and experimental investigation of the acoustic response of cavities in an aerodynamic flow,” WADD-TR- 61–75 (1962).

[16] H.H. Heller, D.G. Holmes, E.E. Covert, “Flow induced pressure oscillations in shallow cavities,” Journal of Sound and Vibration 18 (4) 545-553(1971).

[17] Charawat,A.F., Roos,J.N, Dewy,F.C.,Jr., and Hitz,J.A., “An Investigation of Separated Flows-Part1:The Pressure Field.” Journal of Aerospace Science, 28,457-470 (1961).

[18] Chung,K. “Characteristics of Compressible Rectangular Cavity Flows. Journal of Aircraft,” Vol.40, No.1, 137-142(2003).

[19] Tracy, M.B., Plentovich, E.B., and Julio Chu.“Measurements of Fluctuating Pressure in a Rectangular Cavity in Transonic Flow at High Reynolds Numbers.” NASA TM-4363(1992).

[20] Tracy, M.B., and Plentovich, E. B., “Characterization of Cavity Flow Fields Using Pressure Data Obtained in the Langley 0.3 – Meter Transonic Cryogenic Tunnel.” NASA TM –4436(1993).

[21] D.S. Mironov, “An experimental study of pressure fluctuations generated by an open shallow cavity performed using joint time-frequency techniques of data analysis,” Thermophysics and Aeromechanics, 18 (3): 369- 379(2011).

[22] P. Oshkai, D. Rockwell, M. Pollack. “Shallow cavity flow tones: transformation from large- to small-scale modes,” Journal of Sound and Vibration, 280:777–813(2005).

[23] Clarence W. Rowley, Tim Colonius and Amit J. Basu. “On self-sustained oscillations in two-dimensional compressible flow over rectangular cavities.” Journal Fluid Mechanics, 455: 315-346(2002).

[24] M. Gharib, and A. Roshko. “The effect of flow oscillations on cavity drag.” Journal Fluid Mechanics, 177: 501-530(1987).

[25] R. Camussi, G. Guj, A. Di Marco and Ragni,"Propagation of wall pressure perturbations in a large aspect ratio shallow cavity." Experiments in Fluids 40: 612–620(2006).

[26] Sheryl M. Grace, W. Gary Dewar and Donald E. Wroblewski. "Experimental investigation of the flow characteristics within a shallow wall cavity for both laminar and turbulent upstream boundary layers." Experiments in Fluids, 36:791–804(2004).

[27] B. Farkas, G. Paal and K. G. Szab. "Descriptive analysis of a mode transition of the flow over an open cavity." Physics of Fluids. 24: 027102 (2012).

[28] Hiroshi Yokoyama and Chisachi Kato. "Fluid-acoustic interactions in self-sustained oscillations in turbulent cavity flows I. Fluid-dynamic oscillations," Physics of Fluids. 21, 105103, (2009).

[29] Ben-Yakar, A., and Hanson, R., "Cavity Flame-holders for Ignition and Flame Stabilization in Scramjets: Review and Experimental Study," AIAA Paper 98-3122, July (1998).

[30] Bilanin A.J and Covert.E.E "Estimation of possible excitation frequencies for shallow rectangular cavities." AIAA Journal, 11 (3), 347-351, (1973).

[31] H.H. Heller, D.B. Bliss, "The physical mechanism of flow-induced pressure fluctuations in cavities and concepts for their suppression," AIAA Paper 75-491 (1975).

[32] H. Heller and J. Delfs, "Cavity pressure oscillations: The generation mechanism visualized. Journal of sound and vibration," 196(2): 248-252 (1996).

[33] D. Rockwell and C. Knisely, “The organized nature of the flow impingement upon a corner. Journal of Fluid Mechanics,” 93 (3): 413-432(1979).

[34] Tam,C.K.W.“The acoustic Modes of a Two-Dimensional Rectangular Cavity.” Journal of Sound and Vibration, 49: 353-364(1976).

[35] Tam, C.K.W., and Block,P.J.W.“On the tones and pressure oscillations induced by flow over rectangular cavities.” Journal of Fluid Mechanics, 89 (2): 373-.399(1978).

[36] Rockwell, D and Naudascher, E.“Review-Self sustaining oscillations of flow past Cavities.” Journal of Fluids Engineering (Transactionof ASME), 100: 152-164(1978).

[37] Hankey,W.L., and Shang,J.S. “Analysis of pressure oscillations in an open Cavity.” AIAA Journal, 8 (8), 892-898, (1980).

[38] Rizetta,D.P.(1988) “Numerical simulation of supersonic flow over a three-dimensional cavity.” AIAA Journal, 26 (7): 779-807(1988).

[39] Zhang,X., and Edwards,J.A.“Computational Analysis of Unsteady Supersonic Cavity Flows Driven by Thick Shear Layers,”Aeronautical Journal, 92: 355-364(1988).

[40] Baysal,O., and StallingsJr,R.L. “Computational and experimental investigation of cavity flow fields.” AIAA Journal, 26 (1): 6-7(1988).

[41] Stallings Jr, R.L., and Wilcox Jr, F.J. “Experimental cavity pressure distribution at supersonic speeds,” NACA-TP-2683(1987).

[42] Zhang,X and Edwards,J.A. “An investigation of supersonic oscillatory cavity flows driven by thick shear layer,” Aeronautical Journal, 94(940), 355–364 (1990).

[43] Zhang. X. “Compressible Cavity Flow Oscillation due to Shear Layer Instabilities and Pressure Feedback,” AIAA Journal. 33 (8): 1404-1411(1995).

[44] Tam,C. J., Orkwis, P. D and Disimile, P. J., " Algebraic Turbulence Model Simulations of Supersonic Open-Cavity Flow Physics", AIAA Journal, 34 (11): 2255-2260(1996).

[45] Zhang, X., Rona, A and Edwards, J. A., "An Observation of Pressure Waves Around a Shallow Cavity", Journal of Sound and Vibration, 214 (4): 771-778 (1998).

[46] J. Poggie and A. J. Smits. “Large-Scale Structures in a Compressible Mixing Layer over a Cavity.” AIAA Journal, 41 (12): 2410-2419(2003).

[47] O. H. Unalmis, N. T. Clemens, and D. S. Dolling. “Cavity Oscillation Mechanisms in High-Speed Flows,” AIAA Journal, 42 (10): 2036-2041(2004).

[48] Taro Handa, and Mitsuharu Masuda. “On the jump in the frequency of acoustic oscillations in supersonic flows over rectangular cavity,” Physics of Fluids, 21: 026102 (2009).

[49] Weipeng Li, Taku Nonomura, and Kozo Fujii. “On the feedback mechanism in supersonic cavity flows,” Physics of Fluids, 25: 056101 (2013).

[50] N. S. Vikramaditya and Job Kurian. “Nonlinear aspects of supersonic flow past a cavity,” Experiments in Fluids,52:1389–1399(2012).

[51] Hongbo Wang, Mingbo Sun, Ning Qin, Haiyan Wu and Zhenguo Wang. "Characteristics of Oscillations in Supersonic Open Cavity Flows." Flow Turbulence Combustion 90:121–142(2013)

[52] Ryan F. Schmit, James E. Grove, Frank Semmelmayer, and Mitchell Haverkamp. "Nonlinear Feedback Mechanisms inside a Rectangular Cavity." AIAA Journal, 52 (10): 2128-2142(2014)

[53] K. M. Nair and S. Sarkar. "Large Eddy Simulation of Self- Sustained Cavity Oscillation for Subsonic and Supersonic Flows." ASME Journal of Fluids Engineering, 139: 011102-1(2017).

[54] Vikram Sridhar, Harald Kleine, Sudhir L. Gai. "Visualization of wave propagation within a supersonic two-dimensional cavity by digital streak schlieren." Experiments in Fluids, 56:152(2015).DOI 10.1007/s00348-015-2026-3,1-15 .

[55] Sally J. Moon, Sudhir L. Gai, Harald H. Kleine, and Andrew J. Neely. "Supersonic Flow over Straight Shallow Cavities Including Leading and Trailing Edge Modifications." AIAA-4687(2010).

[56] G. S. Settles, D.R. Williams, B.K. Baca and S.M. Bogdonoff, "Reattachment of a Compressible Turbulent Free Shear Layer", AIAA Journal 20 (1): 60-67 (1982)

[57] L. Timothy, N. Bisek, and J. Poggie, "Detached-Eddy Simulation of a Supersonic Reattaching Shear Layer." AIAA Journal 55 (11): 3722-3733 (2017)

[58] Wei Huang, Li Yan, Jian guo Tan ,"Survey on the mode transition in combined cycle Propulsion system" Aerospace Science and Technology, 39: 685-691 (2014).

[59] Lei Liao, Li Yan, Wei Huang, Lang-quan Li, " Mode transition process in a typical strut based scramjet combustor based on a parametric Study ,"Applied Physics and Engineering,19(6): 431-451, (2018).

[60] Wei Huang, Zhao-bu Du, Li Yan, R Moradi, " Flame propagation and stabilisation in a dual mode scramjet combustor: A survey, " Progress in Aerospace Sciences, 101: 3-30 (2018).

[61] Xi- Peng Li, Wei- Dong Liu, Yu Pan and Shi-Jie Liu," Investigation on Ignition enhancement mechanism in a scramjet combustor with dual cavity," Journal of Propulsion and Power, 32 (2):439-447 (2016).

[62] Chenlin Zhang, Juntao Chang, Jun long Zhang, Wen Bao Daren Yu, "Effect of continuous Mach number variation of incoming flow on ram-scram transition in a dual mode Combustor," Aerospace Science and Technology, 76: 433-441 (2018).

[63] W.H.Heiser and D T Pratt “Aerothermodynamics of Dual Mode Combustion system” Progress in Astronautics and Aeronautics, 189: 569-595 2012.

[64] Brown G. L and A. Roshko, “On Density Effects and Large Scale Structures in Turbulent Mixing Layers,” Journal of Fluid Mechanics, 64: 775-816(1974).

[65] Chinzei N., G. Masuya, T. Komuro, A. Murakami and K. Kudou, "Spreading of Two-Stream Supersonic Turbulent Mixing Layers," Physics of Fluids, 29 (5): 1345-1347 (1986).

[66] Elliot G. S and M. Saimmy,"Compressibility Effects in Free Shear Layers, "Physics of Fluid, 2: 1231- 1240(1990).

[67] Papamoschou D and A. Roshko, "The Compressible Turbulent Shear Layer: An Experimental Study," Journal of Fluid Mechanics, 197, 453-477(1988).

[68] Dimotakis P.E., 1989. "Turbulent Free Shear Layer Mixing," AIAA-89-0262(1989).

[69] Sekar B and H.S. Mukunda,"A Computational Study of Direct Simulation of High Speed Mixing Layers without and with Chemical Heat Release, " 23rd symposium (International) on combustion, Vol 23,Issue 1,707-713(1991) **.**

[70] Clemens N.T and M.G. Mungal, "Two and Three Dimensional Effects in the Supersonic Mixing Layers," AIAA Journal, 20 (4): 973-981(1992).

[71] Papamoschou D., "Effect of Three Dimensionality on Compressible Mixing Layers, "Journal of Propulsion and Power, 8, 247-249(1992).

[72] Erdos J., J. Tamagno, R. Bakos and R. Trucco, "Experiments on Shear Layer Mixing at Hypervelocity Conditions," AIAA-92-0628(1992).

[73] Marble F.E., G.J. Hendricks and E.E. Zukoski,"Progress toward Shock Enhancement of Supersonic Combustion Processes," AIAA-87-1880(1987)

[74] Drummond J.P., M.H. Carpenter, D.W. Riggins and M.S. Adams, "Mixing Enhancement in Supersonic Combustor," AIAA-89-2794(1989).

[75] Pope and Alan," High speed wind tunnel testing" John Wiley publication, 1968

[76] L. Crocco and L. Lees, "A Mixing Theory for the Interaction between Dissipative Flows and Nearly Isentropic Streams," Journal of the Aeronautical Sciences, 19 (10), 640-676(1952).

[77] L. S. Ukeiley, M. K. Ponton, J. M. Seiner, and B. Jansen, “Suppression of Pressure Loads in Cavity Flows,” AIAA Journal, 42 (1), 004, pp. 70–79. 2004

[78] R. Bauer and R. Dix, “Engineering Model of Unsteady Flow in a Cavity,” Arnold Engineering Development Center Technical Report No. AEDCTR- 91-17, Dec. (1991).

[79] L. S. Ukeiley and N. Murray, “Velocity and Surface Pressure Measurements in an Open Cavity,” Experiments in Fluids, 38: 656–671(2005).

[80] N.S. Vikramaditya, J. Kurian, “Pressure oscillations from cavities with ramp,” AIAA. J, 47 (12) 2974–2984(2009).

[81] P.K. Maurya, C. Rajeev, R.R. Vinil Kumar, V. Aravind, “Effect of aft wall offset and ramp on pressure oscillation from confined supersonic flow over cavity”, Experimental Thermal and Fluid Science,68: 559–573(2015).

[82] J. S. Bendat and A. G. Piersol, “Random Data Analysis”, Wiley-Inter science, (1986).

[83] http://www.fil.ion.ucl.ac.uk/~wpenny/course/course.html, Chapter 7.

[84] N. S. Vikramaditya and J. Kurian, “Amplitude and Phase Modulation of Cavity Modes in a supersonic flow,” European Journal of Mechanics B/Fluids(2013).http://dx.doi.org/10.1016/j.euromechflu.2013.06.12.

[85] Mayank Kumar and V. Aravind, “On shock train interaction with cavity oscillations in a confined supersonic flow,” Experimental Thermal and Fluid Science, 90: 260–274(2018).

[86] D. Jordan, R. W. Miksad, and E. J. Powers, “Implementation of the continuous wavelet transform for digital time series analysis,”Review of Scientific Instrument, Vol 68(3), 1484-1494 ,March (1997).

[87] Neumann, E. P, Lustwerk, F, "Supersonic diffusers for wind tunnels". Journal Applied Mechanics, 16 (2): 195-202 (1949).doi.org/10.2514/8.2763

[88] Newman, E. P, Lustwerk, F, "High-efficiency supersonic diffusers". Journal of Aeronautical Sciences, 18(6), 269-274,1951. doi.org/10.2514/8. (1975.)

[89] Lukasiewicz, J, "Diffusers for supersonic wind tunnels". Journal of Aeronaut Sciences, 20(9), 617-626(1953).doi.org/10.2514/8.2763

[90] Shapiro, A.H, "The dynamics and thermodynamics of compressible fluid flow", vols. 1 and 2. New York: Ronald Press, 135 (9): 1153-1156(1953).

[91] Ikui, T, Matsuo, K and Nagai, M, "The mechanism of pseudo-shock waves", Bull JSME, 17(108), 731-9(1974).

[92] Ikui T, Matsuo K, Sasaguchi K. "Modified diffusion model of pseudo-shock waves considering upstream boundary layers", Bull JSME,24(197), 1920-7(1981).

[93] Kim, H. D, "An experimental study of weak normal shock-wave/turbulent boundary-layer interaction in internal flows", PhD Thesis, Kyushu University, Japan, (1991).

[94] Nussdorfer, T. J, "Some observations of shock-induced turbulent separation on supersonic diffusers", NACA R.M. E51L26, (1954).

[95] Matsuo, K, Miyazato, Y and Kim, H. D, "Shock train and pseudo-shock phenomena in internal gas flows", Progress in Aerospace Sciences 35 (1999), 33-100. doi.org/10.1016/S0376-0421 (98)00011-6.

[96] B.F. Carroll, J.C. Dutton, “Characteristics of multiple shock wave/turbulent boundary layer interaction in rectangular ducts,” Journal of Propulsion, 6 (2): 186-193(1990).

[97] G. G. Mateer and J. R. Viegas, “Effect of Mach and Reynolds numbers on a normal shock-wave/turbulent boundary-layer interaction,” AIAA Paper No. 79-1502, (1979).

[98] P. E. Dimotakis, "Two-Dimensional Shear Layer Entrainment," AIAA Journal, 24 (11), 1797-1796, (1986).

[99] B.F. Carroll and J.C. Dutton, “Multiple normal shock wave/turbulent boundary-layer interactions,” Journal of Propulsion and Power, 8 (2):441–448(1992).

[100] N. Zhuang, F. S. Alvi and M. B, Alkislar, C. Shih, “Supersonic cavity flows and their control,”AIAA.J, 44 (9): 2118-2128(2006).

[101] N. S. Vikramaditya and J. Kurian, “Experimental study of influence of trailing wall geometry on cavity oscillations in supersonic flow,” Experimental Thermal and Fluid Science, 54: 102–109(2014).

[102] Chandra BU, Chakravarthy SR “Experimental investigation of cavity-induced acoustic oscillations in confined supersonic flow.” Journal of Fluids Engineering 127:761–769(2005).

[103] Mayank Kumar and Aravind Vaidyanathan “Oscillatory mode transition for supersonic open cavity flows.” Physics of Fluids, 30: 026101(2018).

[104] Marta Marimon Mateu “Study of an Air-Breathing Engine for hypersonic flight” Technical Report, September (2013).

[105] Donggang Cao, Guoqiang, Fei Qin, Xianggeng Wei, Bing Liu and Zhiwei Huang,” Investigation of shear layer growth influenced by shock wave in a Scramjet”, AIAA Journal , Vol54,3,1133-1138,(2016)